



University of Strathclyde
Renewable Energy Marine Structures Centre for Doctoral Training
Department of Naval Architecture, Ocean & Marine Engineering

Reliability-based optimization of floating wind turbine support structures

Mareike Leimeister

A thesis submitted in partial fulfilment of the requirements for the degree of
Doctor of Engineering
2020

Supervisors: Prof Athanasios Kolios
Dr Maurizio Collu

Declaration of authenticity and author's rights

This thesis is the result of the author's original research. It has been composed by the author and has not been previously submitted for examination which has led to the award of a degree.

The copyright of this thesis belongs to the author under the terms of the United Kingdom Copyright Acts as qualified by University of Strathclyde Regulation 3.50. Due acknowledgement must always be made of the use of any material contained in, or derived from, this thesis.

Mareike Leimeister

A handwritten signature in blue ink that reads "Mareike Leimeister". The script is cursive and elegant, with the first letters of the first and last names being capitalized and prominent.

August 2020

Statement on previously published work

In the course of this thesis, a number of papers are published in scientific journals or still under review at the time of writing, as listed in Section 1.5. The author of this thesis was and is in all these publications - even if the paper is co-authored - the main responsible person. The author's contributions to the publications, thus, comprise conceiving the works, administering the studies, realizing the works, performing literature studies, developing the methodologies, performing the researches, developing and applying the approaches, working with and extending the software, curating the data, verifying and validating the methods and results, analyzing and investigating the data and results, post-processing and visualizing the results and findings, writing the papers and preparing the original drafts, interacting with the journals' editors and reviewers, as well as reviewing and editing the papers for the final publications.

Mareike Leimeister

A handwritten signature in blue ink that reads "Mareike Leimeister". The script is cursive and fluid.

August 2020

Abstract

Floating offshore wind technology has high potential due to the renewable energy goals and the vast deep water ocean areas, however, still faces several challenges until achieving commercial market uptake. Floating concepts have to gain economic competitiveness and deal with more complex coupled system dynamics and greater uncertainties. This makes modeling, simulation, and reliability-based design optimization indispensable. However, reliability assessment and design optimization of floating wind turbines has not yet been coupled. - This is precisely the focus of this thesis. The overall aim is to derive guidelines for reliability-based design optimization of floating wind turbine support structures, taking target safety levels and failure mechanisms from existing standards into account and applying them in such novel concepts. To achieve this, reliability methods applied in the offshore and marine renewable energy industry are reviewed, classified, and investigated with respect to suitable procedures for reliability assessment of offshore wind turbine systems. Addressing the aspect of floating wind, the large diversity of existing floating support structures is assessed, focusing on their suitability for offshore wind farm deployment. Based on this, a reference floating wind turbine system is defined, for which an aero-hydro-servo-elastic coupled model of dynamics is developed and verified. Additionally, a holistic framework for automated simulation and optimization is developed and applied to different design optimization tasks: based on global limit states, addressing innovative design solutions or the future trend towards larger MW-class wind turbines, and finally including reliability criteria. The developed model, framework, and approaches - especially the concept for combining floating wind turbine design optimization with reliability assessment in a computationally and time-efficient manner - are of high value for both research and industry. The knowledge and outcomes of this thesis offer a broad range of future applications and pave the way towards economic and reliable floating support structure designs.

Keywords

Reliability-based design optimization (RBDO); Floating offshore wind turbines (FOWTs); Aero-hydro-servo-elastic coupled dynamics; Modelica[®] library for wind turbines (MoWiT); Python; Genetic algorithms; Monte Carlo simulation (MCS); Response surface; Quadratic regression analysis; Reliability index; Limit states; Design load cases (DLCs); Upscaling; Spar-buoy.

Acknowledgements

First and foremost I want to thank my supervisors Prof Athanasios Kolios and Dr Maurizio Collu. I am grateful to Prof Kolios for his valuable support throughout the three and a half years of my research work, for introducing me to and making me highly interested in the topic of risk assessment and reliability analysis - which I have never dealt with before - for having high expectations for my research outcome but always believing in me, for taking his time to discuss concerns, ideas, approaches, and results, as well as for always encouraging when receiving persistent comments from reviewers or rejections of papers submitted to journals. I would also like to thank Dr Collu for his valuable feedback on all topics related to floating wind turbines and hydrodynamics, for long, extensive, and very fruitful discussions, for his time taken for detailed analyses, and for the innovative ideas and valuable suggestions.

Furthermore, I am thankful for being part of the Renewable Energy Marine Structures Centre for Doctoral Training (REMS CDT) program, which gave me the opportunity to further deepen my knowledge and make valuable contacts with both academics and industry representatives, and which finally provided the framework and conditions for conducting and completing my research within these three and a half years. With high pleasure I took the courses within the first months of the program and conducted the group project, allowing me to dive into the health and safety aspects of offshore wind turbine systems, be myself together with my fellow students innovative, and perform lifting tests at the facilities of Cranfield university. Thanks to my fellow students for the quality time together in the REMS CDT. A special thanks goes to the team of the REMS CDT program, in particular to Prof Feargal Brennan and Sally Dring, being always open for any organizational question and concern and making me feeling welcome and being in the right research community.

Thanks as well to the Fraunhofer Institute for Wind Energy Systems (IWES) for enabling me to work as a research associate at the institute and this way to gain valuable insight and experience in applied research works and the management of projects. The combination of the employment at Fraunhofer IWES and the participation in the REMS CDT program only made the research work conducted in this thesis possible, as I was able to utilize and further develop the in-house tools for modeling and simulation of wind turbine systems.

My final thanks go to my friend and family for always being there for me, for giving me the feeling that they are always with me even if I am often on the go, for their sincere interest in my work and studies, and also for their dear nudges to occasionally emerge from my thesis work.

Table of contents

Declaration of authenticity and author’s rights	ii
Statement on previously published work	iii
Abstract	iv
Acknowledgements	v
Table of contents	vi
List of figures	x
List of tables	xiii
List of symbols	xviii
List of abbreviations	xxiii
1 Introduction to the thesis	1
1.1 Potential of floating offshore wind technology	1
1.2 Challenges towards next generation floating offshore wind turbines	3
1.3 Aim and objectives	4
1.4 Thesis structure	5
1.5 Publications in connection with the research thesis	7
2 Review of reliability-based methods for risk analysis and their application in the offshore wind industry	9
2.1 Classification of reliability methods	10
2.1.1 Qualitative reliability methods	11
2.1.2 Semi-quantitative reliability methods	13
2.1.3 Quantitative reliability methods	14
2.2 Qualitative approaches for reliability analyses of offshore wind turbine systems	16
2.2.1 Failure mode analyses	16
2.2.2 Tree and graphical analyses	18
2.2.3 Hazard analyses	19

2.3	Quantitative approaches for reliability analyses of offshore wind turbine systems	19
2.3.1	Analytical methods	20
2.3.2	Stochastic methods	21
2.3.3	Bayesian inference	22
2.3.4	Reliability-based design optimization	23
2.3.5	Multivariate analyses	24
2.3.6	Data foundations	26
2.4	Discussion of reliability methods for offshore wind turbine systems	28
3	Floating offshore wind turbine systems	36
3.1	Critical review of floating support structures for offshore wind farm deployment	36
3.1.1	Review of FOWT support structures	37
3.1.2	Assessment of floating support structures	43
3.2	Reference spar-buoy floating wind turbine system	51
3.2.1	Wind turbine and tower	52
3.2.2	Floating structure and station-keeping system	53
4	Modeling, automated simulation, and optimization	56
4.1	Development and verification of an aero-hydro-servo-elastic coupled model of dynamics for FOWTs, based on MoWiT	57
4.1.1	Modeling of the OC3 phase IV FOWT system in MoWiT	59
4.1.2	Code-to-code comparison	67
4.1.3	Discussion of the code-to-code comparison results	79
4.2	Development of a framework for wind turbine design and optimization	89
4.2.1	Framework for automated simulation	91
4.2.2	Application for DLC simulations	97
4.2.3	Incorporation of optimization functionalities	99
4.2.4	Discussion of the broad application range of the framework to optimization tasks for wind turbine systems	107
5	Design optimization of floating wind turbine support structures	114
5.1	Design optimization of the OC3 phase IV spar-buoy floater, based on global limit states	115
5.1.1	Description of the system to optimize	116
5.1.2	Optimization problem of the global design optimization task	120
5.1.3	Optimization approach for the design optimization based on global limit states	122
5.1.4	Results of the design optimization based on global limit states	127
5.1.5	Discussion of the design optimization approach based on global limit states	138
5.2	Designing a complex geometry offshore wind turbine spar-type floating support structure	144

5.2.1	Advanced spar-type floating wind turbine support structures	146
5.2.2	Definition of the optimization problem for designing an advanced spar-type floater	153
5.2.3	Approach for automated design optimization of an advanced spar-type floater	156
5.2.4	Results of the automated design optimization of an advanced spar-type floater	161
5.2.5	Discussion of the results of the automated design optimization of an advanced spar-type floater	171
5.3	Brief digression and outlook: larger MW-class floater designs without upscaling? - a direct optimization approach	174
5.3.1	Target larger MW-class reference wind turbine	175
5.3.2	Methodology of the direct optimization approach	176
5.3.3	Design conditions for the direct optimization approach	178
5.3.4	Results of the direct optimization application	181
5.3.5	Discussion of the direct optimization approach	186
6	Reliability-based design optimization of a spar-type floating offshore wind turbine support structure	189
6.1	Definition of the RBDO problem	191
6.1.1	The design variables of the RBDO problem	191
6.1.2	The objective functions of the RBDO problem	192
6.1.3	The limit states of the RBDO problem	192
6.1.4	The design load case of the RBDO problem	194
6.1.5	The stochastic variables of the RBDO problem	196
6.1.6	The reliability criteria of the RBDO problem	198
6.1.7	The constraints of the RBDO problem	198
6.2	Numerical implementation of the RBDO problem	200
6.2.1	Pre-processing level one	201
6.2.2	Pre-processing level two	205
6.2.3	RBDO process	211
6.3	Results of the RBDO of the spar-type floating support structure	214
6.3.1	Progression within the iterative RBDO process	214
6.3.2	Selection of the optimized FOWT system design solution	217
6.3.3	Final checks with the optimized FOWT system design solution	219
6.4	Discussion of the RBDO approach applied to floating offshore wind turbine support structures	221
6.4.1	Full convergence of the RBDO	221
6.4.2	DDO and RBDO in comparison	221
6.4.3	Environmental conditions considered within the RBDO	221
6.4.4	Reliability criteria and analysis method within the RBDO approach	222

7 Discussion	224
8 Conclusions	230
8.1 Summary of the chapters	230
8.2 Thesis contributions to knowledge, research, and industry	235
8.3 Future work and outlook	242
8.3.1 Efforts to overcome limitations	242
8.3.2 Future applications of the research outcomes	243
8.4 Concluding remarks	244
Appendix A Additional dissemination activities	246
Appendix B Statistics of DLC 4.2	247
Appendix C Statistics of DLC 5.3	250
Appendix D Potential risks and consequences associated with global system performance criteria	254
Appendix E Pareto filtering	256
Appendix F Characteristics of a two-parameter Weibull distribution	257
Appendix G Characteristics of a three-parameter Weibull distribution	258
Appendix H Python function for closest value	260
References	261

List of figures

1.1	Flowchart of the thesis structure.	5
2.1	Venn diagram for the classification of the presented reliability methods.	11
2.2	Venn diagram for the presented qualitative reliability methods.	16
2.3	Venn diagram for the presented quantitative reliability methods.	20
3.1	Stability triangle for floating structures.	38
3.2	Three main floater categories.	38
3.3	TRL versus potential for wind farm deployment (TOPSIS score).	51
3.4	The OC3 phase IV spar-buoy FOWT system.	51
3.5	Schematic of the OC3 phase IV spar-buoy.	53
4.1	Aero-hydro-servo-elastic modeling approaches of the OC3 phase IV participants and IWES.	57
4.2	Hierarchical modeling structure of a FOWT system in MoWiT.	60
4.3	OC3 phase IV spar-buoy FOWT system modeled in MoWiT and visualized in Dymola [®]	61
4.4	Flowchart representing the structure of MoWiT with inputs and outputs.	62
4.5	Missing and provided parameters of the OC3 phase IV spar-buoy.	66
4.6	Full-system natural frequencies and damping ratios.	71
4.7	Free-decay time series from DLC 1.4a.	72
4.8	Free-decay time series from DLC 1.4c.	72
4.9	Free-decay time series from DLC 1.4e.	73
4.10	Free-decay time series from DLC 1.4f.	73
4.11	Hydro-elastic time series with regular waves from DLC 4.1.	74
4.12	Hydro-elastic power spectra with irregular waves from DLC 4.2.	75
4.13	Aero-hydro-servo-elastic time series with regular waves from DLC 5.1, part I.	76
4.14	Aero-hydro-servo-elastic time series with regular waves from DLC 5.1, part II.	77
4.15	Aero-hydro-servo-elastic power spectra with irregular waves from DLC 5.3, part I.	78
4.16	Aero-hydro-servo-elastic power spectra with irregular waves from DLC 5.3, part II.	79
4.17	Wave power spectra for DLC 4.2 in comparison.	83

4.18	Hydro-elastic power spectra with irregular waves from DLC 4.2, corrected for eliminating the deviations in the irregular wave spectrum.	84
4.19	Wave power spectra for DLC 5.3 in comparison.	85
4.20	Wind power spectra for DLC 5.3 in comparison.	86
4.21	Aero-hydro-servo-elastic power spectra with irregular waves from DLC 5.3, corrected for eliminating the deviations in the irregular wave and turbulent wind spectra, part I.	87
4.22	Aero-hydro-servo-elastic power spectra with irregular waves from DLC 5.3, corrected for eliminating the deviations in the irregular wave and turbulent wind spectra, part II.	88
4.23	Components of the framework for automated simulation and their relations. . .	92
4.24	Incorporation of optimization functionalities into the framework.	100
4.25	Automated optimization process, on the example of an evolutionary algorithm.	106
4.26	Results from the optimization procedure for the plausibility check test case. . .	108
4.27	Results from the optimizations for maximizing the power output or minimizing the thrust force.	110
5.1	Fixed/original and modifiable variables of the global design optimization task. .	118
5.2	Development of the 2,011 individuals throughout generation 0 up to generation 57 within the global design optimization.	131
5.3	Development of the individuals in the design space within the global design optimization.	134
5.4	Design shapes from the global design optimization in comparison.	135
5.5	Development of the individuals and Pareto optimal solutions in the design space within the global design optimization.	141
5.6	Pareto optimum design shape from the global design optimization.	142
5.7	Geometrical definitions of the advanced spar-type floating platform.	148
5.8	Development of the design variables throughout the iterative optimization process for designing an advanced spar-type floater.	162
5.9	Development of the constraints throughout the iterative optimization process for designing an advanced spar-type floater.	163
5.10	Exemplary potential advanced spar-type floater geometries selected from the individuals complying with all constraints.	164
5.11	Development of the objective function throughout the iterative optimization process for designing an advanced spar-type floater.	166
5.12	The optimized advanced spar-type floater geometry in comparison with the original shape.	168
5.13	Development of the individuals throughout the simulated generations in the direct optimization approach.	182
5.14	Spar-buoy geometry obtained from the direct optimization approach.	185

6.1	Flowchart of modular steps for realizing the RBDO problem.	200
6.2	Pre-processing level one flowchart for elaborating the approach and boundary conditions for the reliability assessment of one specific system.	201
6.3	Pre-processing level two flowchart for generating response surfaces in the optimization design space.	206
6.4	Eight closest neighbors of design χ in the optimization design space.	208
6.5	Flowchart of the RBDO approach, including its components and their interaction.	212
6.6	Development of the design variables throughout the iterative RBDO approach. .	214
6.7	Development of the performance constraints throughout the iterative RBDO approach.	215
6.8	Development of the reliability constraints throughout the iterative RBDO approach.	215
6.9	Development of the constraints on the maximum stresses throughout the iterative RBDO approach.	216
6.10	Development of the objective functions throughout the iterative RBDO approach.	216
6.11	Original, RBDO-, and DDO-based optimized design shapes in comparison. . .	218

List of tables

2.1	Wind turbine databases.	26
2.2	Applicability of presented qualitative reliability methods, in summary.	30
2.3	Applicability of presented quantitative reliability methods, in summary.	32
3.1	Representative natural frequencies of the three main floater types.	39
3.2	SWOT analysis of the spar floater concept.	44
3.3	SWOT analysis of the semi-submersible floater concept.	45
3.4	SWOT analysis of the TLP floater concept.	46
3.5	Set of criteria.	47
3.6	Set of alternatives.	48
3.7	Decision matrix, weight vector, and TOPSIS scores and positions, based on survey results.	49
3.8	Standard deviations among survey participants for decision matrix and weight vector.	49
3.9	Properties of the wind turbine RNA of the FOWT system from OC3 phase IV.	52
3.10	Properties of the tower of the FOWT system from OC3 phase IV.	52
3.11	Geometrical parameters of the OC3 phase IV spar-buoy.	54
3.12	Mass-related properties of the OC3 phase IV spar-buoy.	54
3.13	Properties of the station-keeping system of the FOWT system from OC3 phase IV.	55
4.1	Mass-related properties of the FOWT system from OC3 phase IV, MoWiT model results in comparison with the prescribed values.	63
4.2	Assumed values of the undefined spar-buoy and system parameters.	66
4.3	Simulation settings and analysis methods for DLC group 1.x.	68
4.4	Simulation settings and analysis methods for DLC group 4.x.	69
4.5	Simulation settings and analysis methods for DLC group 5.x.	70
4.6	Natural frequencies from OC3 phase IV codes and MoWiT in comparison.	80
4.7	Damping ratios from OC3 phase IV codes and MoWiT in comparison.	81
4.8	Static equilibrium positions from OC3 phase IV codes and MoWiT in comparison.	81
4.9	Overview of different optimizers.	103

5.1	Allowable value ranges of the design variables of the global design optimization task.	117
5.2	Global limit state criteria for the FOWT system performance.	119
5.3	Declaration of the three design variables of the global design optimization task.	121
5.4	Declaration of the three objective functions of the global design optimization task.	121
5.5	Declaration of the ten inequality constraints of the global design optimization task.	122
5.6	Optimizers considered for the global design optimization task in comparison.	125
5.7	Environmental conditions and simulation settings for the pre-selected DLCs.	127
5.8	The five most critical DLCs for each optimization criterion and the constrained mean translational motion.	130
5.9	Design variables of the optimum design of the global design optimization task.	136
5.10	Optimization criteria of the optimum design of the global design optimization task.	136
5.11	Values of the optimization objectives and constrained parameters for the utilized and the most critical DLCs.	138
5.12	Comparison of the centers of buoyancy and mass of the original and optimum FOWT systems.	140
5.13	Design variables of the Pareto optimum design of the global design optimization task.	143
5.14	Optimization criteria of the Pareto optimum design of the global design optimization task.	143
5.15	Allowable value ranges addressing the draft limits for the advanced spar-type floater.	151
5.16	Declaration of the seven design variables of the optimization problem for designing an advanced spar-type floater.	154
5.17	Declaration of the objective function of the optimization problem for designing an advanced spar-type floater.	154
5.18	Definition of the 25 inequality constraints of the optimization problem for designing an advanced spar-type floater.	155
5.19	The highest values for the three performance parameters and corresponding DLC simulation cases, based on the modified reference advanced spar-type floating system.	158
5.20	Simulation settings of the optimization algorithm for designing an advanced spar-type floater.	160
5.21	Key figures of the exemplary potential advanced spar-type floater geometries.	165
5.22	Key figures of the optimized advanced spar-type floater.	168
5.23	The highest values for the three performance parameters and corresponding DLC simulation cases, based on the optimized advanced spar-type floating system.	170

5.24	Properties of the IWT-7.5-164 reference wind turbine RNA.	176
5.25	Properties of the IWT-7.5-164 reference wind turbine support structure.	176
5.26	Properties of the IWT-7.5-164 reference wind turbine drivetrain and blade-pitch controller.	177
5.27	Required initial adaptations of the OC3 phase IV spar-buoy floater model with the IWT-7.5-164 on top.	178
5.28	Design variables and allowable value ranges for the direct optimization application.	179
5.29	Objectives for the direct optimization application, including target values and constraints.	180
5.30	Design variables of the final design obtained from the direct optimization approach.	185
5.31	Comparison of the results for the two generation selection methods for determining the optimum spar-buoy floater geometry resulting from the direct optimization approach.	186
5.32	Performance of the spar-buoy FOWT system design obtained with the direct optimization approach.	186
6.1	Declaration of the three design variables and their allowable value ranges of the RBDO problem.	191
6.2	Declaration of the three objective functions of the RBDO problem.	192
6.3	Criticality of specific DLC settings for evaluated system parameters of the RBDO problem.	195
6.4	Statistical coefficients of the stochastic variable wind speed.	197
6.5	Statistical coefficients of the stochastic variable significant wave height.	198
6.6	Declaration of the 18 inequality constraints of the RBDO problem.	199
6.7	Sample points of the stochastic variable wind speed.	202
6.8	Sample points of the stochastic variable significant wave height.	203
6.9	Comparison of the limit values and the maximum LS parameter values obtained from the 36 stochastic simulations.	205
6.10	Discrete values of the design variables for the selected floater geometries in the optimization design space.	206
6.11	Control design geometries for verifying the accuracy of the interpolation approach.	210
6.12	Key figures of the selected RBDO-based optimized design solution.	219
8.1	Contribution of the successfully realized objectives to knowledge, assessed with respect to novelty, scientific soundness, and value.	237
B.1	Wave elevation statistics from DLC 4.2 from OC3 phase IV codes and MoWiT in comparison.	247

B.2	Platform surge motion statistics from DLC 4.2 from OC3 phase IV codes and MoWiT in comparison.	247
B.3	Platform heave motion statistics from DLC 4.2 from OC3 phase IV codes and MoWiT in comparison.	248
B.4	Platform pitch motion statistics from DLC 4.2 from OC3 phase IV codes and MoWiT in comparison.	248
B.5	Tower-top fore-aft shear force statistics from DLC 4.2 from OC3 phase IV codes and MoWiT in comparison.	248
B.6	Tower-top fore-aft bending moment statistics from DLC 4.2 from OC3 phase IV codes and MoWiT in comparison.	248
B.7	Downstream fairlead tension statistics from DLC 4.2 from OC3 phase IV codes and MoWiT in comparison.	249
C.1	Wave elevation statistics from DLC 5.3 from OC3 phase IV codes and MoWiT in comparison.	250
C.2	Wind speed statistics from DLC 5.3 from OC3 phase IV codes and MoWiT in comparison.	250
C.3	Platform surge motion statistics from DLC 5.3 from OC3 phase IV codes and MoWiT in comparison.	251
C.4	Platform heave motion statistics from DLC 5.3 from OC3 phase IV codes and MoWiT in comparison.	251
C.5	Platform pitch motion statistics from DLC 5.3 from OC3 phase IV codes and MoWiT in comparison.	251
C.6	Platform yaw motion statistics from DLC 5.3 from OC3 phase IV codes and MoWiT in comparison.	251
C.7	Tower-top fore-aft shear force statistics from DLC 5.3 from OC3 phase IV codes and MoWiT in comparison.	252
C.8	Tower-top fore-aft bending moment statistics from DLC 5.3 from OC3 phase IV codes and MoWiT in comparison.	252
C.9	Downstream fairlead tension statistics from DLC 5.3 from OC3 phase IV codes and MoWiT in comparison.	252
C.10	Upstream fairlead tension statistics from DLC 5.3 from OC3 phase IV codes and MoWiT in comparison.	252
C.11	Generator power statistics from DLC 5.3 from OC3 phase IV codes and MoWiT in comparison.	253
C.12	Rotor speed statistics from DLC 5.3 from OC3 phase IV codes and MoWiT in comparison.	253
C.13	Out-of-plane blade-tip deflection statistics from DLC 5.3 from OC3 phase IV codes and MoWiT in comparison.	253

D.1 Potential risks and consequences associated with global system performance
criteria. 254

List of symbols

Latin symbols

A	[–]	Matrix of regression coefficients
A_{β_i}	[–]	Vector of regression coefficients of neighboring point i
A_{χ}	[–]	Vector of regression coefficients of design χ
a	[*]	Location parameter of three-parameter Weibull distribution
$a_{\text{hor,nacelle}}$	[m/s ²]	Horizontal nacelle acceleration
a_i	[–]	Regression coefficient
b	[*]	Scale factor of two- or three-parameter Weibull distribution
C	[kg(m/s) ²]	System stiffness (unit referring to rotational degree of freedom)
c	[–]	Shape factor of two- or three-parameter Weibull distribution
<i>criterion</i>	[*]	Parameter to be optimized
D_{BC}	[m]	Diameter of base column
$D_{\text{BC,low}}$	[m]	Diameter of base column lower part
$D_{\text{BC,mid}}$	[m]	Diameter of base column middle part
$D_{\text{BC,up}}$	[m]	Diameter of base column upper part
$D_{\text{gen,rotor}}$	[m]	Diameter of generator rotor
D_i	[m]	Diameter of component i
$D_{\text{ML}i}$	[m]	Diameter of mooring line i
D_{TB}	[m]	Diameter of tower base
D_{TP}	[m]	Diameter of tapered part
D_{UC}	[m]	Diameter of upper column

D_{WP}	[m]	Diameter of spar-buoy at waterplane
$d_{BC,b}$	[m]	Distance to base of base column (wrt SWL)
$d_{BC,t}$	[m]	Distance to top of base column (wrt SWL)
$d_{UC,b}$	[m]	Distance to base of upper column (wrt SWL)
$d_{UC,t}$	[m]	Distance to top of upper column (wrt SWL)
E	[*]	Error matrix
$F(*)$	[—]	Cumulative density function
F_{MLi}	[N]	Tension in mooring line i
$F_{SSS}(*)$	[—]	Cumulative density function for severe sea state extreme event
$f(*)$	[*]	Probability density function
f_i	[*]	Objective function
f_{nat}	[Hz]	Natural frequency
$f_{SSS}(*)$	[*]	Probability density function for severe sea state extreme event
G	[—]	Generation number
g	[m/s ²]	Gravitational acceleration
g_i	[*]	Inequality constraint
$goal$	[*]	Target value for parameter to be optimized
H	[m]	Wave height
$H_{ballast}$	[m]	Height of ballast within base column
$H_{ballast,required}$	[m]	Height of ballast within base column, required based on the ballast density selected from the optimizer
H_{BC}	[m]	Height of base column
$H_{BC,low}$	[m]	Height of base column lower part
$H_{BC,mid}$	[m]	Height of base column middle part
$H_{BC,up}$	[m]	Height of base column upper part
H_i	[m]	Height of component i
H_s	[m]	Significant wave height
h_i	[*]	Equality constraint
$I_{drivetrain}$	[kg m ²]	Inertia of drivetrain
I_{ref}	[—]	Reference value of the turbulence intensity
j	[—]	Number of failure events

K_I	[-]	Integral controller gain
K_P	[s]	Proportional controller gain
k	[-]	Number of design variables
l	[-]	Number of objective functions
M	[Nm]	Overturning moment
M_{TB}	[Nm]	Bending moment at tower base
m	[-]	Number of equality constraints
m_B	[kg]	Buoyant mass
$m_{gen,rotor}$	[kg]	Mass of generator rotor
$m_{platform}$	[kg]	Platform structural mass
m_{system}	[kg]	Mass of entire floating offshore wind turbine system
N	[-]	Number of extreme events fitting theoretically in one year
n	[-]	Number of inequality constraints
P	[W]	Aerodynamic power
P_i	[-]	Neighboring point i
p	[-]	Percentile
$power_i$	[W]	Rotor power output at iteration i
$power_{orig}$	[W]	Original rotor power output
R^2	[-]	Coefficient of determination
r	[-]	Number of random samples
$s_{dyn,transl}$	[m]	Dynamic translational motion
$s_{mean,transl}$	[m]	Mean translational motion
$system$	[-]	Fully-coupled floating offshore wind turbine system
T	[s]	Wave period
T_p	[s]	Peak period
t	[m]	Wall thickness
t_{BC}	[m]	Wall thickness of base column
t_{cap}	[m]	Cap thickness
t_{TB}	[m]	Wall thickness of tower base
t_{UC}	[m]	Wall thickness of upper column
$thrust_i$	[N]	Rotor thrust force at iteration i
$thrust_{orig}$	[N]	Original rotor thrust force

U_W	[m/s]	Wind-generated current velocity
V	[m/s]	Wind speed
V_{hub}	[m/s]	Wind speed at hub height
w_{P_i}	[–]	Weight for neighboring point i
$weight$	[–]	Weight factor
$weight_{\text{power}}$	[–]	Weight factor for rotor power output objective
$weight_{\text{thrust}}$	[–]	Weight factor for rotor thrust force objective
X	[*]	Design variable vector
x	[m]	Coordinate and position in direction of surge
x_i	[*]	Optimization (or so-called design) variable
\vec{x}_i	[*]	Vector with discrete values of design variable i
$x_{i,\text{left}}$	[*]	Discrete design variable value of left neighbor (smaller compared to the design variable value of design χ)
$x_{i,\text{right}}$	[*]	Discrete design variable value of right neighbor (larger compared to the design variable value of design χ)
$x_{i,\chi}$	[*]	Design variable value of design χ
Y	[*]	Matrix of dependent variables
y	[m]	Coordinate and position in direction of sway
Z	[*]	Matrix of independent variables
z	[m]	Coordinate and position in direction of heave
z_{CoB}	[m]	Vertical position of center of buoyancy
z_{CoG}	[m]	Vertical position of center of gravity

Greek symbols

β	[–]	Reliability index
$\Gamma(*)$	[–]	Gamma function
γ	[–]	Peak shape parameter
Δ_i	[*]	Spacing between discrete values of design variable i
ζ	[–]	Damping ratio
ζ_c	[–]	Damping ratio of the response associated with the equation of motion for the rotor-speed error
θ	[rad]	Rotor-collective blade-pitch angle
ι_{tot}	[deg]	Total inclination angle
κ_i	[–]	Number of discrete values of design variable i
λ_i	[–]	Position factor for design variable i
$\mu(*)$	[*]	Mean value
$\mu_{SSS}(*)$	[*]	Mean value for severe sea state extreme event
$\rho_{ballast}$	[kg/m ³]	Density of ballast material
$\rho_{ballast,selected}$	[kg/m ³]	Density of ballast material, selected from the optimizer
$\rho_{platform}$	[kg/m ³]	Density of platform material
ρ_{water}	[kg/m ³]	Density of water
$\sigma(*)$	[*]	Standard deviation
σ_{MLi}	[N/m ²]	Tensional stress in mooring line i
$\sigma_{SSS}(*)$	[*]	Standard deviation for severe sea state extreme event
σ_{TB}	[N/m ²]	Bending stress at tower base
Φ	[–]	Normal cumulative density function
χ	[–]	Design in optimization design space
Ω_{rated}	[rpm]	Rated rotational speed of drivetrain shaft
$\omega_{c,nat}$	[rad/s]	Natural frequency of controller

List of abbreviations

ADAMS	Automatic Dynamic Analysis of Mechanical Systems
AEP	Annual Energy Production
AFT	Advanced Floating Turbine
AHP	Analytic Hierarchy Process
ALARP	As Low As Reasonably Practicable
ALPSO	Augmented Lagrangian Particle Swarm Optimization
ANP	Analytic Network Process
ATF	Artificial Transfer Function
BBN	Bayesian Belief Network
BC	Base Column
BC _{low}	Base Column lower part
BC _{mid}	Base Column middle part
BC _{up}	Base Column upper part
BEM	Blade Element Momentum
BFGS	Broyden-Fletcher-Goldfarb-Shanno
BS	British Standard
BTA	Bow-Tie Analysis
BTD	Bow-Tie Diagram
C	Construction stage
CapEx	Capital Expenditure
CDF	Cumulative Density Function
CMAES	Covariance Matrix Adaptation Evolution Strategy
COBYLA	Constrained Optimization BY Linear Approximation
CONMIN	CONstrained function MINimization
CPN	Cost Priority Number
Cvode	C-language variable-coefficients ordinary differential equation
D	Design stage
DDO	Deterministic Design Optimization
DLC	Design Load Case
DLL	Dynamic Link Library
DNV	Det Norske Veritas
DNV GL	Det Norske Veritas and Germanischer Lloyd

DOF	Degree Of Freedom
DS	Dynamic Stall
DTU	Technical University of Denmark
Dymola®	Dynamic modeling laboratory
EA	Evolutionary Algorithm
ELECTRE	ELimination Et Choix Traduisant la REalité
EpsMOEA	Steady-state Epsilon Multi-Objective Evolutionary Algorithm
ETA	Event Tree Analysis
ETD	Event Tree Diagram
FAST	Fatigue, Aerodynamics, Structures, and Turbulence
FEM	Finite-Element Method
FEMP	Finite-Element Method for mode Pre-processing
FM	Failure Mode
FMEA	Failure Mode and Effects Analysis
FMECA	Failure Mode Effects and Criticality Analysis
FMMA	Failure Mode and Maintenance Analysis
FORM	First Order Reliability Method
FOWT	Floating Offshore Wind Turbine
FSQP	Feasible Sequential Quadratic Programming
FST	Fuzzy Set Theory
FTA	Fault Tree Analysis
FTD	Fault Tree Diagram
GA	Genetic Algorithm
GDE3	Generalized Differential Evolution 3
GDW	Generalized Dynamic Wake
HAWC2	Horizontal Axis Wind turbine simulation Code 2nd generation
HAZID	HAZard IDentification
HAZOP	HAZard and OPerability
HL	Hasofer and Lind
HL-RF	Hasofer Lind - Rackwitz Fiessler
IBEA	Indicator-Based Evolutionary Algorithm
IEA	International Energy Agency
IEC	International Electrotechnical Commission
IFE-UMB	Institute for Energy Technology at the University of Life Sciences
IPOPT	Interior Point OPTimizer
IS	Importance Sampling
ISM	Importance Sampling Method
ISO	International Organization for Standardization
ISRM	Importance Sampling Reduction Method
IWES	Institute for Wind Energy Systems
JONSWAP	JOint North Sea WAve Project

L-BFGS-B	Limited-memory Broyden-Fletcher-Goldfarb-Shanno with Box constraints
LC	Life Cycle planning stage
LCoE	Levelized Cost of Energy
LHS	Latin Hypercube Sampling
LS	Limit State
LSF	Limit State Function
LSM	Least Squares Method
M	Maintenance stage
MA	Markov Analysis
MADM	Multi-Attribute Decision Making
MARINTEK	Norwegian Marine Technology Research Institute
MBD	MultiBody-Dynamics
MCDA	Multi-Criteria Decision Analysis
MCF	MacCamy-Fuchs
MCS	Monte Carlo Simulation
ME	Morison Equation
ML1	Mooring Line 1, facing in positive x -direction parallel to the x -axis
ML2	Mooring Line 2, facing in negative x -direction and positive y -direction
ML3	Mooring Line 3, facing in negative x -direction and negative y -direction
MO	Multi-Objective
MOEA	Multi-Objective Evolutionary Algorithm
MOEAD	Multi-Objective Evolutionary Algorithm based on Decomposition
MoWiT	Modelica [®] library for Wind Turbines
MSD	Mass-Spring-Damping
MUFOW	Multiple Unit Floating Offshore Wind farm
NaN	Not a Number
Newton-CG	Newton Conjugate Gradient
NOMAD	Non-linear Optimization by Mesh Adaptive Direct search
NPI	Non-parametric Predictive Inference
NREL	National Renewable Energy Laboratory
NSGAI	Non-dominated Sorting Genetic Algorithm II
NSGAIII	Non-dominated Sorting Genetic Algorithm III
O	Operation stage
OC3	Offshore Code Comparison Collaboration
OC4	Offshore Code Comparison Collaboration Continuation
OMOPSO	Our Multi-Objective Particle Swarm Optimization
OpenMDAO	Open-source Multi-disciplinary Design, Analysis, and Optimization
OpEx	Operational Expenditure
OREDA	Offshore RELiability DATa
PDF	Probability Density Function
PDMP	Piecewise Deterministic Markov Process

PEAS	Parallel Evolutionary Algorithms
PESA2	Pareto Envelope-based Selection Algorithm
PF	Potential Flow
PNET	Probability Network Evaluation Technique
PoF	Probability of Failure
PROMETHEE	Preference Ranking Organization METHod for Enrichment Evaluation
PSO	Particle Swarm Optimization
PSQP	Preconditioned Sequential Quadratic Programming
PyGMO	Python parallel Global Multi-objective Optimizer
QSCE	Quasi-Static Catenary Equation
RA	Reliability Analysis
RAMS	Reliability, Availability, Maintainability, and Safety
RBD	Reliability Block Diagram
RBDO	Reliability-Based Design Optimization
RI	Reliability Index
RIF	Risk Influencing Factor
RIV	Reliability Index Vector
Rkfix4	Runge-Kutta fixed-step and 4th order method
RNA	Rotor-Nacelle Assembly
RPN	Risk Priority Number
RS	Response Surface
RSM	Response Surface Method
S	Wind Seed in design load case naming convention
SIMO	Simulation of Marine Operations
SKWID	Savonius Keel & WInd turbine Darrieus
SLSQP	Sequential Least Squares Quadratic Programming
SM	Interface to Simulink with MATLAB®
SMPSO	Speed-constrained Multi-objective Particle Swarm Optimization
SNOPT	Sparse Nonlinear OPTimizer
SORM	Second Order Reliability Method
SPEA2	Strength Pareto Evolutionary Algorithm 2
SQP	Sequential Quadratic Programming
SRSM	Stochastic Response Surface Method
SSS	Severe Sea State
SWIFT	Structured What-IF Technique
SWL	Still Water Level
SWOT	Strengths, Weaknesses, Opportunities, and Threats
TI	Turbulence Intensity
TLP	Tension Leg Platform
TNC	Truncated Newton
TOPSIS	Technique for Order Preference by Similarity to Ideal Solution

TP	Tapered Part
TRL	Technology Readiness Level
UC	Upper Column
UDFD	User-Defined Force-Displacement
UDS	User-Defined Subroutine
VAWT	Vertical Axis Wind Turbine
W	Wind speed in design load case naming convention
WPM	Weighted Product Method
WS	Wheeler Stretching
WSM	Weighted Sum Method
Y	Yaw misalignment angle in design load case naming convention

Chapter 1

Introduction to the thesis

With the end of 2018, the first renewable energy directive from 2009 (European Parliament & Council of the European Union 2009), which set the target of a minimum share of 20% of renewable energy in the European energy demand by 2020, was revised and replaced. The new European goals - now for 2030 - are to reach at least 32% share of renewable energy (European Parliament & Council of the European Union 2018). A large contributor to energy generation from renewable sources is offshore wind. Its worldwide technical potential exceeds the current electricity demand by a factor of more than 18 (IEA 2019).

Depending on the location, water depth, and seabed conditions, different offshore wind turbine systems are required: bottom-fixed solutions - such as monopiles, jackets, tripods, gravity-based structures, or suction buckets - are limited to shallow and intermediate water depths, while for deeper water sites, floating platforms - such as spar-buoys, semi-submersibles, or tension leg platforms - are required to support offshore wind turbines (Arapogianni et al. 2013). The current trend in the offshore wind industry is towards larger wind turbines of higher performance classes, larger distances of wind farms to the shore, and sites with deeper water depths, implying as well the growing interest in floating offshore wind turbine (FOWT) systems (WindEurope 2019*b*). Furthermore, shallow water zones and areas of intermediate water depth, such as the coastal offshore sites in German waters, are, however, an exception. The majority of the world oceans exhibits great water depths (James & Ros 2015, Mast et al. 2015, Govindji et al. 2014). Thus, to exploit these sites for energy generation from offshore wind turbines, floating systems need to be utilized.

1.1 Potential of floating offshore wind technology

With floating support structures for offshore wind turbines, more offshore wind resources can be captured and used for power generation, as around 60% to 80% of the ocean areas (James & Ros 2015, Mast et al. 2015, Govindji et al. 2014, Bossler 2014) cannot be exploited with bottom-fixed structures, which are limited to water depths of up to around 50 m (Arapogianni et al. 2013). The floating offshore wind technology is no longer in its infancy. Over the last decade, the technology readiness level of FOWT systems has significantly increased so that

“floating offshore wind is coming of age”, as WindEurope states in its floating offshore wind vision statement (WindEurope 2017, p.4). The large number of research studies, research projects, scaled model tests, prototype developments, and full scale model test phases paved the way towards this current status. Around 40 floating foundation concepts exist and are under development (Q FWE 2020, Power Technology 2019, James & Ros 2015, Mast et al. 2015). A few selected milestones are (Löfken 2019)

- the Hywind spar-buoy floating system, with a 2.3 MW demonstrator deployed in 2009, the subsequent Hywind Scotland pilot park of five 6 MW turbines operating since 2017, and another wind farm Hywind Tampen with eleven 8 MW turbines planned for 2022;
- the WindFloat semi-submersible floating system by Principle Power, with three 2 MW demonstrators since 2011 and twelve large projects planned for the upcoming years with turbines of up to 8.4 MW;
- the Damping Pool[®] (Floatgen) barge floating system by Ideol, with a 2 MW and a 3 MW demonstrator since 2018 and further large projects with, for example, 6.2 MW wind turbines planned for the future; and
- the TetraSpar spar, semi-submersible, or tension leg platform floating system by Stiesdal A/S, with a demonstrator supporting a 3.6 MW wind turbine planned for 2020.

Apart from the benefit of deploying high potential deep water sites for wind energy utilization and being no longer limited to water depths up to around 50 m when employing floating offshore wind technology, there are further advantages over bottom-fixed offshore wind turbine support structures. (Landbø 2017a, Arapogianni et al. 2013)

- As FOWT systems are moored to the seabed, the design of the support structure is less dependent upon the specific site conditions (soil characteristics and water depth), which can vary within a large offshore wind farm. Hence, one and the same floater design can be utilized for all turbines within a farm. Furthermore, when extending the application to different sites and resulting environmental conditions, as well as to other wind turbines, standardization of the floating support structure design is also possible.
- Significant cost reduction and process acceleration, compared to bottom-fixed offshore wind turbine systems, can be achieved with the floating technology for the installation. Most of the FOWT systems can be fully assembled in the port. This way, high costs for special heavy-lift vessels, required to mount the turbine offshore on a bottom-fixed support structure, can be cut and - in addition - the highly weather dependent installation lead time shortened. The tow out of the fully-assembled FOWT happens with common tug boats, which are again much cheaper than special installation vessels.
- This aspect regarding transport and installation method is not only favorable to time and cost, but also paves the way for the floating technology towards larger MW-class wind turbines, which - based on the current rapid development trend - will be soon no longer

practicable, both economically and feasibly, for offshore installation on bottom-fixed support structures.

1.2 Challenges towards next generation floating offshore wind turbines

Despite the great amount of FOWT projects, most of them are under development and currently the Hywind Scotland pilot park is the one and only operational floating wind farm (Power Technology 2019) - apart from the first prototype floating wind farm within the Fukushima Floating Offshore Wind Farm Demonstration Project FORWARD, in which three different FOWTs connected to the same floating substation were tested for a limited operating life (James & Ros 2015, Main(e) International Consulting LLC 2013). More floating wind projects are planned, as already mentioned in Section 1.1. However, the large diversity in existing floater concepts slows down the development and maturing processes of FOWTs and, for further speed-up of the market uptake of floating wind farms, significant cost-reductions are still required.

Thus, design optimization, focusing on cost reduction while ensuring optimum system performance and reliable operation, plays a key role in achieving the goal of gaining economic competitiveness to allow commercial market uptake. However, the development of such an optimized FOWT system is highly challenging.

- The complexity of FOWT systems, with their coupled motions, aero-hydro-servo-elastic dynamics, as well as non-linear system behavior and components (such as mooring lines), makes modeling and simulation indispensable. To ensure realistic representation of the real system behavior by means of engineering models, the correct implementation of the multi-physics into the codes has to be verified and validated.
- Dimensioning and detailed assessment of FOWTs imply iterative steps for design optimization, as well as load calculations and system performance analyses in various environmental conditions. To cope with the large number of simulations to be performed during the design process, automation of simulation executions and optimization procedures are required.
- Floating wind energy applications are governed by a number of uncertainties relevant to the design process and operational management of assets. Risk and reliability analysis methods can allow for systematic assessment of these uncertainties. Thus, integrating reliability analyses into design optimization procedures of FOWT systems is not only highly relevant for considering prevailing uncertainties, but also benefits the economic efficiency. Furthermore, reliability-based design optimization is a very promising approach in optimizing systems when classification and standardization are not yet fully available. However, the level of difficulty of design optimization already increases when including the reliability aspect, but becomes even more challenging when dealing with the highly complex system of FOWTs, which has not yet been applied.

Apart from these challenges towards reliable and cost-efficient FOWT systems, current trends in the offshore wind industry, as well as emerging technological innovations amplify the demands on and relevance of such automated system simulation and optimization approaches, in particular:

- the trend towards larger MW-class offshore wind turbines implies as well the need for bigger support structures. These are commonly derived from existing structures through upscaling and subsequent optimization. This, however, further increases the number of design steps and, hence, emphasizes the need for a holistic automated optimization approach, which is in addition highly flexible in terms of application and specific optimization problem.
- the design process of FOWT systems is not solely based on reliability- and cost-driven design optimization, but also has to take further related aspects - such as manufacturing, handling, transport, and installation - into account. Thus, recent technological innovations with respect to structural realization approaches, manufacturing limitations, or installation concepts have to be considered when specifying such a FOWT design optimization problem.

1.3 Aim and objectives

In this context and based on the potential (Section 1.1) of, but still prevailing challenges (Section 1.2) for the floating offshore wind technology, this research thesis aims to derive guidelines for reliability-based design optimization of FOWT support structures. It takes into account target safety levels and failure mechanisms from existing standards and applies them in such novel concepts.

To achieve this overall aim, the following research objectives are defined:

1. review and classify reliability methods applied in the offshore and marine renewable energy industry and derive from these methods suitable procedures and potential future approaches for reliability assessment applications to offshore wind turbine systems;
2. assess the large diversity of existing FOWT support structures with respect to their suitability for offshore wind farm deployment and future development trends;
3. develop a verified aero-hydro-servo-elastic coupled numerical model of dynamics for FOWTs, as well as a holistic framework for automated simulation and optimization of FOWT systems;
4. apply the developed model and framework to different design optimization tasks on a FOWT system;
5. develop a proven concept for coupling design optimization with reliability assessment of FOWT systems in a computationally and time-efficient manner.

1.4 Thesis structure

The single research objectives, defined in Section 1.3, form the research steps. Based on this, a general overview of the thesis structure is presented in Figure 1.1 and outlined in some more detail in the following.

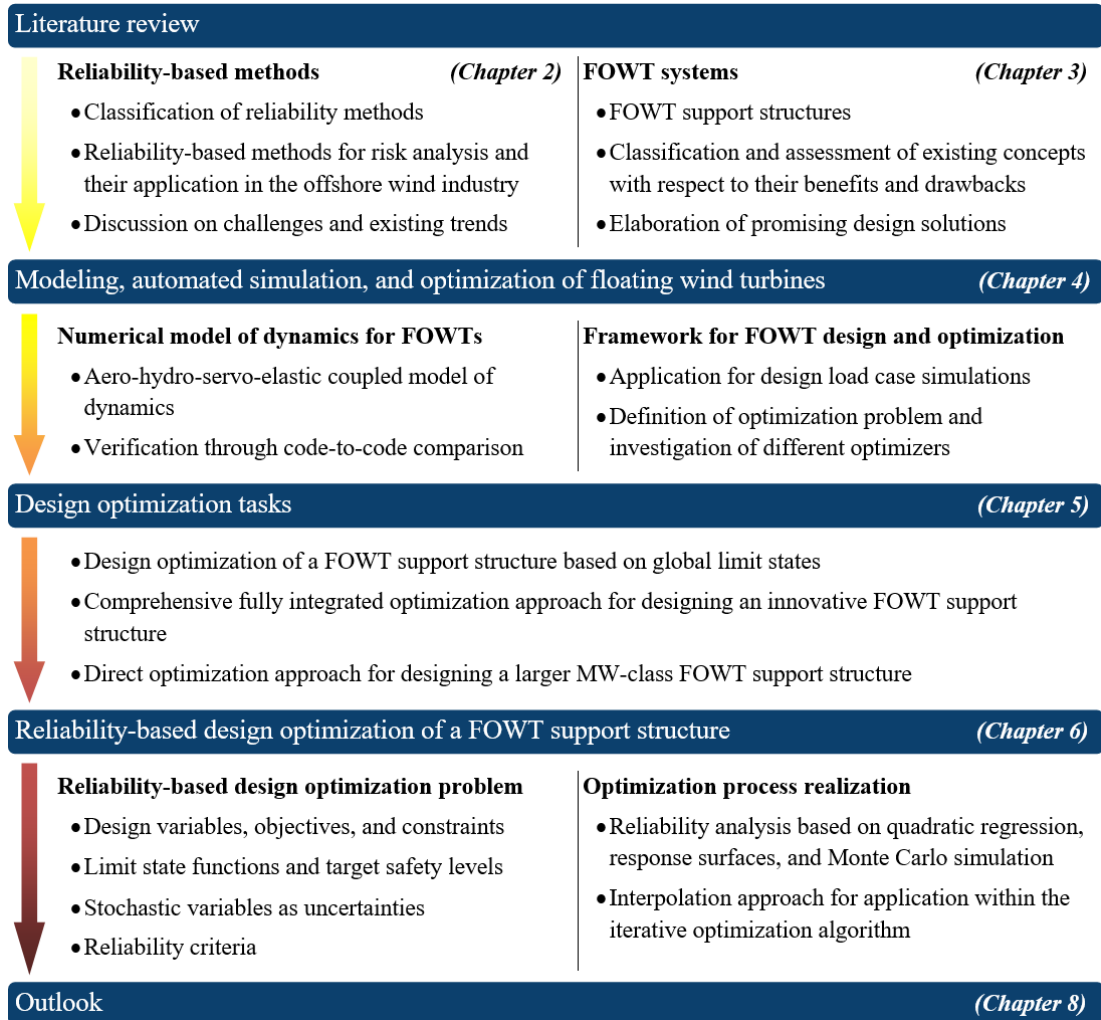


Figure 1.1: Flowchart of the thesis structure.

As the topic on reliability-based design optimization of FOWT support structures has two components, a two-tiered literature review is performed at the beginning of the research. Thus, in Chapter 2, first, risk and reliability methods applied in the offshore and marine renewable energy industry are reviewed and classified. The quite broad differentiation between qualitative and quantitative methods, as well as some which could belong to both groups depending on the way in which they are used, is further differentiated, based on the most common theories applied specifically within the offshore wind industry. Furthermore, the capabilities and limitations of these methods are investigated and current trends, as well as potential future techniques - further developed and advanced - are pointed out.

The second literature review is on FOWT systems. Hence, in Chapter 3, at first different floating support structures are classified and assessed with respect to their suitability for offshore wind farm deployment. For a meaningful valuation, a survey is conducted to examine the capacities of selected floater types, grouped into ten categories, with respect to ten specified criteria focusing on wind farm deployment. By this means, a multi-criteria decision analysis is carried out, using the technique for order preference by similarity to ideal solution. With the individual scores of the different systems, considering the weighting of each criterion, suitable concepts are identified and potential hybrid designs, combining advantages of different solutions, are suggested. Based on the outcomes of the survey and subsequent decision making, a reference spar-buoy floating wind turbine system is defined, which serves as basis for the consecutive research steps.

This reference FOWT system is used in Chapter 4 for developing a numerical model of dynamics, which uses the modeling language Modelica[®], represents the aero-hydro-servo-elastic couplings, and is highly flexible with respect to the modeled wind turbine system and conditions, as well as its application options. To ensure the correct implementation of the multi-physics, the developed engineering model is verified through code-to-code comparison. Having substantiated the capability of the developed model for fully-coupled aero-hydro-servo-elastic simulations of FOWT systems, the complex development process of engineering systems, implying advanced optimizations and iterative simulations, is further addressed. Thus, a holistic simulation and optimization framework is developed, by which means iterative simulations within the wind turbine design process and detailed assessment can be managed and executed in an automated and high-performance manner. The developed framework is very flexible and multifunctional. Its structure allows the use of highly sophisticated optimization tools, so that various optimization tasks, as well as multi-objective problems, can be addressed. However, in addition to optimizations, the developed framework can also be employed for automated execution of simulations, which is for example very useful for dealing with the large number of design load cases recommended by standards.

Based on the developed and verified FOWT system model and the framework for automated simulation and optimization, various design optimization tasks are addressed and performed in Chapter 5. These comprise

- an approach for optimizing a floating concept, utilizing global limit states. The reference FOWT support structure is modified during the optimization regarding its geometrical dimensions and ballasting. The optimization criteria stability, mean and dynamic displacements, as well as tower top acceleration are used for formulating the objective functions. The optimization is carried out for one design load case, which is most critical for the considered criteria, and utilizes a multi-objective genetic algorithm. In post-processing analyses, the convergence of the optimization is examined, the optimum design solution selected, and the overall performance of the optimized FOWT system approved. This approach deals as basis for more advanced design optimization tasks.

- an alternative, fully integrated optimization approach to find innovative floater designs. Three cylindrical sections with individual diameters and heights, as well as the ballast filling height are the modifiable design variables of the optimization problem. Constraints regarding the geometry, ballast, draft, and system performance are specified. The optimization objective to minimize the floater structural material shall represent the overall goal of cost reduction. Pre-processing system simulations are performed to select a critical design load case, which is used within the iterative optimization algorithm. The applied methodology enables to explore alternative structural realization approaches, which frees the design from previous stringent limitations on the structure and dimensions. This way, more innovative cost-efficient floater designs can be captured.
- a direct optimization approach, by which means a FOWT support structure for a larger wind turbine is obtained through an automated optimization procedure, based on a smaller existing system. Only a few initial adaptations in the model are required for taking the different wind turbine geometry and weight into account. Afterwards the larger support structure - appropriate to support the larger MW-class wind turbine and meet the specified optimization objectives of hydrodynamic system behavior - can be obtained through automated optimization of the existing reference design without the intermediate step of upscaling and, hence, with a reduced number of design steps.

Finally, in Chapter 6, an integrated framework for reliability-based design optimization of FOWTs is developed, which combines concepts of optimization with reliability-based design and advanced modeling and requires reasonable computational effort and time expenditure. In pre-processing, the reliability-based optimization problem - in detail the environmental conditions, limit states, and uncertainties, as well as design variables, objectives, constraints, and reliability criteria - are specified. The realization of the reliability-based optimization process happens through quadratic regression, response surface, and Monte Carlo simulation. Furthermore, several response surfaces for various system geometries in the optimization design space are generated ahead of the execution of the optimization process. These are finally used by means of an interpolation approach for the reliability calculation integrated in the iterative design optimization. The developed methodology proves the feasibility of coupling FOWT design optimization with reliability assessment in an efficient manner.

The presented research content, developed methodologies, applied approaches, and obtained results are recapitulatory discussed in Chapter 7.

Chapter 8, finally, summarizes the research work, elaborates on the contributions of the thesis to knowledge, research, as well as industry, addresses possible future work, and draws conclusions.

1.5 Publications in connection with the research thesis

Throughout the research, the following papers are submitted and already published or under review in scientific journals at the time of writing:

- Leimeister, M. & Kolios, A. (2018), ‘A review of reliability-based methods for risk analysis and their application in the offshore wind industry’, *Renewable and Sustainable Energy Reviews* **91**, 1065–1076. doi: <http://dx.doi.org/10.1016/j.rser.2018.04.004>.
- Leimeister, M., Kolios, A. & Collu, M. (2018), ‘Critical review of floating support structures for offshore wind farm deployment’, *Journal of Physics: Conference Series* **1104**, 012007. doi: <http://dx.doi.org/10.1088/1742-6596/1104/1/012007>.
- Leimeister, M., Kolios, A. & Collu, M. (2020a), ‘Development and verification of an aero-hydro-servo-elastic coupled model of dynamics for FOWT, based on the MoWiT library’, *Energies* **13**(8), 1974. doi: <http://dx.doi.org/10.3390/en13081974>.
- Leimeister, M. (2019), Python-Modelica framework for automated simulation and optimization, in ‘Proceedings of the 13th International Modelica Conference, Regensburg, Germany, March 4-6, 2019’, Linköping Electronic Conference Proceedings, Linköping University Electronic Press, Linköping, Sweden, pp. 51–58. doi: <http://dx.doi.org/10.3384/ecp1915751>.
- Leimeister, M., Kolios, A. & Collu, M. (2020b), ‘Development of a framework for wind turbine design and optimization’, *Energy Reports* (in review).
- Leimeister, M., Kolios, A., Collu, M. & Thomas, P. (2020), ‘Design optimization of the OC3 phase IV floating spar-buoy, based on global limit states’, *Ocean Engineering* **202**, 107186. doi: <http://dx.doi.org/10.1016/j.oceaneng.2020.107186>.
- Leimeister, M., Collu, M. & Kolios, A. (2020), ‘A fully integrated optimization framework for designing a complex geometry offshore wind turbine spar-type floating support structure’, *Wind Energy Science Discussions* (in review). doi: <http://dx.doi.org/10.5194/wes-2020-93>.
- Leimeister, M., Kolios, A., Collu, M. & Thomas, P. (2019), Larger MW-class floater designs without upscaling?: a direct optimization approach, in ‘Proceedings of the ASME 38th International Conference on Ocean, Offshore and Arctic Engineering, Glasgow, Scotland, UK, June 9-14, 2019’, American Society of Mechanical Engineers, New York, NY, USA, pp. OMAE2019-95210. doi: <http://dx.doi.org/10.1115/OMAE2019-95210>.
- Leimeister, M. & Kolios, A. (2020), ‘Reliability-based design optimization of a spar-type floating offshore wind turbine support structure’, *Reliability Engineering and System Safety* (in review).

At the beginning of each chapter, it is indicated in a footnote on which publications the chapter is based.

In addition to the paper publications in scientific journals, parts of the research work are presented at scientific conferences, listed in Appendix A.

Chapter 2

Review of reliability-based methods for risk analysis and their application in the offshore wind industry

Offshore wind turbines are exposed to severe environmental conditions. Occurring failures could have environmental impacts, but definitely would lead to considerable financial losses. This is not only due to the lost production output because of the failure, but is especially amplified by the limited accessibility of offshore assets, located some distance from the coast and sometimes even in quite remote areas. Transport of offshore engineers and work on the asset can only be performed in acceptably safe sea states and at medium wind speeds. These prescribed working weather windows sometimes imply quite long delays, until the asset can operate in normal mode again. This moves the point of focus towards risk management and reliability assessment of offshore wind turbines.

According to the British standard BS ISO 31000, risk is the “effect of uncertainty on objectives ... [and] is often expressed in terms of a combination of the consequences of an event (including changes in circumstances) and the associated likelihood ... of occurrence” (BSI 2010a, p. 1). The latter can be influenced by the level of reliability. Reliability itself is defined, based on BS 4778 (BSI 1991), as “the ability of a component or a system to perform its required function without failure during a specified time interval” (DNV GL 2015b, p. 13), but “can also be denoted as a probability or as a success ratio” (O’Connor et al. 2002, p. xxvi). Several different techniques for obtaining qualitative or quantitative measures of reliability exist; however, not every method is suitable to be applied to the assessment of offshore energy systems. Some may be more useful than others, and some have to be adjusted or combined to obtain valuable results.

In this chapter reliability methods used in the offshore and marine renewable energy industry are classified and analyzed with respect to their applicability to offshore wind turbine

Note: This chapter is based on the publication by Leimeister & Kolios (2018).

systems, their benefits and limitations, as well as the elaboration of existing trends and further approaches required to overcome those limits still remaining. The chapter is structured in such a way that first a classification of common reliability methods is given in Section 2.1. After this general overview, qualitative and quantitative reliability assessment procedures, specifically applied within the offshore wind and marine renewable energy industry, are presented and categorized (Sections 2.2 and 2.3). This is based on a systematic literature review, which primarily uses the specific words “reliability” and “offshore”, focuses on the latest research work done, preferably from 2010 onwards, and aims to concentrate on offshore wind turbines; however, some examples of other offshore industries and structures are also included due to the still low information density on offshore renewable energy devices. In total, more than 100 papers are reviewed and further information is taken from recent conferences, as well as industrial experiences. Section 2.4 points out how offshore wind turbine systems challenge common reliability assessment methods, in which way and how far the presented techniques are already able to cope with this, as well as which limits are still existing and which theories will potentially develop further.

2.1 Classification of reliability methods

Reliability analyses (RAs) can be performed for different systems and components, such as mechanical, electronic, or software, as well as at various stages of the engineering process, for example design or manufacture (O’Connor et al. 2002). Due to the broad application of reliability, attempts at categorization are being made. Stapelberg (2009) for example focuses on reliability in engineering design and distinguishes between reliability prediction, assessment, and evaluation, depending on the design stage conceptual, preliminary/schematic, or detailed, respectively. Furthermore, two different levels at which reliability can be applied are defined: component and system level. These already introduce the bottom-up and top-down approaches, which can be found in some reliability methods as well.

Considering the different reliability methods themselves, there are two main categories into which they can be grouped: qualitative methods and quantitative methods, depending on the availability and quality of data (Stapelberg 2009). However, a comparison of different literature, such as the books by O’Connor et al. (2002) or Rausand & Høyland (2004), shows some discrepancies in the assignment of certain reliability methods and indicates the need for a third intermediate category for such semi-quantitative reliability methods. The methods covered in the following, as well as the chosen categorization, are visualized in the form of a Venn diagram, presented in Figure 2.1. The abbreviations used are explained in the following sections.

Furthermore, it has to be noted that some of the presented methods are rather risk assessment tools than reliability methods. However, these risk assessment techniques are still included, as the awareness of the existing risks is the decisive basis for RAs. In the following, it is just stated whether the tool is strictly speaking used for risk or reliability. A detailed list of risk assessment methods can be found in BS EN 31010 (BSI 2010*b*).

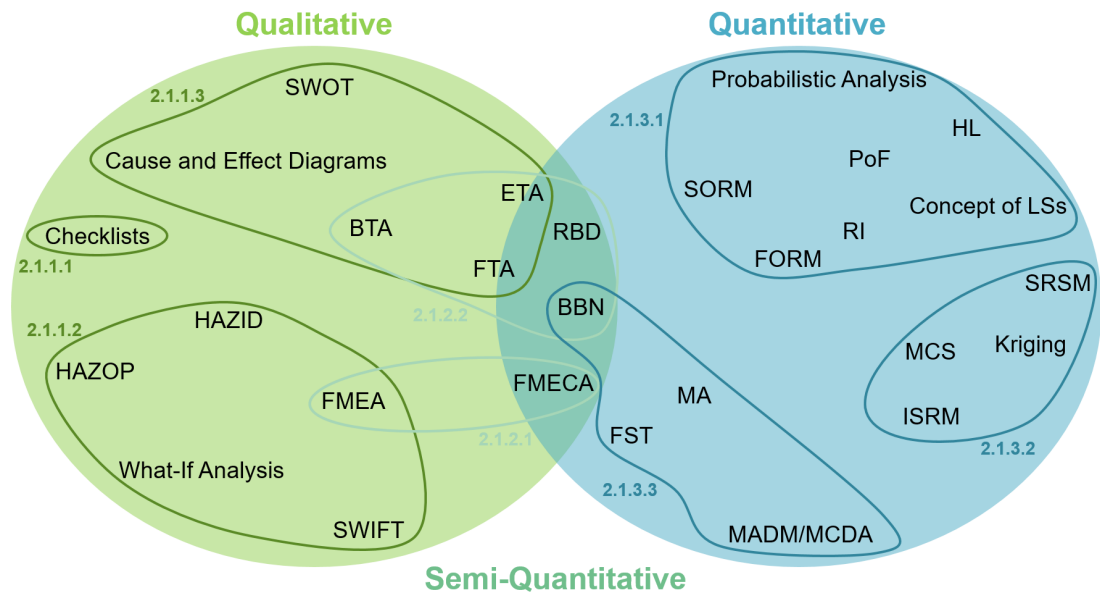


Figure 2.1: Venn diagram for the classification of the presented reliability methods.

2.1.1 Qualitative reliability methods

Missing or insufficient data does not allow for quantitative assessment of reliability. Nevertheless, relations within the system, covering hazards, failure causes, events, failure modes, faults, effects, and consequences, can be shown and this way an estimate of reliability, failure probability, and consequence can still be obtained by using qualitative methods.

Before performing any qualitative RA, first the system structure and functions have to be identified and classified (Rausand & Høyland 2004). On this basis, a qualitative reliability assessment can be carried out. Some of the most common methods are briefly explained in the following, grouped into sheet-based (Section 2.1.1.1), table-based (Section 2.1.1.2), and diagrammatic (Section 2.1.1.3) techniques.

2.1.1.1 Sheet-based qualitative reliability methods

Typical sheet-based qualitative methods are checklists; they are used to assist engineers (Rausand & Høyland 2004) in determining and examining influencing factors and, thus, identifying risks for design operation, maintainability, reliability, safety, and availability. Thus, for each stage there are different question sets, on which basis the contributing parameters can be studied. (Stapelberg 2009)

2.1.1.2 Table-based qualitative reliability methods

The table-based qualitative methods focus either on hazards or failure modes (FMs).

The aim of hazard identification (HAZID) analysis is to determine potential hazards, as well as their causes and consequences. This risk identification method should be applied as early as possible, so that changes and adaptations, which may avoid the hazard or at least reduce

the effects to the system, can be integrated in the early system design. A typical HAZID worksheet starts by naming the investigated component or area, followed by the potential incident. Then, the potential causes and consequences are determined and the severity of the latter is categorized. Finally, recommendations for corrections or precautions are given. (Stapelberg 2009)

A hazard and operability (HAZOP) study, another risk assessment tool, is also used for the identification of hazards, their potential causes and effects; however, this analysis rather focuses on deviations from the normal operation mode as initiating event. Special guide words, such as NO or NOT, MORE, LESS, LATE, or BEFORE, are used for describing these deviations. The HAZOP procedure itself could either start with the guide word or the considered element. A HAZOP worksheet contains, besides the guide word and element, the explicit meaning of the deviation, the potential causes and consequences, already existing safeguards, as well as recommended necessary actions and further comments. (BSI 2001)

More adaptable tools for identifying risks are the what-if analysis or structured what-if technique (SWIFT). The SWIFT starts with collecting potential hazards and uses in addition a checklist, containing typical errors and failures that could also make up hazards. The hazards are then organized in a worksheet, comprising the hazard itself, mentioned in the column headed *What-if?*, its potential causes and effects, as well as presenting safeguards and giving recommendations, similarly to HAZID and HAZOP. (DNV 2002)

Not only focusing on hazards, the failure mode and effects analysis (FMEA) aims to identify FMs in the system function or equipment, their potential impacts and causes, as well as determining existing controls and precautions. Thus, while being originally a risk assessment tool, FMEA can also be used for RA. Three different types of FMEA exist: concept/functional FMEA, design/interface FMEA, and detailed/updated FMEA, implying that FMEA can be used throughout the entire life cycle of an asset. (Rausand & Høyland 2004)

2.1.1.3 Diagrammatic qualitative reliability methods

Qualitative reliability methods in the form of a diagram can be structured from the top down or the bottom up. Such a top-down approach is used in the cause and effect diagram, which is also called the fish-bone diagram due to its shape. The top event, a failure or incident, makes up the head of the fish on the right side. Different cause categories, containing several specific factors, are then added in form of fish-bones to the diagram, allowing a structured risk assessment. (Rausand & Høyland 2004)

The same deductive (top-down) approach is used in the fault tree analysis (FTA), strictly speaking a risk assessment tool, which is visualized in a fault tree diagram (FTD). The tip of the tree is the incident or failure which is then broken down into immediate, intermediate, and basic causes. The relationship between causes and the top event are represented by logical gates, such as AND and OR. (Rausand & Høyland 2004)

An event tree analysis (ETA), also a risk assessment technique, is performed in the opposite direction, meaning from the bottom up. Such an inductive approach uses the incident or failure

as the starting point for identifying all potential event sequences which may result from the initial event. The different levels in the corresponding event tree diagram (ETD) can directly represent safeguards and the two branches of that part of the tree are the options for the success or failure of this safety barrier. (Stapelberg 2009)

A combination of risk assessment methods FTA and ETA is given in the bow-tie analysis (BTA). The corresponding bow-tie diagram (BTD) has the failure or incident in the middle, which is then broken down to the left into its causes, representing the FTA, and to the right into its consequences, such as in the ETA. In both directions safety barriers can be included, safeguards for control and precaution in the FTA part, and safety functions for mitigation in the ETA part. (McLeod 2015)

Besides those linear diagrammatic methods, the strengths, weaknesses, opportunities, and threats (SWOT) technique analyses influence factors and identifies risks in two dimensions. Based on the shape of a compass rose or four-quadrant format, the internal factors i.e. strengths and weaknesses are in the north, while the external factors i.e. opportunities and threats are in the south. In the east-west direction, the factors are distributed such that the positive factors lie in the west and the negative ones in the east. (Pritchard 2015)

2.1.2 Semi-quantitative reliability methods

Some of the qualitative reliability methods can be extended with some quantitative approximate measures and thus also be used for quantitative reliability assessment. These tools can again be grouped into table-based (Section 2.1.2.1) and diagrammatic (Section 2.1.2.2) methods, as presented in the following.

2.1.2.1 Table-based semi-quantitative reliability methods

In Section 2.1.1.2, FMEA is already introduced as a qualitative risk assessment methods, which however can also be used for RA. If this is combined with a criticality analysis, a semi-quantitative reliability method, the so-called failure mode effects and criticality analysis (FMECA), is obtained. The additional parameters are three rating values: for the severity of the effects, the occurrence of the FM, and the detectability of the failure cause. Different tables with recommendations for rating these parameters and assigning a ranking number to them do exist but can also be defined individually. Having determined the severity, occurrence, and detection ratings, the risk priority number (RPN) is computed as a product of these three rating values. This can finally be used to rank the criticality of risks and FMs. As for the FMEA, the worksheet for the FMECA can also either be focused on the component/equipment or on the requirement/function. Furthermore, it is possible to distinguish between product and process FMEA, depending on the items or system under consideration (Rausand & Høyland 2004). (BSI 2006)

2.1.2.2 Diagrammatic semi-quantitative reliability methods

The tree-shaped risk assessment techniques FTA, ETA, and BTA, mentioned in Section 2.1.1.3, can also be used for a quantitative assessment of reliability if probability values are added to the branches. These numbers indicate the occurrence probability of a causal event, in the case of a FTA, and the conditional probability of a safety function being functional or not, in an ETA, respectively. Multiplication of all probability values along one cause or consequence path yields the total probability of this happening. This calculation can be performed in measures for either failure or success; the latter directly represents the reliability value, while in the first case the reliability has to be computed as complementary to the failure probability. (Rausand & Høyland 2004)

Comparable to FTDs and cause and effect diagrams, however, more general are the Bayesian belief networks (BBNs). Similar to the FTA, a BBN uses the top-down approach, starting with the initiating event and breaking this down into different causes or cause categories. Arrows indicate the relationships between the undesired event and the causes, which could result in a quite complex network (Rausand & Høyland 2004). By assigning probabilities to the contributing factors, BBNs can not only be used for risk identification, but also for quantitative reliability assessment. With the help of the Bayes theorem, existing data can be inter- or extrapolated, but also newly available information can be incorporated in the BBN and the reliability estimation updated (Stapelberg 2009).

An alternative way of presenting an FTD or ETD is a reliability block diagram (RBD), which is - as the name already suggests - a reliability assessment tool. The different components are more or less aligned on one common line with the input on the left end and the output on the right end. This way, systems with a flow can also be represented very well. Instead of the AND and OR gates, used in FTDs and ETDs, parallel and series connections are incorporated in the RBD to describe the relationships of the single components, as well as to represent dependencies. If the probabilities of each event or system function, illustrated by the blocks in the diagram, are known, the system reliability can be computed based on the algebraic rules for parallel and series systems. (Stapelberg 2009)

2.1.3 Quantitative reliability methods

For a detailed assessment of the reliability, including ranking of risks, as well as the prioritization of where to focus on and, thus, integrate corrections or precautions, quantitative methods are needed. Typical techniques for quantitative reliability assessment are presented in the following, grouped into analytical (Section 2.1.3.1), stochastic (Section 2.1.3.2), and some sophisticated (Section 2.1.3.3) methods.

2.1.3.1 Analytical quantitative reliability methods

Analytical approaches for quantitative reliability assessment are based on load-strength interference. The difference between the resistance of the system and the acting load is known as

performance or also called limit state function (LSF). Some guidelines, e.g. DNV-OS-C101 (DNV GL 2015*b*) and DNVGL-CG-0128 (DNV GL 2015*a*), provide definitions of limit states (LSs) and analytical expressions for certain failure criteria. Some of the parameters used in these expressions are uncertain and, thus, have to be represented by stochastic or random variables. The performance function is used to show the area of failure, which is the case for negative results. For evaluating the reliability, the LSF has to be solved, which can be done in different ways. (O'Connor et al. 2002)

As the computation of the reliability, based on the condition that the LSF must be positive, could be very complex, the first order reliability method (FORM) or second order reliability method (SORM) are often used for simplifying the analytical expression by applying a first or second order Taylor expansion (Sundararajan 1995). Based on FORM, an iterative approach for determining the reliability index (RI) is given by Hasofer and Lind (HL). The cumulative distribution function relates the RI to the probability of failure (PoF); the latter is just complementary to the reliability (Tichý 1993).

2.1.3.2 Stochastic quantitative reliability methods

As in the analytical quantitative methods, described in Section 2.1.3.1, the stochastic Monte Carlo simulation (MCS) reliability assessment technique is based on the equation for the LSF. In the MCS, several cases are simulated, in which the uncertain variables are randomly sampled based on the defined probability distribution functions and corresponding key parameters, such as mean value and variance. Using direct MCS, conditional expectation, or importance sampling reduction methods (ISRMs) (Ayyub 2014), the reliability or PoF can be estimated based on the results of the iterated simulation calculation. (Stapelberg 2009)

Unlike in the previous techniques, surrogate modeling methods, such as kriging, or stochastic response surface methods (SRSMs) only use an approximated LSF instead of the real one. While SRSM just uses some sample points for interpolating and approximating the response surface, surrogate modeling methods meet all initial data points and are therefore a more accurate method for approximating the LSF, which is then solved for the PoF and reliability by means of FORM, SORM, or MCS. Besides the advantage of SRSMs to reduce the computational effort for solving the iterations, obtained by simplification of the simulation expressions, SRSMs can also link input and output variables (Chopra et al. 2013). (Mahadevan 2013)

2.1.3.3 Sophisticated quantitative reliability methods

Even more sophisticated system conditions can be handled with quantitative reliability methods. Multi-attribute decision making (MADM), also called multi-criteria decision analysis (MCDA), can support selecting the best option when having multiple criteria within an analysis process, whereas fuzzy set theory (FST) can deal with incomplete information or fuzzy data. Both tools can also be combined in the case of several alternatives being vague in nature. (Lazakis & Ölcer 2016)

Finally, dynamic systems can be approached using Markov analysis (MA). This diagrammatic risk and reliability assessment method allows the inclusion of transitions between different states. (O'Connor et al. 2002)

2.2 Qualitative approaches for reliability analyses of offshore wind turbine systems

The qualitative reliability assessment methods, applied to offshore and marine energy devices, which are presented in this section are categorized, based on the classification given in Section 2.1, into FM analyses (Section 2.2.1), tree and diagrammatic analyses (Section 2.2.2), and hazard analyses (Section 2.2.3). The techniques and their grouping are shown in Figure 2.2.

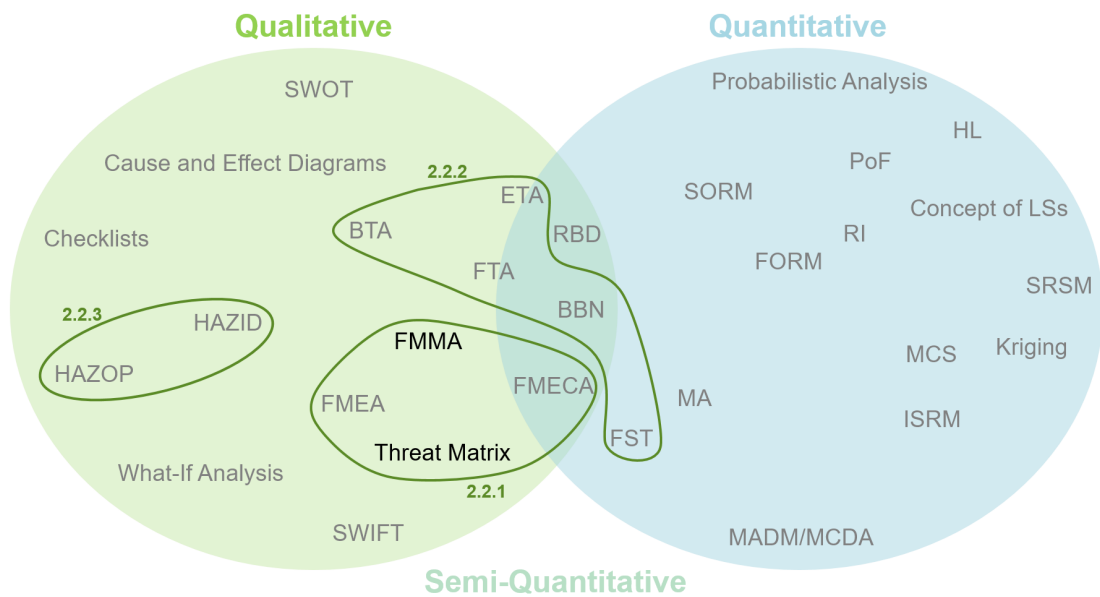


Figure 2.2: Venn diagram for the presented qualitative reliability methods.

2.2.1 Failure mode analyses

FM analyses are already frequently applied to offshore wind turbines and used in both qualitative and quantitative ways, but also in other variations.

2.2.1.1 FMMA, FMEA, and FMECA

An entire RA of the 5 MW wind turbine REpower 5M (Hanke 2004) is performed by Bharatbhai (2015). This consists of a failure mode and maintenance analysis (FMMA) for determining the system components that require focused monitoring, a semi-quantitative FMEA including a criticality rating indicating the risk, based on the two factors of probability and consequence, and an FMECA for identifying those system components which are very prone to failures.

Failure mode identification, based on FMEA, FMECA, as well as FTA, is performed by Luengo & Kolios (2015) to analyze different end of life scenarios for offshore wind turbines.

2.2.1.2 Quantitative FMEA

Similarly to the work of Bharatbhai (2015), mentioned in Section 2.2.1.1, Arabian-Hoseynabadi et al. (2010) deal with FMEA for wind turbines; however, they focus on a quantitative FMEA. The three factors (severity, occurrence, and detectability) of a traditional FMECA are adhered to, but the rating scales are modified and adapted to a wind turbine system. Furthermore, the software Relx Reliability Studio 2007 V2 (PTC 2011) is also adjusted and the component FMEA is chosen to be the most suitable type of FMEA for performing a reliability assessment of a wind turbine. Finally, the benefits of an FMEA, especially for offshore wind turbine systems but also for further improvements towards higher economic efficiency and competitiveness of wind energy, are pointed out.

Shafiee & Dinmohammadi (2014), as well as Kahrobaee & Asgarpour (2011), elaborate the limitations of a traditional FMEA or FMECA when being applied to the assessment of a wind turbine or wind farm, especially offshore. The RPN, used for prioritization, has very little informative value when comparing different wind turbine types and is also difficult to be determined accurately due to deficient failure data. Furthermore, economic aspects, which are becoming more relevant offshore, are not considered in the standard approaches. Thus, a modified FMEA, or by Kahrobaee & Asgarpour (2011) called risk-based FMEA, is proposed which includes both qualitative and quantitative measures. In addition, the cost priority number (CPN) is computed based on the PoF, the cost consequences of a failure, and the detectability. This economic measure is more tangible than the abstract and poor RPN and allows a better and more realistic comparison of different wind turbine systems with respect to criticality.

2.2.1.3 Correlation-FMEA

When dealing with complex systems, such as a FOWT, FMEA could be extremely extensive due to the amount of FMs and the prioritization could become more difficult as many RPNs could have the same order of magnitude. Furthermore, if some FMs are correlated, a direct isolated analysis of each single FM would be more difficult but also less accurate. Thus, Kang et al. (2017) and Bai et al. (2012) propose a correlation-FMEA for the risk assessment of offshore assets. While Kang et al. (2017) applies just the traditional FMECA and uses these FMs with the highest RPN, Bai et al. (2012) modifies the FMECA and determines the RPN based on the ALARP (as low as reasonably practicable) principle, which is also mentioned by Onoufriou & Forbes (2001) as a common approach for defining target safety levels. In both procedures by Kang et al. (2017) and Bai et al. (2012), the correlation of different FMs is then incorporated by means of the reliability index vector (RIV) method. The RIV contains the reliability indices and correlation coefficients of the FMs. The final ranking of these correlated FMs happens through the probability network evaluation technique (PNET) and the most crucial FMs can be determined in this way.

2.2.1.4 Threat matrix and FMECA

A preparatory action for an effective FMECA is described by Baker (2014): the threat matrix. This is meant to be used to estimate the operational expenditure early in the design stage, to identify the most critical components with respect to reliability and maintainability, as well as to be able to optimize the design with respect to cost-efficiency. Using the example of a wave or tidal energy system, a threat matrix is set up by collecting all potential threats or FMs and corresponding failure mechanisms, which are listed on the x-axis, while the y-axis contains all components obtained by a system breakdown. Within the matrix it is marked which threats could occur to which component. This can be used afterwards as a basis for an FMECA in which the possibility of a failure mechanism is supplemented by the probability measure.

2.2.2 Tree and graphical analyses

Just like FM analyses, tree and diagrammatic reliability methods are applied in many cases for the assessment of offshore energy devices; however, these methods are rarely used separately but rather in combination with other tools or in a modified version.

2.2.2.1 FTA, ETA, and BBN

Several techniques are integrated in a complete risk analysis for collision impact on offshore wind turbines, performed by Dai et al. (2013). First, the causes or sequence of events are determined based on FTA or ETA, respectively. Secondly, data for frequencies and probabilities are required. At this stage it is emphasized that in the offshore renewable energy industry sufficient data are often missing; however, existing data from other similar industries, such as offshore oil and gas, with already long-lasting experiences can be taken as a basis. In the third step, potential risk influencing factors (RIFs) affecting event or barrier failure probabilities need to be estimated. With these RIFs, complex BBNs can be created, on which basis the RIFs can be ranked. Finally, the probabilities of undesired events are computed based on the RIFs. For further evaluation of the risk, the consequences and their severity have to be analyzed and then both proactive and reactive actions can be proposed and ranked according to their importance and degree of necessity.

2.2.2.2 Dynamic FTA

A qualitative RA with additional quantitative assessments for complex systems with dynamic characteristics, such as FOWTs, is presented by Zhang et al. (2016). System grading for dealing with the complex composition of the asset is performed in two respects: focused on the system function and based on the structure. For the qualitative assessment of the FMs, dependencies, sequences, and redundancies are taken into account by adapting the traditional FTA to a dynamic FTA, which uses special dynamic logic gates. The quantitative analysis, based on the dynamic FTDs, requires failure rates data, which, however, are not or just insufficiently

available for such a floating wind turbine system. Based on databases for onshore wind turbines and offshore energy assets, which is covered in more detail in Section 2.3.6.1, the failure rates for a floating wind turbine are approximated by the inclusion of marine environmental influences.

2.2.2.3 BTA

The combination of FTA and ETA, in the form of a BTA, is used by Mokhtari et al. (2011) for the assessment of offshore terminals and ports. In the first step, the risk factors are determined by means of HAZID. However, due to vague and imprecise data for failure rates and event occurrences, FST, using the fuzzy analytical hierarchy process method with triangular fuzzy numbers, is applied for prioritizing these identified risk factors. The highest ranked risk factors are then assessed via BTA.

Adjusted BTAs for quantitative and dynamic reliability assessment can be found in literature (Song et al. 2016, Abimbola et al. 2014, Khakzad et al. 2013, Ferdous et al. 2012). The quantitative aspect is covered by FST or evidence theory for dealing with uncertain and vague data, and is applied after the creation of the BTD based on expert knowledge as input for the event probabilities (Ferdous et al. 2012). With such a quantitative BTA, the likelihood of consequences can be set in relation to failure rates of system components and safety barriers (Abimbola et al. 2014). But in order to include dynamics, dependencies, and common causes (Khakzad et al. 2013) as well, or also update the probability estimates based on newly available data (Abimbola et al. 2014, Ferdous et al. 2012), Bayesian updating approaches (Abimbola et al. 2014, Ferdous et al. 2012) and BBNs (Song et al. 2016), which could also be object-oriented (Khakzad et al. 2013), are also used.

2.2.3 Hazard analyses

Contrary to FM, tree, and diagrammatic analyses, hazard analysis techniques are more rarely found to be applied for the reliability assessment of offshore and marine renewable energy assets. HAZID is mentioned once by Mokhtari et al. (2011) for identifying the risk factors of an offshore system. HAZID is more likely to be used preparatory to an FMEA, compared to HAZOP, as the latter requires that the entire design is already fixed and everything is in place. Thus, these two hazard analysis tools are more suitable for reviewing the final design (NOPSEMA 2017) or within integrity management for scheduling inspection and maintenance, based on the determined hazards (Nwofor 2010).

2.3 Quantitative approaches for reliability analyses of offshore wind turbine systems

The quantitative reliability assessment methods, applied to offshore and marine energy devices, which are presented in this section are categorized, based on the classification given in Section 2.1, into analytical methods (Section 2.3.1), stochastic methods (Section 2.3.2), Bayesian

approaches (Section 2.3.3), reliability-based design optimization methods (Section 2.3.4), multivariate analyses (Section 2.3.5), and data foundations (Section 2.3.6). The techniques and their grouping are shown in Figure 2.3.

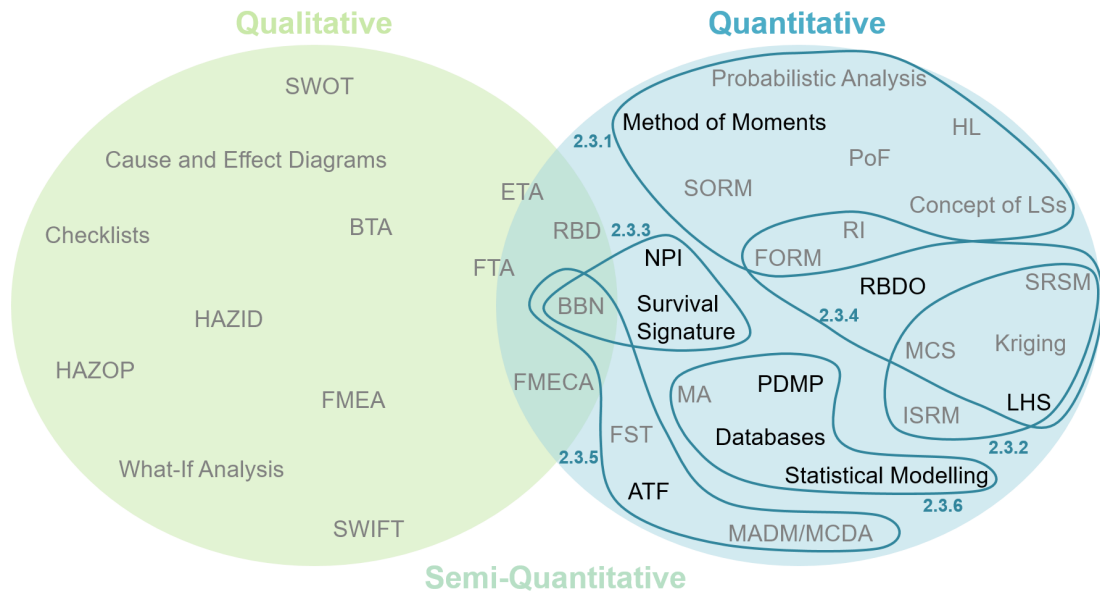


Figure 2.3: Venn diagram for the presented quantitative reliability methods.

2.3.1 Analytical methods

The analytical quantitative reliability methods, found to be used for the assessment of offshore wind turbines, are mainly based on performance functions and focus on the determination of the RI.

2.3.1.1 Concept of LSs

LSFs, RI, and PoF are mentioned frequently as a basis for assessing the reliability of whole offshore systems or single components (Olle 2016, Yeter et al. 2016, Kim & Lee 2015, Kolios et al. 2015, Rendón-Conde & Heredia-Zavoni 2015, Carswell et al. 2013, Kolios, Collu & Brennan 2010, Lu et al. 2010, Kolios & Brennan 2009). Furthermore, the hazard rate function is used by Zitrou et al. (2016) for developing an availability growth model, which accounts already in the early design stage for innovations and later changes.

In the IRPWind-project (Olle 2016), safety factors are used for creating the equations for the LSFs in a study into the reliability of support structures for offshore wind turbines, focusing on degradation due to operational and environmental impact. The benefits of partial safety factors - thus, the LS method - are also emphasized by Kolios & Brennan (2009) by pointing out the applicability of this reliability-based design concept to novel offshore structures, where existing standards may only be used to a limited extent, as well as the upside of having optimization possibilities and other advantages over global safety factor approaches.

2.3.1.2 Analytical probabilistic analyses

FORM and/or SORM are frequently applied for the reliability assessment of different assets, such as FOWTs (Kolios et al. 2015, Kolios, Collu & Brennan 2010), mooring lines for a floating device (Rendón-Conde & Heredia-Zavoni 2015), offshore support structures (Yeter et al. 2016, Kim & Lee 2015), or the welded tubular joints of an offshore structure (Dong et al. 2012). Kolios, Collu & Brennan (2010) emphasize the capability of these indirect methods to estimate joint probability density functions, as well as their advantage over MCS regarding the computational effort. A direct comparison by Kang et al. (2016) of the results from FORM and SORM with these obtained by MCS is satisfactory. Furthermore, Rendón-Conde & Heredia-Zavoni (2015) apply FORM to show how the reliability is affected by uncertainties in system parameters. Finally, Kolios et al. (2015) indicate the HL method as an example for FORM and point out the higher accuracy of SORM, which can also handle non-linear LSFs.

Different methods, however, related to FORM and SORM - as they are also based on derivatives of the LSF - are the first order second moment approach (Carswell et al. 2013) and the method of moments (Lu et al. 2010); the latter is used for estimating the reliability sensitivity. The computational efficiency of the moment-based reliability assessment and its applicability to systems with several FMs is underlined by Lu et al. (2010). Furthermore, Llado (2015) mentions the advanced mean value method as a tool for reliability assessment and reliability-based design optimization.

2.3.2 Stochastic methods

Besides the above mentioned analytical quantitative reliability methods (Section 2.3.1), stochastic techniques, such as MCS, importance sampling method (ISM), or SRSM, are also applied for the reliability assessment of offshore wind turbine systems.

2.3.2.1 MCS

Scheu et al. (2017), Kolios et al. (2015), Llado (2015), Yang et al. (2015), Lee et al. (2014), and Kolios, Collu & Brennan (2010) all refer to MCS as a method for assessing system reliability. One reason for using this method is the demanding approximation of the PoF, as stated by Kolios et al. (2015), especially when complex systems such as FOWTs are considered. However, Kolios, Collu & Brennan (2010) also point out the corresponding disadvantage of MCS, which often comes with high computational effort. The number of iterations is lower for Latin hypercube sampling (LHS) (Lee et al. 2014), while uncertainties can still be accounted for in the design (Yang et al. 2015).

A specific category within MCS is ISM, which only samples a selected region of interest. Thus, Thöns et al. (2010) first identify the converged design point based on an adaptive response surface (RS) algorithm, which is introduced in Section 2.3.2.2, and then carry out the RA with the help of an importance sampling (IS) Monte Carlo scheme to determine the PoFs. Due to the preceding RS-based approach, this IS algorithm only requires the LSs and

corresponding uncertainties as input. Similarly, IS follows the surrogate modeling within the stochastic simulation by Taflanidis et al. (2013) to quantify the importance of uncertain parameters.

2.3.2.2 SRSM

RAs of offshore (wind turbine) support structures are also conducted by means of SRSM, as for example by Kim & Lee (2015) for obtaining the RI. A special approach in this reliability assessment has to be mentioned: due to the time-consuming analysis of systems with dynamic characteristics - as prevailing in the environmental conditions of an offshore wind turbine support structure - the dynamic response is approximated by applying a peak response factor for the dynamic amplification to the static response.

Similarly to Kim & Lee (2015), Thöns et al. (2010) examine the reliability of an offshore wind turbine support structure. An adaptive RS algorithm is proposed for obtaining the design point, which is later used for the RA based on IS, covered in Section 2.3.2.1. First, an experimental design is created, which is used for finite element computations. Afterwards, a regression analysis is performed and the design point is determined. This is an iterative process until the design points converge.

Response surface method (RSM) and regression analysis are also used by Zhang & Lam (2015), while Yang et al. (2015) apply the kriging RSM for building an approximate model including uncertainties and Taflanidis et al. (2013) use moving least squares RS approximations within the surrogate modeling approach for obtaining higher computational efficiency.

2.3.3 Bayesian inference

The system reliability can be investigated in more detail by means of the Bayesian approach. This combines and processes expert knowledge, providing prior distributions, and test data, representing sample distributions (Walter et al. 2017). Bayesian inference can also be used for dealing with uncertainties or conflicts in the prior probability distributions (Walter & Coolen 2016, Troffaes et al. 2014, Walter & Augustin 2009).

2.3.3.1 Bayesian updating

Garbatov & Soares (2002) use the Bayesian approach for updating the reliability and the resulting maintenance schedule of a floating offshore structure. However, not all parameters are updated after each inspection - only those which are very prone to uncertainties. Nielsen & Sørensen (2011) also make use of previous experiences, inspections, and Bayesian pre-posterior decision theory in order to optimize maintenance planning.

A non-parametric Bayesian updating approach is presented by Ramirez & Sørensen (2011) for the reliability assessment of a support structure for an offshore wind turbine. For integrating uncertainties in the RA, a polynomial chaos expansion approximation, based on Hermite polynomials and Gaussian variable, is applied. Furthermore, discrete semi- or non-conjugated updating is recommended for multi-parametric updating.

2.3.3.2 Survival signature

A kind of Bayesian inference can also be obtained by combining the survival signature, which is equal to the system signature if only one type of component exists, with non-parametric predictive inference (NPI). NPI does not provide exact probabilities, but a lower and upper bound for the survival probability function. (Walter et al. 2017)

The survival signature can also be used within optimization models for more efficient opportunistic condition-based maintenance strategies (Shafiee et al. 2015).

2.3.4 Reliability-based design optimization

Several quantitative reliability methods are used together in reliability-based design optimization (RBDO) processes. The structure of RBDO is always quite similar. However, three different approaches for the design optimization of offshore wind turbine support structures are presented in the following.

2.3.4.1 RBDO vs. deterministic design optimization

The comparison of RBDO and deterministic design optimization (DDO) is shown by Lee et al. (2014). The optimization procedures aim at reducing the mass of the structure by taking reliability into account. For both approaches, first, design loads are determined by conducting a dynamic response analysis with a finite element model. The DDO, based on progressive quadratic RSM optimizes the mass and fulfills the LS requirements; however, the reliability of the structure is not necessarily ensured. In contrast, RBDO yields an optimized design and achieves the target reliability at the same time. In the RBDO procedure, the mean values of the random design variables are processed. The boundary conditions for the computations are given by the LSFs and required reliability. The iterative calculation procedure consists of an inner loop for the reliability and structural analyses, applying LHS, and the outer optimization process, including RA and using a micro genetic algorithm. With this RBDO procedure, a reliable and cost-effective design is aimed to be obtained.

2.3.4.2 Dynamic RBDO

A dynamic RBDO is elaborated by Yang et al. (2015). Due to the integrated dynamics, these RBDO processes have a quite high computational effort. Commonly, deterministic techniques are used in optimization procedures; however, these do not account for uncertainties, for which probabilistic methods are required. The proposed dynamic RBDO process also starts with a finite element model of the considered structure. With the focus on the inclusion of uncertainties in the RBDO approach and the reduction of computational effort, an approximate metamodel is created by means of kriging RSM or LHS, based on the generated finite element model. This approximate model is used within the iterative optimization process, incorporating uncertainties and focusing on the weight of the structure. For comparative purposes, MCS is used to

estimate the reliability of the resulting optimum design. This shows higher reliability values than are obtained by DDO.

2.3.4.3 Integrated RBDO

For the realization of RBDO, an integrated algorithms system is presented by Karadeniz et al. (2009). This integrated RBDO algorithm consists itself of three interacting numerical algorithms for structural analysis, RA, and the optimization process. By means of the structural analysis, which is based on a finite element model and performed with a stochastic analysis program for offshore structures, the LSF, as well as the cost or weight and their gradients, are computed as function of the design variables. LSF and its gradient, as well as the probabilistic data, are given as input to the RA algorithm. Using FORM, the RI is determined iteratively and for the converged value also the gradient is calculated. These parameters, together with the cost/weight function and its gradient from the structural analysis, are integrated into the optimization process, using sequential quadratic programming. The iterative loop computes the objective function - thus, cost/weight - based on the provided design variables, proves the requirements for reliability, and is iterated until convergence, and, thus, the optimized design is achieved. This integrated RBDO algorithm requires an initial estimate for the optimization design variables as input and then runs in a closed loop until the final optimum design variables are found. Despite the functionality and applicability of this integrated RBDO algorithm, it also brings the disadvantage of high computational effort.

2.3.5 Multivariate analyses

The category of multivariate quantitative reliability assessment methods comprises analyses, which contain various criteria, handle several hazards, or deal with complex systems.

2.3.5.1 FST in MADM

MADM is commonly used to find a preferred solution from a pool of alternatives. Different MCDA methods are applied and compared by Kolios, Mytilinou, Lozano-Minguez & Salonitis (2016) for determining the most suitable support structure for wind turbines at specific locations, while Lozano-Minguez et al. (2011) focus on the technique for order preference by similarity to ideal solution (TOPSIS), which is one typical method within MADM (Gumus et al. 2016). This is also applied by Lavasani et al. (2012) to select the best barrier for offshore wells with respect to costs and benefits. In order to deal with fuzzy data, a fuzzy analytical hierarchy process is integrated in MADM. Similarly, an intuitionistic fuzzy entropy method within an MCDA model allows to choose the most appropriate wind energy technology for a specific site under consideration of vagueness and uncertainties in environmental, economic, and social factors (Gumus et al. 2016). Kolios et al. (2017) apply as well a fuzzy-TOPSIS method for prioritization of FMs of a subsea control module, while Kolios, Rodriguez-Tsouroukdissian & Salonitis (2016) and Martin et al. (2013) extend the TOPSIS method to take stochastic inputs and uncertainties into account.

Besides these more traditional applications of MADM, Okoro et al. (2017) use TOPSIS for risk-based prioritization of offshore energy asset components. The proposed multi-criteria risk assessment approach is similar to FMEA; however, it overcomes the disadvantageous subjective ranking of FMs within FMEA, as each single variable of one FM is weighted instead. The entire risk assessment contains, as usual, risk identification, risk analysis (with collection of information, multi-criteria analysis, and final integration to an overall ranking), and risk evaluation. Within the multi-criteria RA, first, all FMs are investigated and broken down into all risk parameters, which are finally weighted, as already mentioned. In a second step, all relevant FMs of each system component are determined. Based on these estimates, FMs and risk parameters are ranked by means of the TOPSIS method.

Apart from TOPSIS, the analytic hierarchy process (AHP) and the analytic network process (ANP) are two further MCDAs that can be applied within risk and reliability assessments. While the hierarchical approach in AHP only shows the relation between elements, the network view in ANP provides a more sophisticated analysis, which takes dependencies and feedbacks into account (Figueira et al. 2005). This capacity benefits the utilization of ANP in multi-criteria decision tasks within complex systems, for which reason it is applied by Shafiee & Kolios (2015) in the field of offshore wind energy in order to find the best strategy for mitigating operational risks.

2.3.5.2 Multi-hazard reliability assessment

Also, for supporting the decision-making process within the planning and design of offshore wind energy projects, Mardfekri & Gardoni (2015) present a multi-hazard reliability assessment method. A finite element model for an offshore wind turbine is set up to represent the dynamic response by taking aero-elastic coupling and soil-structure interaction into account. Probabilistic demand models for the support structure are obtained in a deterministic procedure, which is supplemented by adjustment terms to consider uncertainties in the statistics, as well as model errors and uncertainties. These demand models are updated by incorporating existing data, using the Bayesian approach. With wind and seismic hazard data for a particular site, the fragility curves are estimated, based on LSFs. These fragility curves give information about the expected structural damage, but also the degree of sensitivity of single random variables, which could then provide a measure of importance.

2.3.5.3 Artificial transfer function

Structural RA of offshore structures, evaluated with respect to fatigue behavior and considering each single failure scenario, could be computationally intensive and time-consuming. To deal with this, an artificial transfer function (ATF) is used by Gholizad et al. (2012). The real transfer function, used in the fatigue calculations, is approximated by a two-parameter ATF with a predefined shape, similar to the Pierson-Moskowitz spectrum. The two parameters are determined by evaluating the real and ATF at two points. With these parameters and the

eigenperiod of the structure, the wave scatter, and the in-service life time, the RIs of different components can be determined and, thus, used as a measure of the structural reliability.

2.3.6 Data foundations

Quantitative reliability methods depend, as their name suggests, on quantitative measures. The required data do not always exist, are incomplete, or not accurate enough. Thus, data often have to be modeled based on available information or estimates.

2.3.6.1 Databases

Several long-term surveys have been performed in different countries for collecting data on installed wind turbines, as summarized in Table 2.1. These could be of various types, such as fixed or variable speed wind turbines, with geared or direct drives. Furthermore, the amount and concrete type of collected data depend on the specific survey. (Tavner 2012)

Table 2.1: Wind turbine databases, based on the publications by Tavner (2012) and Faulstich et al. (2009).

Name	Country	Period	# Units	Reliability-relevant collected data
WMEP	Germany	1989-2006	1500	Maintenance and repair events, disruptions, malfunctions, failures, downtimes
LWK	Germany	1993-2006	241	Failures, downtimes
Windstats WSD	Germany	1995-2004	4285	Failures, downtimes
Windstats WSDK	Denmark	1994-2003	904	Failures, downtimes
VTT	Finland	2000-2004	92	Failures, downtimes
Elforsk	Sweden	1997-2004	723	Failures, downtimes
ReliaWind	Europe	2004-2010	~350	Failures, downtimes, FMEA

These data, however, are only for onshore wind turbines and, thus, show an example for a case where data of similar, but not the finally considered, assets are available. Faulstich et al. (2009) already mention a transfer of the existing data to offshore wind turbines, which are, however, affected by the concrete type of asset, as well as the different environmental conditions, and, thus, require a very rich database. WMEP is quite extensive but not broad enough, therefore a new research project for an Offshore-WMEP has been undertaken in Germany. In accordance and cooperation with the Offshore-WMEP, Great Britain has set up the offshore wind data platform SPARTA, which focuses on availability and reliability to improve the system performance (Offshore Renewable Energy 2014). Within another recent research project, WInD-Pool (Fraunhofer IWES 2015), a broad database is provided by amalgamating compatible data, including among others also the Offshore-WMEP. Similar to the databases presented in Table 2.1, however, considering offshore wind turbines, Carroll et al. (2016) have

analyzed and collected failure rate, repair time, and operation and maintenance data of around 350 offshore wind turbines in Europe.

The need for a database for offshore wind turbines is also emphasized by Hameed et al. (2011). With respect to offshore energy industries, there is a reliability, availability, maintainability, and safety (RAMS) database existing for the oil and gas industry, called offshore reliability data (OREDA). However, comprehensive data collections for reliability and safety of offshore and marine renewable energy assets are lacking. Thus, it is proposed to make use of already existing databases, such as OREDA, and transfer this knowledge to other industries for setting up RAMS databases for offshore renewable energy systems, such as offshore wind turbines. The structure of the RAMS database, proposed by Hameed et al. (2011), is inspired by the concept of the Offshore-WMEP presented by Faulstich et al. (2009). Thus, Hameed et al. (2011) construct a RAMS database, which uses operational, equipment, failure, and maintenance data, as well as condition monitoring information as input. Furthermore, already existing experiences from OREDA, as well as from onshore and offshore wind turbines, are used as information sources. Directly linked to the RAMS database is the data analysis, which provides outputs that are valuable for design and manufacturing, self-maintenance machines, operation and maintenance strategies, life cycle cost and profit estimates, as well as the assessment of qualifications for new technologies. Despite the suspected powerfulness of this RAMS database, Hameed et al. (2011) also mention challenges which come with the data collection. Besides cost factors, information protection and specific client needs, as well as data quality and management, technological changes and optimization strategies have to be faced.

The method of using existing reliability databases from other energy industries as basis for assessing reliability data for offshore wind turbines is applied by Delorm et al. (2016). By transferring the existing data to the specific offshore environmental and operational condition of the considered asset, a so-called surrogate data portfolio is generated. The aspect of dealing with different environmental conditions is considered by applying a failure rate estimate approach. By means of reliability modeling and prediction analysis - a combination of diagrammatic and analytical models - the reliability of the system and its components can be assessed.

2.3.6.2 Statistical modeling

In case of a lack of failure rate data, statistical modeling techniques can be applied. The Weibull distribution is commonly used (Walter et al. 2017, Tavner et al. 2007) for estimating the failure rate of a system. By changing the shape parameter of the Weibull distribution, the entire life cycle can be covered and the bathtub curve of the failure rate represented. As this power law process is very suitable for complex repairable systems, it can also be utilized to assess the reliability of large (offshore) wind turbines (Tavner et al. 2007).

2.3.6.3 Markov chain approach for data modeling

The capability of MA to deal with transitions between states, mentioned in Section 2.1.3.3, can be utilized for modeling developing data, such as environmental conditions or degradation and

maintenance processes. Thus, Hagen et al. (2013), Scheu et al. (2012), as well as Castro Sayas & Allan (1996), use the Markov chain for modeling the sea state parameters of wave height and wind speed. Ziegler et al. (2016) and Hagen et al. (2013) generate Markov chain weather models, also representing seasonal characteristics. Furthermore, deterioration processes are sometimes modeled by using the Markov property, as done by Besnard & Bertling (2010). This presented Markov chain maintenance model considers degradation of components, but also includes inspection processes. An alternative to this are Petri net models combined with MCS, which can also take degradation, inspection, and maintenance into account and provide information about condition, failure estimates, as well as basic details helpful for planning maintenance strategies (Le & Andrews 2016).

Alternative applications of the Markov property can as well be found in literature (Strauss 2016, Zhang et al. 2014). Strauss (2016) uses a Markov chain model and semi-Markov chain model for assessing the fatigue reliability of concrete structures, including Bayesian updating for considering actual information from monitoring activities. Broader capabilities of the Markov property are opened up with a piecewise deterministic Markov process (PDMP), as applied by Zhang et al. (2014). With PDMP, discrete failure events, as well as continuous processes, can be modeled. Due to this ability, PDMP combined with MCS can make a quite powerful tool for the reliability assessment of offshore systems.

2.4 Discussion of reliability methods for offshore wind turbine systems

Some challenges that come with the reliability assessment of offshore wind turbine systems are already mentioned in Sections 2.2 and 2.3. The main ones, as well as the customized proposed solution methods, are collated and presented in the following.

- **RPN and ranking of FMs**

The ranking of FMs within an FMECA is often quite subjective (Okoro et al. 2017) and the RPN does not always provide meaningful information, especially when different technologies and types of wind turbine systems have to be compared (Shafiee & Dinmohammadi 2014). Thus, Okoro et al. (2017) recommend subdividing the FMs into their risk factors and applying the weights directly to these parameters, and Kolios et al. (2017) use a fuzzy-TOPSIS MCDA method in addition to FMEA and RPN to prioritize FMs. Shafiee & Dinmohammadi (2014), as well as Kahrobaee & Asgarpour (2011), on the other hand, introduce the CPN for inclusion of economic aspects and in order to work with a more tangible monetary ranking value within the prioritization process.

- **Complex and novel systems**

Offshore wind turbines are often very complex systems and prone to several different, correlated, and dynamic FMs. Kang et al. (2017), Bai et al. (2012), and Onoufriou & Forbes (2001) propose a correlation-FMEA, based on the ALARP principle and using

RIV as well as PNET, to cope with this difficulty, while Zhang et al. (2016) use system grading and a dynamic FTA. An additional challenge, especially within the relatively recent offshore renewable energy technologies, is that of novel designs, to which existing standards can only be applied to a limited extent. The concept of LSs (Kolios & Brennan 2009), as well as RBDO procedures (Section 2.3.4) could be a helpful support.

- **The problem with the data**

Missing, insufficient, and vague data, especially in the offshore wind energy industry, is a big issue in detailed and meaningful reliability assessment of such assets. FST and evidence theory can help dealing with vague data (Ferdous et al. 2012, Mokhtari et al. 2011). However, this does not replace the need for a RAMS database for offshore wind turbines. Existing data from other offshore industries, such as oil and gas, or even on-shore renewable energy equivalents, which already have long-lasting experience, can serve as a basis for setting up a useful RAMS database for these assets (Dai et al. 2013). Besides the need for modifications to take different (environmental) conditions into account (Zhang et al. 2016), further challenges, such as cost aspects, richness of data, or fast developing technologies, have still to be faced (Hameed et al. 2011).

These above mentioned challenges are still current working areas within the reliability assessment of offshore wind turbines. The most recent theories show that computational simplifications, through FORM or SORM, are still of interest; however, the main research focus has shifted towards more comprehensive and adjusted approaches for complex, dynamic systems with correlated FMs, multivariate problems, as well as data collection and modeling. Based on this existing trend and including the characteristics of offshore wind turbine systems, as well as the specific capabilities of different reliability methods, Bayesian approaches, MCDMs, Markov analyses, and especially combined theories, are likely to come more to the fore.

A summary of the presented qualitative and quantitative methods, their applicability with respect to stage, specific challenges, and aimed outcomes, as well as their limitations, is presented in Tables 2.2 and 2.3, respectively. The considered stages are divided into design (D), construction (C), operation (O), maintenance (M), and life cycle planning (LC).

It can clearly be seen that for the early stages of the process life cycle qualitative methods are more suitable than quantitative methods, as not sufficient data is yet available. However, when proceeding towards later stages in which more and more data is already gained and available, more quantitative methods can be used and are also favored due to their more comprehensive capabilities. Thus, qualitative methods are mostly used in the design stage and some also in the construction stage. Only a few qualitative methods, such as dynamic FTA or BTA, are utilized in operation and maintenance when it comes to monitoring. Furthermore, advanced qualitative methods, such as correlation-FMEA, threat matrix, and FMECA, can support life cycle planning. On the other hand, quantitative methods are mostly used in operation, maintenance, and life cycle planning, while only a few, e.g. analytical methods, RBDO, and some multivariate analyses, can be applied in the design stage for the purpose of design optimization.

Table 2.2: Applicability of presented qualitative reliability methods, in summary.

Method	Stages	Results	Capabilities	Limitations	References
FMMA, FMEA, and FMECA	D	FMs	Easy implementation; employable from the beginning of the project	Competent facilitator for reaching consensus in scoring is required	(Luengo & Kolios 2015, Hanke 2004)
Quantitative FMEA	D, C	Prioritization of FMs	Straightforward application due to well-defined bands of scores	Appropriate scoring for different classes of application	(Shafiee & Dinmohammadi 2014, PTC 2011, Arabian-Hoseynabadi et al. 2010)
Correlation-FMEA	D, LC	Weak points	Coping with mutual correlated FMs	Complexity in case of multiple FMs	(Kang et al. 2017, Bai et al. 2012, Onoufriou & Forbes 2001)
Threat matrix and FMECA	D, LC	Components requiring high reliability or good maintainability	Visual representation of FMs and associated consequences	No incorporation of detectability factor in 2D representation	(Baker 2014)

Table 2.2: Applicability of presented qualitative reliability methods, in summary. (cont.)

Category: Tree and graphical analyses					
Method	Stages	Results	Capabilities	Limitations	References
FTA, ETA, and BBN	D, C	Decision making	Visual representation of interdependencies of events	Cumbersomeness in case of highly granulated system analysis	(Dai et al. 2013)
Dynamic FTA	D, C, O, M	Maintenance references	Coping with sequentially dependent and redundancy failures	Effect of inappropriate sequencing of events on analysis results	(Zhang et al. 2016)
BTA	O, M	Real time risk monitoring	Efficient link of ETA and FTA; visualization of dependencies	Common cause and dependency failures	(Song et al. 2016, Abimbola et al. 2014, Khakzad et al. 2013, Mokhtari et al. 2011)
Category: Hazard analyses					
Method	Stages	Results	Capabilities	Limitations	References
HAZID/HAZOP	D, O, M	Monitor operational risk factors	Structured description of hazards and system effects of deviations from design intent	Extensive documentation only to be applied to well-defined system	(NOPSEMA 2017, Mokhtari et al. 2011, Nwofor 2010)

Table 2.3: Applicability of presented quantitative reliability methods, in summary.

Category: Analytical methods					
Method	Stages	Results	Capabilities	Limitations	References
Concept of LSS	D, O, LC	Design optimization and novel design signs	Systematically considered uncertainties; no global safety factors	Combined FMs vs. their individual contributions	(Olle 2016, Yeter et al. 2016, Zitrou et al. 2016, Kolios et al. 2015, Rendón-Conde & Heredia-Zavoni 2015, Carswell et al. 2013, Kolios & Brennan 2009)
Analytical probabilistic analyses	D, C, O, LC	Reliability sensitivity	Robust consideration of input uncertainties	Complex derivation of joint probability distribution functions	(Kang et al. 2016, Yeter et al. 2016, Kim & Lee 2015, Rendón-Conde & Heredia-Zavoni 2015, Carswell et al. 2013, Dong et al. 2012, Lu et al. 2010)
Category: Stochastic methods					
Method	Stages	Results	Capabilities	Limitations	References
MCS	O, M	Decision making	Easy to implement due to direct simulations	Large computational effort	(Scheu et al. 2017, Llado 2015, Kolios, Collu & Brennan 2010)
SRSM	O	Computational efficiency	Time-varying and dependent variables	Sensitive to initial assumption of RS shape	(Kim & Lee 2015, Yang et al. 2015, Zhang & Lam 2015, Taflanidis et al. 2013, Thöns et al. 2010)
ISM	O	Computational efficiency	Overcome limitations of direct MCS	Performance in multiple variables; modeling requirements	(Taflanidis et al. 2013, Thöns et al. 2010)

Table 2.3: Applicability of presented quantitative reliability methods, in summary. (cont.)

Category: Bayesian inference					
Method	Stages	Results	Capabilities	Limitations	References
Bayesian updating	O, M	Optimized/updated inspection planning	Uncertainty in prior; application with condition monitoring	Appropriate data to update probabilities	(Walter et al. 2017, Walter & Coolen 2016, Troffaes et al. 2014, Nielsen & Sørensen 2011, Ramirez & Sørensen 2011, Walter & Augustin 2009, Garbatov & Soares 2002)
Survival nature	sig- LC	System survivability	Incorporation of condition monitoring	Resilience and maintenance effects	(Walter et al. 2017, Shafiee et al. 2015, Troffaes et al. 2014)
Category: RBDO					
Method	Stages	Results	Capabilities	Limitations	References
(Dynamic, integrated) RBDO	D	Optimized design (reliability, mass, performance, cost)	Consideration of uncertainties	Computational effort	(Yang et al. 2015, Lee et al. 2014, Karadeniz et al. 2009)

Table 2.3: Applicability of presented quantitative reliability methods, in summary. (cont.)

Category: Multivariate analyses

Method	Stages	Results	Capabilities	Limitations	References
FST MADM	D, O, M, LC	Decision making; prioritization of interventions	Easy implementation due to intuition-based input data	Skewness of results due to extreme values	(Kolios et al. 2017, Okoro et al. 2017, Gumus et al. 2016, Kolios, Mytilinou, Lozano-Minguez & Salonitis 2016, Ko- lios, Rodriguez-Tsouroukdissian & Salonitis 2016, Shafiee & Kolios 2015, Martin et al. 2013, Lavasani et al. 2012, Lozano-Minguez et al. 2011)
Multi-hazard reliability assessment	D	Design optimiza- tion	Consideration of uncertain- ties; level of importance of variables in LSF	Complex derivation of joint probability density func- tions in case of correlated hazards	(Mardfekri & Gardoni 2015)
ATF	O, LC	Inspection plan- ning	Approximation of complex processes	Lost information further from expected value	(Gholizad et al. 2012)

Table 2.3: Applicability of presented quantitative reliability methods, in summary. (cont.)

Method	Stages	Results	Capabilities	Limitations	References
Databases	D, O, M	Data collection; optimized operation and maintenance	Availability of generic occurrence frequencies	Processed data; different sources and reporting protocols forms	(Delorm et al. 2016, Tavner 2012, Hameed et al. 2011, Faulstich et al. 2009)
Statistical modeling	O	Optimization (design, operation and control strategies)	Failure prediction in complex and repairable systems	Sufficiently accurate system modeling required (e.g. supervised learning)	(Tavner et al. 2007)
Markov chain approach for data modeling	O, M	Sensitivity to parameter variations	Coping with dynamic reliability problems, degradation, and maintenance processes	Non-explicit expression of dependencies between hidden states; computational effort	(Le & Andrews 2016, Zhang et al. 2014, Hagen et al. 2013, Scheu et al. 2012, Besnard & Bertling 2010, Castro Sayas & Allan 1996)

Chapter 3

Floating offshore wind turbine systems

Around 40 FOWT concepts are already proposed (Q FWE 2020, James & Ros 2015, Mast et al. 2015); however, this broad range of floater types being up to now investigated - either as research designs, under development, in prototype stage, or already in demonstration projects - inhibits fast achievement of high technology readiness levels (TRLs). Furthermore, less diversity in floating support structures would allow more focused research, development of required infrastructure, specification and adaption of suppliers and manufacturers, as well as realization of serial production (Butterfield et al. 2007). Then, FOWTs could become soon cost-competitive with bottom-fixed offshore wind turbine systems. Thus, in this chapter, first (Section 3.1), different floaters are assessed and examined in detail by means of a MCDA, emphasizing their suitability for deployment in offshore wind farms. Based on the outcomes, a reference FOWT system is defined in Section 3.2, which serves as starting point for the optimization applications covered in Chapters 5 and 6.

3.1 Critical review of floating support structures for offshore wind farm deployment

As fundamental basis for examining floating platform concepts for offshore wind turbines, a literature review on FOWT support structures, their characteristics, and the state-of-the-art is conducted. The main classification and the wide variety of existing floater concepts are presented in Section 3.1.1. For the assessment of floating support structures (Section 3.1.2), first, a SWOT analysis is carried out for the three main categories (Section 3.1.2.1). This already indicates benefits and drawbacks of the technologies and, hence, supports the investigation of other concepts. On this basis, a set of criteria for assessing the potential of floating support structures for wind farm deployment is specified in Section 3.1.2.2. The examined alternatives are defined in Section 3.1.2.3. To obtain more meaningful results and to allow ranking of the

Note: This chapter is primarily based on the publication by Leimeister et al. (2018), as well as the publications by Leimeister, Collu & Kolios (2020), Leimeister & Kolios (2020), Leimeister, Kolios & Collu (2020a), and Leimeister, Kolios, Collu & Thomas (2020, 2019) in excerpts.

different support structures, a MCDA is carried out in Section 3.1.2.4, based on survey results and using the TOPSIS method. Finally, the TRLs are assessed in Section 3.1.2.5.

3.1.1 Review of FOWT support structures

In 2015, FOWTs counted already over 30 types (James & Ros 2015, Mast et al. 2015), while just five years later Q FWE (2020) already states around 40 floating projects. This broad range and huge diversity of floating support structures for offshore wind turbines are presented in Section 3.1.1.2. Even if always new concepts and technologies are coming up, there are three main categories, which are introduced in the following Section 3.1.1.1.

3.1.1.1 Main classification of floaters

Floating support structures can be categorized based on the primary mechanism adopted to fulfill the static stability requirements. There are three main stabilizing mechanisms (Borg & Collu 2015, Taboada 2015, Butterfield et al. 2007).

- **Ballast stabilized**

Having large ballast deep at the bottom of the floating structure moves the center of gravity of the total system below the center of buoyancy. This leads, when tilting the platform, to a stabilizing righting moment which counteracts rotational displacements.

- **Waterplane (or buoyancy) stabilized**

The waterplane area is the main contributor to the restoring moment of the floater. Having a large second moment of area with respect to the rotational axis, either due to a large waterplane area or due to smaller cross-sectional areas at some distance from the system central axis, creates a stabilizing righting moment in case of rotational displacement.

- **Mooring stabilized**

High tensioned mooring lines generate the restoring moment when the structure is inclined.

Spars, semi-submersibles or barges, and tension leg platforms (TLPs) rely, respectively, on the above mentioned stabilizing mechanisms and, thus, make up the three cornerstones of floating support structures. This is visualized in Figure 3.1 in form of a stability triangle.

Spars, the ballast stabilized floaters (Figure 3.2(a)), usually consist of a long cylindrical structure which is filled with ballast at the bottom. For station-keeping, the floater is commonly equipped with three catenary mooring lines. The same mooring system is used for semi-submersibles, shown in Figure 3.2(b). To obtain waterplane-based stability, this floater type is mostly made out of three or four columns placed on the edges of a triangle. The wind turbine is either mounted on one of these columns or supported by a fourth one in the center of the triangle. Braces interconnect the columns. Unlike the multi-cylindrical semi-submersible, the waterplane-area stabilized barge is rather a plane structure. Finally, the mooring stabilized TLP (Figure 3.2(c)) commonly has a central column to support the turbine. At the floater base

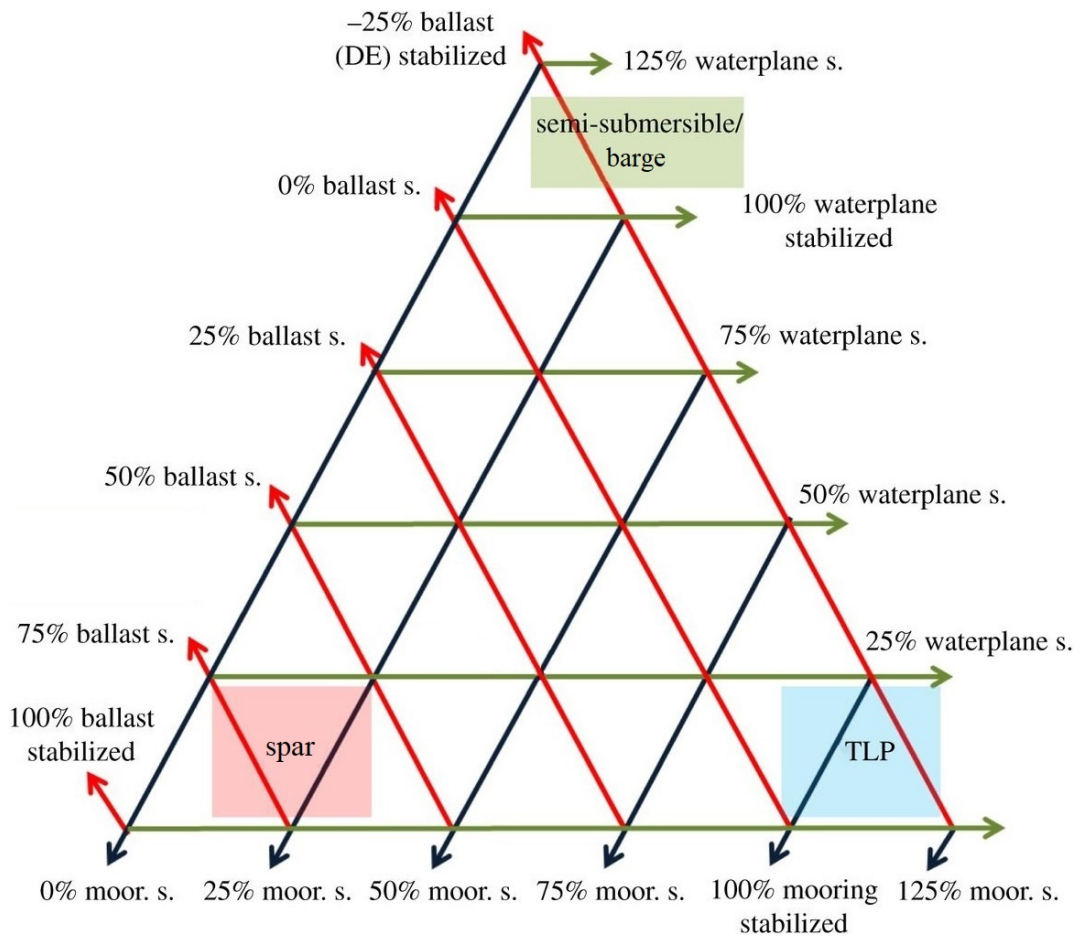


Figure 3.1: Stability triangle for floating structures, adapted from Borg & Collu (2015).

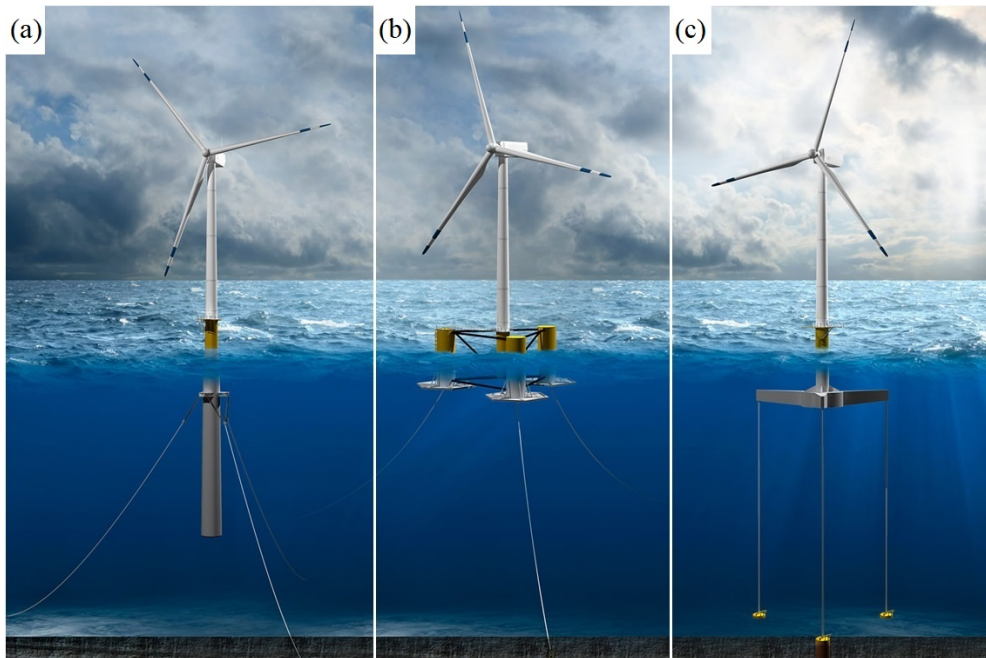


Figure 3.2: Three main floater categories (DNV GL 2017): (a) Spar, (b) Semi-submersible, (c) TLP.

at least three arms reach out where the tendons are connected. The displaced volume should be high enough to provide excess buoyancy to ensure that the mooring lines are always under tension. Special vertical load anchors are required for the mooring lines going straight down to the seabed. (Taboada 2015, Nilsson & Westin 2014)

Due to the different mooring systems (catenary mooring for spar, semi-submersible, and barge; tendons for TLP), the floaters differ in their dynamics. For the catenary-moored floaters, the natural frequencies lie below the range of wave frequencies; however, for the TLP heave, roll, and pitch natural frequencies are above the first order wave load frequencies. Some typical numbers for the system natural frequencies are presented in Table 3.1. (Taboada 2015)

Table 3.1: Representative natural frequencies of the three main floater types (Taboada 2015).

Degree of freedom	Spar	Semi-submersible/barge	TLP
Surge	0.02 Hz	0.02 Hz	0.04 Hz
Sway	0.02 Hz	0.02 Hz	0.04 Hz
Heave	0.07 Hz	0.07 Hz	0.44 Hz
Roll	0.05 Hz	0.05 Hz	0.43 Hz
Pitch	0.05 Hz	0.05 Hz	0.43 Hz
Yaw	0.02 Hz	0.02 Hz	0.04 Hz

3.1.1.2 Broad range of existing floater concepts

Most of the existing FOWT support structures can be assigned to the main categories presented in Section 3.1.1.1. Some other designs are found to be a combination of different floater types, termed hybrid concepts in the following. Finally, multi-purpose floaters exist: a structure that carries more than just one wind turbine, so-called multi-turbine concepts, or a mixed-energy design, by means of which not only wind energy but also another energy source is captured. In the following, examples of existing FOWT concepts are shortly presented. References with more details about each design are mentioned for further reading. Market study reports about existing concepts and projects are presented as well by Q FWE (2020), James & Ros (2015), Mast et al. (2015), Govindji et al. (2014), and Arapogianni et al. (2013).

Spar concepts The general principle of spar floaters is introduced in Section 3.1.1.1: a long cylindrical structure, ballasted at the bottom to obtain stability, and moored with three catenary lines. Some modifications for improving performance and floater characteristics could be a delta-connection of the mooring lines to the floater, damping or so-called vacillation fins, or a reduced draft.

Already in the 1970s a spar-type floater was proposed - Heronemus - which, however, was not technologically developed (Seymour 1992). Nowadays, the most well-known spar FOWT is the Norwegian project Hywind by Equinor (formerly Statoil), which - at that time - could

still benefit from further optimization, as the structure was heavily over-designed (Henderson & Witcher 2010). However, after just one single prototype, this floating concept is already used in the Hywind Scotland pilot park off the Scottish coast, while another larger floating wind farm - Hywind Tampen - is planned for installation in 2022 off the Norwegian coast (James & Ros 2015, ORE Catapult 2015, Rummelhoff & Bull 2015, Henderson & Witcher 2010, Matha 2009). Research is also conducted on the use of concrete: FLOAT by GH-Tecnomare is a concrete buoy (Cruz & Atcheson 2016, Henderson & Witcher 2010), the Hybrid spar by Toda Construction uses steel at the upper and concrete at the lower section (James & Ros 2015), the Universitat Politècnica de Catalunya designed an one-piece concrete structure for tower and floater (James & Ros 2015), and within the Kabashima Island Project in Japan a hybrid (concrete/steel) spar floater is developed (Mast et al. 2015, Bossler 2014). Even some advanced spars, modified for improved performance, exist already. The delta-connection, also called crowfoot connection, of the mooring lines to the structure is often used, as well as redundant mooring lines, as for example for the double taut leg buoy by Massachusetts Institute of Technology (Butterfield et al. 2007). More advanced improvements, such as reduced draft or stabilizing fins for improving sway and heave response, are integrated in the advanced spar floater within the Fukushima Floating Offshore Wind Farm Demonstration Project FORWARD in Japan by Japan Marine United (Fukushima Offshore Wind Consortium 2017, James & Ros 2015, Bossler 2014). Finally, some quite different spar floaters are developed to support a vertical axis wind turbine (VAWT). In these designs, such as the SeaTwirl by SeaTwirl Engineering in Sweden (James & Ros 2015) or the DeepWind Spar by the DeepWind Consortium (James & Ros 2015), the support structure is rotating together with the turbine.

Semi-submersible concepts The semi-submersible floater is explained in Section 3.1.1.1. In addition to the catenary-moored three- or four-cylindrical structure, heave plates are often attached to the bottom of the columns to reduce heave motion. Further improvements with respect to stability can be achieved by designing the geometry for wave-cancellation or by using an active ballast system (Liu et al. 2016). A braceless design would simplify manufacturing and inspection.

The floating structure developed by Mitsui Engineering & Shipbuilding within the Fukushima Floating Offshore Wind Farm Demonstration Project FORWARD in Japan (Fukushima Offshore Wind Consortium 2017, Liu et al. 2016, James & Ros 2015, Bossler 2014), as well as WINFLO in France (Liu et al. 2016, Henderson & Witcher 2010), VoltturnUS by the DeepCwind Consortium (James & Ros 2015), Drijfwind or FloatWind from the Netherlands (Liu et al. 2016, Henderson & Witcher 2010, Bulder et al. 2002), and VERTIWIND in France by Technip and Nenuphar for a VAWT (James & Ros 2015), represent the basic semi-submersible type with three or four columns, braces, and catenary moorings. Some simplified floaters without braces are the Dutch Tri-Floater by GustoMSC (James & Ros 2015, Butterfield et al. 2007, Musial et al. 2004), SeaReed by DCNS (James & Ros 2015), OO-Star Wind Floater in Norway by Olav Olsen (Landbø 2017b), SPINFLOAT by EOLFI for a VAWT (James & Ros 2015), and TetraFloat by TetraFloat - a special light-weight design of the entire FOWT system (James

& Ros 2015). As well braceless, but more innovative are the V-shape semi-submersible of the Japanese Fukushima Floating Offshore Wind Farm Demonstration Project FORWARD by Mitsubishi Heavy Industries (Fukushima Offshore Wind Consortium 2017, Liu et al. 2016, James & Ros 2015, Bossler 2014) and Nezy SCD by aerodyn engineering, which is a turret-moored Y-shaped structure but uses plastic-composite buoys instead of cylindrical columns (James & Ros 2015). Active ballast system is additionally used in the NAUTILUS concept by NAUTILUS Floating Solutions (NAUTILUS 2020, James & Ros 2015) and the WindFloat by Principle Power in Portugal (Liu et al. 2016, James & Ros 2015, ORE Catapult 2015, Principle Power 2015, Myhr et al. 2014, Henderson & Witcher 2010).

Barge concepts Just as a semi-submersible, a barge floater is a waterplane area stabilized structure. The main difference between these floaters, however, is that a semi-submersible has distributed buoyancy and consists of columns, while a barge is typically flat without inter-spaces.

Only a few barge-type FOWT systems exist. ITI Energy Barge (Matha 2009) is a very standard one. Floatgen by the French Ideol, however, is quite special with its concrete ring-shaped support structure utilizing a moonpool, also called damping pool, system for motion reduction (Ideol 2017, Liu et al. 2016, James & Ros 2015).

TLP concepts The TLP system is explained in Section 3.1.1.1. As a TLP is most reliant on the tendons and highly dependent on the soil conditions, improvements can be achieved through redundant mooring lines and different, more soil-insensitive, anchors.

An early design is the Eolomar ring-shaped TLP (Henderson & Witcher 2010). More contemporary and very basic is the TLP by Massachusetts Institute of Technology and National Renewable Energy Laboratory (Henderson & Witcher 2010, Matha 2009, Musial et al. 2004). GICON in Germany with GICON[®]-SOF (GICON 2016, James & Ros 2015), the American Glosten Associates with PelaStar (James & Ros 2015, ORE Catapult 2015), Iberdrola with TLPWind (ORE Catapult 2016, James & Ros 2015), and I.D.E.A.S with the TLWT (Myhr et al. 2014) have addressed the high risk problem by equipping the floater with additional mooring lines, either via an increased number of arms or a supporting redundant mooring system. The strong soil dependence is solved by DBD Systems (Eco TLP) (James & Ros 2015), Arcadis in Germany (Henderson & Witcher 2010), and the Dutch Blue H Group (BlueH) (Blue H Engineering 2017, James & Ros 2015, Henderson & Witcher 2010) with (concrete) gravity anchors.

Hybrid concepts Combination of any of the three stability mechanisms, represented by spar, semi-submersible or barge, and TLP in Figure 3.1, leads to so-called hybrid floating concepts. In this way, advantages of different systems can be combined in one floating structure.

Quite common is the tension leg buoy (TLB), which is a spar floater moored with tendons, such as the Floating Haliade by Alstom in France (Arapogianni et al. 2013), the Ocean Breeze by Xanthus Energy in UK (Arapogianni et al. 2013), the TLB series by the Norwegian Univer-

sity of Life Science (Myhr et al. 2014), and the SWAY or Karmøy in Norway (James & Ros 2015, Myhr et al. 2014, Henderson & Witcher 2010). Nautica Windpower in the US combined in the single-point moored AFT (advanced floating turbine) a TLP with a semi-submersible to support a two-bladed wind turbine (James & Ros 2015), while Concept Marine Associates added to a TLP a barge-shaped structure, which is ballasted offshore and, thus, functions as gravity-based anchor (Butterfield et al. 2007). A mixture of all three main floater categories can be found in a pendulum-stabilized floater, as realized in the AFLOWT project, where a counterweight is connected via tendons to a lightweight structure (Richard 2019). Similarly, within the Tetra Project by Stiesdal A/S, the TetraSpar allows for realization of all three floater categories - spar, semi-submersible, and TLP - by means of different arrangements of a keel which is connected with tendons to the floating structure (Stiesdal 2019).

Multi-turbine concepts Placing more than one wind turbine on top of one floater reduces the structural mass (James & Ros 2015), as well as the mooring and anchoring costs per turbine, and increases the stability (Musial et al. 2004). On the other hand, the loads on the structure might increase, the overall size is enlarged, which complicates manufacturing and handling, and the turbines are likely to operate sometimes in the wake of the other turbine(s) (James & Ros 2015, Musial et al. 2004). This needs to be considered when designing a support structure for multi-turbine utilization.

Two turbines are deployed on Hakata Bay Scale Pilot Wind Lens by the Japanese Kyushu University (Bossler 2014) and the in 2020 launched test model of Nezy² by aerodyn engineering supports from one central column twin turbines while utilizing rather a semi-submersible floater of common braceless shape and comparable size as for one single turbine (Siegfriedsen & Klumpp 2020). The semi-submersibles MUFOW (multiple unit floating offshore wind farm) (Cruz & Atcheson 2016, Henderson & Witcher 2010) and the design by Lagerwey and Herema (Henderson & Witcher 2010) even support several turbines. Hexicon by Hexicon in Sweden carries three turbines in a row (James & Ros 2015) and WindSea by FORCE Technology in Norway is a tri-floater with two upwind and one downwind turbine (James & Ros 2015, Henderson & Witcher 2010).

Mixed-energy concepts Another option for higher utilization of one floating support structure is to capture not only wind but also another energy source, such as wave, current, tidal, or solar energy. This way, the power density can be increased and the fluctuations in the power production can be balanced to some extent. However, as for the multi-turbine floater, the complexity and overall dimension of the system, as well as the loads on the system are increased (James & Ros 2015).

Such multi-energy floaters are examined in the TROPOS, MERMAID, H2OCEAN, and MARINA projects (Koundouri et al. 2017, Arapogianni et al. 2013). A quite common combination is wind and wave energy, as realized by W2power in Norway with the Pelagic Power floater (James & Ros 2015) and by Floating Power Plant in Denmark with the Poseidon P80 semi-submersible (James & Ros 2015). Wind and ocean current turbines are combined in the

SKWID (Savonius keel & wind turbine Darrieus) by MODEC in Japan (James & Ros 2015, Bossler 2014). Finally, the multi-turbine floater Hakata Bay Scale Pilot Wind Lens accommodates also solar panels (James & Ros 2015, Bossler 2014).

3.1.2 Assessment of floating support structures

The assessment of different floating support structures is carried out in two steps: first (Section 3.1.2.1), a basic SWOT analysis is performed for the three main floater categories mentioned in Section 3.1.1.1, and secondly (Section 3.1.2.4), a MCDA is carried out. The criteria, focusing on the potential for offshore wind farm deployment, as well as the selected floater concepts used in the MCDA, are defined and specified beforehand in Sections 3.1.2.2 and 3.1.2.3, respectively. Based on the results of the MCDA, the TRLs and potentials to scale up to serial production for multi-MW wind farm deployment are finally estimated (Section 3.1.2.5).

3.1.2.1 SWOT analysis

Based on the initially performed literature study the benefits and drawbacks of spars, semi-submersibles, and TLPs are presented in form of a SWOT analysis in Tables 3.2, 3.3, and 3.4, respectively.

3.1.2.2 Set of criteria

FOWT support structures can be assessed based on different criteria, as realized by Mone et al. (2017), Kolios, Mytilinou, Lozano-Minguez & Salonitis (2016), Kolios, Rodriguez-Tsouroukdissian & Salonitis (2016), Taboada (2015), Lozano-Minguez et al. (2011), and Kolios, Collu, Chahardehi, Brennan & Patel (2010). This study, however, focuses on offshore wind farm deployment. Thus, the following ten criteria are specified as presented in Table 3.5, with a (+)/(-) indicating a positive/negative criterion, meaning that a higher score corresponds to a more positive/negative aspect for the floater.

3.1.2.3 Set of alternatives

The assessed floaters are specified in Table 3.6 according to the categorization in Section 3.1.1.2.

Table 3.2: SWOT analysis of the spar floater concept.

Strengths	Weaknesses
<ul style="list-style-type: none"> ● Inherent stability (Kolios, Rodriguez-Tsouroukdissian & Salonitis 2016, Liu et al. 2016, James & Ros 2015, Mast et al. 2015, Taboada 2015, Nilsson & Westin 2014, Bossler 2014, Kolios, Collu, Chahardehi, Brennan & Patel 2010, Butterfield et al. 2007) ● Suitability for even higher sea states (Butterfield et al. 2007) ● Soil condition insensitivity (Nilsson & Westin 2014, Butterfield et al. 2007) ● Simple mooring system, as well as cheap and simple anchoring system (Liu et al. 2016, Taboada 2015, Musial et al. 2004) ● Low operational risk (Bossler 2014) ● Little susceptibility to corrosion (Butterfield et al. 2007) ● Simple structure, easy manufacturing and maintenance (James & Ros 2015, Mast et al. 2015, Taboada 2015, Nilsson & Westin 2014, Butterfield et al. 2007) 	<ul style="list-style-type: none"> ● Relative large motions (Henderson & Witcher 2010) ● Unsuitability for shallow water (Kolios, Rodriguez-Tsouroukdissian & Salonitis 2016, James & Ros 2015, Mast et al. 2015, Taboada 2015, Govindji et al. 2014, Nilsson & Westin 2014, Bossler 2014, Henderson & Witcher 2010, Kolios, Collu, Chahardehi, Brennan & Patel 2010, Butterfield et al. 2007) ● Large seabed footprint (Mast et al. 2015) ● Long mooring lines (costs) (Butterfield et al. 2007) ● Assembly in sheltered deep water (Liu et al. 2016, Mast et al. 2015, Nilsson & Westin 2014, Bossler 2014) ● Challenging, time-consuming, and costly float-out and installation (Liu et al. 2016, James & Ros 2015, Mast et al. 2015, Nilsson & Westin 2014, Bossler 2014, Butterfield et al. 2007) ● Long and heavy structure (costs) (Taboada 2015, Butterfield et al. 2007) ● High fatigue loads in tower base (Mast et al. 2015)
Opportunities	Threats
<ul style="list-style-type: none"> ● Serial fabrication and synergies with tower manufacturing (James & Ros 2015, Mast et al. 2015, Taboada 2015, Nilsson & Westin 2014, Butterfield et al. 2007) ● Delta-connection for yaw stabilization ● Stabilizing fins for sway and heave stabilization (James & Ros 2015, Govindji et al. 2014) ● Horizontal transportation (Butterfield et al. 2007) ● High TRL (Nilsson & Westin 2014) 	<ul style="list-style-type: none"> ● Need for special purpose vessels (Nilsson & Westin 2014) ● No global market (Nilsson & Westin 2014)

Table 3.3: SWOT analysis of the semi-submersible floater concept.

Strengths	Weaknesses
<ul style="list-style-type: none"> • Heave plates for heave response reduction (Liu et al. 2016, Mast et al. 2015) • Wide weather window for float-out and installation (Butterfield et al. 2007) • Depth independence (Kolios, Rodriguez-Tsouroukdissian & Salonitis 2016, James & Ros 2015, Mast et al. 2015, Taboada 2015, Nilsson & Westin 2014, Henderson & Witcher 2010, Kolios, Collu, Chahardehi, Brennan & Patel 2010, Butterfield et al. 2007) • Soil condition insensitivity (Mast et al. 2015, Nilsson & Westin 2014, Butterfield et al. 2007) • Simple mooring system, as well as cheap and simple anchoring system (Liu et al. 2016, Taboada 2015, Butterfield et al. 2007, Musial et al. 2004) • Low overall risk (Zhang et al. 2016, Nilsson & Westin 2014) • Onshore or dry dock assembly (Liu et al. 2016, Taboada 2015, Nilsson & Westin 2014, Butterfield et al. 2007) • Simple installation and decommissioning (Kolios, Rodriguez-Tsouroukdissian & Salonitis 2016, James & Ros 2015, Mast et al. 2015, Nilsson & Westin 2014, Henderson & Witcher 2010, Butterfield et al. 2007) 	<ul style="list-style-type: none"> • Lower stability and higher motions (Kolios, Rodriguez-Tsouroukdissian & Salonitis 2016, Mast et al. 2015, Nilsson & Westin 2014, Bossler 2014, Kolios, Collu, Chahardehi, Brennan & Patel 2010, Butterfield et al. 2007) • Wave sensitivity • Large seabed footprint (Mast et al. 2015) • Long mooring lines (costs) (Butterfield et al. 2007) • Susceptibility to corrosion and ice-loads (Mast et al. 2015, Taboada 2015, Nilsson & Westin 2014, Butterfield et al. 2007, Musial et al. 2004) • Challenging manufacturing and maintenance due to large and complex structure (James & Ros 2015, Mast et al. 2015, Taboada 2015, Nilsson & Westin 2014) • Large and heavy structure (costs) (James & Ros 2015, Taboada 2015, Nilsson & Westin 2014, Henderson & Witcher 2010, Butterfield et al. 2007) • Larger impact on turbine due to motions (Kolios, Rodriguez-Tsouroukdissian & Salonitis 2016, Mast et al. 2015, Nilsson & Westin 2014, Kolios, Collu, Chahardehi, Brennan & Patel 2010, Butterfield et al. 2007)
Opportunities	Threats
<ul style="list-style-type: none"> • Cost reduction through mass production and braceless design (Nilsson & Westin 2014) • Geometry for wave-cancellation (Liu et al. 2016, Taboada 2015) • Stabilizing active ballast system (James & Ros 2015) • High TRL (Nilsson & Westin 2014) • Large global market (Nilsson & Westin 2014) • Suitability for multi-turbine concepts (Taboada 2015) 	<ul style="list-style-type: none"> • Large internal forces if geometry designed for wave-cancellation (Taboada 2015) • Costly active ballast system (James & Ros 2015) • High competition (Nilsson & Westin 2014)

Table 3.4: SWOT analysis of the TLP floater concept.

Strengths	Weaknesses
<ul style="list-style-type: none"> • High stability and low motions (Liu et al. 2016, James & Ros 2015, Mast et al. 2015, Taboada 2015, Nilsson & Westin 2014, Bossler 2014, Henderson & Witcher 2010, Musial et al. 2004) • Little wave sensitivity (in case of submerged platform) (Kolios, Rodriguez-Tsouroukdissian & Salonitis 2016, Kolios, Collu, Chahardehi, Brennan & Patel 2010) • Suitability for even high sea states (in case of submerged platform) (Butterfield et al. 2007) • Suitability for intermediate depths (Mast et al. 2015, Henderson & Witcher 2010) • Small seabed footprint (Mast et al. 2015, Taboada 2015, Nilsson & Westin 2014, Butterfield et al. 2007, Musial et al. 2004) • Short mooring lines (Nilsson & Westin 2014, Butterfield et al. 2007) • Little susceptibility to corrosion (in case of submerged platform) (Butterfield et al. 2007) • Simple, small, and light structure and easy maintenance (James & Ros 2015, Mast et al. 2015, Taboada 2015) • Onshore or dry dock assembly (James & Ros 2015, Mast et al. 2015) 	<ul style="list-style-type: none"> • Unsuitability for strong tidal currents or storm surges (Mast et al. 2015, Taboada 2015, Govindji et al. 2014, Nilsson & Westin 2014, Bossler 2014, Butterfield et al. 2007) • Unsuitability for shallow water • Unsuitability for challenging soil conditions (Mast et al. 2015, Taboada 2015, Govindji et al. 2014, Nilsson & Westin 2014, Bossler 2014, Butterfield et al. 2007) • Complex and costly mooring and anchoring system (Liu et al. 2016, James & Ros 2015, Nilsson & Westin 2014, Butterfield et al. 2007, Musial et al. 2004) • High risk if tendon or anchor fails (Liu et al. 2016, James & Ros 2015, Taboada 2015, Bossler 2014, Henderson & Witcher 2010) • Complex and risky installation and disconnection for onshore maintenance (Kolios, Rodriguez-Tsouroukdissian & Salonitis 2016, Liu et al. 2016, James & Ros 2015, Mast et al. 2015, Taboada 2015, Nilsson & Westin 2014, Henderson & Witcher 2010, Kolios, Collu, Chahardehi, Brennan & Patel 2010, Butterfield et al. 2007, Musial et al. 2004) • Large stresses in structure (James & Ros 2015, Butterfield et al. 2007)
Opportunities	Threats
<ul style="list-style-type: none"> • Low mass production cost (Nilsson & Westin 2014) • Redundant moorings for risk reduction • Less soil dependent gravity anchors • Low competition (Nilsson & Westin 2014) 	<ul style="list-style-type: none"> • Need for special purpose installation ships (Nilsson & Westin 2014) • Low TRL (Nilsson & Westin 2014) • No global market (Nilsson & Westin 2014)

Table 3.5: Set of criteria.

Criterion	Included aspects	Type
1. LCoE	Levelized cost of energy (LCoE), rate of return, power density, outer dimension, mooring footprint, turbine spacing	(-)
2. Volume production	Ease of manufacturing, modular structure, fabrication time, on-shore fabrication	(+)
3. Ease of handling	Outer dimension, total weight, assembly, transport, installation, decommissioning, required equipment and vessels	(+)
4. Durability	Corrosion resistance, fatigue resistance, redundancy, aging	(+)
5. Flexibility	Offshore site, water depth, soil condition, environmental loading	(+)
6. Certification	Time to achieve, ease to achieve, TRL	(+)
7. Performance	Deflections, displacements, nacelle acceleration, dynamic response, overturning resistance, torsion resistance	(+)
8. Maintenance	Frequency, redundant components, costs, downtime	(-)
9. Time-efficiency	Assembly, transport, installation, maintenance, decommissioning	(+)
10. Mooring requirements	Number of mooring lines, motions with respect to need of flexible cables, length of lines, anchoring system costs	(-)

3.1.2.4 MCDA via TOPSIS

Several approaches, such as weighted sum or product methods (WSM/WPM), TOPSIS, AHP, ELECTRE (elimination et choix traduisant la réalité), and PROMETHEE (preference ranking organization method for enrichment evaluation) can be used to rank alternatives, taking account of multiple criteria. Based on studies applying and comparing MCDA methods for the assessment of offshore wind turbine support structures (Kolios, Mytilinou, Lozano-Minguez & Salonitis 2016, Kolios, Rodriguez-Tsouroukdissian & Salonitis 2016, Lozano-Minguez et al. 2011, Kolios, Collu, Chahardehi, Brennan & Patel 2010), TOPSIS is selected in this work, as it is based on easy, robust calculation methods, deals with criteria of quantitative or qualitative nature, and incorporates expert opinions (Lozano-Minguez et al. 2011, Kolios, Collu, Chahardehi, Brennan & Patel 2010). The basis of TOPSIS is a set of alternatives and criteria, as specified in Sections 3.1.2.2 and 3.1.2.3. By means of a survey, scores for each criterion are assigned to each alternative, in this study from 1 (least applicable) to 5 (most applicable), and weights are set to represent the importance of each criterion with respect to offshore wind farm deployment, here again values between 1 (not important) and 5 (very important). The scores yield a decision matrix, which is - after normalization - multiplied with the weight vector. The final ranking of the alternatives is obtained based on their closeness to the positive ideal solution and distance to the negative ideal solution. (Kolios, Rodriguez-Tsouroukdissian & Salonitis 2016, Kolios, Collu, Chahardehi, Brennan & Patel 2010)

Table 3.6: Set of alternatives.

Alternative	Description
I. Spar - standard	Common spar floater type
II. Spar - advanced	Improved spar (reduced draft, vacillation fins, crowfoot/delta mooring connection, horizontal transportation methodology)
III. Semi-submersible - standard	Common semi-submersible floater type
IV. Semi-submersible - advanced	Improved semi-submersible (braceless, wave-cancelling geometry, inclined/shape-optimized columns, active ballast system)
V. Barge floater	Common barge floater type
VI. TLP - standard	Common TLP floater type
VII. TLP - advanced	Improved TLP (redundant mooring lines, gravity anchors)
VIII. Hybrid floater	Mixed spar, semi-submersible, TLP floater types
IX. Multi-turbine floater	Floater supporting more than one wind turbine
X. Mixed-energy floater	Floater for wind and wave/tidal/current/photovoltaic utilization

The survey is sent to knowledgeable academic, as well as industrial experts in the field of floating offshore wind and is answered completely by seven individuals. These seven participants have on average more than five and a half years of experience in floating offshore wind energy, ranging individually from one and a half year to even ten years.

The survey results are presented in Table 3.7 in form of the mean values of scores (decision matrix) and weights (weight vector), as well as the final TOPSIS score and position. Even if the results depend on the specified categorization and general assumptions, e.g. use of the same wind turbine, costs (indicated in green) proved to be still most important, as Habib Dagher stated (Kosowatz 2015): “Each solution has its pros and cons. There’s lots of solutions out there. The bottom line is what is most cost-effective at the end of the day.” Flexibility - on the other hand - is judged to be least important, as stressed out by a red colored value. From the considered concepts, the advanced spar ranks first - emphasized through green colored values - directly followed by standard spar and advanced semi-submersible, whereas the TLP (written in red) makes up the tail. Thus, advanced spars and semi-submersibles are assessed to be most suitable for deployment in offshore wind farms, which is especially due to the high opportunity for volume production and certification, as well as the low LCoE and mooring requirements in case of the advanced or standard spar, and due to the easy handling, high flexibility and low mooring requirements for the advanced semi-submersible. On the other hand, handling, certification, mooring requirements, and also maintenance are the criteria that let TLPs fail in the comparison.

Table 3.7: Decision matrix, weight vector, and TOPSIS scores and positions, based on survey results; most/least important criteria and alternatives with highest/lowest scores are written in green/red.

	1	2	3	4	5	6	7	8	9	10	Score	Pos.
I	3.20	4.00	3.00	3.00	3.20	3.40	3.00	3.40	3.20	3.40	0.651	2
II	3.17	4.33	3.17	3.33	3.33	3.17	3.17	3.50	3.17	2.83	0.763	1
III	3.50	2.83	3.50	3.33	3.50	3.17	2.83	3.50	2.83	3.00	0.532	5
IV	3.50	3.17	3.67	3.50	3.50	2.83	3.17	3.33	2.83	2.83	0.600	3
V	3.67	3.67	3.17	3.00	2.67	3.20	2.67	3.00	2.67	3.00	0.549	4
VI	3.43	3.00	2.57	3.14	2.43	2.83	3.33	3.50	3.33	4.33	0.319	10
VII	3.33	3.00	2.17	3.50	3.00	2.50	3.33	3.50	3.33	4.00	0.335	9
VIII	3.67	3.17	3.17	3.17	2.83	2.83	3.17	3.33	3.17	3.83	0.425	7
IX	3.33	3.00	2.83	3.33	3.00	2.50	3.33	3.17	3.00	3.33	0.436	6
X	3.67	2.83	2.67	3.17	3.50	2.67	2.67	3.17	2.83	3.17	0.390	8
Wgt.	4.26	3.43	2.91	3.24	2.33	3.40	3.38	3.59	3.02	3.06		

Apart from the mean values of the survey results, the standard deviations among the answers from the survey participants are at least as important. These are presented for the decision matrix and weight vector in Table 3.8, including also averaged values for the standard devia-

Table 3.8: Standard deviations among survey participants for decision matrix and weight vector; highest/lowest agreement indicated through green/red colored values.

	1	2	3	4	5	6	7	8	9	10	Avg.
I	1.48	1.41	1.22	0.71	1.30	0.89	0.00	0.55	1.30	1.34	1.02
II	1.33	1.03	1.17	0.82	1.21	0.98	0.75	0.55	1.17	1.17	1.02
III	1.05	1.17	1.05	0.82	0.84	0.98	0.75	0.84	0.75	1.10	0.93
IV	1.05	0.98	1.03	0.55	1.22	0.75	0.75	0.82	0.75	0.98	0.89
V	1.03	0.82	0.41	1.67	0.52	0.45	1.21	1.10	0.82	1.10	0.91
VI	1.27	1.10	1.51	0.69	0.79	1.17	1.03	1.05	1.37	1.21	1.12
VII	1.37	1.10	1.17	0.55	0.63	1.05	1.03	0.55	1.37	1.10	0.99
VIII	0.82	1.17	1.17	0.75	0.75	1.33	0.75	1.03	0.75	0.75	0.93
IX	1.03	1.10	1.33	1.03	0.89	1.38	1.21	1.33	1.10	1.21	1.16
X	1.51	0.98	1.37	1.17	1.38	1.51	1.21	1.60	1.33	1.47	1.35
Avg.	1.19	1.09	1.14	0.88	0.95	1.05	0.87	0.94	1.07	1.14	
Wgt.	1.83	1.47	1.45	1.44	1.50	1.55	1.60	1.46	1.61	1.40	

tions of each concept alternative and each criterion. This shows that all survey respondents agree on the performance of standard spars, while on average they are most confident with the advanced semi-submersible, as emphasized through green colored values. This good agreement underlines the meaningfulness of the TOPSIS result for the most potential floater concepts. The largest discrepancy in the survey responses is found in the durability of barge floaters; however, the survey participants seem to be most uncertain about mixed-energy floaters in general - both stressed through red colored values. Looking at the criteria, the difference in the answers is the largest for the LCoE, both in decision matrix and weight vector. This large deviation is striking, but still does not affect the clear outcome that cost is the most important criterion. The best agreement in weighting the criteria concerns the mooring requirements, while on average the smallest deviation in the decision matrix has the performance of floating concepts.

3.1.2.5 TRLs of floater concepts

The TRL gives a measure of the development status of a technology, which is - according to Horizon 2020 definition (European Commission 2013) - as follows:

1. basic principles observed;
2. technology concept formulated;
3. experimental proof of concept;
4. technology validated in lab;
5. technology validated in relevant environment;
6. technology demonstrated in relevant environment;
7. system prototype demonstration in operational environment;
8. system complete and qualified;
9. actual system proven in operational environment.

TRL estimates for different FOWT concepts are given by James & Ros (2015) and ORE Catapult (2015) and are also obtained through the survey. Based on this, the different floater categories are ranked with respect to their TRLs, as well as their potential to scale up to mass production for multi-MW wind farm deployment (TOPSIS score), as visualized in Figure 3.3, with the size of the bubbles representing the standard deviation among the answers from the survey participants for the TRL values.

From Figure 3.3 it becomes clear that TRLs and TOPSIS scores are kind of correlated. While the standard concepts of spar, semi-submersible, and TLP are located above the imaginary correlation line, their advanced equivalents are positioned lower. This emphasizes the already high maturity of the standard concepts for FOWT platforms, as well as their increased potential after further improvements and advancements.

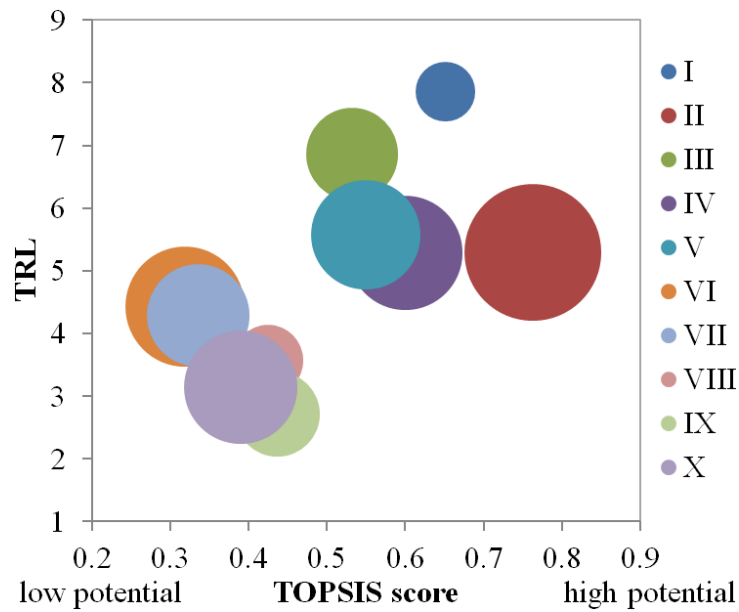


Figure 3.3: TRL (with the standard deviation represented by the size of the bubble) versus potential for wind farm deployment (TOPSIS score).

3.2 Reference spar-buoy floating wind turbine system

As the survey, conducted and analyzed in Section 3.1.2.4, reveals that the advanced spar - directly followed by the most developed standard spar - has the highest potential for multi-MW wind farm deployment, the well-known reference FOWT system from phase IV of the OC3 (offshore code comparison collaboration) project (Jonkman & Musial 2010), as visualized in Figure 3.4, is selected as basis for the optimization applications presented in Chapters 5 and



Figure 3.4: The OC3 phase IV spar-buoy FOWT system (Jonkman 2010).

6. This floating system consists of the NREL (National Renewable Energy Laboratory) 5 MW reference wind turbine (Jonkman et al. 2009) with an offshore adapted tower (Section 3.2.1), supported by a moored spar-buoy floating structure (Section 3.2.2). The entire FOWT system is specified for a site with 320 m water depth and a water density of 1025 kg/m^3 , and the overall system structural mass - rotor-nacelle assembly (RNA), tower, and floater including ballast - amounts to $8.066 \times 10^6 \text{ kg}$.

3.2.1 Wind turbine and tower

The OC3 phase IV floating platform carries the upwind, three-bladed NREL 5 MW reference wind turbine (wind turbine class I) (Jonkman et al. 2009), adjusted for the floating system. While the RNA, as well as the blade (aerodynamic) properties remain unchanged as defined for the NREL 5 MW turbine by Jonkman et al. (2009), a modified tower (Jonkman 2010) is used for the OC3 phase IV spar-buoy floating wind turbine system to fit the platform top cylinder diameter and to maintain the hub height. Furthermore, the wind turbine control system parameters are retuned in phase IV of OC3, to avoid negative damping effects due to the floating system. The specified wind turbine properties of the RNA and tapered tower are presented in Tables 3.9 and 3.10, respectively, with elevations given as distance above the still water level (SWL).

Table 3.9: Properties of the wind turbine RNA of the FOWT system from OC3 phase IV (Jonkman 2010, Jonkman et al. 2009).

Parameter	Value
Rotor diameter	126.0 m
Hub height	90.0 m
Mass	$350.0 \times 10^3 \text{ kg}$
Cut-in, rated, cut-out wind speed	3.0 m/s, 11.4 m/s, 25.0 m/s
Integral controller gain	0.0008965149
Proportional controller gain	0.006275604 s

Table 3.10: Properties of the tower of the FOWT system from OC3 phase IV (Jonkman 2010).

Parameter	Value
Top elevation, diameter, thickness	87.6 m, 3.9 m, 0.019 m
Base elevation, diameter, thickness	10.0 m, 6.5 m, 0.027 m
Material density	$8,500 \text{ kg/m}^3$
Mass	$249.7 \times 10^3 \text{ kg}$
Center of tower mass (above SWL along central axis)	43.4 m

3.2.2 Floating structure and station-keeping system

The platform of the OC3 phase IV FOWT system is a spar-buoy, which is based on the Hywind floater. The spar-buoy floater consists of two cylindrical elements - an upper column (UC), which matches the tower base diameter of 6.5 m, and a base column (BC) - with one tapered part between them and is partially filled with ballast. The main structural parameters are provided in the definition of the FOWT system (Jonkman 2010). Comparison of the specified values shows that the dimensions - apart from the improved and reduced draft of the real systems - lie in between the dimensions of the Hywind Demo for a 2.3 MW wind turbine and the Hywind Scotland floater supporting a 6.0 MW wind turbine (Equinor 2020a). The geometrical parameters are presented in Table 3.11 and indicated, using green color, in a schematic drawing of the OC3 phase IV spar-buoy (Figure 3.5). Distances to the top and bottom ends of the floating structure are measured with respect to SWL.

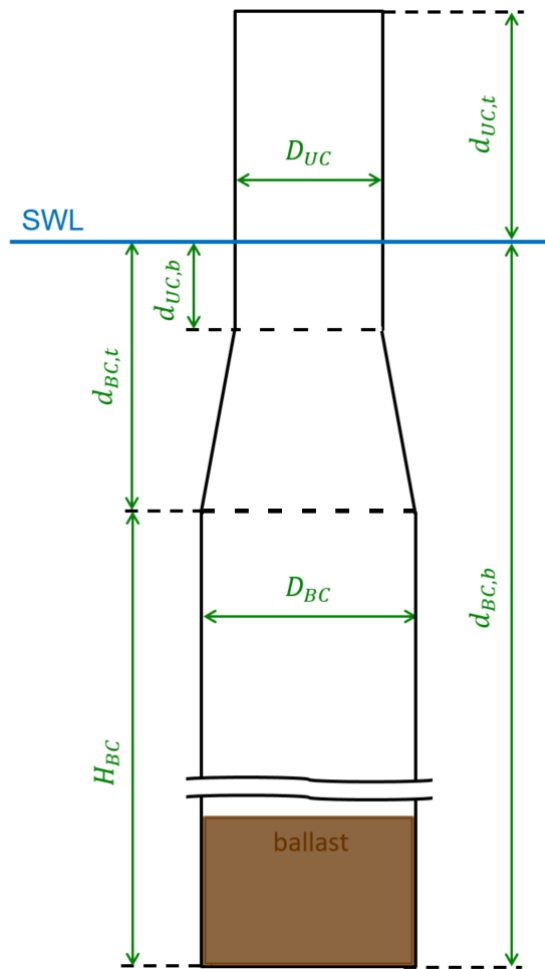


Figure 3.5: Schematic of the OC3 phase IV spar-buoy, geometric parameters indicated in green.

Table 3.11: Geometrical parameters of the OC3 phase IV spar-buoy (Jonkman 2010).

Parameter	Symbol	Value
Upper column diameter	D_{UC}	6.5 m
Base column diameter	D_{BC}	9.4 m
Distance to top of upper column	$d_{UC,t}$	10.0 m
Distance to base of upper column	$d_{UC,b}$	4.0 m
Distance to top of base column	$d_{BC,t}$	12.0 m
Distance to base of base column	$d_{BC,b}$	120.0 m
Height of base column	H_{BC}	108.0 m

In addition to the geometrical spar-buoy parameters, given in Table 3.11, some mass-related properties are provided by Jonkman (2010) and presented in Table 3.12. Furthermore, for the hydrodynamic characteristics of the floating platform, the added mass coefficient is given as 0.969954 (Jonkman 2010), which is close to the typical value of 1 for circular cylinders (Sumer & Fredsøe 2006), while the viscous-drag coefficient amounts to 0.6 (Jonkman 2010) and corresponds to the common value at high Reynolds number, which is already prevailing at low flow velocities for a large diameter structure as this spar-buoy (Sumer & Fredsøe 2006, Clauss et al. 1992). The hydrostatic buoyancy force, determined from the displaced water volume, is stated as 80,708,100 N (Jonkman 2010). To get closer to the Hywind floater characteristics, additional linear damping in surge and sway of 100×10^3 Ns/m each, in heave of 130×10^3 Ns/m, and in yaw of 13×10^6 Nms/rad are applied per definition by Jonkman (2010).

Table 3.12: Mass-related properties of the OC3 phase IV spar-buoy (Jonkman 2010).

Parameter	Value
Platform mass (including ballast)	746.63×10^4 kg
Center of platform mass (below SWL along central axis)	89.9155 m
Platform roll inertia (about center of mass)	422.923×10^7 kgm ²
Platform pitch inertia (about center of mass)	422.923×10^7 kgm ²
Platform yaw inertia (about central axis)	164.23×10^6 kgm ²

The floating spar-buoy is moored to the seabed by means of three evenly spaced catenary mooring lines. The main properties of the station-keeping system are presented in Table 3.13. As this mooring system is a simplified version of the station-keeping system used for the Hywind floater, in which a delta connection is realized, an additional yaw spring stiffness of 98.34×10^6 Nm/rad has to be considered to correct for this (Jonkman 2010).

Table 3.13: Properties of the station-keeping system of the FOWT system from OC3 phase IV (Jonkman 2010).

Parameter	Value
Fairleads depth, radius from centerline	70.0 m, 5.2 m
Anchors depth, radius from centerline	320.0 m, 853.9 m
Mooring line length (unstretched), diameter	902.2 m, 0.09 m
Mooring line mass density	77.7066 kg/m
Mooring line length-related weight in water	698.094 N/m
Mooring line extensional stiffness	384.243×10^3 N

Chapter 4

Modeling, automated simulation, and optimization

FOWTs have to withstand various loadings, static and dynamic, structural and environmental. In comparison to onshore systems, offshore wind turbines have to deal with hydrodynamic loads in addition to wind loads. For FOWTs, the system complexity increases even more. Apart from the environmental loads from wind, waves, currents, tides, and sea ice, the motion of the floating system leads to relative velocities, which have to be accounted for in the aerodynamic and hydrodynamic load calculations. Variable buoyancy loads are as well a consequence of the free motion of the system. Nevertheless, to keep the floater within a specific site, FOWTs have an additional component - the mooring system. Thus, a FOWT system implies motion couplings, several different loading components, as well as non-linearities. In addition to the external factors, which place already high demands on the design of a wind turbine system, also other requirements related to costs, manufacturing, size, performance, and system safety have to be met. This makes the development of FOWTs a highly iterative process, in which the evolving designs are tested, analyzed, and modified accordingly until an optimized design is achieved. (Sirnivas et al. 2014, Zhang et al. 2013, Butterfield et al. 2007, Wayman 2006)

For this reason, modeling, simulation, and optimization techniques are crucial for the highly complex, labor-intensive, and extensive assessment and development of FOWT system designs. However, it has to be ensured that the physical equations are correctly implemented in the code and the system behavior is realistically represented by the model. This is to be proved through verification and validation, with the latter requiring in addition real measurements or test data. Afterwards, to cope with the large number of simulations, needed to assess and develop such a FOWT system design in detail, but also to support design optimization processes, in which iterative simulations have to be performed, automation of simulation executions and optimization procedures is indispensable. Thus, in this chapter, first (Section 4.1), an aero-hydro-servo-elastic coupled model of dynamics for the reference spar-buoy FOWT

Note: This chapter is based on the publication by Leimeister, Kolios & Collu (2020a), as well as the publications by Leimeister, Kolios & Collu (2020b) and Leimeister (2019).

system, specified in Section 3.2, is developed and verified. This model can then be integrated in a holistic simulation and optimization framework, which is presented in Section 4.2 and by which means iterative simulations within the FOWT design assessment and development process can be managed and executed in an automated and high-performance manner.

4.1 Development and verification of an aero-hydro-servo-elastic coupled model of dynamics for FOWTs, based on MoWiT

Within the IEA (International Energy Agency) Wind Task 23 Subtask 2, the OC3 project was developed to verify offshore wind turbine codes based on code-to-code comparison works (Jonkman & Musial 2010). The participants of OC3 phase IV, which is on verifying a model of a spar-buoy FOWT system as described in Section 3.2 (Jonkman 2010), used various aero-hydro-servo-elastic modeling approaches as presented in Figure 4.1. Very common and widely used tools are among others Bladed, HAWC2, and FAST. The wind turbine design software Bladed is a commercial software by DNV GL (Det Norske Veritas and Germanischer Lloyd), which is highly established and continuously enhanced in each newer version, is applied for system simulations, design, and certification, and has further advanced modules for specific applications such as advanced hydrodynamic calculations (DNV GL 2018a,b). Another commercial aero-elastic code for wind turbine system simulation and response calculation is HAWC2 (horizontal axis wind turbine simulation code 2nd generation) developed at DTU (Technical University of Denmark) Risø Campus, which no longer only is used for aero-elastic simulations but also can represent floating systems (Larsen & Hansen 2015). As well commercial, but right now also transferred to open-source development, is FAST (fatigue, aerodynamics, structures, and turbulence) - a simulation tool developed and used at NREL for coupled analyses of horizontal axis wind turbines, which can be combined with several other programs and

Bladed	HAWC2	FAST	ADAMS	SESAM/DeepC	Simo	3Dfloat	MoWiT
Code developer							
GH	Risø-DTU	NREL	MSC + NREL + LUH	DNV	MARINTEK	IFE-UMB	IWES
OC3 participant							
GH	Risø-DTU	NREL POSTECH	NREL LUH	Acciona NTNU	MARINTEK	IFE-UMB	IWES
Aerodynamics (aero)							
(BEM / GDW) + DS				none	BEM	(BEM / GDW)	(BEM / GDW) + DS
Hydrodynamics (hydro)							
(Airy+ / Stream) + ME	Airy + ME	(Airy+ + ME) / (Airy + ME + PF)			Airy + ME + PF	Airy + ME	Airy + WS + (ME / MCF)
Control system (servo)							
DLL	DLL / UDS / SM		DLL / UDS		none	DLL	UDS
Structural dynamics (elastic)							
Turbine							
FEMP	MBD / FEM	FEMP + (Modal / MBD)	MBD		MBD	FEM	(FEM / Modal) + MBD
Mooring							
UDFD		QSCE	QSCE / UDFD	QSCE / FEM	QSCE / MBD	FEM / UDFD	MBD

Figure 4.1: Aero-hydro-servo-elastic modeling approaches of the OC3 phase IV participants (Jonkman & Musial 2010) and IWES.

packages for further advanced and detailed analyses, such as structural finite element analysis (Jonkman & Buhl 2005). Further software and modeling tools are for example ADAMS (automatic dynamic analysis of mechanical systems) by MSC Software for simulating multi-body dynamics of mechanical systems, which can as well be applied to FOWTs (Withee 2004); SIMO (simulation of marine operations) by the Norwegian Marine Technology Research Institute (MARINTEK) for floating systems (originally mainly vessels) simulation, which can be advanced by means of the code RIFLEX for non-linear mooring line dynamics, coupled with HAWC2, and also be used for wind turbine systems by incorporating an external aerodynamic module (SINTEF Ocean 2017); 3Dfloat developed at the Institute for Energy Technology at the (then called) University of Life Sciences (IFE-UMB) for fully-coupled simulation and advanced analyses of offshore structures, such as FOWTs (Nygaard et al. 2016); or SESAM software with the DeepC module by DNV GL for simulation and (un-)coupled analyses of floating structures and station-keeping systems, which however require a separate approach for integrating aerodynamics for a full offshore wind turbine system (Zhang et al. 2013). More detailed reviews of the utilized modeling tools are provided by Liu et al. (2016) and Cordle & Jonkman (2011) and the physics and theories implemented in the tools - all abbreviations mentioned under aerodynamics, hydrodynamics, control system, and structural dynamics in Figure 4.1 - are described in more detail in Sections 4.1.1.1 and 4.1.2.2.

The results from these offshore code-to-code comparisons are used to verify a model of the floating spar-buoy wind turbine system from phase IV of OC3 (Jonkman 2010) - particularized in Section 3.2 - which is implemented in MoWiT (Modelica[®] library for wind turbines)¹, a library developed at Fraunhofer IWES (Institute for Wind Energy Systems), based on the object-oriented and equation-based modeling language Modelica[®] (Modelica Association 2020a). One advantage - out of several more highlighted in more detail in Section 4.2.1.4 - of using Modelica[®] for modeling wind turbine systems is the hierarchical programming, by which means the complex system can be subdivided into single components. Thus, this component-based library MoWiT allows for modifications and replacements of individual component models, so that modeling and simulation of different system designs and boundary conditions can be realized. Furthermore, due to the possibility to couple MoWiT models to Python scripts - as done and described in Section 4.2 - many more doors are being open for automated simulations, such as for design load case calculations, post-processing and analyses of simulation results, as well as other extensive tasks and applications, such as system optimization. However, all these benefits would be as good as useless if the model and code is not yet verified.

Thus, a fully-coupled system model of dynamics for the FOWT from phase IV of OC3, defined in Section 3.2, is developed based on MoWiT (Section 4.1.1). Afterwards, the main task of verifying this model is performed based on code-to-code comparison works and results are presented in Section 4.1.2. More detailed discussion and analyses of the results follow in Section 4.1.3.

¹Formerly OneWind Modelica library.

4.1.1 Modeling of the OC3 phase IV FOWT system in MoWiT

Modeling of a FOWT system can be done by means of various software architectures, which are based on different simulation codes with varying capabilities for aero-hydro-servo-elastic calculations, as pointed out by Liu et al. (2016) and Cordle & Jonkman (2011). Within the OC3 project, the floating spar-buoy wind turbine system from phase IV, as described in Section 3.2, was modeled by the project participants in different codes and tools for wind turbine system simulation, as already introduced and presented in Figure 4.1, to be compared and verified within the study (Jonkman & Musial 2010). For the same purpose of code verification and to add one more result to the cross-code comparison, the OC3 phase IV FOWT is implemented in the modeling language Modelica[®], using MoWiT for fully-coupled aero-hydro-servo-elastic dynamic simulation of wind turbine systems. In the following, first (Section 4.1.1.1), this library and the modeling environment is introduced briefly to point out the advantages and capabilities of this tool. Afterwards (Section 4.1.1.2), the methodology of implementing the OC3 phase IV FOWT system is outlined, demonstrating as well difficulties which arose and assumptions that had to be made.

4.1.1.1 MoWiT - the Modelica[®] library for wind turbines

MoWiT, which is developed at Fraunhofer IWES, allows modeling of state-of-the-art onshore or offshore wind turbine systems to be simulated in Dymola[®], the dynamic modeling laboratory by Dassault Systèmes (Dassault Systèmes 2015*a,b*), for load calculations and further analyses. The component-based library is based on the object-oriented and equation-based open-source modeling language Modelica[®]. The hierarchical structure of programming in Modelica[®], as well as the multibody approach adopted in Modelica[®], benefit the modeling of such a complex system as a FOWT. Hence, the wind turbine system is broken down into single components (main and subcomponents), as shown in Figure 4.2, which are modeled separately and interconnected to represent correctly couplings and interactions between them. This structure also allows fast and easy exchange of single components to model different wind turbine technologies, turbine or support structure designs, control strategies, or site and environmental conditions. Furthermore, as MoWiT is under development by Fraunhofer IWES, code modifications, optimizations, and enhancements are always possible. (Leimeister & Thomas 2017*a*, Thomas et al. 2014, Strobel et al. 2011)

As presented in Figure 4.2, a FOWT - such as the OC3 phase IV spar-buoy system shown as well in Figure 4.3, together with the corresponding global coordinate system, system degrees of freedom (DOFs), and normal wind inflow direction - consists of six main components, of which two are for the environmental parameters. Within these main components there are several subcomponents and options to be modeled. Hence, apart from the hub, a specified number of blades (for common wind turbines mostly three or two), represented as either rigid or flexible structures, make up the wind turbine rotor. This is, among others, connected to the nacelle with the structural models of drivetrain (rigid or flexible in one torsional DOF) and generator (fixed or variable speed). The nacelle as well contains the yaw controller; however, the

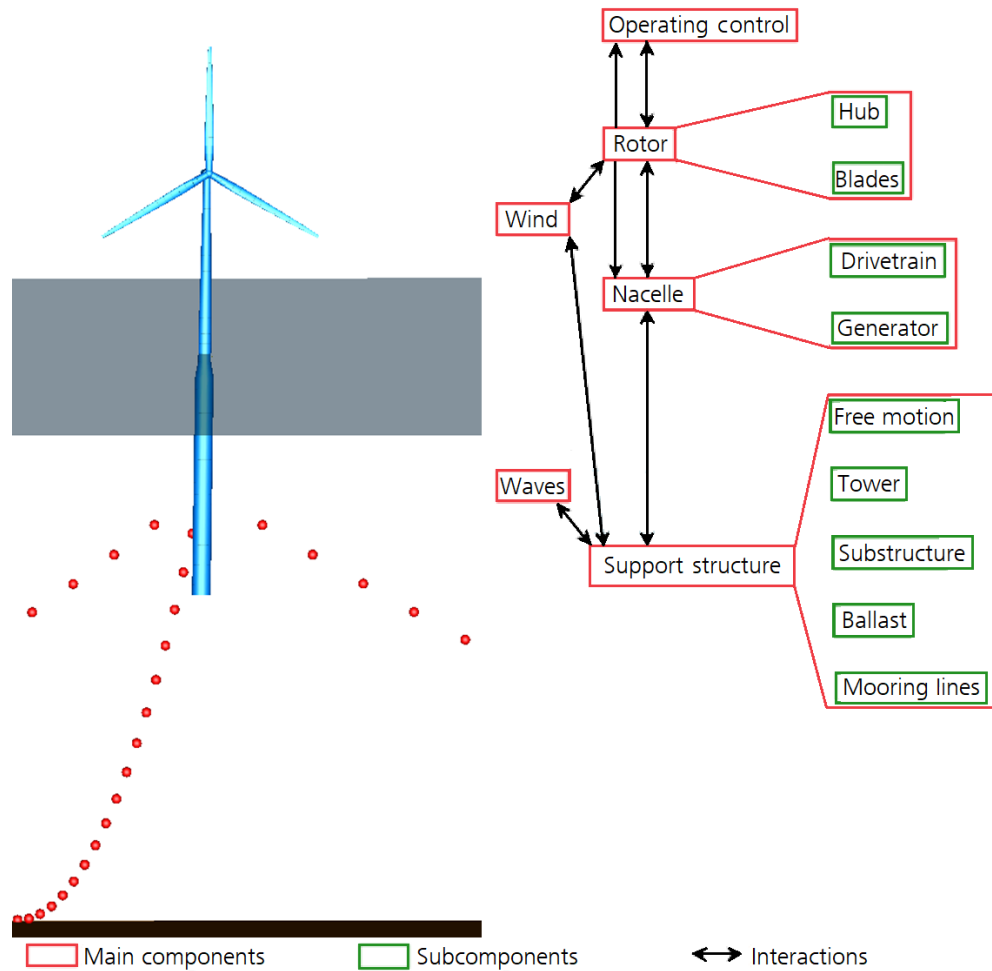


Figure 4.2: Hierarchical modeling structure of a FOWT system in MoWiT, adapted from the publication by Leimeister & Thomas (2017a).

remaining control systems for pitch and torque control, following PI-algorithms or an external dynamic link library (DLL) for running various operating phases, are incorporated in the operating control. The whole representation of the floating structure - including the tower, potential ballast, and the station-keeping system - is done in the support structure model, comprising as well the determination of all (aerodynamic, hydrostatic, and hydrodynamic) loads and motions. With respect to the aerodynamics, the calculations in MoWiT can be based on the blade element momentum (BEM) theory (Glauert 1935, Betz 1920, Froude 1889, Rankine 1865) or the generalized dynamic wake (GDW) model (Suzuki 2000, He 1989) and incorporate corrections for dynamic wake and dynamic stall (DS). Regarding the hydrodynamics, MoWiT is capable of linear Airy (Airy 1845) or non-linear Stokes wave theory (Clauss et al. 1992, Fenton 1985), Wheeler stretching (WS) or delta stretching (Journée & Massie 2001), Morison equation (ME) (Morison et al. 1950), and MacCamy-Fuchs (MCF) approach (MacCamy & Fuchs 1954). For the structural dynamics, the finite-element method (FEM), based on Euler-Bernoulli or Timoshenko beam theory, or modal reduction can be used for the floater and turbine representation, while the mooring lines are modeled through a mass-spring-damping (MSD) system, which

considers - apart from the dynamic inertial motion of the mooring system - hydrodynamic and internal damping, elastic deformation, as well as soil contact, and uses the catenary equation for determining the initial shape and position of the mooring line elements. Finally, the two environmental models for wind and waves, including also currents, allow the realization of various steady or turbulent, regular or irregular, aligned or misaligned, and normal or extreme environmental conditions and sea states. (Leimeister & Thomas 2017a, Thomas et al. 2014, Strobel et al. 2011)

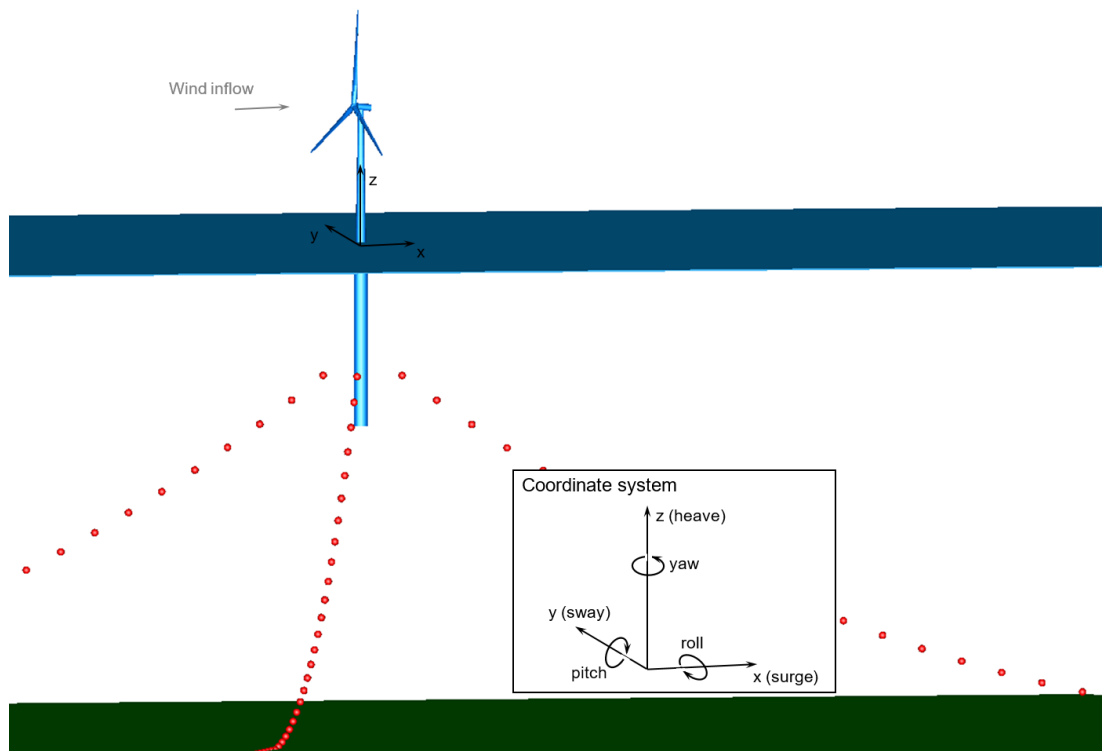


Figure 4.3: OC3 phase IV spar-buoy FOWT system modeled in MoWiT and visualized in Dymola[®] (structural elements shown in blue, mooring lines represented as chains of small red spheres, and SWL as well as seabed visualized as flat surfaces), including coordinate system and system DOFs, as well as wind inflow direction.

An overview of the structure of MoWiT is presented in Figure 4.4. It shows the required inputs for the wind turbine system and the environment and points out the approaches for the fully-coupled aero-hydro-servo-elastic dynamic calculations, based on which the final system responses are determined and obtained as outputs.

The simulations of models developed in MoWiT are performed in the time-domain and executed in Dymola[®]. This simulation engine is highly suited for modeling complex systems, such as FOWTs, which come with a large number of system equations. Dymola[®] provides various solvers with fixed or variable step size and following an implicit or explicit method, to cope with a broad range of problems and system equation types.

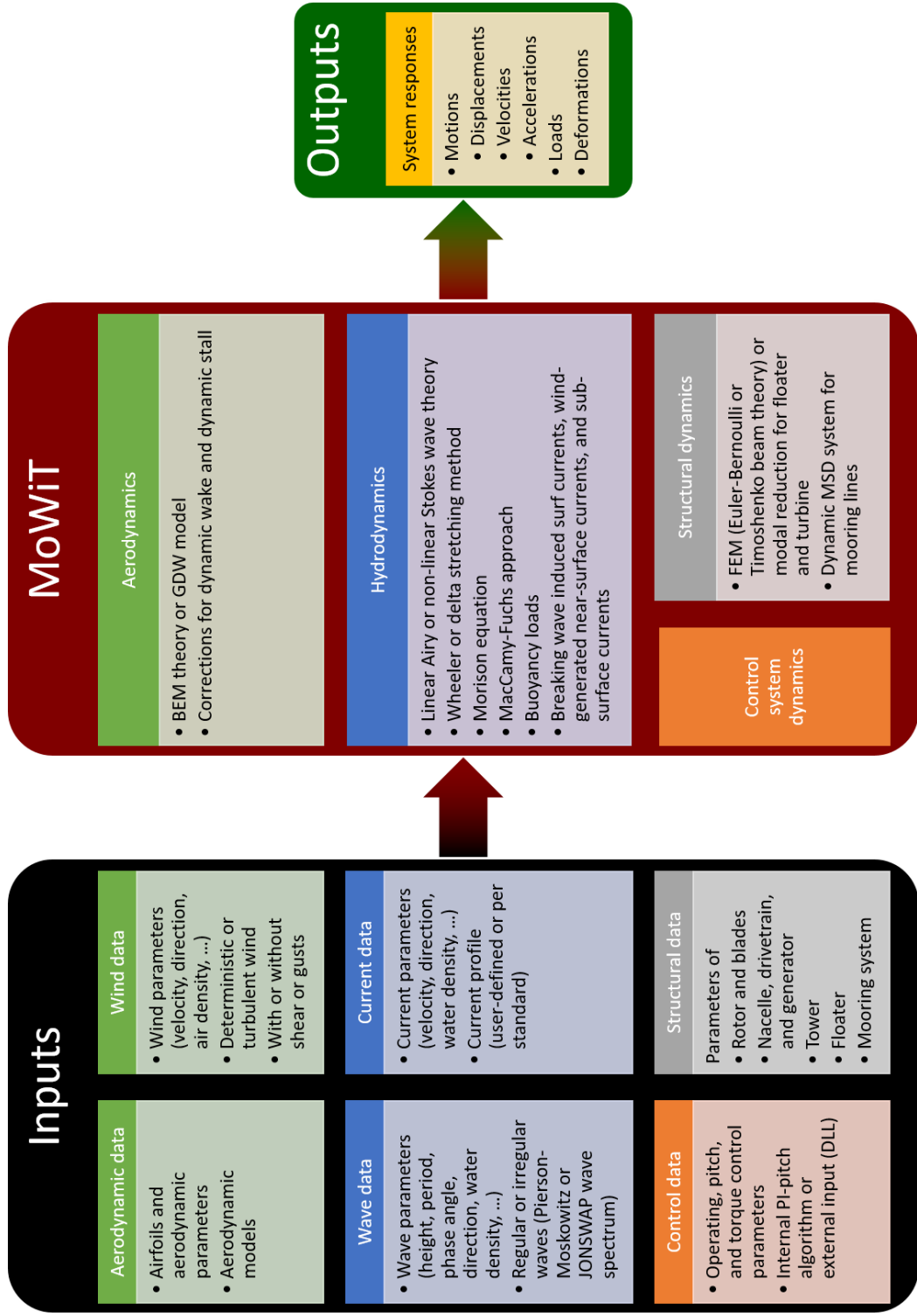


Figure 4.4: Flowchart representing the structure of MoWiT with inputs and outputs.

4.1.1.2 Implementation of the OC3 phase IV FOWT system in MoWiT

The OC3 phase IV FOWT system is modeled in MoWiT according to the definitions given by Jonkman (2010) and Jonkman et al. (2009) and as presented in Section 3.2. However, not all data relevant for modeling the system correctly are specified explicitly in these documents. Hence, in the following, the used - either prescribed or derived - parameters of the system components are addressed.

For the wind turbine - both the rotor and nacelle, as well as the operating control system - extensive data are available from Jonkman et al. (2009), as well as from Jonkman (2010) for the adaptations made specifically for the OC3 phase IV spar-buoy floating wind turbine system. Thus, the entire RNA (modeled as flexible structure with modal reduced blades) and operating control can be implemented correctly in MoWiT according to the definitions. The comparison of the total RNA mass, presented in Table 4.1, shows perfect agreement.

Table 4.1: Mass-related properties of the FOWT system from OC3 phase IV, MoWiT model results in comparison with the prescribed values given in Tables 3.9, 3.10, and 3.12.

Parameter	Value based on MoWiT model	Deviation from prescribed value
RNA mass	350.0×10^3 kg	0.0 kg
Tower mass	249.6×10^3 kg	-108.7 kg
Center of tower mass (above SWL along central axis)	43.4 m	0.0 kg
Platform mass (including ballast)	746.63×10^4 kg	0.0 kg
Center of platform mass (below SWL along central axis)	89.9136 m	-1.9×10^{-3} m
Platform roll inertia (about center of mass)	422.923×10^7 kgm ²	-18.6 kgm ²
Platform pitch inertia (about center of mass)	422.923×10^7 kgm ²	-18.6 kgm ²
Platform yaw inertia (about central axis)	92.67×10^6 kgm ²	-71.56×10^6 kgm ²

The support structure model comprises tower and floater, as already mentioned in Section 4.1.1.1. Within the code-to-code comparisons of OC3 phase IV, the spar-buoy is considered as rigid structure throughout all load cases (Jonkman & Musial 2010), which are introduced in Section 4.1.2.1. Only the tower is sometimes represented as rigid or flexible structure in the OC3 phase IV code-to-code comparisons. As the focus of the verification is on the floating platform, a rigid support structure model is utilized in MoWiT.

The structural part of the support structure, concerning the wind turbine tower, is described in-depth by Jonkman (2010), on which basis the tower with its distributed properties can be implemented from the top of the floating platform up to the RNA position through individual rigid cylindrical segments. The overall tower mass and corresponding center of mass are presented in Table 4.1 and compared to the specified values. There is just a minor deviation in the

tower mass, which might be due to the fact that the tower is conical, however, each element is modeled as straight cylinder based on its averaged top and bottom diameter.

For the floating platform, however, only the main parameters for geometry, outer dimensions, as well as total mass and inertia properties are provided by Jonkman (2010). Other parameters, relevant for modeling the structure and its characteristics properly, such as cap and (distributed) wall thickness values, material properties, or any information regarding the ballast system, are missing, as indicated in Figure 4.5. To overcome this issue, the unavailable parameters are determined - in the following way and based on the assumptions described hereinafter - to match the existing data resulting for the total system, accordingly the resulting mass-related properties (Table 3.12), as good as possible.

- The floating platform, being part of the support structure model, is implemented as the tower through rigid cylindrical segments. As no distributed properties are available for the spar-buoy, four cylindrical bodies are used based on the geometry of the floater: (1) one for BC with given length and diameter; (2) one for the tapered part, as connection between BC and UC, with determined length and averaged diameter of D_{BC} and D_{UC} ; (3) one for UC with given length and diameter; and (4) one for modeling the ballast within BC.
- As no structural analysis is going to be carried out within the OC3 phase IV code-to-code comparisons, the cap thickness (t_{cap}) - meaning the thickness of the bottom cap of BC, as well as the thickness of the cap on the upper end of UC - is set equal to 1.0×10^{-4} m to avoid large contribution of the caps to the total mass due to any too large assumed value.
- Each of the three structural cylinders (1) - (3), described in the first bullet point, is defined through its outer diameter and length, which are both provided or - in case of the tapered (2) part - determined as described beforehand, its wall thickness, as well as its material density. The latter two are assumed to be the same for the three cylindrical parts of the floating structure.

As the platform inertia values are relevant for the dynamic response of the floating system, it is tried to match these inertia values as good as possible by modifying assumed values for the material density ($\rho_{platform}$) and wall thickness (t) of the spar-buoy. First, it is presumed that the specified parameters for the inertia values are for the platform including ballast, because no separate values are given for the ballast and the total inertia is important for the dynamics. Furthermore, as it is not possible to match all (roll, pitch, and yaw) inertias at the same time under the assumptions made, it is focused on achieving correct values at least for the roll and pitch inertias, as these are usually more important than the yaw inertia.

The calculations are based on the target value search in Excel. The starting value for the material density is $7,850 \text{ kg/m}^3$, assuming typical steel properties, and an upper bound is set at $10,000 \text{ kg/m}^3$. For the wall thickness, taking on one constant value for the entire platform ($t = t_{UC} = t_{BC}$) for reasons of simplicity and as already mentioned above, the

starting value is 0.1 m, which is at the same time the upper bound. With these settings, the target value search results in a material density of $10,000 \text{ kg/m}^3$ and a wall thickness of 0.0314 m. With these parameters, the difference in the platform roll and pitch inertias is with $4.4 \times 10^{-7}\%$ negligible, while the achieved yaw inertia is 43.6% smaller than the defined value, as presented in Table 4.1.

As the upper bound for the material density is reached, the target value search is again executed with removed upper limit. The result, however, is that an unfeasible high material density is reached, while the wall thickness would be unrealistically thin and the discrepancy between better matching the platform roll and pitch inertias, however, higher deviation in the yaw inertia becomes greater. Thus, the results obtained when limiting the material density to common and feasible values are kept.

A better match of the yaw inertia value could have been achieved by segmentation of the cylindrical structural elements of the spar-buoy. However, with unknown number of segments and length distributions, a full match of all inertia values at the same time is questionable to be obtained. Thus, as the focus lies on the verification of the modeling approach and implemented theories and coupled dynamics, a compromise is needed between available data and perfect match of resulting system properties. As mentioned above, the main focus is on the most important inertia components, namely for roll and pitch, and, hence, the discrepancy in the system yaw inertia is accepted and accounted for when analyzing the results of the code-to-code comparison, as covered in Section 4.1.3.

- Having the material density and wall thickness set, the ballast density (ρ_{ballast}) and ballast height (H_{ballast}) are determined to match the total platform mass including ballast of $746.63 \times 10^4 \text{ kg}$, as specified in Table 3.12. Due to the small difference in the tower mass, outlined before and in Table 4.1, the second criterion for determining the ballast parameters would either be
 1. the same center of mass of platform including ballast at 89.9155 m below SWL;
 2. or the same resulting center of mass of tower and platform including ballast at 85.6009 m below SWL;
 3. or the same total restoring moment due to tower, platform, and ballast.

Due to the minor discrepancy in the tower mass, all three options for the second criterion yield very similar ballast parameters. Nevertheless, the second option to meet the same total center of mass is selected to avoid altering the response in pitch and roll by a shifted center of gravity. This results in a ballast density of $1,907 \text{ kg/m}^3$ and a ballast height of 48.4 m, which yields a perfect match in the total platform mass and a minor deviation in the position of the center of mass of the floater, as presented in Table 4.1.

Table 4.2 summarizes the settings of the unavailable floater parameters, used for the modeling in MoWiT. With these settings, a resulting hydrostatic buoyancy force, determined based on the geometry and presuming a gravitational acceleration (g) of 9.81 m/s^2 , of 80,724,636 N is

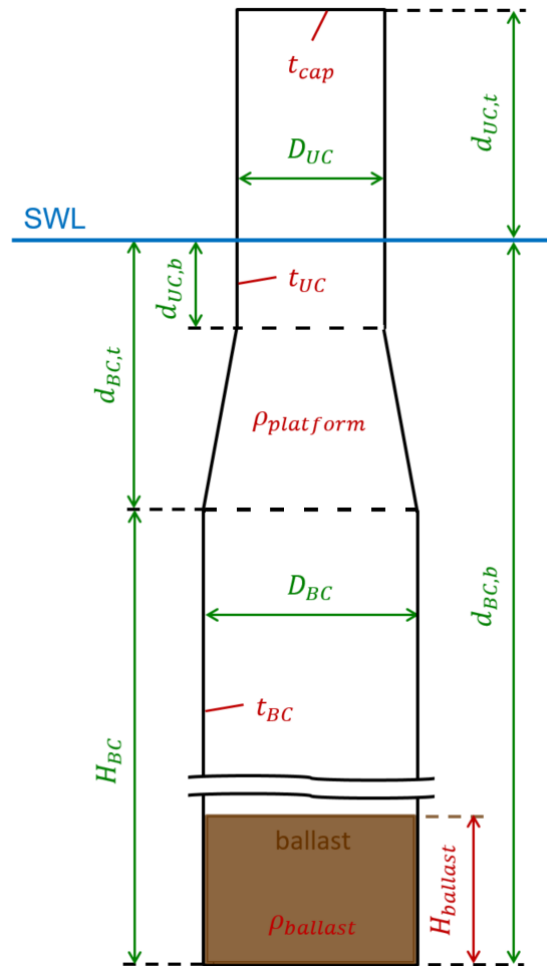


Figure 4.5: Missing parameters indicated in red in the schematic of the OC3 phase IV spar-buoy; provided parameters, as given in Figure 3.5, are written in green.

Table 4.2: Assumed values of the undefined spar-buoy and system parameters.

Parameter	Symbol	Value
Cap thickness	t_{cap}	1.0×10^{-4} m
Wall thickness of upper column	t_{UC}	0.0314 m
Wall thickness of base column	t_{BC}	0.0314 m
Density of platform material	$\rho_{platform}$	10,000 kg/m ³
Density of ballast material	$\rho_{ballast}$	1,907 kg/m ³
Height of ballast within base column	$H_{ballast}$	48.4 m
Gravitational acceleration	g	9.81 m/s ²

obtained. This deviates by $2.0 \times 10^{-2}\%$ from the specified value, mentioned in Section 3.2.2, what is mainly expected to come from a slightly different gravitational acceleration value taken in the OC3 phase IV definition. The hydrostatic restoring is, as opposed to the OC3 phase IV system definition by Jonkman (2010), not explicitly defined within MoWiT but a result of the

implemented system properties. Hence, a quantitative comparison of the hydrostatic restoring values is not directly possible without additional analyses, such as stepwise simulations for generating the corresponding curve of static stability. However, the precise representation of the floater geometry and its center of mass allow to draw conclusions on the correct representation of the hydrostatic restoring. This as well can be examined indirectly when analyzing the simulation results. In contrast to the hydrostatic restoring values, the additional damping parameters, outlined in Section 3.2.2 and stated by Jonkman (2010), are implemented separately in MoWiT and the hydrodynamic coefficients are set according to the definitions.

The mooring system properties, including as well the additional yaw spring stiffness, specified by Jonkman (2010) and mentioned in Section 3.2.2, are implemented in MoWiT according to the definitions.

Finally, the OC3 phase IV spar-buoy FOWT model, implemented as described above in MoWiT, is simulated in Dymola[®]. The specific simulation and solver settings are stated in Section 4.1.2.1 for each simulation case separately. A visualization of the modeled system is given in Figures 4.2 and 4.3, with the structural elements shown in blue, the mooring lines represented as chains of small red spheres, and the SWL as well as the seabed visualized as flat surfaces.

4.1.2 Code-to-code comparison

To verify the OC3 phase IV spar-buoy FOWT system model, implemented in MoWiT as described in Section 4.1.1, the design load case (DLC) simulations are executed with this model and the code-to-code comparison is performed, as done in the OC3 project (Jonkman & Musial 2010). Hereinafter, first (Section 4.1.2.1), the simulated DLCs are presented together with the settings used in Dymola[®] for executing the simulations, while in the subsequent Section 4.1.2.2 the results of the simulations with the MoWiT model are presented in comparison with the other code results from the OC3 project. Further discussion and analyses of these results follow in Section 4.1.3.

4.1.2.1 Simulated load cases

For the analyses of offshore wind turbine systems, various DLCs are recommended by standards (IEC 2019*b,c,a*, DNV GL 2018*c*, 2016*a*, DNV 2014). Based on these guidelines, only a reduced number of design relevant DLCs and environmental conditions are selected for the application in research studies (Krieger et al. 2015, Matha et al. 2014, Bachynski et al. 2013). Within phase IV of OC3, a separate set of DLCs is specified, which is grouped into three categories: (1) DLC 1.x for system-only analyses; (2) DLC 4.x for hydro-elastic response analyses, hence, only with waves; and (3) DLC 5.x for aero-hydro-servo-elastic response analyses, thus, with environmental impact from both wind and waves (Jonkman & Musial 2010). To allow a code-to-code comparison of the spar-buoy FOWT model in MoWiT with the other codes and tools used in OC3 phase IV, the same DLCs are simulated with the implemented model as presented in Section 4.1.1.2.

DLC 1.x In the DLCs for system-only analyses, neither wind nor waves are considered. Hence, the air density is set equal to 0 kg/m^3 in order to have no aerodynamic loads acting, and still water condition is applied so that no waves exist. For the wind turbine control and operating system, the brake is active and the control is disabled. In the OC3 phase IV code-to-code comparisons, the entire wind turbine system is modeled as a rigid structure, which is as well realized in MoWiT, as described in Section 4.1.1.2. Case-specific simulation configurations, with additional choices (highlighted in red) for undefined settings are summarized in Table 4.3. Thus, in addition to the six free-decay tests DLC 1.4a to 1.4f with initial deflections in one of the six DOFs taken as starting position of the floater, which are as well utilized for the evaluation of the eigenanalysis (DLC 1.2), one “neutral” free-decay test without any initial deflection is simulated to be used for determining the static equilibrium (DLC 1.3). All simulations in the DLC group 1.x are executed in Dymola[®], using the Rkfix4 (Runge-Kutta fixed-step and 4th order method) solver with a fixed integrator step-size of 0.01 s. The output interval length of the resulting time series amounts to 0.05 s. The simulation settings are chosen based on preceding sensitivity studies on the solver and time step-size for the specific FOWT system.

Table 4.3: Simulation settings and analysis methods for DLC group 1.x, **assumptions** are written in red.

DLC	Type	Initial conditions	Simulation length	Analyzed output for code-to-code comparison
1.2	Eigenanalysis	N/A	N/D	f_{nat} and ζ taken from DLC 1.4a–f
1.3	Static equilibrium	N/A	N/D	Static equilibrium taken from DLC 1.4 at 600 s
1.4	Free-decay		600 s	Time series
	a	Surge: 21 m		
	b	Sway: 18 m		
	c	Heave: 5 m		
	d	Roll: -10°		
	e	Pitch: 10°		
	f	Yaw: -6°		

DLC 4.x In the DLC group 4.x only the hydro-elastic response should be analyzed. Hence, the aerodynamics are turned off by setting again the air density equal to 0 kg/m^3 . The brake is still enabled and the control switched off. Contrary to the OC3 phase IV definition by Jonkman & Musial (2010) that the tower is considered to be flexible, not only the floater, but the entire FOWT system is modeled as rigid structure in MoWiT, as spar-buoy and tower are implemented as one continuous structure, which is already pointed out in Section 4.1.1.2. The two DLCs in group 4.x differ in the considered wave type, as presented in Table 4.4. The regular wave is defined through the wave theory, wave height H , and wave period T , while the irregular wave is

specified by the wave theory and spectrum type used, as well as the significant wave height H_s and peak period T_p . As nothing specifically is stated for the hydrodynamic load calculation, the more sophisticated MCF approach, as well as the Wheeler stretching, are applied in MoWiT. Both DLCs, for which no initial conditions are required, are simulated in Dymola[®], using the same integration, solver, and output settings as in the DLC group 1.x, namely Rkfix4 solver with fixed integrator step-size of 0.01 s and 0.05 s output interval length.

Table 4.4: Simulation settings and analysis methods for DLC group 4.x, **assumptions** are written in **red**.

DLC	Type	Wave conditions	Simulation length	Analyzed output for code-to-code comparison
4.1	Regular waves	Airy wave theory $H = 6$ m; $T = 10$ s	120 s	Time series
4.2	Irregular waves	Airy wave theory JONSWAP spectrum $H_s = 6$ m; $T_p = 10$ s	600 s	min, mean, max taken from last 120 s Power spectra taken from entire 600 s

DLC 5.x Finally, the DLC group 5.x represents full aero-hydro-servo-elastic simulations. Hence, the air density is now set equal to 1.225 kg/m^3 - based on the offshore aerodynamic properties specified for the NREL 5 MW wind turbine (Jonkman et al. 2009) - and the operating control system is turned on. The wind is either considered to be constant with a specified wind speed V_{hub} at hub height, or turbulent, defined additionally through the turbulence model and reference value of the turbulence intensity I_{ref} . Contrary to the OC3 phase IV specification (Jonkman & Musial 2010), which uses the Mann turbulent wind model, the turbulent wind time series in MoWiT follows the Kaimal model as it can easily be generated by means of TurbSim (Jonkman 2009), which only supports Kaimal or von Karman normal turbulence models. The waves and hydrodynamic load calculations are realized just like in the DLC group 4.x. The specific parameter settings for the different DLCs are presented in Table 4.5. As defined in OC3 phase IV (Jonkman & Musial 2010) for both DLC groups 4.x and 5.x, the tower is originally considered to be flexible; however, it is modeled in MoWiT together with the spar-buoy as rigid structure, while the RNA is implemented as flexible structure as prescribed. For the DLC 5.1 simulation the same integration, solver, and output settings as in the DLC groups 1.x and 4.x are used (solver: Rkfix4, fixed integrator step-size: 0.01 s, output interval length: 0.05 s), while for DLC 5.2 and 5.3, which both deal with turbulent wind and irregular waves, the variable-step Ccode (C-language variable-coefficients ordinary differential equation) solver with tolerance of 1.0×10^{-4} is utilized. Originally, there is also a fourth DLC (5.4) defined in phase IV of OC3 for generating effective response amplitude operators (Jonkman & Musial 2010), which, however, is not employed in the code-to-code comparison with the MoWiT model in this verification study.

Table 4.5: Simulation settings and analysis methods for DLC group 5.x, **assumptions and modifications** are written in **red**.

DLC	Wind conditions	Wave conditions	Initial conditions	Simulation length	Analyzed output for code-to-code comparison
5.1	Steady, uniform wind $V_{\text{hub}} = 8 \text{ m/s}$	Regular Airy waves $H = 6 \text{ m}$ $T = 10 \text{ s}$	Rotor speed: 9 rpm	120 s	Time series
5.2	Turbulent wind (Mann) Kaimal model $V_{\text{hub}} = 11.4 \text{ m/s}$ $I_{\text{ref}} = 0.14$	Irregular Airy waves JONSWAP spectrum $H_s = 6 \text{ m}$ $T_p = 10 \text{ s}$	Rotor speed: 12 rpm	(600 s) 650 s	min, mean, max taken from last 120 s Power spectra taken from last 600 s
5.3	Turbulent wind (Mann) Kaimal model $V_{\text{hub}} = 18 \text{ m/s}$ $I_{\text{ref}} = 0.14$	Irregular Airy waves JONSWAP spectrum $H_s = 6 \text{ m}$ $T_p = 10 \text{ s}$	Rotor speed: 12 rpm Blade pitch: 15°	(600 s) 650 s	min, mean, max taken from last 120 s Power spectra taken from last 600 s

4.1.2.2 Results of the simulations and the code-to-code comparison

For the comparison of the DLC simulation results only a few results are presented, mostly based on the selection in the OC3 phase IV code-to-code comparison (Jonkman & Musial 2010). An overview of the different codes, tools, and modeling approaches used by the OC3 phase IV participants (Jonkman & Musial 2010) and described in Section 4.1 is given in Figure 4.1, including as well the color-coding, used for comparing the results from the ten OC3 phase IV participants. In addition to the theories and modeling approaches mentioned in Section 4.1.1.1, stream functions or Airy wave theory with free surface connections, indicated by Airy+, as well as linear potential flow (PF) theory with radiation and diffraction are utilized to deal with the hydrodynamics. The MCF approach, used in MoWiT for taking diffraction effects into account, applies as well PF theory. Regarding the control system, two more options are available in the OC3 phase IV participants' codes: either the implementation through an user-defined subroutine (UDS), or the interface to Simulink with MATLAB® (SM). The structural dynamics of turbine and mooring system can be formulated by means of multibody-dynamics (MBD). For the turbine dynamics, FEM could as well be used just for mode pre-processing (FEMP). Finally, the quasi-static catenary equation (QSCE) and implementation through user-defined force-displacement (UDFD) relationships provide two more options for modeling the mooring system dynamics. (Jonkman & Musial 2010)

In the following, the results are mainly presented by comparative plots. The comparison of numbers, more detailed discussion of reasons for differences, as well as performed in-depth analyses follow in Section 4.1.3.

Results for DLC 1.x From the full-system eigenanalysis DLC 1.2, both the natural frequencies f_{nat} and the damping ratios ζ in the six DOFs surge, sway, heave, roll, pitch, and yaw are compared. These, however, as mentioned in Table 4.3, are taken from analysis of the free-decay time series from DLCs 1.4a to 1.4f. The natural frequencies obtained with the MoWiT model could be compared with nine other codes, whereas results for the damping ratios are only available from three OC3 phase IV participants, as presented both in Figure 4.6. In general, it can be seen that MoWiT-based results are within the limits of the results from the OC3 phase IV participants, with just some minor differences in the surge and sway natural frequencies, as well as some higher deviations in the yaw natural frequency and the damping ratio in heave. A more in-depth comparison, based on numerical values and including analyses and justification of the deviations, is given in Section 4.1.3.1.

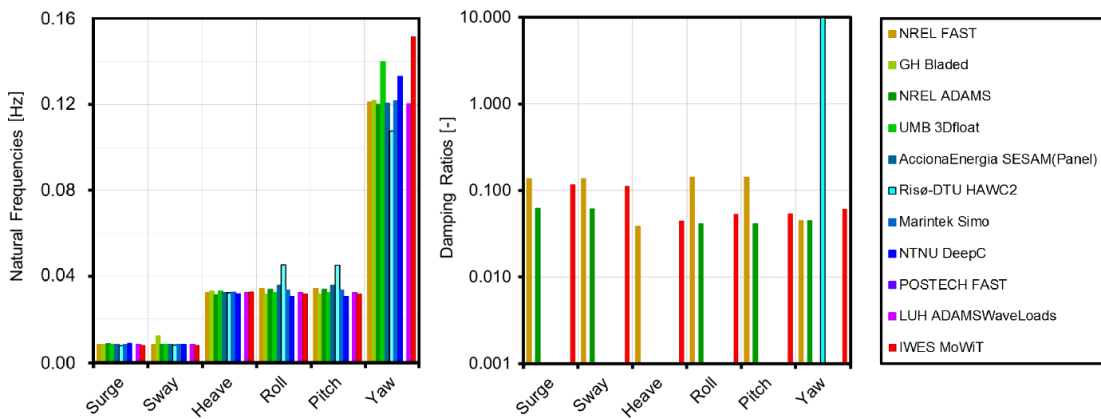


Figure 4.6: Full-system natural frequencies and damping ratios.

The results for the static equilibrium analysis, which are obtained from the “neutral” free-decay simulation in DLC 1.4 at the end of the simulation time, are only presented in numerical format in Table 4.8 in Section 4.1.3.1 and show, except for the heave DOF, good agreement with the results from the OC3 phase IV participants.

The time series of the free-decay simulations are presented in Figures 4.7 to 4.9 for DLCs 1.4a, 1.4c, and 1.4e for the responses in the surge, heave, and pitch DOFs, as well as in Figure 4.10 for DLC 1.4f for the response in the yaw DOF. The time series represent very well the above mentioned findings from the natural frequencies, damping ratios, and static equilibrium analyses, and show also couplings in the responses of different DOFs.

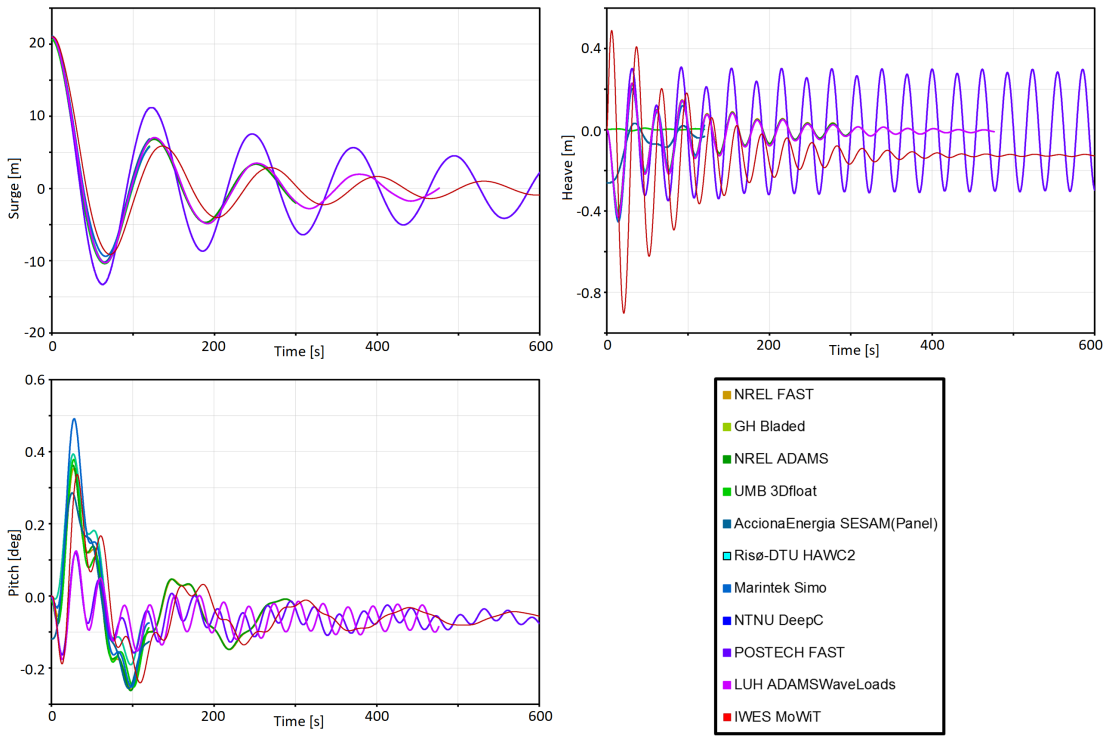


Figure 4.7: Free-decay time series from DLC 1.4a.

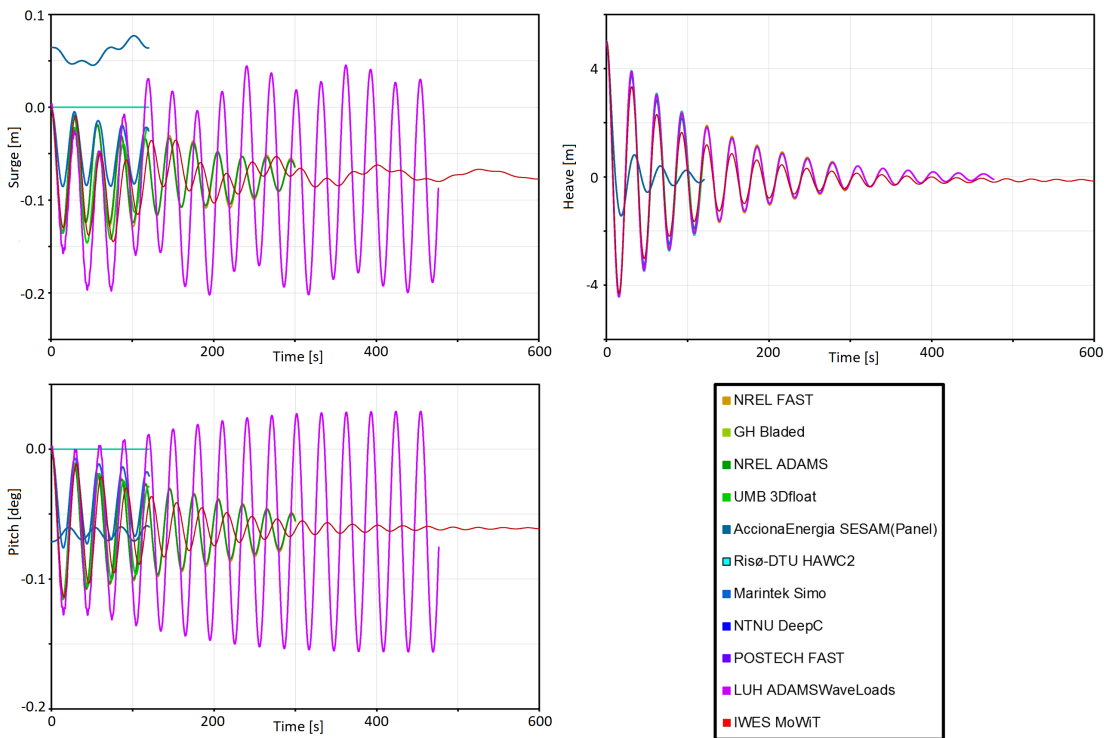


Figure 4.8: Free-decay time series from DLC 1.4c.

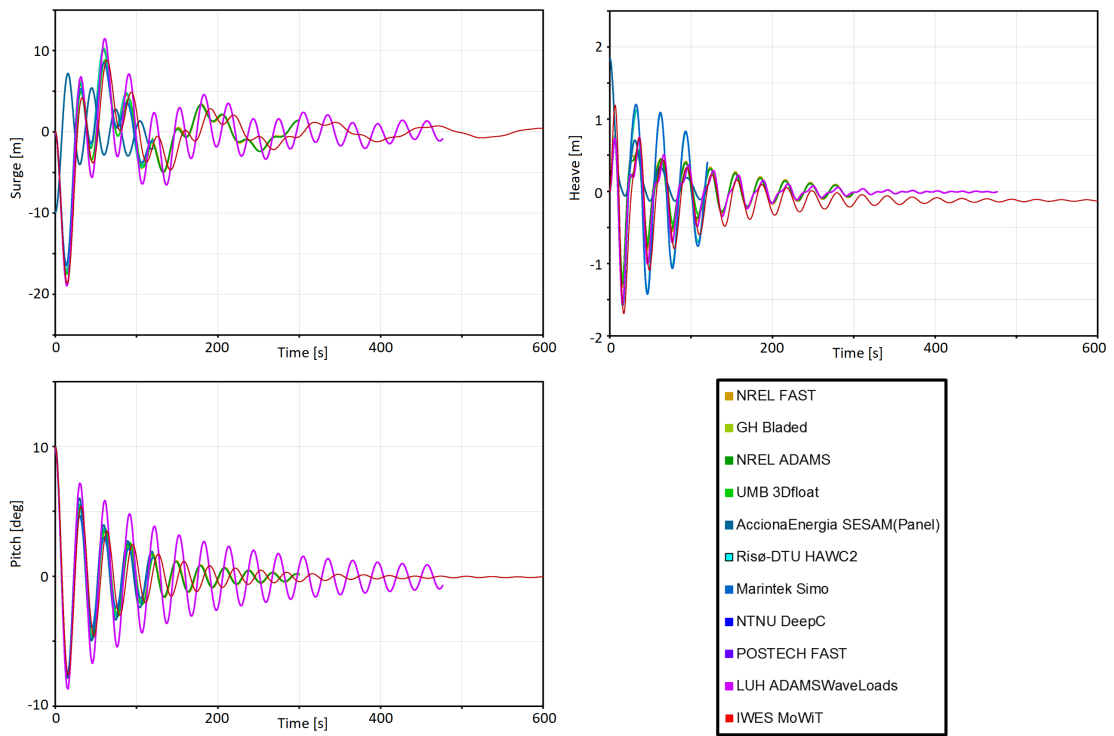


Figure 4.9: Free-decay time series from DLC 1.4e.

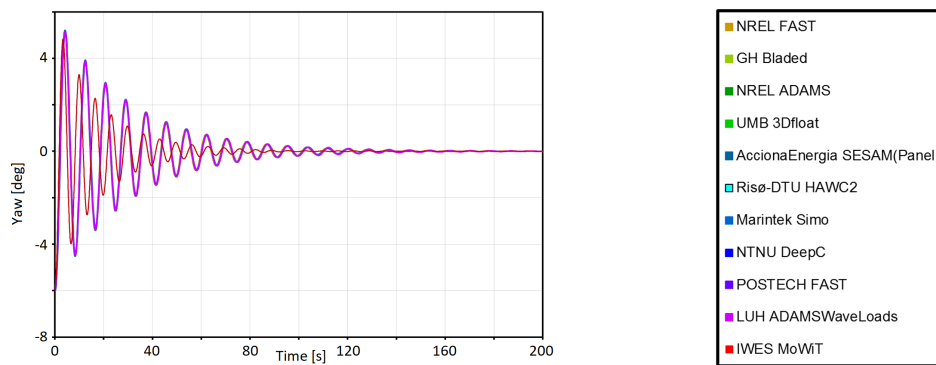


Figure 4.10: Free-decay time series from DLC 1.4f.

Results for DLC 4.x For the hydro-elastic response analyses in DLC group 4.x, first, the simulations with regular waves are presented. These comprise time series for the surge, heave, and pitch DOFs (Figures 4.11(a) to 4.11(c)), as well as for the downstream fairlead tension (Figure 4.11(f)). Originally, also tower-top fore-aft deflection and shear force are compared within the OC3 phase IV activities; however, as the tower is modeled throughout the DLCs together with the spar-buoy floater as rigid structure in MoWiT, no tower-top deflections are obtained. Hence, in addition to the tower-top fore-aft shear force (Figure 4.11(d)), also the tower-top fore-aft bending moment is presented (Figure 4.11(e)). For the latter two, the results from the MoWiT model match the time series from the OC3 phase IV participants, while more motion is seen in the platform DOFs, as well as the downstream fairlead tension. This behavior is analyzed and discussed in more detail in Section 4.1.3.2.

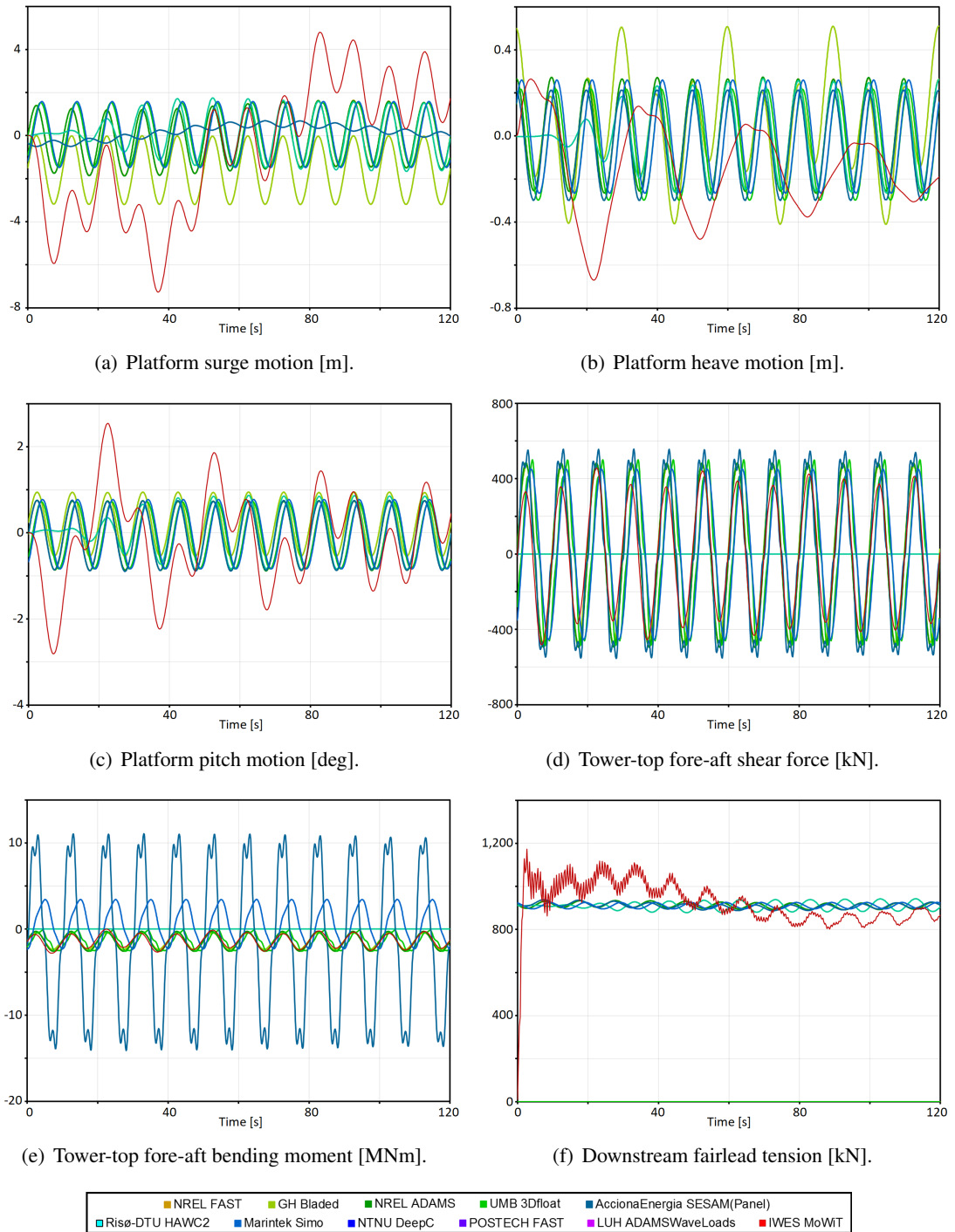


Figure 4.11: Hydro-elastic time series with regular waves from DLC 4.1.

For the hydro-elastic response analyses with irregular waves from DLC 4.2, the statistics are taken from the final fifth of the time series, while the power spectra are generated by using the entire length of the simulation, as indicated in Table 4.4. Figure 4.12 demonstrates the power spectra for the same parameters as considered already in DLC 4.1 for presentation of the results. The comparison of the statistics of the time series, presented in Appendix B,

shows good agreement between the results from MoWiT and the OC3 phase IV codes for the tower-top fore-aft shear force and bending moment, as well as the downstream fairlead tension; however, the statistics for the platform motions from MoWiT yield overall some smaller values by amount. The platform motions response spectra, on the other hand, match the power spectra from the OC3 phase IV participants for frequencies below the irregular wave frequency. For higher frequencies, as well as for the response spectra of the other parameters, there are significant deviations between the codes. In-depth analyses of these are given in Section 4.1.3.2.

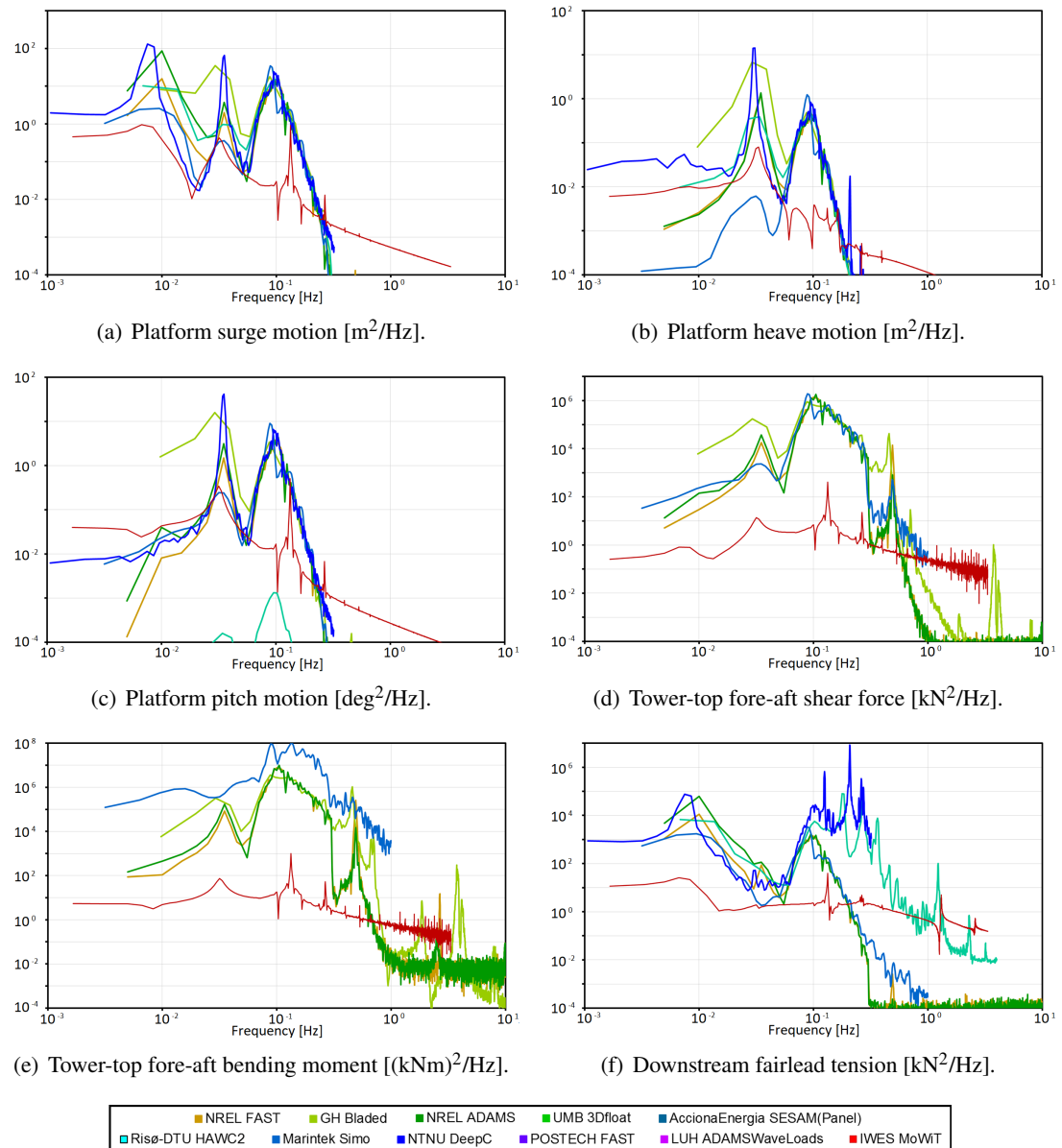


Figure 4.12: Hydro-elastic power spectra with irregular waves from DLC 4.2.

Results for DLC 5.x In the DLC group 5.x, the aero-hydro-servo-elastic response of the FOWT system is analyzed firstly under regular conditions, and then for irregular waves and

turbulent wind. Beginning with the regular waves and steady wind case DLC 5.1, the time series of the parameters considered already in DLC 4.x (namely the surge, heave, and pitch DOFs, the tower-top fore-aft shear force and bending moment, as well as the downstream fairlead tension) and additionally the upstream fairlead tension, the generator power and the rotor speed, as well as the out-of-plane blade-tip deflection are presented in Figures 4.13 and 4.14. The MoWiT-based time series for the tower-top fore-aft shear force and bending moment, the out-of-plane blade-tip deflection, the generator power and rotor speed, the platform pitch

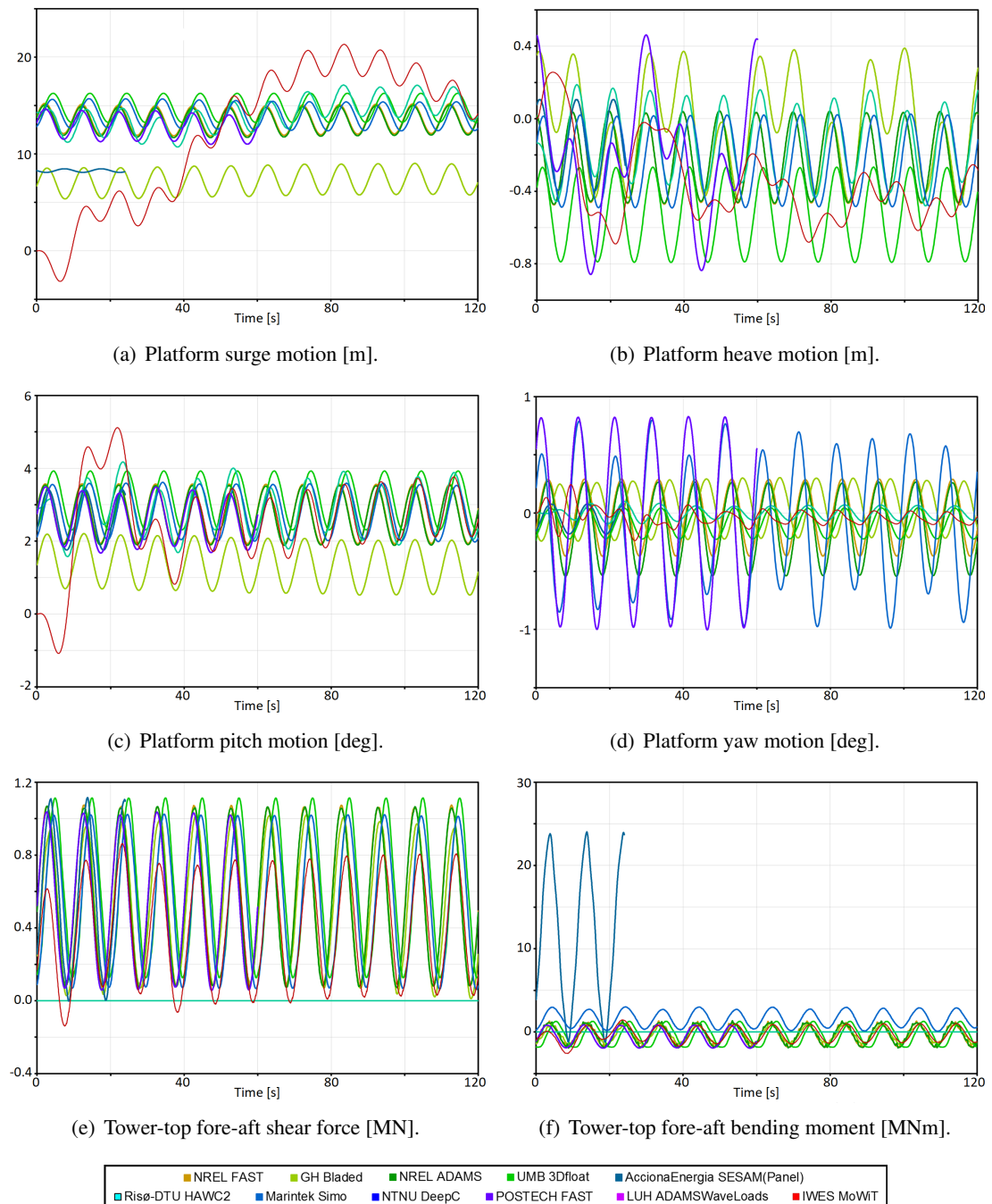


Figure 4.13: Aero-hydro-servo-elastic time series with regular waves from DLC 5.1, part I.

and yaw motions, as well as the downstream and upstream fairlead tensions are comparable to the OC3 phase IV participants' results with more or less long lasting deviations at the beginning of the time series. However, larger discrepancies are observed in the platform surge and heave motions time series. These findings are discussed in-depth and reasoned in Section 4.1.3.3.

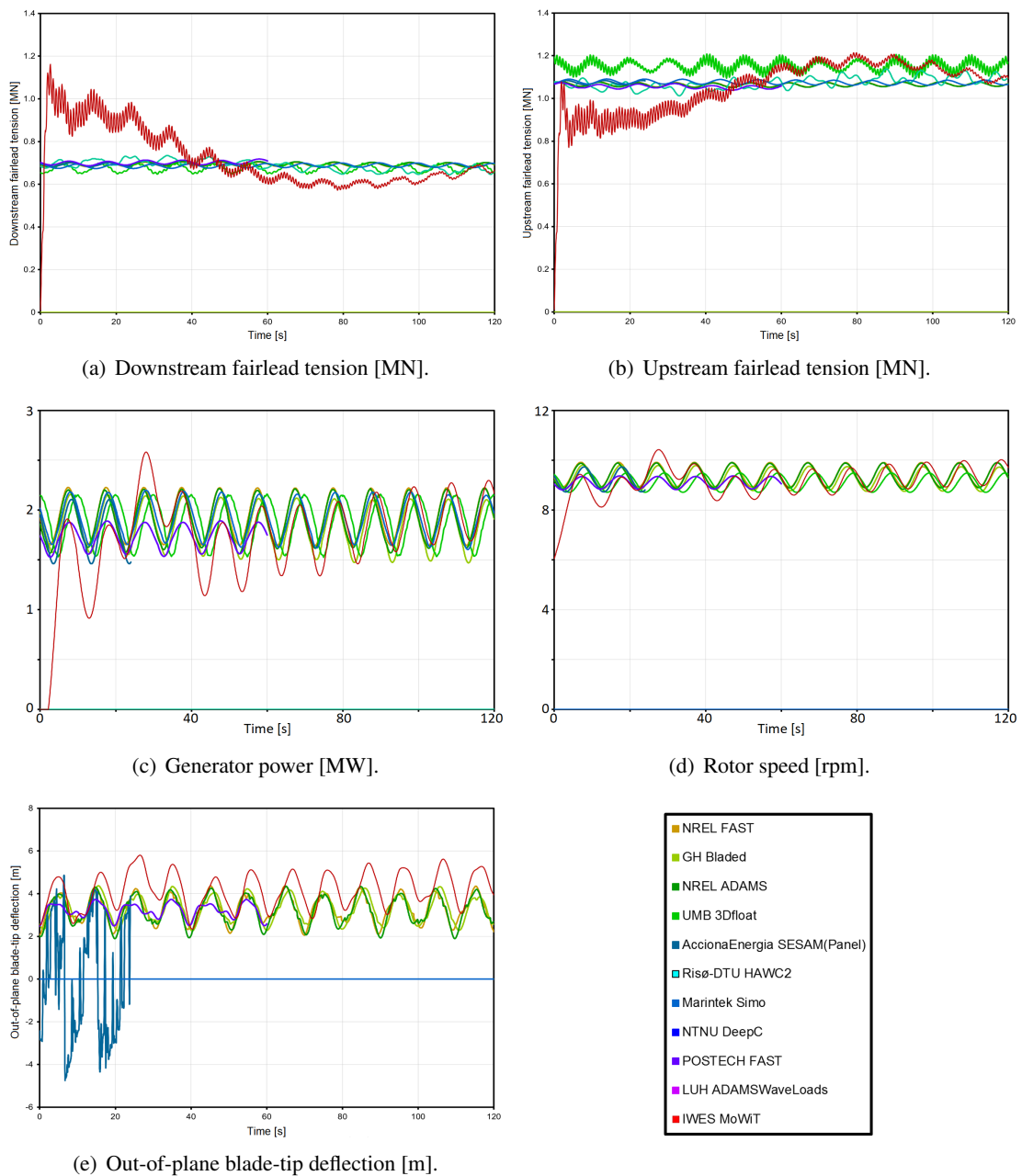


Figure 4.14: Aero-hydro-servo-elastic time series with regular waves from DLC 5.1, part II.

The simulations with irregular waves and turbulent wind in DLCs 5.2 and 5.3 are - similarly to DLC 4.2 and as indicated in Table 4.5 - analyzed with respect to their statistics, determined based on the last fifth of the simulated time, and response power spectra, generated based on the last 600 s. The results for DLCs 5.2 and 5.3 provide similar findings and, hence, everything presented and discussed in the following for the above rated DLC 5.3 can be related to DLC 5.2

as well. Figures 4.15 and 4.16 demonstrate the power spectra for DLC 5.3 for the same parameters as considered already in DLC 5.1 for presentation of the results. The statistical results from the MoWiT model, presented in Appendix C, fall for most of the analyzed parameters within the range of the results from the OC3 phase IV participants. Only for the tower-top fore-aft responses they deviate slightly from the OC3 phase IV results: smaller values by amount for the shear force and larger values for the bending moment. The power spectra, presented in Figures 4.15 and 4.16, show - similarly to the results from DLC 4.2 - some significant deviations from the OC3 phase IV results. Additionally to the differences in the range of the wave peak frequency in the surge, heave, and pitch motions (Figures 4.15(a) to 4.15(c)), as well as the fairlead tensions (Figures 4.16(a) and 4.16(b)), there are some high oscillations striking in

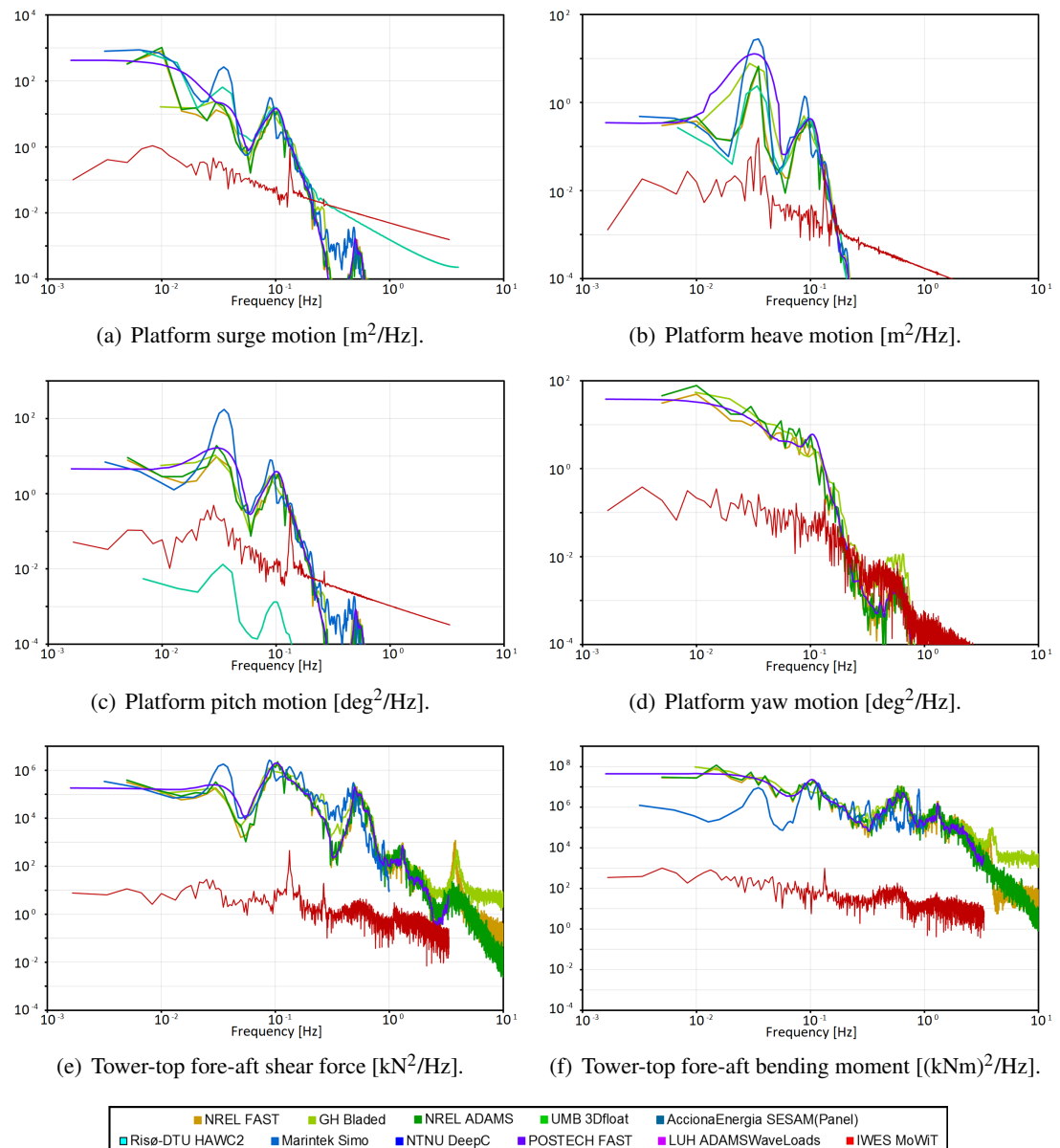


Figure 4.15: Aero-hydro-servo-elastic power spectra with irregular waves from DLC 5.3, part I.

the higher frequency ranges in the yaw motion (Figure 4.15(d)), tower-top fore-aft responses (Figures 4.15(e) and 4.15(f)), out-of-plane blade-tip deflection (Figure 4.16(e)), as well as generator power and rotor speed (Figures 4.16(c) and 4.16(d)). These findings and behaviors are analyzed in more detail in Section 4.1.3.3.

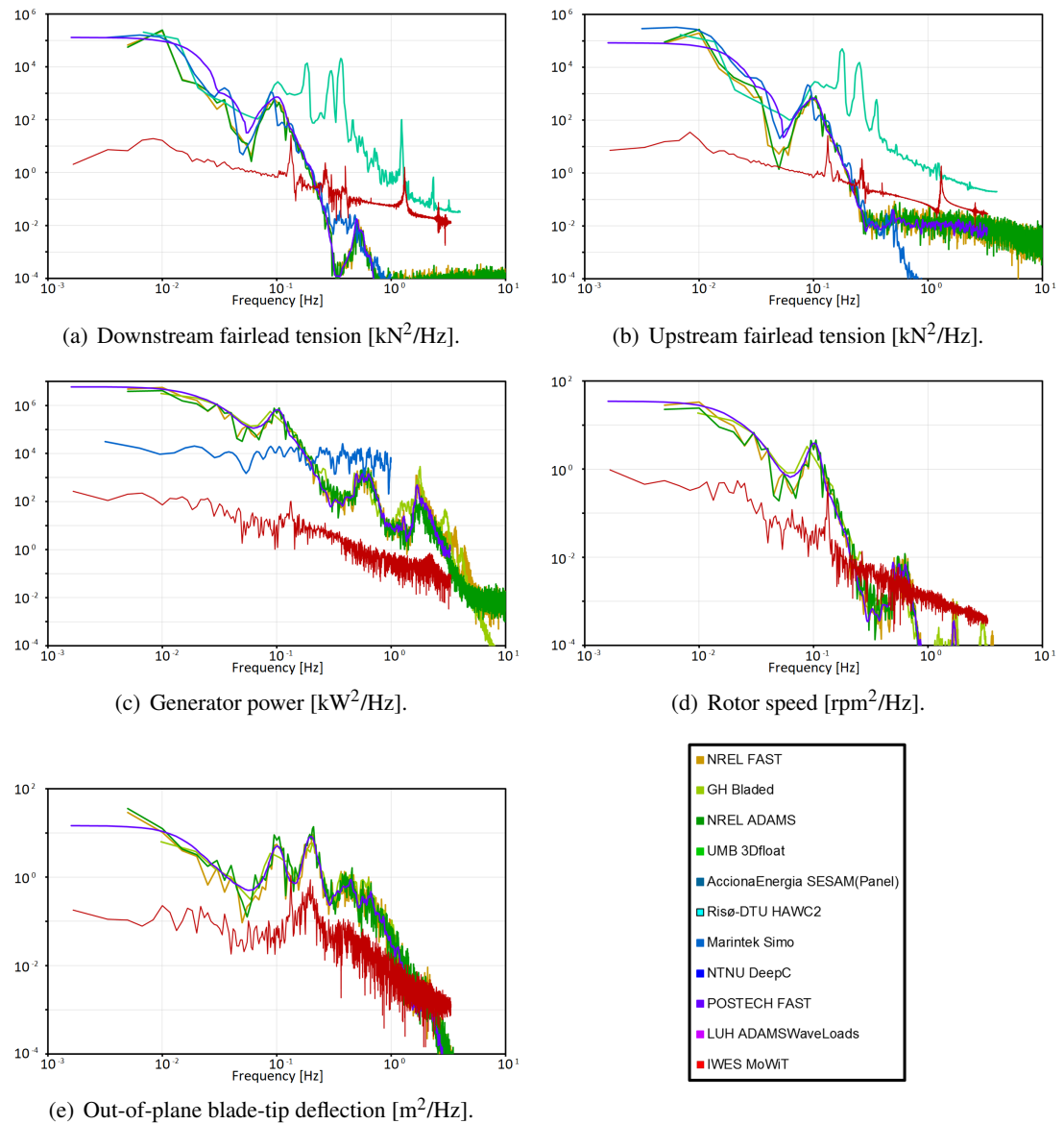


Figure 4.16: Aero-hydro-servo-elastic power spectra with irregular waves from DLC 5.3, part II.

4.1.3 Discussion of the code-to-code comparison results

Some results of the code-to-code comparison DLC simulations are presented in Section 4.1.2.2, where already minor comments on the degree of agreement are included. A more detailed analysis, including discussion of deviations, more in-depth evaluations, as well as final remarks and holistic reflections on the findings, is performed and presented hereinafter. As a general remark, it has to be noted that the presented results from simulations with Dymola[®] based on

the system model created by means of MoWiT are just adding one more result to the cross-code comparison. For a final statement on the accuracy of the codes, the comparison would need to be repeated when real data is available to validate the codes as well.

4.1.3.1 System-only analyses

The full-system eigenanalysis of DLC 1.2 shows overall mostly good agreement, as already indicated in Section 4.1.2.2. The numerical comparison of the natural frequency and damping ratio results, as presented in Tables 4.6 and 4.7, respectively, is done based on the range of the results from the OC3 phase IV participants (minimum value up to maximum value), including also the mean value for comparison with the results obtained by means of the MoWiT model. The deviations in the surge and sway natural frequencies are very small and might be caused by the implemented mooring system in MoWiT, which accounts for a varying stiffness matrix, however, uses constant damping coefficients. The eigenfrequency in yaw, by contrast, is with some larger deviation slightly higher than the results from the OC3 phase IV participants: ranging from +8.3% up to even +40.9%, with around +23.4% deviation when taking the mean value of the OC3 phase IV participants' results. This discrepancy in the yaw eigenfrequency is mainly due to the different platform yaw inertia of the modeled system, which is 43.6% smaller than the defined value, as already outlined and explained in Section 4.1.1.2. The natural frequencies in heave, roll, and pitch are in good agreement with the OC3 results.

Table 4.6: Natural frequencies (in Hz) from OC3 phase IV codes and MoWiT in comparison, deviations are highlighted in red.

DOF	OC3 mean	OC3 min	OC3 max	MoWiT	MoWiT deviation
Surge	0.0081	0.0077	0.0087	0.0075	-13.4% to -2.0%
Sway	0.0085	0.0077	0.0120	0.0075	-37.2% to -2.5%
Heave	0.0323	0.0313	0.0330	0.0325	-1.4% to +3.9%
Roll	0.0343	0.0305	0.0453	0.0316	-30.2% to +3.7%
Pitch	0.0343	0.0305	0.0452	0.0316	-30.0% to +3.8%
Yaw	0.1229	0.1076	0.1400	0.1516	+8.3% to +40.9%

With regards to the damping ratios, it first has to be emphasized that only three OC3 phase IV participants have contributed their results, which reduces significantly their representativeness (see for example the outlier in the yaw DOF in Figure 4.6 or some very low values - not visible in Figure 4.6 - in the other DOFs). Based on this little data available, it can be seen that there is only a small deviation for the heave DOF, where a slightly higher damping ratio is obtained in the MoWiT model; however, this is even the case where only one OC3 phase IV participants' result is valuable for comparison, as the other two results show unreasonable low values.

Table 4.7: Damping ratios from OC3 phase IV codes and MoWiT in comparison, **deviations** are highlighted in **red**.

DOF	OC3 mean	OC3 min	OC3 max	MoWiT	MoWiT deviation
Surge	0.0663	0.0001	0.1369	0.1169	−14.6% to $+1.2 \times 10^5\%$
Sway	0.0661	0.00001	0.1368	0.1122	−18.0% to $+1.1 \times 10^6\%$
Heave	0.0128	0.00001	0.0384	0.0445	+15.8% to $+4.4 \times 10^5\%$
Roll	0.0609	0.0001	0.1415	0.0534	−62.3% to $+3.8 \times 10^4\%$
Pitch	0.0611	0.0008	0.1415	0.0536	−62.1% to $+6.4 \times 10^3\%$
Yaw	3.3197	0.0446	9.8696	0.0605	−99.4% to $+35.7\%$

Apart from the heave DOF, the MoWiT model yields very comparable results for the static equilibrium positions for DLC 1.3 (Table 4.8). The slightly deeper equilibrium position in heave is opposite the expected deviation based on the difference in the hydrostatic buoyancy force, outlined in Section 4.1.1.2. The deviation might come from any differences in the mooring system or a different value taken for the gravitational acceleration; however, this deviation in the static heave equilibrium position is just minor when comparing the corresponding resulting difference in mass with the total system mass. The horizontal tension forces from the MoWiT model, however, are matching the OC3 phase IV results.

Table 4.8: Static equilibrium positions from OC3 phase IV codes and MoWiT in comparison, **deviations** are highlighted in **red**.

DOF	OC3 mean	OC3 min	OC3 max	MoWiT	MoWiT deviation
Surge [m]	−0.0352	−0.1100	0.0662	−0.0742	−212.1% to +31.9%
Sway [m]	−0.0002	−0.0010	2.89×10^{-5}	9.76×10^{-6}	−66.3% to +101.0%
Heave [m]	-2.83×10^{-5}	−0.0309	0.0400	−0.1290	−422.5% to −317.8%
Roll [deg]	-2.99×10^{-5}	−0.0002	5.59×10^{-7}	1.05×10^{-7}	−81.3% to +100.0%
Pitch [deg]	−0.0566	−0.1185	-4.34×10^{-7}	−0.0605	$-1.4 \times 10^7\%$ to +48.9%
Yaw [deg]	-4.61×10^{-7}	-5.8×10^{-6}	1.48×10^{-6}	1.04×10^{-7}	−93.0% to +101.8%

The degrees of agreement in the natural frequencies, damping ratios, and static equilibrium solutions, obtained in the previous analysis, are clearly visible in the free-decay time series of DLC 1.4: the surge free-decay test DLC 1.4a (Figure 4.7) shows a slightly higher eigenperiod,

but comparable damping; the heave response in DLC 1.4c (Figure 4.8) fits very well with respect to the eigenfrequency, but is slightly higher damped and reaches static equilibrium at a slightly deeper position; the pitch response in DLC 1.4e (Figure 4.9) shows a slightly higher eigenperiod, but comparable damping; and the yaw response in DLC 1.4f (Figure 4.10) has a slightly higher eigenfrequency and is a little bit stronger damped than most of the other codes. Furthermore, the coupled responses between the DOFs are clearly visible in the free-decay time series.

4.1.3.2 Hydro-elastic response analyses

Within the hydro-elastic response analyses with regular waves in DLC 4.1, no additional time is simulated in Dymola[®], for which reason the response time series in Figure 4.11 show some start-up transients in the curves from the MoWiT model, while these have been removed from the results from the OC3 phase IV participants. These start-up transients influence especially the results for the platform motions (Figures 4.11(a) to 4.11(c)), as the equilibrium is not yet achieved. But still, the wave oscillation and coupled response in surge and pitch is clearly visible, while in heave the eigenfrequency is more dominating. The tower-top fore-aft bending moment, induced by the oscillating mass of the RNA, agrees very well with the OC3 phase IV results (Figure 4.11(e)), whereas the tower-top fore-aft shear force time series (Figure 4.11(d)) shows a difference in the peak amplitude and a lack of higher frequency content, which is due to the fact that the tower flexibility is not captured in the MoWiT model. For the downstream fairlead tension, presented in Figure 4.11(f), the start-up transients are again visible; however, it can be clearly seen that the time series approaches the steady-state conditions presented by the OC3 phase IV participants.

When evaluating the hydro-elastic response due to irregular waves, first, it is realized that some statistics of the time series from the MoWiT model, presented in Appendix B, are slightly smaller by amount than obtained from the OC3 phase IV simulation results. However, here it has to be mentioned that not all OC3 phase IV participants have removed the start-up transients for the statistical analyses, which - by contrast - is covered in MoWiT by evaluating only the final fifth of the time series. But still, looking at the power spectra obtained with the MoWiT model, as shown in Figure 4.12, there are significant discrepancies within the results, for which the argumentation on start-up transients does not apply.

Comparing the DLC 4.2 irregular wave spectrum (Figure 4.17(a)) already indicates that the simulated irregular wave in MoWiT differs from the wave in the simulations by the OC3 phase IV participants. Commonly, a large number (in the order of a few hundred) of regular wavelets of different periods and wave heights are superimposed for representing an irregular wave. However, as apart from the spectral information (see Table 4.4) no more details are provided in the OC3 phase IV simulation descriptions, and for reasons of computational effort, the irregular wave in MoWiT is simulated using just one seed. This explains the differences presented in Figure 4.17(a), but also indicates that all other results for response spectra are affected by this. To prove this expectation that the discrepancies in the simulation results stem from the

implemented irregular wave, the different wave input is “eliminated” in the response spectra by multiplying the latter with a “correction factor”. This correction factor is rather to be seen as a transfer function as it is directly the fraction of the OC3 phase IV wave spectrum (averaged over the participants’ results) and the MoWiT wave spectrum; both mathematical operations (averaging and division) are performed for each frequency value separately. Multiplication of the response spectra with this correction transfer function happens as well frequency value by frequency value. To show this effect, first, the corrected wave spectrum is presented in Figure 4.17(b), which corresponds, as intended, to the averaged course of the OC3 phase IV wave spectra.

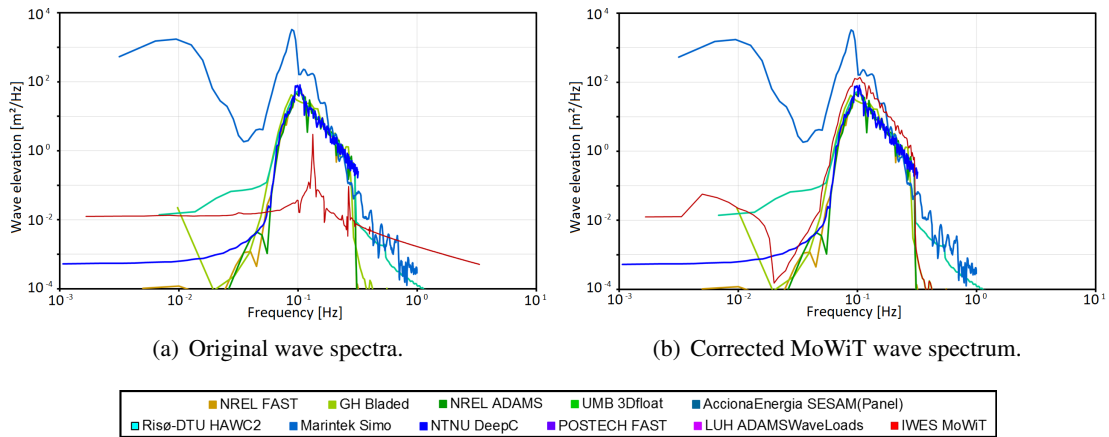


Figure 4.17: Wave power spectra for DLC 4.2 in comparison.

The corrected response spectra (with eliminated difference in the wave input), generated in the way as described above, are presented in Figure 4.18, which already at first glance show significant improvements compared to the unmodified results presented in Figure 4.12. In the power spectra of the platform motions (Figures 4.18(a) to 4.18(c)), now, the peaks at the wave peak period and at the eigenfrequency in the considered DOF, as well as peaks due to couplings between different DOFs are clearly visible and better fit the OC3 phase IV results in the range of the wave peak frequency, compared to the initial spectra presented in Figures 4.12(a) to 4.12(c). Similarly, after applying the correction transfer function, the power spectra for the tower-top fore-aft shear force and moment, as well as for the downstream fairlead tension (Figures 4.18(d) to 4.18(f)) better resemble the trend obtained by the OC3 phase IV participants, while there are still significant differences in the amount for the tower-top fore-aft loadings, which might as well be induced due the rigid modeling of the tower in MoWiT. Furthermore, it has to be noted that this approach of utilizing such a correction transfer function cannot capture any nonlinearities coming from, for example, hydrodynamic viscous forces or nonlinear mooring forces.

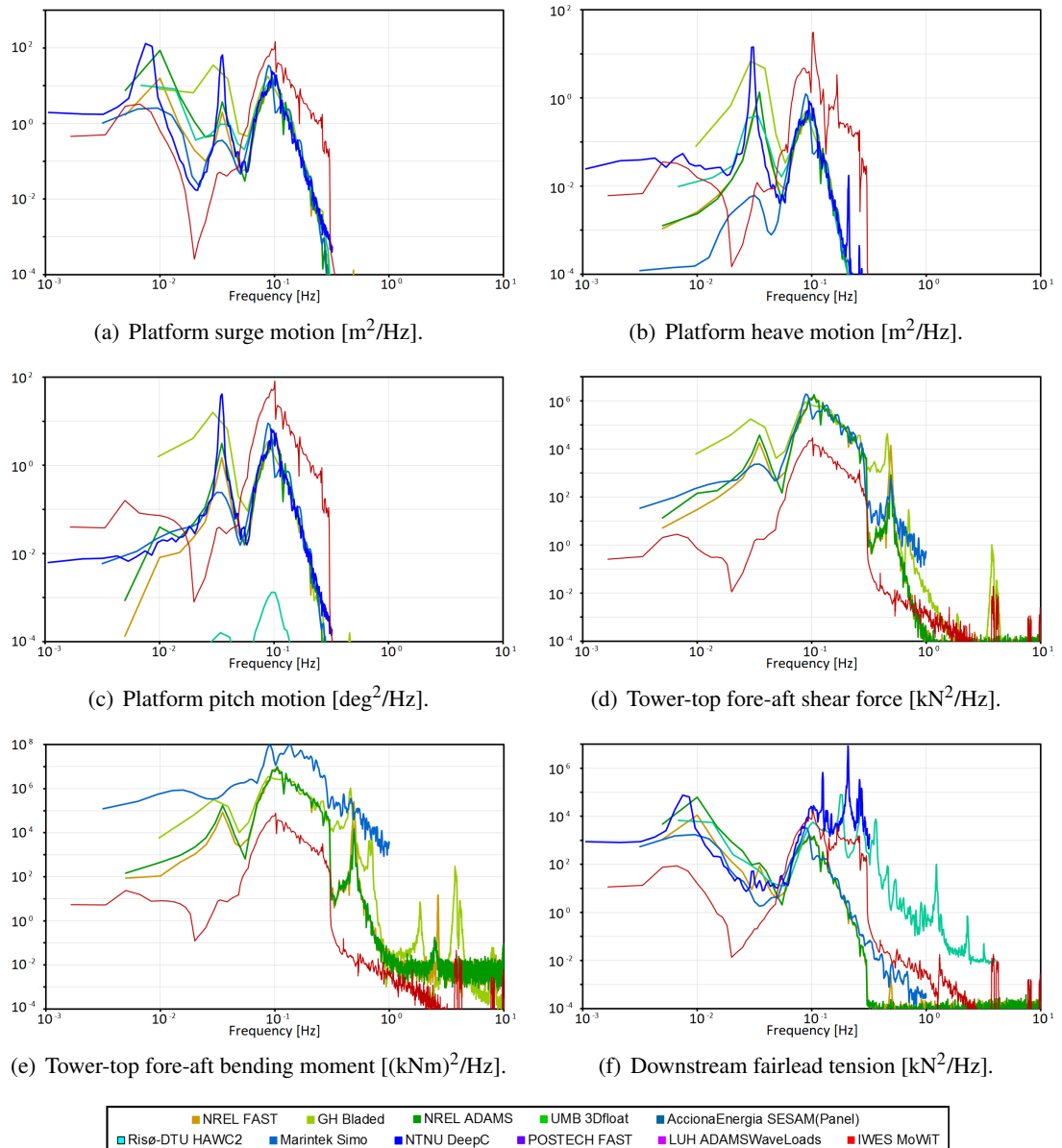


Figure 4.18: Hydro-elastic power spectra with irregular waves from DLC 4.2, corrected for eliminating the deviations in the irregular wave spectrum.

4.1.3.3 Aero-hydro-servo-elastic response analyses

With respect to the comparability of the time series of DLC 5.1 for the aero-hydro-servo-elastic response analyses with regular waves and steady wind, the same aspect has to be commented, as already indicated in Section 4.1.3.2: the OC3 phase IV results show the steady-state response, while the time series from MoWiT still contain start-up transients. These are mainly visible in the time series of the platform motions (Figures 4.13(a) to 4.13(d)) and fairlead tensions (Figures 4.14(a) and 4.14(b)), however, already diminish over the short simulation time. Hence, nevertheless, the wave oscillation is clearly visible in these time series. In the remaining presented parameters for tower-top fore-aft shear force and bending moment (Figures 4.13(e)

and 4.13(f)), out-of-plane blade-tip deflection (Figure 4.14(e)), as well as generator power and rotor speed (Figures 4.14(c) and 4.14(d)), the transients are very short or almost not noticeable and their time series are in good agreement with the results from the OC3 phase IV participants.

For the case with irregular waves and turbulent wind, looking at DLC 5.3 with above rated wind speed (which represents similar findings and conclusions as DLC 5.2 at rated wind speed, as pointed out in Section 4.1.2.2), the statistical results from the MoWiT model, presented in Appendix C, show - apart from the tower-top fore-aft loads - good agreement with the OC3 phase IV values. The outcome that the statistics for the tower-top shear force are predicted with MoWiT smaller by amount than in OC3 phase IV might be due to the fact that the tower is modeled as rigid structure in MoWiT instead of a flexible tower as defined in OC3 phase IV, due to the reasons stated in Section 4.1.1.2. This affects as well the results in the tower-top fore-aft bending moment statistics.

With regard to the power spectra for DLC 5.3, as presented in Figures 4.15 and 4.16, there are again large discrepancies between MoWiT and OC3 phase IV results observed. Hence, and based on the findings from DLC 4.2, described in Section 4.1.3.2, the power spectrum for the irregular wave in MoWiT is examined (Figure 4.19(a)), displaying a similar different behavior, due to the same reason of how the irregular wave is modeled in MoWiT (using - for computational reasons - just one seed for describing the irregular wave, which is not further defined in the OC3 phase IV descriptions), as explained in Section 4.1.3.2. Thus, a correction transfer function is determined accordingly to the approach followed for DLC 4.2 in Section 4.1.3.2. The corrected wave spectrum (Figure 4.19(b)) matches well the wave spectrum from OC3 phase IV, averaged over the participants' individual results.

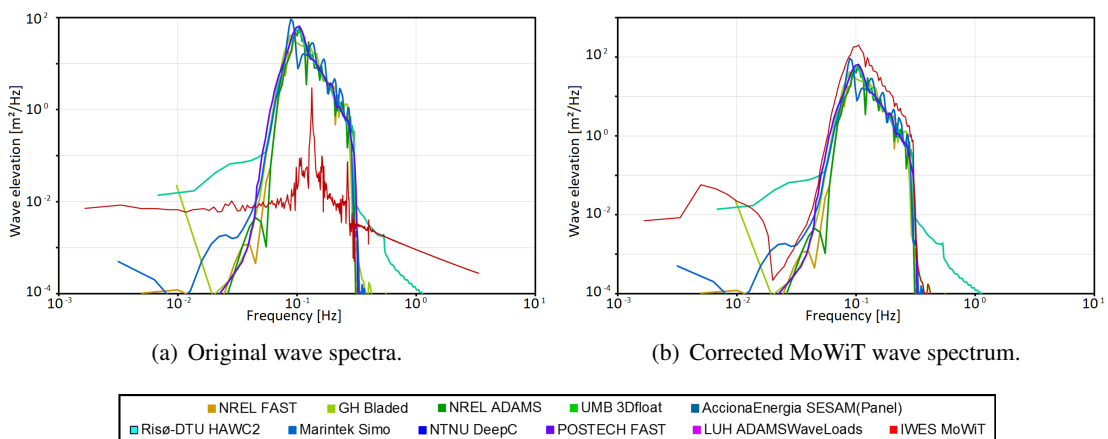


Figure 4.19: Wave power spectra for DLC 5.3 in comparison.

However, as DLC 5.3 also deals with turbulent wind, the power spectrum of the wind is analyzed as well, as presented in Figure 4.20(a). This shows, despite the good match of the statistics for the turbulent wind, some different curve than obtained from the OC3 phase IV participants: the power spectrum from MoWiT is much less steep and has some larger oscillations in the higher frequency range. The difference in the spectrum could be due to the fact that the Kaimal model is used for generating the turbulent wind time series in MoWiT instead of the

prescribed Mann model in OC3 phase IV, as indicated and explained in Section 4.1.2.1. Due to the fact that this discrepancy in the wind spectrum is as well expected to affect the response spectra, another correction transfer function, now for the wind spectrum, is determined, according to the same approach used for the irregular wave spectrum, as explained in Section 4.1.3.2. The corrected wind spectrum is presented in Figure 4.20(b) and now shows a comparable trend similar to the OC3 phase IV (averaged) results.

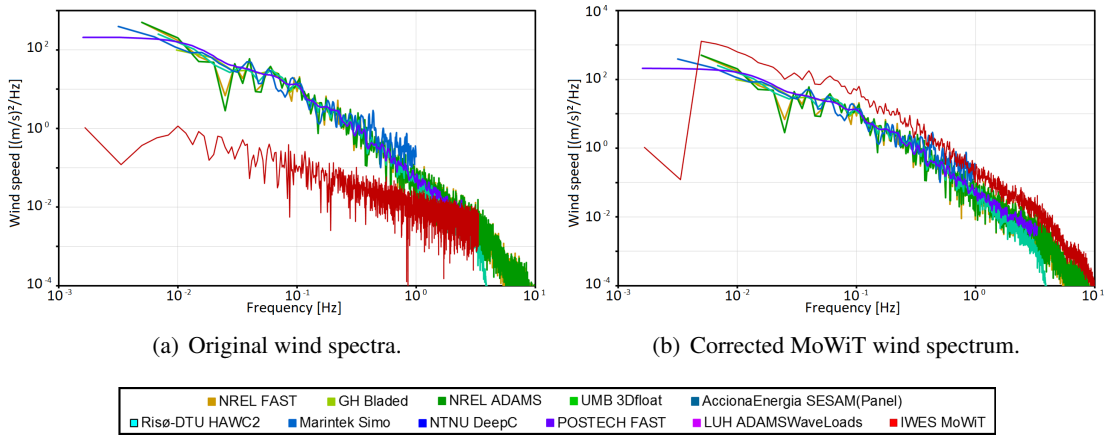


Figure 4.20: Wind power spectra for DLC 5.3 in comparison.

In order to eliminate the differences in the input for the irregular wave, as well as for the turbulent wind, the power spectra of the responses are to be multiplied with the correction transfer functions. However, as now two deficient inputs play a role, it is important to take care of the influence of wind and wave on the single system parameter. Hence, the power spectra of the platform motions in surge, heave, pitch, and yaw, presented in Figures 4.15(a) to 4.15(d) and in which the trend of the original wave spectrum from MoWiT (Figure 4.19(a)) shines through in some frequency ranges, are adjusted by applying the wave correction transfer function, as, in addition, the platform motions are expected to be mainly affected by the hydrodynamics. This yields the corrected power spectra for the platform motions, as visualized in Figures 4.21(a) to 4.21(d). The shapes of the power spectra for the surge, heave, and pitch DOFs have improved, while the power spectrum for the yaw motion is still quite different. This might be due to the fact that a turbulent wind could cause yaw motion of the entire floating system; however, utilizing the wind correction transfer function instead of the wave correction transfer function would result into much too high values.

The tower-top fore-aft loadings, as well as the out-of-plane blade-tip deflection, generator power, and rotor speed are mostly influenced by the aerodynamics. Furthermore, in the original spectra (Figures 4.15(e), 4.15(f), and 4.16(c) to 4.16(e)) the wind spectrum from MoWiT (Figure 4.20(a)) is partially visible. Thus, these power spectra are corrected by applying the wind correction transfer function, which yields some improvement, as presented in Figures 4.21(e), 4.21(f), and 4.22(c) to 4.22(e). While there are still quite large oscillations at high frequencies, the steepness of the spectra are now much more comparable.

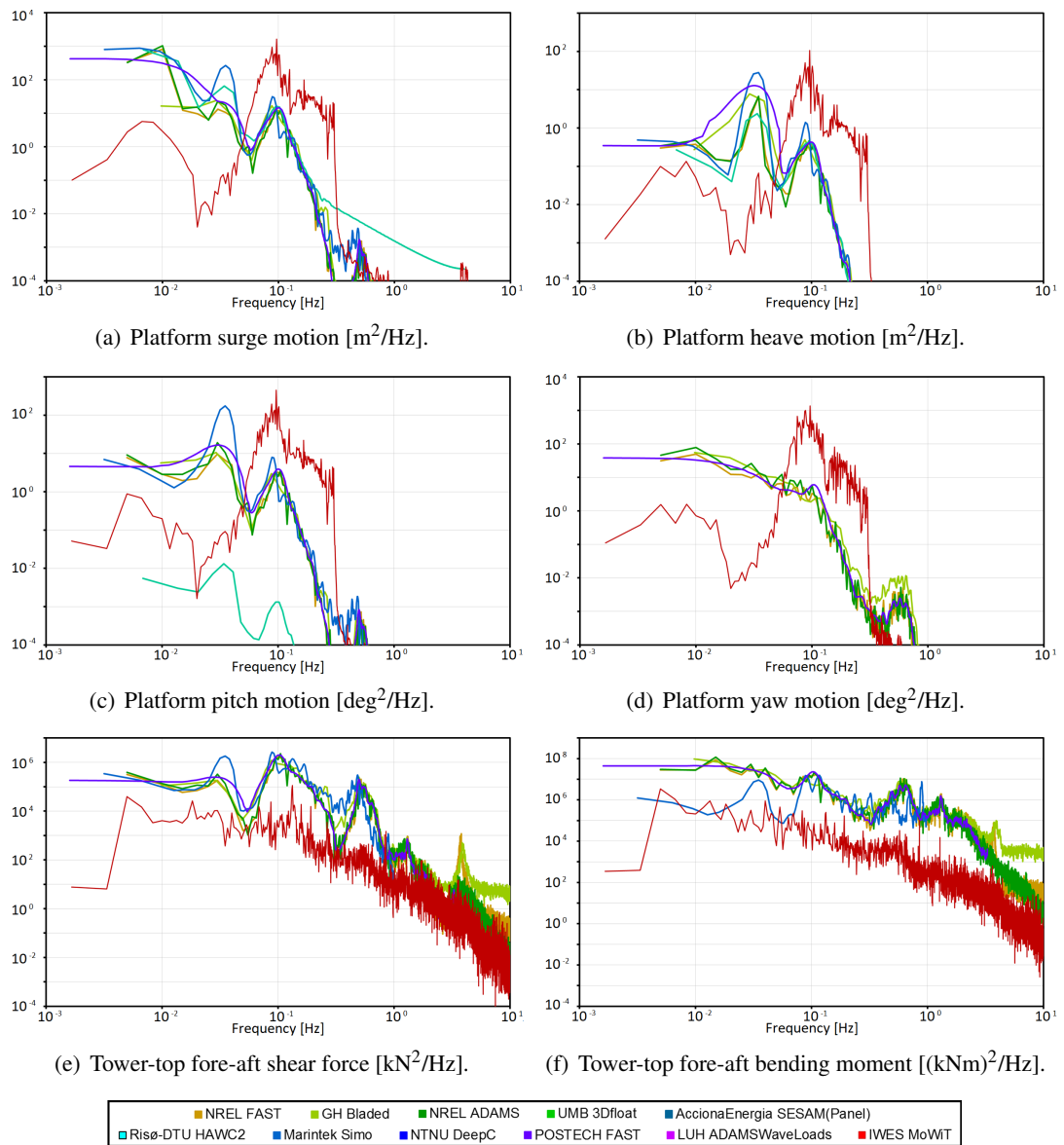


Figure 4.21: Aero-hydro-servo-elastic power spectra with irregular waves from DLC 5.3, corrected for eliminating the deviations in the irregular wave and turbulent wind spectra, part I.

Finally, for the remaining two parameters to be analyzed - the downstream and upstream fairlead tensions - the wave correction transfer function is again applied to the original spectra (Figures 4.16(a) and 4.16(b)), as the hydrodynamics are expected to be the primary influencing factor. This way, a significant improvement, especially in the range of the wave peak frequency, can be achieved, as presented in Figures 4.22(a) and 4.22(b).

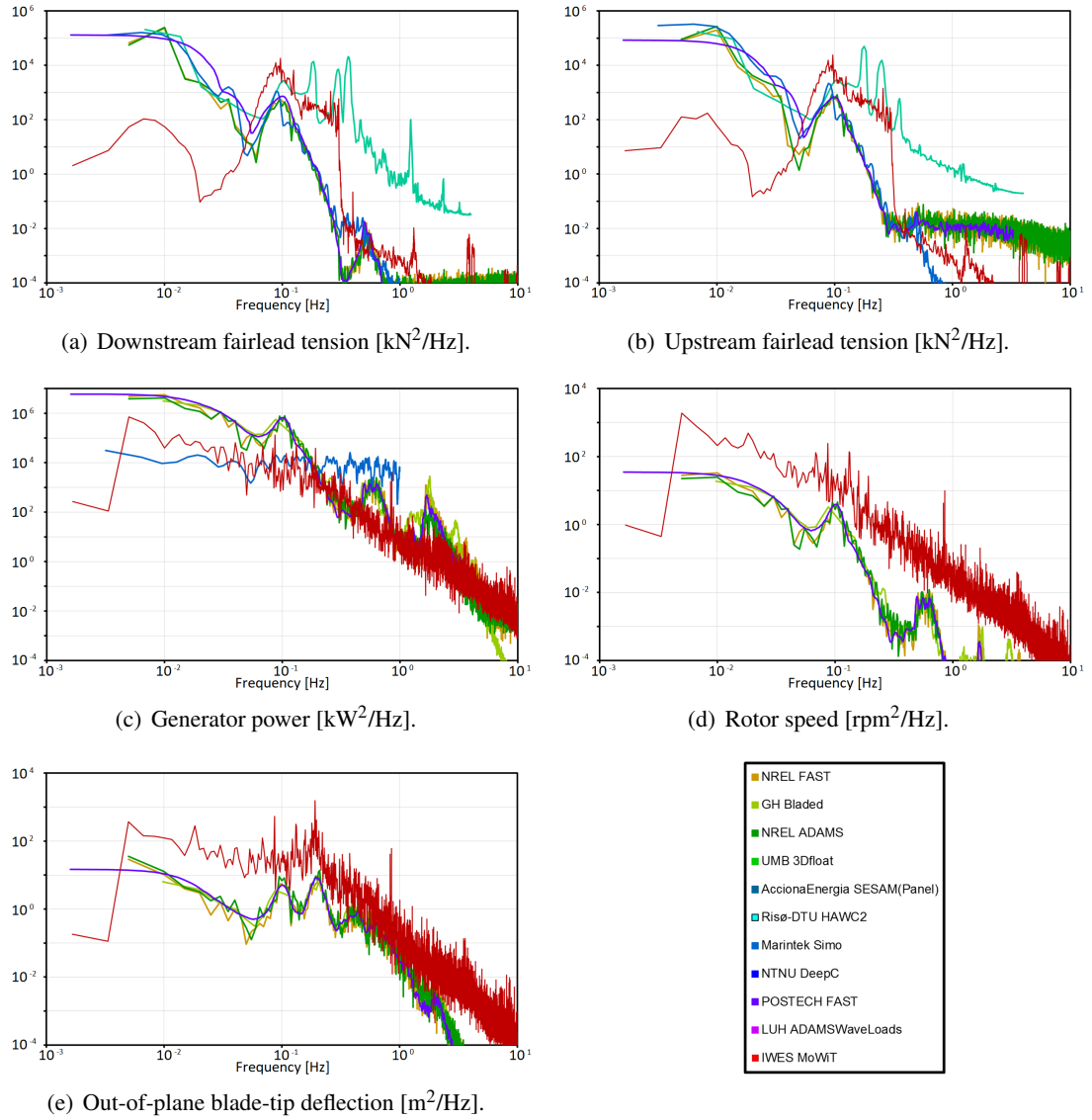


Figure 4.22: Aero-hydro-servo-elastic power spectra with irregular waves from DLC 5.3, corrected for eliminating the deviations in the irregular wave and turbulent wind spectra, part II.

4.1.3.4 Brief résumé of the model verification

In consequence of missing data and incomplete information, assumptions are required to develop an aero-hydro-servo-elastic coupled model of dynamics for the OC3 phase IV spar-buoy FOWT system, based on MoWiT. Due to these assumptions, some (minor) deviations in the model characteristics are obtained and corresponding differences in the simulation results expected, which, however, can be taken into account in the analyses of the code-to-code comparisons. In this regard, the code-to-code comparisons of the MoWiT simulation results show for the system-only analyses, as well as for the hydro-elastic and aero-hydro-servo-elastic response analyses in regular and steady environmental conditions, overall good agreement with the results from various other wind turbine system tools used by the OC3 phase IV participants. In irregular and turbulent environmental conditions, however, further discrepancies are obtained

due to differences in the environmental inputs, start-up transients still contained in the time series and resultant power spectra, and unconsidered tower flexibility in the MoWiT model. The comparability of the power spectra of the system responses can already be improved by applying a correction transfer function, however, nonlinearities or effects of the start-up transients cannot be captured with this approach. Thus, MoWiT can already be utilized for fully-coupled aero-hydro-servo-elastic simulations, as well as design assessment and development of FOWT systems; however, for a full verification of the FOWT system model, more detailed results assessments - including new simulations of the DLCs based on an updated system model, as well as environmental inputs that are adjusted and verified beforehand - are needed.

4.2 Development of a framework for wind turbine design and optimization

Standards or technical specifications by Det Norske Veritas DNV (2014), DNV GL (2018c, 2016a), or International Electrotechnical Commission IEC (2019b,c,a) describe DLCs, which are grouped into normal, fault, and other (transport or installation) design situations. DLCs are used to assess ultimate and fatigue loads on the system and this way to approve its integrity and to show that the wind turbine can withstand environmental conditions during its design life. Considering various normal and extreme conditions for the different design situations leads to a huge set of load cases, for which prescribed parameters have to be set. For this application an automated simulation framework is valuable.

Furthermore, to support the development of a wind turbine design through an optimization process, iterative simulations have to be executed. In these, a number of design variables have to be modified until an appropriate design, optimized with respect to a range of prescribed criteria, is achieved. However, due to the complexity of wind turbine systems, as well as their non-linear and fully-coupled aero-hydro-servo-elastic behavior, this optimum solution has to be derived through modeling and simulation. Thus, a framework for automated optimization of wind turbine systems is essential.

A huge variety of optimization methods is available and finds application to optimization tasks for the complex engineering systems in the field of renewable energies (Momoh & Suren-der Reddy 2014, Baños et al. 2011). In the particular case of wind turbine systems, not only the optimization approaches, but also the optimization objectives are multifaceted. Apart from the most common and overall goal of reducing the system costs or LCoE (Hou et al. 2019, Mytilinou & Kolios 2019, Mytilinou et al. 2018, Lemmer et al. 2017, Mytilinou & Kolios 2017, Wang et al. 2016, Ashuri et al. 2014, Herbert-Acero et al. 2014, Muskulus & Schafhirt 2014, Sandner et al. 2014, Valverde et al. 2014, Härer 2013, Fylling & Berthelsen 2011), the optimization focus also often lies on the loads on the system, including fatigue (Lemmer et al. 2017, Chew et al. 2016, Ashuri et al. 2014, Muskulus & Schafhirt 2014, Sandner et al. 2014, Härer 2013, Fylling & Berthelsen 2011), as well as the dynamic system response (Lemmer et al. 2017, Sandner et al. 2014, Fylling & Berthelsen 2011, Clauss & Birk 1996). The compo-

ment of interest, which is to be optimized, ranges from the blades (Ashuri et al. 2014), the tower (Wang et al. 2016, Ashuri et al. 2014, Muskulus & Schafhirt 2014), and the support structure (Chew et al. 2016, Muskulus & Schafhirt 2014, Clauss & Birk 1996), which might even be floating (Lemmer et al. 2017, 2016, Sandner et al. 2014, Härer 2013, Fylling & Berthelsen 2011, Clauss & Birk 1996), to the mooring lines and power cable (Fylling & Berthelsen 2011), and even to wind farms, which might be optimized with respect to their location, layout, or utilized turbines (Hou et al. 2019, Mytilinou & Kolios 2019, Mytilinou et al. 2018, Mytilinou & Kolios 2017, Herbert-Acero et al. 2014, Valverde et al. 2014). The optimization itself can be done analytically and gradient-based (Chew et al. 2016, Ashuri et al. 2014, Clauss & Birk 1996); however, most commonly evolutionary and genetic algorithms are applied (Mytilinou & Kolios 2019, Mytilinou et al. 2018, Mytilinou & Kolios 2017, Wang et al. 2016, Härer 2013). Furthermore, due to the high complexity of wind turbine systems, simplified models, such as multibody or reduced-order models, are utilized for the application in optimization tasks (Lemmer et al. 2017, 2016, Sandner et al. 2014, Härer 2013, Fylling & Berthelsen 2011). Even in the already quite established field of wind farm design and layout optimization, the single wind turbine system is extremely simplified, as the main emphasis is on the farm economics and not on the fully-coupled system dynamics of each single wind turbine within the farm.

The presented literature shows the need and relevance of design optimization methods for wind turbine systems; however, apart from a few multidisciplinary approaches focusing on more than just one system component (Ashuri et al. 2014, Muskulus & Schafhirt 2014, Fylling & Berthelsen 2011), the available optimization methods are mostly tailored to the specific optimization task and component of interest. This is reflected as well by the manner, in which the system is implemented: simplified and reduced-order models for the wind turbine system are utilized (Lemmer et al. 2017, 2016, Sandner et al. 2014, Härer 2013), as well as aero-, hydro-, control, and structural dynamics are only selectively and/or just rudimentary represented (Wang et al. 2016, Fylling & Berthelsen 2011, Clauss & Birk 1996). Each method presented in the literature is valuable but limited to certain optimization problems. Thus, a holistic approach for optimization of wind turbine systems, involving all system components, as well as their fully-coupled aero-hydro-servo-elastic behavior, is the next development step and level of wind turbine design and optimization. Such a holistic and highly flexible optimization framework is developed and presented in this section. This framework is not only suitable for systematic optimization of wind turbine systems, but also for automated execution of simulation and optimization tasks. Furthermore, it implies fully-coupled simulations of any wind turbine system - even floating.

Thus, first (Section 4.2.1), a generic description of such a framework for automated wind turbine system simulation is presented. The application of this for automated DLC simulations is shown afterwards in Section 4.2.2. To cope also with optimization tasks, additional features need to be considered and incorporated in the framework (Section 4.2.3). The broad range of applications of the framework for optimization problems is outlined and discussed in Section 4.2.4, while the framework is utilized for the design optimization tasks presented in Chapters 5 and 6.

4.2.1 Framework for automated simulation

To establish a framework for automated simulation of wind turbine systems, three main components, as presented in Figure 4.23 and described hereafter, are considered to be required. This modular structure allows the utilization of unique modules, which are sophisticated for the particular application. The selected tools for the framework utilized in this work are presented in the end (Section 4.2.1.4) and denoted as well in Figure 4.23.

4.2.1.1 Modeling environment

First, there is the need for a modeling environment, which is capable of representing the non-linear and fully-coupled aero-hydro-servo-elastic behavior of an onshore or offshore wind turbine system, which might be in the latter case bottom-fixed or even floating. Within the model all components of the system, corresponding parameters and variables, as well as their physical relations and the systems of equations have to be specified.

Various codes and tools for wind turbine modeling, load calculation, and fully-coupled aero-hydro-servo-elastic simulation - as presented and described in more detail in Section 4.1 and applied to code-to-code comparison tasks - are already developed, such as:

- Bladed (DNV GL 2020) by DNV GL, which is a wind turbine design and simulation software, by which means both the wind turbine and its environment can be modeled (DNV GL 2018a);
- FAST (Jonkman 2018) by NREL, which is an aero-elastic simulation tool for horizontal axis wind turbines, based on a code containing models for aero-, hydro-, control, and structural dynamics (Jonkman & Buhl 2005);
- HAWC2 (Kristiansen 2020) developed at Risø National Laboratory in Denmark, which is an aero-elastic code for wind turbine design and load simulation and covers various models for dealing with aero-, hydro-, control, and structural dynamics (Larsen & Hansen 2015);
- MoWiT developed at Fraunhofer IWES in Bremerhaven, Germany, which is based on the open-source object-oriented and equation-based modeling language Modelica[®] (Modelica Association 2020a) and by which means the entire wind turbine system can be represented through models for each single component, including the environment and aero-hydro-servo-elastic dynamics (Leimeister & Thomas 2017a, Thomas et al. 2014, Strobel et al. 2011).

4.2.1.2 Simulation tool

Having created the wind turbine system model, it needs to be passed on to a simulation tool. Additionally, simulation settings, such as simulation duration, solver type, step size, and tolerance have to be defined.

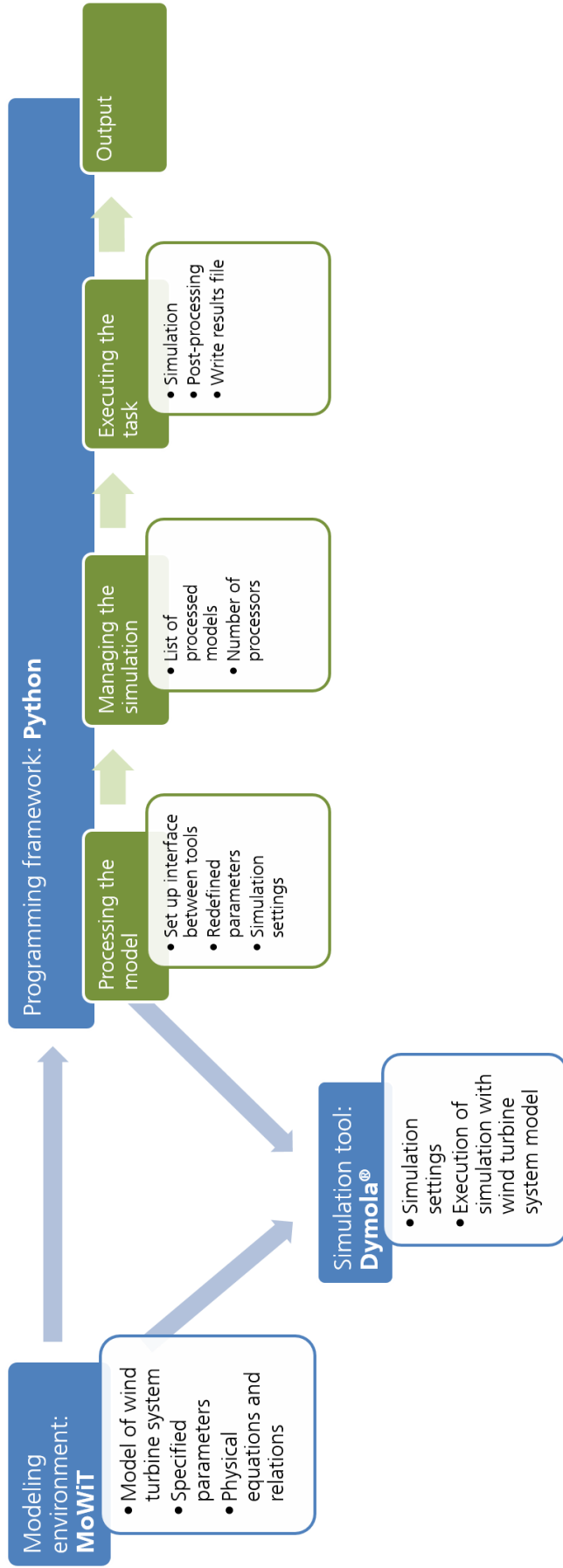


Figure 4.23: Components of the framework for automated simulation and their relations, with selected tools for utilized framework being denoted.

The simulation tool could either be already integrated in one tool together with the code for modeling or could be separated from the modeling environment. For the modeling tools, presented in Section 4.2.1.1, the corresponding simulation environments are as follows:

- the Bladed software package directly contains modules for simulations execution, results analyses and post-processing, as well as batch calculations (DNV GL 2018a);
- the FAST tool also not only contains code and models, but is as well capable of executing time-domain simulations (Jonkman & Buhl 2005);
- within the HAWC2 code there is directly a simulation command block, which specifies the simulation settings when executing the file (Larsen & Hansen 2015);
- however, in order to translate and simulate Modelica[®] models, a separate simulation environment is required. There is a huge number of commercial and free tools (Modelica association 2020b), which can be used together with Modelica[®]. At Fraunhofer IWES, Dymola[®] by Dassault Systèmes (2015a,b) is utilized for simulating models based on MoWiT in time-domain, due to the available interfaces to MATLAB[®] and Simulink and as Dymola[®] is highly suitable for system models which obey a large number of equations.

4.2.1.3 Programming framework

Finally, a programming framework, capable of interfacing with both the modeling environment and the simulation tool, needs to be established. Within this programming framework all steps required for automated execution and control of wind turbine system simulations are defined, from model processing, through simulation management and execution, to the final output.

Processing the model In the first step, the wind turbine system model created in the modeling environment (see Section 4.2.1.1) and passed to the simulation tool (see Section 4.2.1.2) is processed. Thus, an interface between the modeling environment and the programming framework has to be set up, but also already the link to the simulation tool has to be established. Through this interface, on the one hand, the specified model is provided and given as input to the programming framework. Apart from this, however, the interface should also allow to some degree for modifications of model and initial defined settings. This is highly relevant when it comes to DLC simulations or optimization tasks, in which one and the same base model is used, however, either environmental parameters or turbine operational stage (in case of DLC simulations) or design variables (in case of optimization tasks) differ from simulation to simulation. Hence, it should be possible to redefine system parameter values, but also to specify the simulation settings, which are then further processed to the simulation tool when executing the task. Furthermore, within the model processing step, the output parameters are defined and - depending on the capability of and interface with the simulation tool - additional code for saving the results in an output file is written. Finally, the model processing step should also

extract from the model and simulation settings the number of simulations which are to be run. This is relevant for managing the simulations, as explained hereinafter.

Managing the simulation When managing the simulation, one and the same or several different processed models can be dealt with at the same time and in different ways. Thus, it can be specified that the model is just translated or as well simulated, or even only some partial or preparative simulation tasks, such as creation of turbulent wind speed time series, are executed. Having declared the manner, in which the models are to be dealt with, now the number of simulations, which is provided for each processed model as mentioned before, and the number of processors, which can be used for executing the task, are important. The latter has to be specified by the user and has to be consistent with the available logical processors. Thus, depending on the settings and user preferences, as well as the computer or system capabilities, the simulations of the models in the simulation tool can be run one by one after each other or executed simultaneously, using several processors in parallel. The latter option, of course, is of high interest and advantage (with respect to time-efficiency) when having to handle a large number of simulation tasks, as is the case with DLC simulations and optimization processes.

Executing the task Based on the model processing and simulation management done beforehand, commands are written in the programming framework for finally executing the specific task. Thus, the interface from the modeling environment through the programming framework to the simulation tool is used to simulate the model or just to create other wind turbine system input files, for example a time series of the wind speed for representing turbulent wind. Furthermore, additional code for post-processing of the results or for extending the framework to the application for optimization tasks can be written at this point in the programming framework. More information on the incorporation of optimization functionalities in the programming framework are given in detail in Section 4.2.3.

Output After execution of the simulation tasks, the specified parameters are given as output and the corresponding results and/or the further post-processed results are written in an output file, according to the commands given when processing the model and the additional code defined in the last step within the programming framework for executing the task, as described before.

4.2.1.4 Selected tools for utilized framework

In Figure 4.23 the tools, which are selected to be incorporated in one framework for automated simulation, are denoted:

1. MoWiT as modeling environment;
2. Dymola[®] as corresponding simulation tool for executing time-domain simulations; and

3. Python (Python Software Foundation 2020) as programming interface for external and automated control of the simulations.

These tools stand in perfect mutual complement. The Modelica[®] based modeling environment in combination with the Dymola[®] simulation engine is very suitable for time-domain simulations of complex multi-physics engineering problems. Programming in Python, on the other hand, facilitates the management and handling of simulations, controls the entire simulation process, and creates a set framework for automated application to engineering system models and problems.

MoWiT and Dymola[®] for modeling and simulation MoWiT is selected as modeling environment due to its beneficial properties.

- **High flexibility**

Due to the object-oriented and equation-based modeling language Modelica[®], its hierarchical programming structure, and its multibody approach, the complex wind turbine system can be represented through component-based numerical models, as described in detail with respect to their physics in Section 4.1.1.1. Thus, MoWiT contains six main components (rotor, nacelle, operating control, support structure, wind, and waves), which comprise further subcomponents, such as the hub and blades within the rotor component, the drivetrain and generator within the nacelle component, or within the support structure component the tower, substructure, as well as ballast and mooring lines in case of a floating system. The single components and models are interconnected to represent the fully-coupled aero-hydro-servo-elastic behavior of wind turbine systems, as presented in Figure 4.2. By adapting or exchanging single components, any state-of-the-art wind turbine system type (onshore or offshore, bottom-fixed or floating), various environmental conditions, and different simulation settings can be modeled.

- **Continuous enhancement and extension**

The development of MoWiT directly happens at Fraunhofer IWES, which has the code and knowledge at its own disposal. This allows continuous enhancement and extension of the library - as done by Leimeister & Thomas (2017a), Thomas et al. (2014), and Strobel et al. (2011) - and including also verification and validation of the code - as covered in Section 4.1 and performed by Robertson et al. (2020), Popko et al. (2019), Leimeister & Dose (2018), Popko, Huhn, Robertson, Jonkman, Wendt, Müller, Kretschmer, Vorpahl, Hagen, Galinos, Le Dreff, Gilbert, Auriac, Villora, Schünemann, Bayati, Belloli, Oh, Totsuka, Qvist, Bachynski, Sørnum, Thomassen, Shin, Vittori, Galván, Molins, Bonnet, van der Zee, Bergua, Wang, Fu & Cai (2018), and Leimeister & Thomas (2017b). Thus, different theories and approaches are implemented to represent the aero-hydro-servo-elastic dynamics of a wind turbine system and the degree of detail is refined on and on. The current capability of the in-house library MoWiT is presented in detail in Section 4.1.1.1 and shortly summarized as follows (Leimeister & Thomas 2017a, Thomas et al. 2014, Strobel et al. 2011).

- The BEM theory with dynamic stall and dynamic wake, or the generalized dynamic wake model with dynamic stall, or stochastic wind and gust models can be utilized to represent unsteady aerodynamics.
- The hydrodynamic loads of regular or irregular waves can be determined based on the Morison equation or the MacCamy-Fuchs approach, with having different wave theories (linear Airy or non-linear Stokes) available and optionally accounting for wave stretching (Wheeler or linear extrapolation). The buoyancy force and righting moment are calculated in time-domain depending on the actual local surface elevation and the current position of the offshore structure. Additionally, loads from different current types (breaking wave induced, wind-generated, or sub-surface) are considered.
- The servo dynamics are represented by means of a built-in operating control or a generic dynamic link library interface.
- Finally, the elastic behavior is addressed with the aid of the multibody approach, using Euler-Bernoulli or Timoshenko beam elements. Blades and tower can as well be represented by modal reduced anisotropic beams, considering deflection and torsion, and even accounting for bent-twist coupling effects in the blades.

- **Broad range of applications**

Apart from the fully-coupled time-domain simulation of wind turbine systems, MoWiT serves as basis for a wide range of other applications, such as

- real-time simulations in a hardware-in-the-loop environment;
- usage of components in MATLAB[®] and Simulink;
- automated simulation of design load cases;
- automated system and component optimization.

The latter two are realized by means of the framework for wind turbine design and optimization presented in this work.

In Modelica[®], using MoWiT, the considered wind turbine system is specified and all parameters are set, so that the model can be simulated in the corresponding utilized simulation tool Dymola[®]. This way a Modelica[®] package is created, which is the main input to the programming framework as it contains all necessary information about the simulated model (structure, components, parameters, equations, states, ...). In order to modify specific parameter values and settings according to specific simulation requirements still when processing the model in the programming framework, the foundation has to be laid already in the model set up based on MoWiT. In the Modelica[®] modeling language, it can be stated - by adding `annotation(Evaluate=false)` to certain variables, when defining them in MoWiT - that these variables are not evaluated and replaced by the predefined value, but remain with their variable name in the model and, hence, can still be addressed when processing the model in the programming framework.

Python for the programming framework The programming framework, used in this work in conjunction with MoWiT and Dymola[®], is written in Python. Python is among others a commonly used programming language (Python Software Foundation 2020), but has important advantages over some other well-known programming languages. First of all, Python is not commercial, furthermore, several open-source libraries exist, moreover, the area of application is very broad, and Python is judged to be very suitable for different programming levels and purposes (McKinney 2013). Thus, for example packages defining interfaces between certain tools are already available, such as the Python package BuildingsPy (The Regents of the University of California 2020), which links Python with Modelica[®] and Dymola[®], or the code for tools like HAWC2 can directly be generated using Python scripts. Also wind turbine specific tools, such as TurbSim (Jonkman 2009) for generating turbulent wind fields can be addressed through Python.

In specific for the MoWiT-Dymola[®]-Python framework, when processing the model, the interface between the utilized tools can directly be defined by means of the available Python package BuildingsPy. The further steps within the model processing - model parameters redefinition, simulation settings, and output definitions, as explained in Section 4.2.1.3 - are specified in Python scripts. For the simulation management, the option to generate turbulent wind fields is available to be selected, as the above mentioned tool TurbSim (Jonkman 2009) is integrated in the Python programming framework. This way, a turbulent wind speed time series can be obtained by means of the framework and then directly used when simulating the processed model in a consecutive step. Finally, Python offers wide possibilities, when intending to add code for post-processing or further extension of the framework, as this can be dealt with by means of additional scripts and by utilizing available Python packages, for example for addressing optimization tasks, which will be investigated in more detail in Section 4.2.3.

4.2.2 Application for DLC simulations

The framework for automated simulation gains meaningful importance for the application for lifetime and fatigue analyses of wind turbine systems, as these come usually with a huge number of DLC simulations.

4.2.2.1 The role of DLCs for wind turbine systems

For examining a wind turbine design, load calculations are essential to analyze the wind turbine performance in different environmental and operational conditions, determine ultimate and fatigue loads on turbine components, estimate damage, integrity, and lifetime of the system, as well as assess the system performance in fault conditions.

Several distinct DLCs for wind turbine systems are proposed by standards like DNVGL-ST-0437 (DNV GL 2016a) and IEC 61400-1 (IEC 2019a), or DNVGL-ST-0119 (DNV GL 2018c), DNV-OS-J101 (DNV 2014), IEC 61400-3-1 (IEC 2019b), and IEC TS 61400-3-2 (IEC 2019c) with special focus on offshore (floating) wind turbine systems. These cluster different design situations, meaning the operating state of the wind turbine, such as power production with or

without occurrence of a fault, start-up, normal or emergency shut-down procedures, parked conditions with or without occurrence of a fault, as well as other situations (e.g. transport, assembly, maintenance, or repair). For each design situation various environmental conditions have to be considered. One essential parameter is of course the wind, which could be steady or follow a normal or extreme turbulence model, range from cut-in to cut-out wind speeds of the operating system or take on extreme values for 50-year events, represent extreme operating gusts, or contain extreme direction changes. In case of offshore wind turbines, additional environmental factors play a role. Thus, the sea state, represented by regular or irregular waves for normal or extreme events, is to be defined. Furthermore, wind and waves could be uni- or multi-directional, but also misaligned with respect to the wind turbine. Apart from waves, also currents have to be taken into account when dealing with an offshore system. These can either consist of sub-surface currents and/or wind generated, near surface currents, and/or breaking wave induced surf currents. Finally, in some DLCs fault conditions have to be considered, which could for example be the loss of electrical network or a fault in the control system to pitch the blades or yaw the nacelle.

Thus, there is a large number of different simulations with one and the same wind turbine system model, in which specific settings and parameter values are to be defined. To reduce the dimension of the system analysis task, often only the prevailing DLCs and environmental conditions, which are assessed as most relevant for the considered system and problem of interest, are utilized (Stieng & Muskulus 2019, Krieger et al. 2015, Matha et al. 2014, Bachynski et al. 2013). But still, several iterative simulations have to be performed and the number of simulations will multiply quickly if the wind turbine system develops within the design process. Hence, automated DLC generation and simulation are relevant for repetitive detailed analyses of various wind turbine systems.

4.2.2.2 Realization of DLC simulations with the framework for automated simulation

When using the programming framework for DLC simulations, several parameters have to be specified and additional information has to be provided when processing the model. One DLC comes with different wind speeds, seeds for turbulent wind, yaw misalignment angles of the turbine with respect to the incoming wind direction, initial rotor positions, direction angles of gusts if applicable, as well as - additionally for offshore systems - wave heights, wave periods, seeds in case of irregular waves, and wind-wave-misalignment angles. Therefore, many simulation cases result from one DLC. An effective implementation with respect to computational effort allows combination of different parameter settings, for example by splitting the wind seed numbers and distributing them to the yaw misalignment angles. To uniquely denominate the single simulations within one DLC, a suffix follows the DLC name. This suffix is constructed according to a predefined naming convention, which uses the values in combination with the coefficients (similar to an abbreviation) of the above mentioned parameters. This naming convention could be for example $DLC_x_wW_sY$, with x indicating the number of the DLC, W being replaced by the considered mean wind speed, S referring to the seed number for the

random generation of the turbulent wind conditions, and Y specifying the yaw misalignment angle between wind direction and the perpendicular to the rotor plane. As the characteristic irregular wave parameters are mostly different depending on the considered wind speed case and for each wind seed also an unique seed number for the random phase angle is commonly used, these values do not need to appear in the naming convention. However, this can further be extended, if additional aspects - such as wind-wave misalignment - have to be considered.

Thus, in the model processing step within the programming framework (Section 4.2.1.3), additionally the name of the simulation file needs to be specified according to the naming convention and the simulation parameters are set, both based on the values of the coefficients for wind and wave parameters. For the sake of clarity, it makes sense to use separate programming scripts for each DLC to prescribe these values and settings. The DLC specification scripts can be based on a standard or technical specification by IEC (IEC 61400-1 (IEC 2019a), IEC 61400-3-1 (IEC 2019b), or IEC TS 61400-3-2 (IEC 2019c)) or a standard by DNV GL (DNVGL-ST-0437 (DNV GL 2016a), DNVGL-ST-0119 (DNV GL 2018c), or DNV-OS-J101 (DNV 2014)). The determination of the single parameter values for each simulation within one DLC, as well as the assignment of the values to the parameters within the wind turbine system model follow directly the coding in the model processing step and the DLC definition scripts. Thus, only the basic settings and system parameters are needed as input, on which basis then the framework internally and automatically sets up and simulates all the single DLC subcases.

In addition, the programming framework - within the final step when defining everything for the task execution - can also be used to code a post-processing method to write the results from the DLC simulations in a MLife-compatible output file. By means of this post-processed output file, the simulation results can further be evaluated using MLife (Hayman 2018). The MATLAB[®]-based tool allows statistical, short-term, and lifetime analyses of the considered wind turbine system. This way, extreme and mean values of structural loads, as well as their standard deviations can be determined, but also fatigue calculations for short-term damage-equivalent loads or for the lifetime damage performed. (Hayman & Buhl 2012, Hayman 2012)

4.2.3 Incorporation of optimization functionalities

By incorporating additional functionalities and features, the framework for automated simulation can be extended to be also used for simulation-based optimization, as defined by Gosavi (2015). Such an automated optimization procedure is highly beneficial because wind turbine systems cannot directly be optimized just by utilizing mathematical operations, as the non-linear system is too complex (with even much greater complexity in case of FOWTs), and, thus, optimization tasks on wind turbine systems come with several iterations (corresponding to a large number of simulations) until an optimum solution is found.

The programming framework introduced in Section 4.2.1.3 serves as basis. The extension happens in the task execution step, as visualized in Figure 4.24. At this point, the optimization task has to be introduced, specified through the optimization problem (Section 4.2.3.1), the optimizer (Section 4.2.3.2), and the optimization algorithm (Section 4.2.3.3).

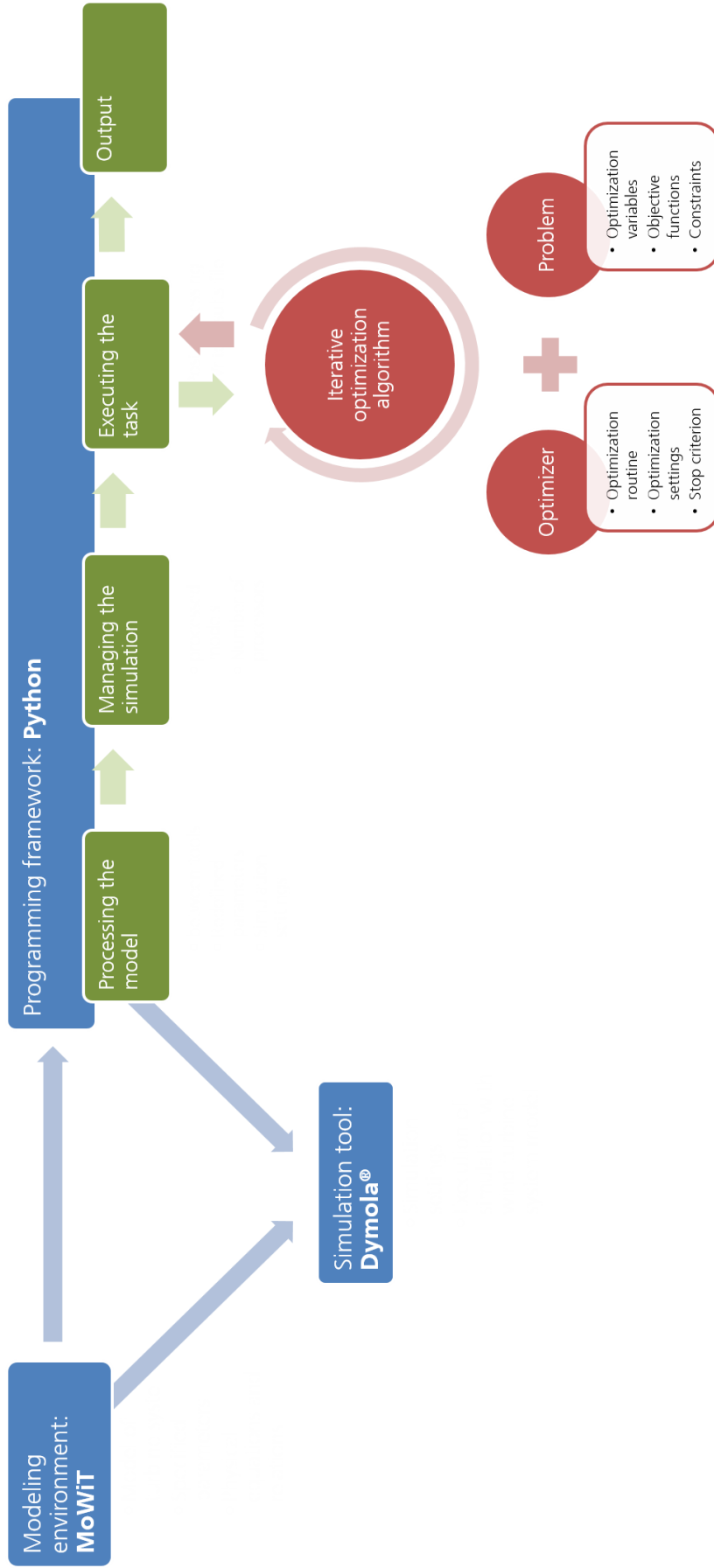


Figure 4.24: Incorporation of optimization functionalities into the framework.

4.2.3.1 The optimization problem

The optimization problem, meaning the optimization task, has to be defined. This comprises the declaration of optimization (or so-called design) variables (x_i), which are to be modified during the optimization process; objective functions (f_i), which describe the targets of the optimization and are (depending on the optimization routine) mostly formulated in such a way that the functions are to be minimized; and (in-)equality constraints ($g_i \leq 0$ and $h_i = 0$, respectively) for optimization criteria and parameters, if they are only allowed to take on specific values or for instance the target value should be approached from only one side on the numerical scale. The general formulation of such an optimization problem with multiple objective functions can be written as

$$\begin{aligned}
 &\text{find} && X = \{x_1, \dots, x_k\} \\
 &\text{to minimize} && f_i(X, \text{system}(X)) \quad , \quad i = 1, \dots, l \\
 &\text{subject to} && h_i(X, \text{system}(X)) = 0 \quad , \quad i = 1, \dots, m \\
 &\text{subject to} && g_i(X, \text{system}(X)) \leq 0 \quad , \quad i = 1, \dots, n
 \end{aligned}$$

The functions are either directly depend on the design variables, collated in the design variables vector X , or also on the resulting fully-coupled floating wind turbine. Due to the complexity of the considered FOWT system, a new external function $\text{system}(X)$ is introduced, which means that the fully-coupled FOWT system with the specified design variables is evaluated externally by means of the model definitions based on MoWiT and corresponding simulation analyses, to finally derive the parameters for the objective functions and constraints.

Design variables Within an optimization task there are parameters of the wind turbine system selected, which may be modified during the optimization. These optimization variables are specified, using the parameter names according to the model definition. Since these parameters are assigned new values during the optimization, it is important that they are still existing in the compiled model (see the remark in Section 4.2.1.4).

Objective functions Apart from the modifiable wind turbine system parameters, the specific goal of the optimization has to be specified, but also several objectives can be pursued within one optimization task. These goals are defined through objective functions - expressions which are to be (depending on the specific optimization routine, but typically) minimized. Using a parameter (*criterion*), taken from simulation results or from further processing of these, and having the target value (*goal*) for this criterion, possible notations of the objective function could be for example Equations 4.1 and 4.2, with or without using a normalization, respectively. If no target value is prescribed and the parameter directly is to be minimized (or maximized), just *criterion* (or $-criterion$) is given as expression.

$$\frac{|criterion - goal|}{goal} \tag{4.1}$$

$$|criterion - goal| \quad (4.2)$$

Such expressions can be set up for each objective; however, in that case, the optimizer has to be capable of processing multiple objective functions at the same time. In the other case, if the used optimizer is not a multi-objective (MO) one and thus can only cope with one single objective function, all goals have to be combined in one equation. In this case, typically weight factors (*weight*) are incorporated, which allow for differentiating the importance of the single objectives. Thus, the objective function for l goals could be written for example as in Equations 4.3 and 4.4, considering the same two cases with or without normalization of the objective.

$$\sum_{i=1}^l weight_i \frac{|criterion_i - goal_i|}{goal_i} \quad (4.3)$$

$$\sum_{i=1}^l weight_i |criterion_i - goal_i| \quad (4.4)$$

(In-)equality constraints The two key elements of the optimization problem are already specified by means of the optimization variables and the objective functions; however, further input can be given in form of constraints. These can apply to the design variables, goals or further other parameters, if only certain values are allowed or if dependencies or relations exist.

The values, which the design variables may take on, are commonly constrained. Thus, the allowable value ranges, provided in terms of lower and upper limits, have to be declared for each of the optimization variable, which limits the design space investigated. The lower and upper bounds can be written in form of inequality constraints; however, if only discrete values are allowed to be taken on, equality constraints are utilized.

Furthermore, the goals within the objective functions might also be constrained or have to stand in a defined relation to each other. In such a case of having a constrained problem, additional equations for the limiting conditions are to be provided. When, for example, using the objective function given in either Equation 4.1 or Equation 4.2, which is to be minimized, but also wanting to constrain the criterion to approach the goal from the left side on the numerical scale, meaning not exceeding the target value, the constraint can be defined as given in Equation 4.5.

$$criterion - goal \leq 0 \quad (4.5)$$

In optimization scripts, which separate the parameter relation (left-hand side of Equation 4.5) from the (in-)equality constraint ($\leq \#$, $\geq \#$, $= \#$, $\neq \#$, with a number $\#$), the code might be simplified if all constraint equations are converted into such a formulation, that all use the same (in-)equality constraint. Then, the left-hand side expressions can be provided as vector input, while for the (in-)equality constraint only one type needs to be specified.

4.2.3.2 The optimizer

Having the optimization problem defined, an optimizer has to be selected for executing the optimization algorithm, and thus solving the optimization task. A variety of available optimizers is presented in Table 4.9. The optimizers are grouped according to their basic method into quasi-Newton methods, sequential quadratic programming (SQP), evolutionary algorithms (EAs), particle swarm optimization (PSO), and other types. Furthermore, it is indicated if the optimization routine requires gradients or if it is a gradient-free method. This might be relevant when dealing with complex systems, such as an aero-hydro-servo-elastic wind turbine, where the system complexity cannot be minimized and represented by means of one single system equation. Another important feature is the capableness of the optimizer to handle MO problems, which is already mentioned in Section 4.2.3.1. Thus, in Table 4.9 it is additionally indicated which optimizers can process multiple objective functions.

For the application in a Python environment - as the utilized programming framework specified in Section 4.2.1.4 - there are several open-source optimizers available, such as optimization routines from OpenMDAO (open-source multi-disciplinary design, analysis, and optimization), an open-source framework for efficient multi-disciplinary optimization, (openmdao.org 2016); PyGMO (Python parallel global multi-objective optimizer), focusing on (MO) optimization, (Izzo & Biscani 2015); or Platypus with a special focus on MOEAs (multi-objective evolutionary algorithms) (Hadka 2015) - just to name a few examples.

Table 4.9: Overview of different optimizers (openmdao.org 2016, Hadka 2015, Izzo & Biscani 2015).

Category: Quasi-Newton methods			
Optimizer	Meaning	Gradient-	MO
Newton-CG	Newton conjugate gradient	based	
TNC	Truncated Newton	based	
Powell		based	
BFGS	Broyden-Fletcher-Goldfarb-Shanno	based	
L-BFGS-B	Limited-memory BFGS with box constraints	based	
Category: SQP			
Optimizer	Meaning	Gradient-	MO
FSQP	Feasible SQP	based	
PSQP	Preconditioned SQP	based	
SLSQP	Sequential least squares quadratic programming	based	

Table 4.9: Overview of different optimizers. (cont.)

Category: EA			
Optimizer	Meaning	Gradient-	MO
GA	Genetic algorithm	free	x
NSGAI	Non-dominated sorting GA II	free	x
NSGAIII	Non-dominated sorting GA III	free	x
EpsMOEA	Steady-state epsilon-MO EA	free	x
MOEAD	MO EA based on decomposition	free	x
GDE3	Generalized differential evolution 3	free	x
SPEA2	Strength Pareto EA 2	free	x
IBEA	Indicator-based EA	free	x
PEAS	Parallel EAs	free	x
PESA2	Pareto envelope-based selection algorithm	free	x
CMAES	Covariance matrix adaptation evolution strategy	free	

Category: PSO			
Optimizer	Meaning	Gradient-	MO
ALPSO	Augmented Lagrangian PSO	free	
OMOPSO	Our MO PSO	free	x
SMPSO	Speed-constrained MO PSO	free	x

Category: Others			
Optimizer	Meaning	Gradient-	MO
NOMAD	Non-linear optimization by mesh adaptive direct search	free	x
SNOPT	Sparse nonlinear optimizer	based	
CONMIN	Constrained function minimization	based	
IPOPT	Interior point optimizer	based	
Nelder-Mead		free	
COBYLA	Constrained optimization by linear approximation	free	

Due to the iterative character of optimization routines, there is the need to specify a stop criterion to limit the number of iterations and terminate the optimization algorithm at a specific point. Most commonly, two options for setting such a stop criterion exist: defining a convergence tolerance for terminating the optimization routine or setting an upper limit to the number of iterations performed.

When using optimizers which fall in the category of EAs, some more additional parameters have to be defined. EAs basically work according to the same principle as Darwin's theory of evolution. The main inputs, required for EA-based optimization routines, are presented in the following.

- **Population size**

As EAs work with populations, in which the individuals are modified from generation to generation, the number of individuals in each generation, meaning the size of the population, has to be provided. According to this number, a randomly distributed start population (generation 0: $G = 0$) is created within the prescribed value ranges of the design variables, and depending on the fitness of each individual - meaning how well the individual performs in terms of the objectives -, as well as their compliance with the specified constraints, some individuals are selected, or recombined, or mutated, and a new set of individuals is created as population of the next generation.

- **Number of generations**

The iterative generation of populations continues until a stop criterion is reached. This is mostly a maximum number of generations to be created and simulated. Alternatively, the total number of simulations, which is just *population size * number of generations*, can be required as input to the optimizer.

- **Number of processors**

With the ability of running simulations in parallel (depending on the capabilities of the programming framework and computer system), the number of processors can be provided as well. This option of multi-processing is highly beneficial for optimization applications, as it allows for parallel simulation of several individuals of one generation.

4.2.3.3 The optimization algorithm

The final step is the execution of the iterative optimization algorithm, following the specified optimization problem (Section 4.2.3.1) and using the defined optimizer (Section 4.2.3.2). According to the optimization routine and prescribed value ranges, values for the design variables are set and the corresponding wind turbine system model is simulated. In each consecutive run, the design variables are modified, based on the analyses of objectives and constraints from previous simulations, and still complying with the defined value ranges of the optimization variables, as well as following the optimizer-specific routine. Depending on the specified processing method, several simulations within the optimization routine may be executed in

parallel. Finally, the iterative optimization simulations are terminated as soon as the specified stop criterion is fulfilled.

All simulation results are analyzed internally by the optimizer, based on the prescribed objective functions and constraints. However, due to the fact that - especially at the beginning of the optimization routine - also suboptimal settings might be selected by the optimizer, it could happen that simulations of individual models are aborted before the specified simulation duration and, hence, the criterion for evaluating the objective function might not be existing or used. To handle these or similar failures a query condition can be incorporated when analyzing the results for evaluating the objective functions. The success of a simulation can be directly checked by evaluating the last entry in the time output. For the case of aborted simulations, a different approach, handling such unsuccessful simulations, can be coded within the optimization algorithm. This might be, for instance, to directly set the goals to suboptimal values and therefore step over the evaluation of the objective functions. This way, it can be ensured that these unsuccessful and hence suboptimal individuals are excluded and not considered further by the optimizer.

On the example of an EA-based optimization routine, the optimization algorithm - including the specified optimization problem and optimizer - is presented in Figure 4.25. In this case, several simulations - namely all individuals in one generation - are executed within each iteration, so that *population size * number of generations* simulations are run during the entire optimization procedure. The optimization procedure starts with generating the first individuals according to the set value ranges of the optimization variables. Afterwards, each individual wind turbine system model is simulated, the criteria are extracted from the simulation results, and the objective functions, as well as the constraints, are evaluated - either directly or by means of the alternative approach in case of a failed system simulation as described above.

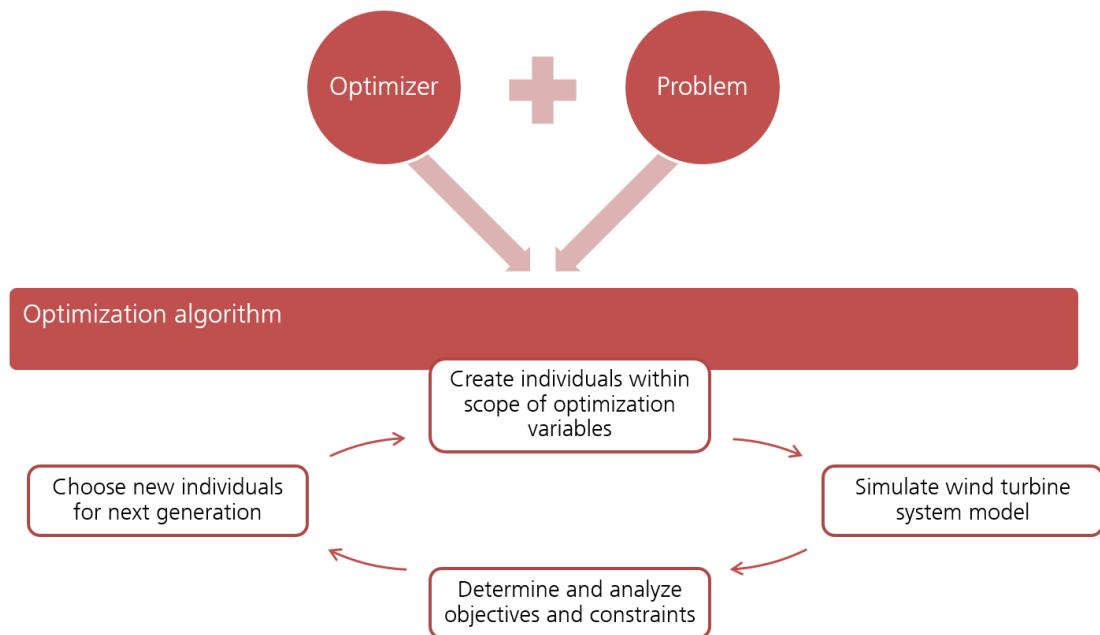


Figure 4.25: Automated optimization process, on the example of an evolutionary algorithm.

Based on these analyses, a new set of individuals for the next generation is chosen by the optimizer, again complying with the allowable value ranges of the design variables. At this point, the optimization procedure is repeated until the specified maximum number of generations or total number of simulations, and, thus, the stop criterion, is reached.

To save the results of each simulated wind turbine system model, which is created during the optimization algorithm, the already coded commands when processing the model in the programming framework (as mentioned in Section 4.2.1.3) might be supplemented by additional code. This way, for example, also the evaluated objectives of each simulation can be written in addition to the output parameters in an output file and used later on for further post-processing or visualization of the progression of the objective functions and design variables.

4.2.4 Discussion of the broad application range of the framework to optimization tasks for wind turbine systems

Optimization tasks in the development of wind turbine systems are wide-ranging. Mostly costs and, thus, indirectly also material demand are the main drivers, but optimization problems can for instance as well be related to system performance and response, noise emissions, dimensions, loads, and lifetime. In the following, a few examples are presented and further applications are discussed to show the functionality, technical feasibility, and the broad application range of the MoWiT-Dymola[®]-Python framework for automated simulation and optimization, as specified in Section 4.2.1.4.

4.2.4.1 Plausibility check of an optimization routine

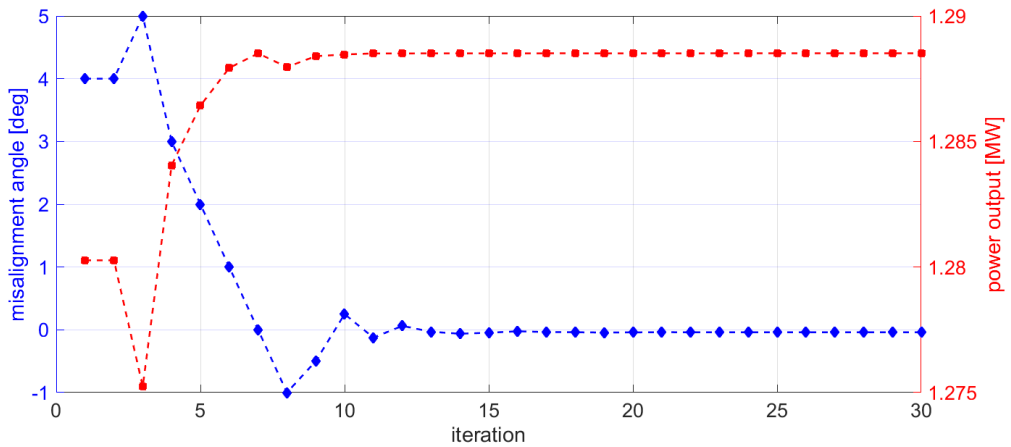
Since optimization problems and wind turbine systems are very complex, it is difficult to assess the results from an optimization procedure. Thus, first, a test case is implemented in the MoWiT-Dymola[®]-Python framework to check the proper functioning of the established framework, as well as the plausibility of the optimization routine. The NREL 5 MW reference wind turbine (Jonkman et al. 2009) is used, with its RNA as specified in Section 3.2.1 and operating at a constant wind speed of 7 m/s, which is below rated wind speed. Now, any control system, apart from the generator control, is turned off, so that neither the blades are pitched nor the RNA is yawed for controlling optimum operation. Having the control systems disabled, an initial misalignment between the wind direction and the normal of the rotor plane is initiated. The optimization problem is then to change the value of the misalignment angle in order to achieve maximum power output. From wind physics theory, the maximum power output is expected when the wind direction is perpendicular to the rotor plane (meaning having a zero misalignment angle), as in this case the projected area facing the wind is maximum.

As this optimization problem has a single objective, optimizers from the list presented in Table 4.9 are selected, which are not MO but gradient-free, as this is required due to the high complexity of the considered wind turbine system. Owing to its good performance in preceding comparative simulations, the presented optimization problem is realized with the optimizer COBYLA from OpenMDAO (openmdao.org 2016). Here, it has to be noted that the frame-

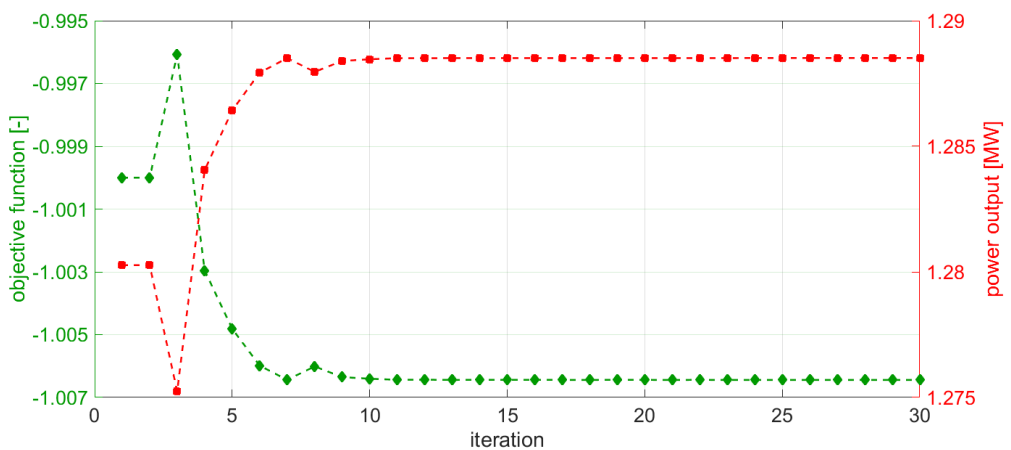
work does not rely on this specific optimizer, which is just selected because of its computational efficiency for the presented optimization problem to verify the correct functioning of the developed optimization framework. For defining the objective function, the mean power output is taken from the simulation time series, excluding any transients at the beginning. The objective function of iteration i , which is to be minimized, is then determined following Equation 4.6.

$$f = -\frac{power_i}{power_1} \quad (4.6)$$

The initial misalignment angle is exemplarily set equal to 4° ; another value would only affect slightly the convergence rate. The results of the optimization procedure are shown in Figure 4.26, presenting the progression of the optimization variable in terms of the misalignment angle (Figure 4.26(a)), as well as the trend of the objective function (Figure 4.26(b)), both together with the resulting power output - the optimization goal. 30 iterations are performed and presented; however, it can be seen that a steady state is already reached after around 15 iterations. Furthermore, the results match the expectations and, thus, the functionality of the optimization routine, incorporated in the framework, is approved.



(a) Progression of the optimization variable, presented in blue, and the goal, plotted in red.



(b) Progression of the objective function, presented in green, and the goal, plotted in red.

Figure 4.26: Results from the optimization procedure for the plausibility check test case.

4.2.4.2 Optimization task with contradictory objectives

Within the wind industry, yield increase, governed by the power output of a wind turbine, is a common goal; however, one should not forget about the loads on the wind turbine, represented for example by the thrust force on the rotor. These two parameters show contradictory demands: maximum exploitation of the wind resource and, hence, increasing the power output for one and the same wind speed leads to an increase in the rotor thrust as well, and vice versa. Both parameters are influenced by the shape of the rotor blades. Thus, in this optimization problem, the NREL 5 MW reference wind turbine (Jonkman et al. 2009) is used again, with its RNA as specified in Section 3.2.1, operating at a constant wind speed, and having each blade defined through 17 sections. The optimization variable is now the chord length, which independently can be modified at each of the 17 sections along the rotor blade. If doing this professionally, also other blade parameters would have to be adjusted and the simulations would have to be performed at different wind speeds and evaluated according to the wind speed distribution prevailing at the considered site; however, in this example the optimization problem is kept simple, as it should mainly deal as a demonstration case for optimization with two contrary objectives.

Basically, two objectives are then to be defined: firstly, the maximization of the rotor power output and, secondly, the minimization of the rotor thrust force. The combination of both objectives into one objective function is realized by utilizing weight factors ($weight_{power}$ and $weight_{thrust}$) for power and thrust, respectively, as presented in Equation 4.7.

$$f = weight_{thrust} \frac{thrust_i}{thrust_1} - weight_{power} \frac{power_i}{power_1} \quad (4.7)$$

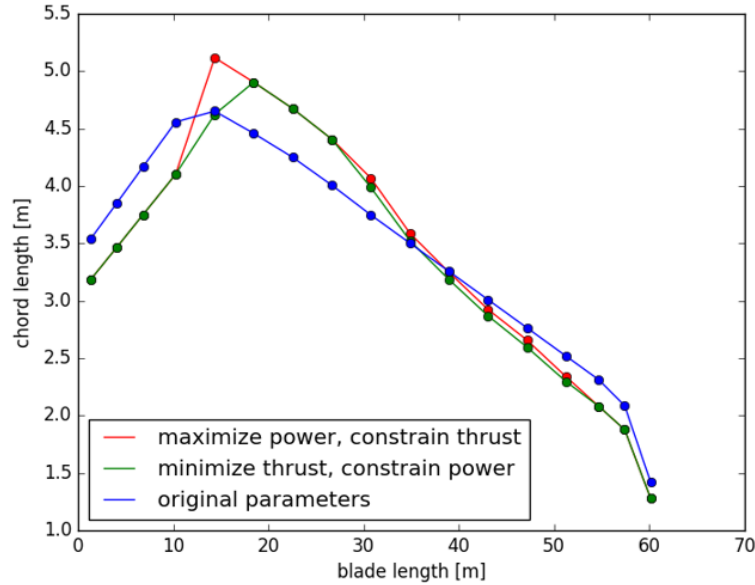
Optimization simulations are performed with different optimizers from OpenMDAO, such as COBYLA and ALPSO (openmdao.org 2016), as it is intended to test the capability of single-objective optimizers to deal with multiple, and besides, contradictory objectives. The opposing goals challenge the optimizers and show the limited use of single-objective optimizers, which still can work with several goals, which, however, have to be written in one objective function as done in Equation 4.7. The final “optimum” solution highly depends on the user-defined and, hence, quite arbitrary chosen weight factors for the objectives and, thus, cannot represent one real unbiased optimum.

The influence of the weight factors can be demonstrated when considering the two boundary events: only one of the objectives is relevant, the other one is neglected. Thus, still using the OpenMDAO optimizers, the optimization problem is modified and adjusted so that in one task (f_{power}) the power output is to be maximized and the thrust force is limited by not exceeding the original value $thrust_{orig}$ (as represented by Equation 4.8), while in the other task (f_{thrust}) the thrust force minimization is defined as objective and the power output is constrained by not falling below the original value $power_{orig}$ (as written in Equation 4.9).

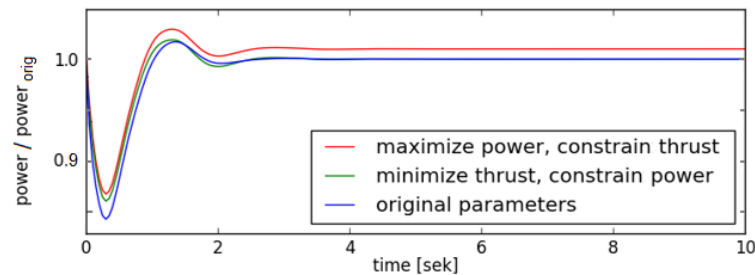
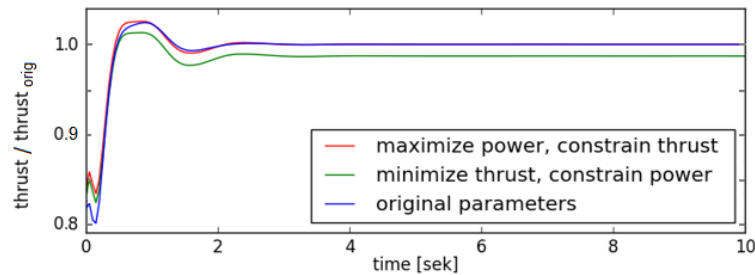
$$f_{power} = -\frac{power_i}{power_1} \quad \text{and} \quad thrust_i \leq thrust_{orig} \quad (4.8)$$

$$f_{\text{thrust}} = \frac{\text{thrust}_i}{\text{thrust}_1} \text{ and } \text{power}_i \geq \text{power}_{\text{orig}} \quad (4.9)$$

For each of the two optimization tasks, an optimum is obtained; however, with this approach also two different optimum blade shapes are achieved, as visualized in Figure 4.27(a), for which each is only the best for each case, as shown in Figure 4.27(b). Thus, this emphasizes the relevance of using optimizers, which are capable of handling multiple objectives at the same time - especially in case of complex MO optimization problems.



(a) Original and power/thrust-optimized blade shapes, presented in blue and red/green, in comparison.



(b) Performance of the original and power/thrust-optimized blades, presented in blue and red/green, with respect to the objectives.

Figure 4.27: Results from the optimizations for maximizing the power output or minimizing the thrust force.

4.2.4.3 Controller tuning and optimization

The control system of a wind turbine needs to be tuned and optimized for the specific purpose. The control system is an essential component, which regulates the wind turbine performance. By pitching the blades, the amount of power extracted from the wind, as well as the thrust force acting on the rotor, are influenced. Below rated wind speed, the blades are not pitched so that the maximum possible power can be extracted, while above rated wind speed, the blade pitch angle is regulated to maintain constant power output or generator torque (depending on the wind turbine control method), which at the same time reduces the thrust force on the rotor.

By tuning the controller parameters, which could be among others the proportional and integral gains, different optimization goals can be pursued.

- **Controller optimization for load reduction**

The control strategy can be optimized to reduce oscillations in the sensor generator speed and to achieve as early as possible a steady state. This implies at the same time also reduced oscillations and an earlier steady state in the power output, blade pitch angle, and the loads on the turbine.

- **Controller adaption for floating systems**

Wind turbine controllers measure the wind speed in certain intervals. In case of a floating system, the measured wind speed is not undisturbed but the resulting speed due to wind inflow and motion of the floating system. A common onshore or bottom-fixed offshore wind turbine controller is much faster than the floating platform motions. This means that the time intervals for taking measurements are so small, that the controller would perceive a decreasing wind speed (corresponding to a decreasing rotor thrust) if the floating system moves with the wind. The reaction of the controller would then be to pitch the blades into the wind to avoid a reduction of the power output. This, however, will increase the thrust force and the system will continue moving backwards. This negative damping effect, which would be introduced when using a common onshore-type wind turbine controller for a floating offshore system, therefore leads to an unstable system behavior. For this reason, the controller parameters have to be adjusted. Thus, the optimization goal in this case is to tune the controller in order to obtain a stable floating system, with a controller frequency lower than the smallest eigenfrequency of the FOWT system. This tuning can be done through running iterative simulations within an optimization algorithm. (Larsen & Hanson 2007)

- **Operational management of a wind farm**

Considering an entire wind farm, optimization tasks can be related to the space utilized and power extracted, which can be addressed by optimizing the wind farm layout. Another option for maximizing the power output of the entire wind farm - having a fixed layout - is to adjust the control and operational management of the single wind turbines by, for instance, changing the yaw angle of the first rows' turbines to influence the wake direction and the flow condition reaching the turbines behind.

4.2.4.4 Design optimization

Design optimization is a key application of the MoWiT-Dymola[®]-Python framework, as it is useful and required within the highly iterative design process of a wind turbine system - either the whole system or only single components, such as the tower, support structure, or even the mooring system in case of FOWTs. Design drivers in the wind industry are among others costs, both capital and operational expenditure (CapEx and OpEx) and, thus, in total LCoE. Especially for the emerging sector of floating wind energy, economic efficiency is very important for achieving competitiveness with conventional and other renewable energy sources. Thus, design optimization of floating wind turbine systems is a relevant topic.

This optimization task can be approached in different ways. Mostly, optimization variables in a design process are geometric parameters. Thus, shape, dimensions, and structural properties of the floating platform might be modified, while the supported wind turbine remains in most respects - and apart from for example controller tuning, as pointed out in Section 4.2.4.3 - unchanged. Based on the survey results presented in Section 3.1.2, relevant objective criteria are besides LCoE also maintenance aspects (including the reliability of the components), the potential of serial production (meaning for example modular structures), and the system performance. The latter criterion implies certain requirements and limits for the system response, such as nacelle acceleration, platform inclination, or translational motion, which are prescribed by specifications of single wind turbine components.

Thus, the developed MoWiT-Dymola[®]-Python framework is applied in detail in Chapters 5 and 6 to design optimization tasks, using the reference FOWT system specified in Section 3.2. These comprise global design optimization focusing on the FOWT system performance (Section 5.1), as well as the cost-driven design of a complex geometry offshore wind turbine system supported by an advanced spar-type floater (Section 5.2). Apart from that, future use of the developed framework for automated simulation and optimization is demonstrated by means of a direct optimization approach for obtaining larger MW-class floater designs without upscaling (Section 5.3). Finally, reliability criteria can as well be incorporated in the design optimization and realized by means of the MoWiT-Dymola[®]-Python framework as presented in Chapter 6.

Thus, for industrial application, the presented framework can be used, for example, just for obtaining a fast preliminary design to do a cost estimation for the initial planning of ((floating) offshore) wind turbines or, on the other hand, for a very detailed reliability-based design optimization to improve the system reliability and this way reduce the downtime of an offshore (floating) system due to defects and long waiting times for proper weather windows for doing maintenance and repair work.

4.2.4.5 Flexibility and sensitivity of the framework for automated simulation and optimization

In addition to the high flexibility in the application to optimization tasks, the MoWiT-Dymola[®]-Python framework is not only suitable for optimization problems, but also directly for executing automatically a large number of simulations, which is for example required in DLC analyses, as

presented in Section 4.2.2. Both capabilities of the framework can be utilized at the same time by incorporating a set of DLC simulations within the execution of the optimization algorithm. Furthermore, if using another library - instead of MoWiT - as basis, the framework is not limited to wind turbine systems and can be applied to other complex engineering systems.

However, in any application of the framework for automated simulation and optimization, especially when using it for optimization tasks, the specific settings have to be chosen carefully, including a sensitivity study where appropriate. Thus, for instance, the results and success of the optimization highly depend on the optimization settings and employed optimizer. The example in Section 4.2.4.1 approves the proper and fast functioning of the single-objective optimizer COBYLA, while the optimization task in Section 4.2.4.2 shows its limited suitability for two (or more) contrary objectives. On the other hand, a MO optimizer, such as NSGAI, proves to be capable of easily handling complex problems with several design variables, objectives, and constraints, as presented in the following Chapters 5 and 6.

Chapter 5

Design optimization of floating wind turbine support structures

Floating support structures for offshore wind turbines are a convenient solution for deep water sites. However, higher costs, especially for the substructure, additional equipment (such as moorings and anchors), and installation challenge the market uptake of floating offshore wind technology (Mast et al. 2015). First floating prototypes, for instance the Hywind spar floater, are highly over-dimensioned for safety reasons and due to the - at that time - still low TRL of and experience with FOWTs. This, however, inhibits fast gain of economic competitiveness. Hence, design optimization of FOWTs with respect to their costs and performance is of high relevance to make them economically viable and to accelerate their market uptake.

Other studies show also the relevance of applying optimization approaches for the hydrodynamic response of (Karimi et al. 2017, Lemmer et al. 2017, Hall et al. 2014, Sandner et al. 2014, Hall 2013, Fylling & Berthelsen 2011, Clauss & Birk 1996) and loads on (Lemmer et al. 2017, Sandner et al. 2014, Härer 2013, Fylling & Berthelsen 2011) floating systems, as well as for cost reduction of FOWTs (Karimi et al. 2017, Lemmer et al. 2017, Hall et al. 2014, Sandner et al. 2014, Hall 2013, Härer 2013, Fylling & Berthelsen 2011). While a variety of optimization approaches is available in the literature for bottom-fixed offshore wind turbine systems, focusing on the optimization of either the bottom-fixed support structure (Stieng & Muskulus 2020, Gentils et al. 2017, Chew et al. 2016, Muskulus & Schafhirt 2014, Clauss & Birk 1996), or the blades (Ashuri et al. 2014) and tower (Wang et al. 2016, Ashuri et al. 2014, Muskulus & Schafhirt 2014), or even an entire wind farm (Hou et al. 2019, Mytilinou & Kolios 2019, Mytilinou et al. 2018, Mytilinou & Kolios 2017, Herbert-Acero et al. 2014, Valverde et al. 2014), the number of optimization approaches, dealing with the highly complex FOWT system, is very limited. While for bottom-fixed offshore wind turbine systems both optimization methodologies of analytical nature based on gradients (Stieng & Muskulus 2020, Chew et al. 2016) and evolutionary optimization approaches (Mytilinou & Kolios 2019, Mytilinou et al. 2018, Mytili-

Note: This chapter is based on the publications by Leimeister, Collu & Kolios (2020), and Leimeister, Kolios, Collu & Thomas (2020, 2019).

nou & Kolios 2017, Wang et al. 2016) can be found, for FOWT systems more typically genetic algorithm optimization approaches are applied (Karimi et al. 2017, Hall et al. 2014, Hall 2013, Härer 2013). However, especially because of the complexity of FOWT systems, which come with coupled motions, aero-hydro-servo-elastic dynamics, non-linear behavior, and additional components such as mooring lines, the optimization approaches presented in the literature are tailored to a specific optimization task. The implementation of the FOWT system is often simplified by using reduced-order models (Lemmer et al. 2017, 2016, Sandner et al. 2014, Härer 2013) and even the fully-coupled dynamics, as mentioned above, are sometimes only partially modeled (Fylling & Berthelsen 2011, Clauss & Birk 1996). Thus, in Section 4.2, a modular framework for automated simulation and optimization is developed and presented. This framework utilizes MoWiT, as presented in Section 4.1.1, for modeling the entire wind turbine system including the environmental conditions and representing the fully-coupled aero-hydro-servo-elastic dynamics. The modeling happens component-based, which brings high flexibility in modeling of any state-of-the-art onshore or offshore bottom-fixed or even floating wind turbine system. Coupling MoWiT to the Python-based programming environment allows automated execution of fully-coupled simulations, as well as solution of optimization problems of any kind, as addressed in Section 4.2.4. This high versatility of the modular MoWiT-Dymola[®]-Python framework is even supplemented by the option of parallelized processing of simulation and/or optimization tasks.

The survey-based study in Section 3.1.2 shows that - apart from LCoE - ease of maintenance and manufacturing, as well as system performance are most important criteria for FOWTs. Furthermore, an advanced spar-buoy floater design turned out to have the highest potential for a fast and successful market uptake. Hence, the floating offshore spar-buoy wind turbine system from phase IV of the OC3 project (Jonkman 2010), as presented in Section 3.2, is used to apply different design optimization tasks, utilizing the MoWiT-Dymola[®]-Python framework. These are: a design optimization based on global LSs for the FOWT system performance (Section 5.1); an optimization-based and cost-driven design development of an advanced spar-type floater (Section 5.2); and a design of a larger MW-class floater obtained through direct optimization, eliminating the intermediate step of upscaling (Section 5.3).

5.1 Design optimization of the OC3 phase IV spar-buoy floater, based on global limit states

The objectives of this global design optimization are to reduce the degree of over-dimensioning of the spar-buoy floater - which benefits the overall system costs, as well as the manufacturability and handleability of the structure - but at the same time to maintain reasonable and safe global system performance even in critical environmental conditions. The presented design optimization approach is kept deliberately simple at the first stage, not including load analyses of the structure, so that it can be used afterwards as basis for well-founded development of

more sophisticated optimization strategies and concepts which consider more detailed criteria, such as local LSs, structural integrity, as well as reliability aspects (Chapter 6).

Thus, first, the reference system to be analyzed and used for applying the developed optimization approach is presented in Section 5.1.1, covering the selected design variables, as well as the defined global LSs. Based on this, the formal declaration of the optimization problem, comprising the design variables, objective functions, and constraints, is given in Section 5.1.2. The optimization approach is then presented in Section 5.1.3, ranging from the design load cases used for simulations and analyses to the specific optimization settings for applying the MoWiT-Dymola[®]-Python framework for automated simulation and optimization. Afterwards (Section 5.1.4), the results of the optimization are analyzed and the selection procedure for determining the optimum spar-buoy design is outlined. Further evaluation of the optimization approach and results are covered in Section 5.1.5.

5.1.1 Description of the system to optimize

To deploy the design optimization approach, first, a reference framework has to be set up. This comprises - apart from and based on the reference spar-buoy floating wind turbine system specified in Section 3.2 - the system variables that can be modified during the optimization process (Section 5.1.1.1), as well as the global LS criteria (Section 5.1.1.2), on which basis the objective functions are then defined.

5.1.1.1 Design variables

The purpose of this optimization task is the design optimization of the floating wind turbine support structure, because this has a significantly larger contribution to the system costs compared to bottom-fixed designs. Hence, the focus lies on the floating platform, meaning that wind turbine (tower and RNA), as well as the station-keeping system properties remain unchanged, while some of the floater system variables are free to be altered. In the following, these design variables, which are modifiable during the optimization, are defined.

Geometric design variables Geometric system variables of the floater are diameters, thicknesses, and lengths of the floating structure. The top diameter (D_{UC}) and elevation ($d_{UC,t}$) should retain their original values to ensure that the floater top fits the tower base and the hub height remains the same. Furthermore, it is decided to keep the total length of the upper column, as well as the length of the taper fixed to avoid significantly changed effects due to the wave impact on the upper part of the structure. Thus, the top end of the base column ($d_{BC,t}$) remains unchanged at 12 m below SWL. However, length (H_{BC}) and diameter (D_{BC}) of the base column are chosen to be the two modifiable geometric design variables, as it is also intended to decrease the outer dimensions - and hence the material costs - while still fulfilling global LS criteria without losing performance.

To apply the basic working principle of a common spar floater, as the OC3 phase IV spar-buoy concept is, and to allow utilization of the same supply chain and manufacturing process

as used for the original design, other (more extraordinary) concepts of spar floaters, such as designs with a deep ballast tank connected with tendons to the floating structure, are not considered - this will be, however, addressed in Section 5.2. Thus, the base diameter of the spar-buoy should not fall below the diameter of the upper column of 6.5 m, which, hence, defines the lower bound for the diameter of the base column. The original diameter value is given in Table 3.11 with 9.4 m. This is directly taken as the maximum tolerated value for the base diameter, as the overall goal is the reduction of the outer dimensions. To allow a reduction in the total length of the spar-buoy, the original height of the base column (108.0 m) is again used as upper bound, while the minimum allowable value is set to 8.0 m. This corresponds to a minimum draft of the floating system of 20.0 m, which on the one hand allows higher survival sea states compared to the recommended initial estimate of 15.0 m for the minimum draft (Ng & Ran 2016) and on the other hand does not fall below the draft of another floater type equivalent, the semi-submersible from OC4 (offshore code comparison collaboration continuation) phase II (Robertson et al. 2014). Figure 5.1 sketches the fixed parameters and modifiable (specified and dependent) design variables of the spar-buoy, while their original values and defined allowable value ranges are stated in Table 5.1.

Table 5.1: Allowable value ranges of the design variables of the global design optimization task.

Parameter	Allowable value range	Original value
D_{BC}	[6.5 m, 9.4 m]	9.4 m
H_{BC}	[8.0 m, 108.0 m]	108.0 m
$\rho_{ballast}$	[1,281 kg/m ³ , 2,600 kg/m ³]	1,907 kg/m ³

Finally, as (local) structural integrity checks are not yet performed at this stage, the wall thickness of the floater ($t = t_{UC} = t_{BC}$) remains unchanged at its original value of 0.0314 m, as determined within the verification process covered in Section 4.1.1.2. Furthermore, the same stiffness provided by the mooring system is used throughout the optimization, as the mooring system design would require a separate in-depth optimization approach, which is not yet included. To overcome the problem of re-designing the mooring system properties for maintaining the resulting stiffness for each different draft of the floater and corresponding change in the fairlead position, in the modeling the original positions of fairleads and anchors, as well as the original mooring system properties are used and the maintained mooring stiffness is passed to the floating structure.

Ballast design variables With changing the geometric variables as stated before, the structural mass, as well as the displaced water volume and resulting buoyancy change as well. In order to maintain the hub height and thus the 10 m elevation of the floater top, but also to allow for a variable center of mass which influences the system performance and, hence, the global LS criteria, which are defined later on in Section 5.1.1.2, ballast amount and density are set to be modifiable, too, as indicated in Figure 5.1.

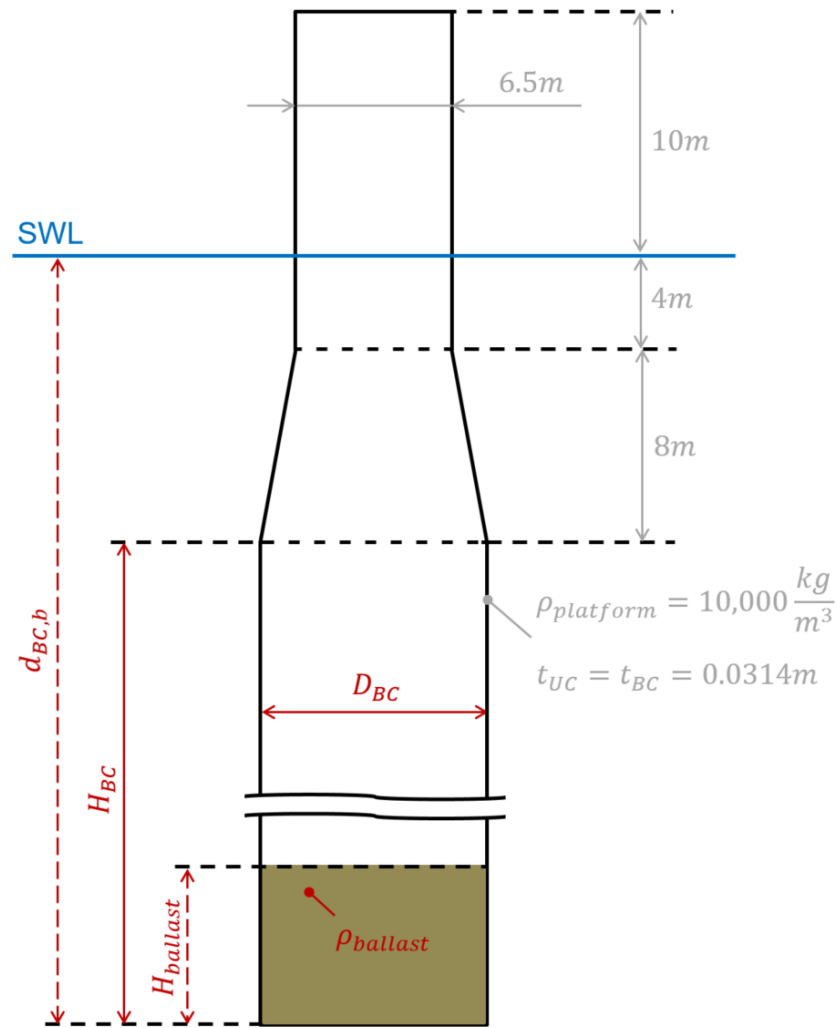


Figure 5.1: Fixed/original and modifiable variables of the global design optimization task, presented in gray and red, while dependent variables are indicated with dashed lines.

The required ballast mass can be determined from the chosen geometric design variables and predefined system dimensions. For the ballast density ($\rho_{ballast}$) range it is decided to make use of common and cheap materials, such as sand with a density range from around 1,281 kg/m³ to 2,082 kg/m³ depending on the water content (Engineering ToolBox 2010), concrete with a density between 1,750 kg/m³ and 2,400 kg/m³ (Dorf 1996), or other rocks like sandstone with a density of 2,600 kg/m³ (BG BAU 2000). Thus, the range for the modifiable ballast density - as presented in Table 5.1 - is chosen to be between 1,281 kg/m³ and 2,600 kg/m³, assuming that every density value can be achieved through mixture of the above mentioned common and cheap ballast types with each other and/or with water. With the selected ballast density, the required ballast height ($H_{ballast,required}$) can be calculated from the determined ballast mass needed; however, it also has to be ensured that the computed ballast height lies within 0 m and the length of the base column. If this is not the case, the selected variable values have to be adjusted according to the following case distinction, which is directly incorporated when modeling the floater based on MoWiT.

- If the required ballast filling height exceeds the chosen length of the base column ($H_{\text{ballast,required}} > H_{\text{BC}}$), the entire base column is filled ($H_{\text{ballast}} = H_{\text{BC}}$), however, the ballast density ($\rho_{\text{ballast,selected}}$), which is initially selected from the optimizer, is increased proportionately, as shown in Equation 5.1.

$$\rho_{\text{ballast}} = \frac{H_{\text{ballast,required}}}{H_{\text{BC}}} \cdot \rho_{\text{ballast,selected}} \quad (5.1)$$

- If mass needs to be removed from the system to make it floatable, meaning if the resulting ballast height is negative ($H_{\text{ballast,required}} < 0$ m), the ballast filling height is set equal to zero ($H_{\text{ballast}} = 0$ m) and the floater structure material density (ρ_{platform}) is reduced respectively, as given in Equation 5.2, to compensate for the excessive weight that needs to be removed.

$$\rho_{\text{platform}} = \frac{(\text{structural weight}) - (\text{excessive weight})}{\text{structure volume}} \quad (5.2)$$

5.1.1.2 Global limit states

The objectives for the optimization focus on the global system performance. Thus, the system rotational stability, nacelle acceleration, and translational displacements make up the global LS criteria used for setting up the objective functions. Their descriptions and envisaged values are given hereinafter and summarized in Table 5.2. Due to the overall goal of reducing the degree of over-dimensioning of the floating support structure, common operational limits for the global system performance of a FOWT are directly used as the target values. Potential risks and consequences associated with these global system performance criteria are investigated in Table D.1 included in Appendix D.

Table 5.2: Global limit state criteria for the FOWT system performance.

Criterion	Symbol	Objective	Constraint
Total inclination angle	$\max(t_{\text{tot}})$	10.0°	$\leq 10.0^\circ$
Horizontal nacelle acceleration	$\max(a_{\text{hor,nacelle}})$	1.962 m/s ²	$\leq 1.962 \text{ m/s}^2$
Dynamic translational motion	$\max(s_{\text{dyn,transl}})$	minimized	$\geq 0.0 \text{ m}$
Mean translational motion	$s_{\text{mean,transl}}$	-	$\leq 64.0 \text{ m}$

System rotational stability The stability criterion of a FOWT system is represented by the maximum combined rotation angle, meaning the total inclination angle t_{tot} (combined roll and pitch motion). Based on conventional values (Katsouris & Marina 2016, Kolios et al. 2015, Huijs et al. 2013), the targeted operational total inclination is set equal to 10.0°, which must not be exceeded.

Nacelle acceleration For the wind turbine being placed on top of a floating platform the motions are most critical, especially the acceleration at the tower top. Due to the fact that the nacelle contains sensitive components - such as gearbox, generator, and bearings - its motion has to be restricted, as otherwise (when exceeding certain acceleration limits) the turbine has to stop operation. The common operational limit for the maximum allowable nacelle acceleration $a_{hor,nacelle}$ is 20% to 30% of the gravitational acceleration (Nejad et al. 2017, Huijs et al. 2013, Suzuki et al. 2011), which corresponds to an acceleration of around 1.962 m/s^2 to 2.943 m/s^2 . The final tolerated acceleration highly depends on the specific turbine. Thus, the more conservative value of 1.962 m/s^2 is used in this study as upper bound for the nacelle acceleration.

Translational motions Floating wind turbines will drift away from their initial position during operation due to wind and wave loading; however, some motion restrictions apply to FOWT systems. For example for wind turbines supported by TLPs, the translational motion restrictions are quite stringent because of the tendons used for station-keeping (Bachynski & Moan 2012). This is not applicable to the spar-buoy FOWT system, as this is moored with catenary lines. However, there are no publically available specific limits for allowable translational displacements of a spar-type floating wind turbine; but for all FOWTs the allowable motion of the power cable is the key factor for restricting the translational displacement of the operating system.

There are two components of the total translational displacement (combined surge, sway, and heave motion) that need to be distinguished in the analyses: the static, meaning average, displacement $s_{mean,transl}$, which is mainly due to the thrust on the wind turbine, and the dynamic displacement $s_{dyn,transl}$, representing the oscillatory motion due to turbulent wind loading and alternating wave loads. As there will always be a mean translational displacement, due to the thrust force, which is coupled to the power production mode of the wind turbine, it is not advisable to target a certain static displacement. Thus, the mean translational motion is not selected as optimization objective, but a constraint for the maximum static displacement is specified, following a rule of thumb, as 20% of the water depth (320.0 m), leading to 64.0 m. The dynamic translational motion, however, is selected as optimization objective and aimed for being minimized to keep the oscillatory motion of the power cable as low as possible.

5.1.2 Optimization problem of the global design optimization task

Based on the information and descriptions outlined in Section 5.1.1, the optimization problem, as generally formulated in Section 4.2.3.1, is defined by declaring the design variables (Section 5.1.2.1), objective functions (Section 5.1.2.2), and constraints (Section 5.1.2.3).

5.1.2.1 Declaration of the design variables

The three selected design variables of the OC3 phase IV spar-buoy floater are the base column diameter, the height of the base column, as well as the density of the ballast, as derived and

described in detail in Section 5.1.1.1. Thus, the design variables vector $X = \{x_1, x_2, x_3\}$ contains the following three elements, as given in Table 5.3.

Table 5.3: Declaration of the three design variables of the global design optimization task.

Design variable	Formal expression	Description
x_1	D_{BC}	Diameter of base column
x_2	H_{BC}	Height of base column
x_3	$\rho_{ballast}$	Density of ballast material

5.1.2.2 Declaration of the objective functions

Three global LSs, as specified in Section 5.1.1.2, are used for setting up the objective functions. As the optimization problem itself is MO, the objective functions are formulated separately and not just in one single objective function. The three objective functions are declared in Table 5.4. The objective functions for inclination and acceleration criteria are both normalized with respect to their target values, while for the objective function for the dynamic translational motion no normalization is carried out.

Table 5.4: Declaration of the three objective functions of the global design optimization task.

Objective function	Formal expression	Description
$f_1(system(X))$	$\frac{ \max(\iota_{tot}) - 10.0^\circ }{10.0^\circ}$	Total inclination angle criterion
$f_2(system(X))$	$\frac{ \max(a_{hor,nacelle}) - 1.962 \text{ m/s}^2 }{1.962 \text{ m/s}^2}$	Horizontal nacelle acceleration criterion
$f_3(system(X))$	$\max(s_{dyn,transl})$	Dynamic translational motion criterion

5.1.2.3 Declaration of the constraints

Both the design variables and the global LS criteria are constrained, as stated in Sections 5.1.1.1 and 5.1.1.2, respectively. For each design variable a lower and upper bound is set, which limits the design space investigated. Furthermore, each criterion, used for defining the objective functions, is constrained from one side as well, and one more additional parameter, namely the mean translational motion, is bounded from one side. As all these constraints follow inequality, there are in total ten inequality constraints ($n = 10$) and no equality constraint ($m = 0$). The assignment and formulation of the inequality constraints is as given in Table 5.5.

Table 5.5: Declaration of the ten inequality constraints of the global design optimization task.

Inequality constraint	Formal expression	Description
$g_1(x_1)$	$6.5 \text{ m} - x_1$	Allowable value range of x_1
$g_2(x_1)$	$x_1 - 9.4 \text{ m}$	Allowable value range of x_1
$g_3(x_2)$	$8.0 \text{ m} - x_2$	Allowable value range of x_2
$g_4(x_2)$	$x_2 - 108.0 \text{ m}$	Allowable value range of x_2
$g_5(x_3)$	$1,281 \text{ kg/m}^3 - x_3$	Allowable value range of x_3
$g_6(x_3)$	$x_3 - 2,600 \text{ kg/m}^3$	Allowable value range of x_3
$g_7(\text{system}(X))$	$\max(t_{\text{tot}}) - 10.0^\circ$	Maximum total inclination angle
$g_8(\text{system}(X))$	$\max(a_{\text{hor,nacelle}}) - 1.962 \text{ m/s}^2$	Maximum horizontal nacelle acceleration
$g_9(\text{system}(X))$	$-\max(s_{\text{dyn,transl}})$	Maximum dynamic translational motion
$g_{10}(\text{system}(X))$	$s_{\text{mean,transl}} - 64.0 \text{ m}$	Mean translational motion

5.1.3 Optimization approach for the design optimization based on global limit states

The design optimization approach requires a FOWT system model, which is simulated and evaluated for a certain environmental condition. Thus, first (Section 5.1.3.1), DLCs which are proposed by standards are analyzed and a most critical DLC is worked out, which represents the environmental condition considered within the optimization simulations. The automated execution of the DLCs, as well as the iterative optimization procedure are both comprised by and performed with the MoWiT-Dymola[®]-Python framework, as described in detail in Section 4.2. Afterwards (Section 5.1.3.2), the specific settings, used for the optimization of the OC3 phase IV spar-buoy floating wind turbine system, are defined.

5.1.3.1 Design load cases

In order to analyze the wind turbine system performance and to evaluate the critical parameters, selected in Section 5.1.1.2 as global LSs for setting up the objective functions, as specified in Section 5.1.2.2, at least the DLCs defined in the IEC technical specification 61400-3-2 (IEC 2019c), based on the IEC standards 61400-3-1 (IEC 2019b) and 61400-1 (IEC 2019a), have to be considered in general. However, as not every DLC is relevant for the particular global LS criteria, commonly, specific critical load cases and environmental conditions are selected and used for the subsequent analyses (Krieger et al. 2015, Matha et al. 2014, Bachynski et al. 2013, Huijs et al. 2013, Bachynski & Moan 2012, Suzuki et al. 2011). Furthermore, in light of the computational effort and time that it would take when simulating several DLCs in each loop of the optimization process, in this application example, it is decided to use only one critical

DLC within the optimization. The choice of this most critical DLC is based on the following approach.

1. All DLCs given in IEC 61400-3-1 (IEC 2019*b*, p. 46-48) are evaluated and an initial selection of the DLCs most relevant for the specified optimization objectives is made.
2. These pre-screened DLCs are simulated with the reference floating wind turbine system presented in Section 3.2. The simulations are performed in Dymola[®], based on the system model created by means of MoWiT and utilizing the MoWiT-Dymola[®]-Python framework for automated simulation.
3. All simulated DLCs are evaluated regarding the selected objective functions. Based on this, the DLC(s) yielding the most critical results, meaning the highest values for the specified optimization objectives, is/are determined.
4. If all optimization criteria are most critical in one and the same DLC, this load case can directly be taken for the optimization. However, if different DLCs yield the most critical global LS criteria, an appropriate DLC - combining all these worst load case conditions - is defined and used for the optimization.
5. This means that only one DLC is used in the optimization process; however, to validate the suitability and representative nature of the chosen critical DLC, all DLCs, based on the initial selection done in 1., are simulated again for the final optimized floating wind turbine system design. This way it can be checked if the load case conditions, yielding the most critical optimization criteria for the original design, have switched to another DLC for the optimized system. If this was the case, the DLC selected for the use during the optimization procedure would have to be modified according to the new findings and the optimization and subsequent validation would have to be performed once again.

Based on the global LSs, defined in Section 5.1.1.2, the pre-screening of the large number of DLCs, recommended in the international standard IEC 61400-3-1 (IEC 2019*b*), is done. At first and even though wind turbine foundation designs are often governed by fatigue, all DLCs defined for fatigue analyses are directly excluded, as the optimization objectives focus on global extreme system behavior without considering structural loads and integrity. From the remaining DLCs for ultimate loads, three operational design conditions are selected as design-relevant load cases with regards to the specified optimization objectives:

- DLC 1.1 at three different wind speeds (10.0 m/s, 11.4 m/s, and 13.0 m/s) slightly below, at, and slightly above rated wind speed of the NREL 5 MW wind turbine.
 - The DLC 1.1 uses normal environmental conditions, hence, normal turbulent wind model, as well as normal irregular sea state and normal current model. The wind turbine is in normal power production.
 - Around rated wind speeds, the highest thrust force is experienced by a wind turbine in operation. This loading is correlated to the platform inclination as response to

the resulting overturning moment, as well as to a mean translational displacement of the floating system.

- Hence, DLC 1.1 at the mentioned three wind speeds is expected to yield critical total inclination angles, as well as critical values for the mean translational motion, which, however, is not a direct optimization objective, but is constrained.
- DLC 1.3 at three different wind speeds (8.0 m/s, 11.4 m/s, and 25.0 m/s) below and at rated wind speed, as well as at the maximum operating wind speed (cut-out) of the NREL 5 MW wind turbine.
 - The DLC 1.3 uses an extreme turbulent wind model, while the irregular sea state and current model are considered to be normal. The wind turbine is in normal power production.
 - This DLC represents critical conditions for a wind turbine at a wind-dominated site. The extreme turbulences in the wind speed time series contain high fluctuations, which excite the floating wind turbine system in oscillatory motions.
 - Hence, if the wind turbine is wind-sensitive, DLC 1.3 is expected to yield critical values for the nacelle acceleration, as well as for the dynamic translational motion.
- DLC 1.6 at three different wind speeds (8.0 m/s, 11.4 m/s, and 25.0 m/s) below and at rated wind speed, as well as at the maximum operating wind speed (cut-out) of the NREL 5 MW wind turbine.
 - The DLC 1.6 considers, opposite to DLC 1.3, a severe irregular sea state, while normal current and turbulent wind models are used. The wind turbine is in normal power production.
 - This DLC represents critical conditions for a wind turbine at a wave-dominated site. The severe irregular sea state comes with high fluctuations in the wave elevation time series, which excite the floating wind turbine system in oscillatory motions.
 - Hence, if the wind turbine is wave-sensitive, DLC 1.6 is expected to yield critical values for the nacelle acceleration, as well as for the dynamic translational motion.

In addition, a fourth DLC in parked condition, namely DLC 6.1b - taken at the time of study from IEC 61400-3 (IEC 2009) - which uses extreme steady wind and reduced wave height models, both with 50-year recurrence period, is considered as in such an extreme event the highest loads, implying critical values for the total inclination angle and mean translational motion, are expected. However, the OC3 phase IV FOWT system turns out to be not properly designed for such an extreme environmental condition given in DLC 6.1b. Thus, for the further investigations, only the three operational DLCs (1.1, 1.3, 1.6) are considered.

5.1.3.2 Optimization settings

For the realization of the optimization task with the MoWiT-Dymola[®]-Python framework - following the descriptions given in Section 4.2.3 - first, the optimization problem and opti-

mizer have to be defined and, then, the optimization algorithm, implying the simulation of the specified wind turbine system model with redefined design variables, is executed.

Optimizer and optimization problem Only gradient-free optimizers can be utilized for MoWiT models due to the complexity of the considered FOWT system, as already indicated in Sections 4.2.3.2 and 4.2.4.1. Hence, from the various optimizers presented in Table 4.9, a few optimizers - namely ALPSO, COBYLA, NSGAI, NSGAIII, and SPEA2 - which are all gradient-free are implemented in the MoWiT-Dymola[®]-Python framework and tested (Section 4.2.4). Furthermore, the optimization problem, as described in Section 5.1.2, comes with three design variables and corresponding lower and upper bounds (corresponding to six inequality constraints), three objective functions, as well as four additional inequality constraints. Thus, for this specific optimization task and application, the optimizer should be capable of processing MO problems. Hence, the three MO optimizers NSGAI, NSGAIII, and SPEA2 from Platypus, which are already utilized by Mytilinou & Kolios (2017), are selected and tested in more detail on the specific optimization problem. It turns out that SPEA2 is converging very slow, while both SPEA2 and NSGAIII have a lower compliance rate of the defined constraints compared to NSGAI. The pros and cons of the considered and compared optimizers are summarized in Table 5.6. Based on this, NSGAI is selected to be used as optimizer within the global design optimization of the OC3 phase IV spar-buoy FOWT system.

Table 5.6: Optimizers considered for the global design optimization task in comparison*.

Optimizer	Gradient-free	MO	Compliance with constraints	Convergence rate
ALPSO	✓	✗		
COBYLA	✓	✗		
NSGAI	✓	✓	+	++
NSGAIII	✓	✓	0	+
SPEA2	✓	✓	0	-

* Optimizer has (✓) or has not (✗) the feature; optimizer performs very good (++), good (+), neutral (0), or bad (-).

NSGAI is a genetic algorithm and, thus, falls in the category of EAs, which obey the principle of Darwin's theory of evolution, as explained in Section 4.2.3.2. Hence, for the additionally required parameters the following values are chosen.

- For the population size, 36 individuals are used within each generation. This number is based on the available number of cores on the utilized Intel[®] Xeon[®] CPU E7-8850 @2.00 GHz with 64-bit system and 80 virtual processors, so that all simulations within one generation can be executed in parallel at the same time.
- Based on the definition of the NSGAI optimizer from Platypus, the total number of simulations is required as input instead of the number of generations. The number of

generations used within the optimization algorithm needs to be high enough to allow for convergence of the optimization. One option to determine the appropriate number of generations is by means of a sensitivity study. In this work, however, a more direct approach is utilized, as information on the performance and convergence rate of NSGAI is already available from the initial optimizer tests on the specific optimization problem. Based on this, the total number of simulations is increased significantly above the expected point of convergence and selected to be 2,000, which would correspond to more than 55 full generations simulated. The convergence is finally approved in the analysis of the simulation results, covered in Section 5.1.4.3.

Optimization algorithm With the specified optimization problem and the selected optimizer and corresponding parameter settings, the optimization algorithm is executed. This iterative process runs until the stop criterion is reached, which is - based on the functionalities of the NSGAI optimizer from Platypus - in this application the total number of simulations. The following steps are then iterated, based on the general working principle of an EA described in Section 4.2.3.3.

0. Choosing from the prescribed value ranges, the design variables are redefined for each individual in the start generation ($G = 0$).
1. The individual floating wind turbine system designs are simulated (in parallel) each for 600 s, using the selected critical DLC as simulation case.
2. Based on the simulation results, the objective functions are evaluated by selecting the largest value for the global LS criteria obtained in the time series (excluding a pre-simulation time of 200 s to avoid transients) and the prescribed constraints are checked.
3. Based on the performance of each individual with respect to the optimization objectives and constraints, the design variables for the individuals of the next generation ($G + 1$) are specified, complying with the boundaries for the design variables values.
4. Steps 1 to 4 are repeated until the total number of simulations is reached.

In step 2, some error handling in case of unsuccessful simulations due to unstable designs with undesirable large motions and/or negative metacentric heights is incorporated, as suggested in Section 4.2.3.3. Before evaluating the objective functions, the last entry of the time series is analyzed. If this time value is the specified simulation length, the simulation was successful and the results evaluation is done as described in step 2. However, if the time value is below the specified simulation length, the simulation failed. Thus, the corresponding design is imperfect and should be excluded from further consideration. Hence, the objective functions are not evaluated, but undesirable values (beyond the valid value ranges) are set for the optimization criteria. These are for the total inclination angle, horizontal nacelle acceleration, and mean translational motion criteria each twice the maximum allowable value given as constraint in Table 5.2 (hence: 20.0° , 3.924 m/s^2 , and 128.0 m , respectively), while for the dynamic translational motion a negative value (-1.0 m) is set.

5.1.4 Results of the design optimization based on global limit states

Based on the descriptions of the reference system (Section 3.2), the system to optimize (Section 5.1.1), the optimization problem (Section 5.1.2), and the optimization approach (Section 5.1.3), first, the critical DLC is to be determined, covered in Section 5.1.4.1, which is later on used for the optimization. All simulations are performed on an Intel[®] Xeon[®] CPU E7-8850 @2.00 GHz with 64-bit system and 80 virtual processors, of which 36 cores are available - as mentioned in Section 5.1.3.2 when specifying the population size. The results of the iterative optimization approach are presented in Section 5.1.4.2, analyzed with respect to the optimized spar-buoy design in Section 5.1.4.3, and further discussed in Section 5.1.5.

5.1.4.1 Selection of the critical DLC

According to the approach, outlined in Section 5.1.3.1, and the performed pre-screening of the DLCs, 54 simulations (18 each selected DLC) are executed in Dymola[®] with the original OC3 phase IV spar-buoy FOWT system, modeled by means of MoWiT. The specific settings and descriptions of these DLC simulation cases are summarized in Table 5.7 and described in more detail in the following. Furthermore, the naming convention DLC_x_wW_sS_yY, as introduced and explained in Section 4.2.2.2, is used.

Table 5.7: Environmental conditions and simulation settings for the pre-selected DLCs.

D L C	Wind conditions				Sea conditions			
	W [m/s]	Long. TI [%]	S [-]	Y [°]	H_s [m]	T_p [s]	Wave seed [-]	Current speed [m/s]
1.1	10.0	18.34	1 ... 6	-8, 0, 8	1.74	6.03	7 ... 12	0.074
	11.4	17.38	7 ... 12	-8, 0, 8	1.99	6.44	13 ... 18	0.084
	13.0	16.53	13 ... 18	-8, 0, 8	2.30	6.92	19 ... 24	0.096
1.3	8.0	35.00	1 ... 6	-8, 0, 8	1.44	5.48	7 ... 12	0.059
	11.4	26.97	7 ... 12	-8, 0, 8	1.99	6.44	13 ... 18	0.084
	25.0	16.68	13 ... 18	-8, 0, 8	4.94	10.14	19 ... 24	0.184
1.6	8.0	20.30	1 ... 6	-8, 0, 8	10.37	14.70	7 ... 12	0.059
	11.4	17.38	7 ... 12	-8, 0, 8	10.37	14.70	13 ... 18	0.084
	25.0	13.64	13 ... 18	-8, 0, 8	10.37	14.70	19 ... 24	0.184

Wind conditions For the wind conditions, the Kaimal spectrum for turbulent wind, according to IEC standard 61400-1 (IEC 2019a), is used. With regard to the turbulence intensity (TI), the lateral and transverse TIs are 80% and 50%, respectively, of the specified longitudinal TI. For each wind speed, three different yaw misalignment angles are considered, as well as six seeds. These are combined in such a way, that the first two seeds go with the first yaw angle, the

third and fourth seeds go with the second yaw angle, and the last two seeds go with the third yaw angle, leading to the following six ending terms of the simulation cases for DLC11_w10.: s1_y-8, s2_y-8, s3_y0, s4_y0, s5_y8, and s6_y8.

Sea conditions For the sea conditions, the JONSWAP (joint North Sea wave project) wave spectrum is utilized. The significant wave height (H_s) is determined depending on the wind speed (W), according to Equation 5.3 (Bredmose et al. 2012). For DLC 1.6, which considers a severe irregular sea state, however, the ten-minutes average wind speed with recurrence period of 50 years from the turbulent extreme wind speed model is used for W in Equation 5.3, based on the recommendation given by IEC (2019b) to use the 50-year extreme significant wave height to be on the conservative side. According to IEC (2019a), the value for the ten-minutes average turbulent extreme wind speed with recurrence period of 50 years equals the reference wind speed average over ten minutes for the IEC wind turbine class I, which amounts to 50 m/s.

$$H_s = H_0 \left(1 + 2.6 \frac{\left(\frac{W}{V_0}\right)^3}{1 + \left(\frac{W}{V_0}\right)^2} \right) \quad ; H_0 = 1 \text{ m} , V_0 = 13 \text{ m/s} \quad (5.3)$$

The common relation between the significant wave height and the peak period (T_p) is given in Equation 5.4, based on IEC (2009).

$$11.1 \sqrt{\frac{H_s}{g}} \leq T_p \leq 14.3 \sqrt{\frac{H_s}{g}} \quad (5.4)$$

The peak-shape parameter (γ) of the JONSWAP wave spectrum depends on the relation of peak period and significant wave height, as expressed in Equation 5.5 (IEC 2009).

$$\gamma = \begin{cases} 5 & \text{for } \frac{T_p}{\sqrt{H_s}} \leq 3.6 \\ \exp\left(5.75 - 1.15 \frac{T_p}{\sqrt{H_s}}\right) & \text{for } 3.6 \leq \frac{T_p}{\sqrt{H_s}} \leq 5 \\ 1 & \text{for } \frac{T_p}{\sqrt{H_s}} > 5 \end{cases} \quad (5.5)$$

Due to the fact that a Pierson-Moskowitz spectrum, having a peak-shape parameter of $\gamma = 1$ would be most realistic for deep water conditions, the lowest possible value for the peak-shape parameter is tried to be obtained. Hence, the peak period is derived based on Equation 5.6, leading to a peak-shape parameter of $\gamma = 1.65$ for all simulation cases. This way, also the highest possible value for the peak period is obtained, which is as well most critical for spar-buoy floating systems with respect to their system eigenfrequencies.

$$T_p = 14.3 \sqrt{\frac{H_s}{g}} \quad (5.6)$$

Finally, as all pre-selected DLCs use the normal current model, no sub-surface currents have to be considered (IEC 2019b). Furthermore, no breaking wave surf induced currents are included due to the large distance of the floater to any coastal breaking wave zone. Hence, only

wind-generated near-surface currents are employed. This current speed (U_W) is determined, depending on the depth ($z \leq 0$ m) below SWL, following Equation 5.7 (IEC 2019b).

$$U_W(z) = \begin{cases} U_W(0 \text{ m}) \left(1 + \frac{z}{20 \text{ m}}\right) & \text{for } -20 \text{ m} \leq z \leq 0 \text{ m} \\ 0 & \text{for } z \leq -20 \text{ m} \end{cases} \quad (5.7)$$

The wind-generated current velocity at the sea surface ($U_W(0 \text{ m})$) is obtained from Equation 5.8, based on IEC 61400-3-1 (IEC 2019b) and utilizing the power law for a normal wind profile (IEC 2019a) to derive the wind speed at 10 m above SWL from the wind speed at hub height of 90 m.

$$U_W(0 \text{ m}) = 0.01W \left(\frac{10 \text{ m}}{90 \text{ m}}\right)^{0.14} \quad (5.8)$$

DLCs evaluation With these settings and definitions, all 54 DLC simulation cases are run for 600 s, using the solver Rkfix4 with a fixed integrator step-size of 0.01 s, which is a suitable value to obtain conservative values for the global dynamic response of the floating wind turbine system. Each 18 simulations per defined DLC category are run in parallel, which takes approximately three hours, leading to around nine hours in total for all 54 DLC simulations. The resulting time series of these simulations are evaluated just from 200 s on to exclude any transients at the beginning of the simulations. Thus, the maximum inclination (combined roll and pitch angle), the maximum horizontal acceleration at the tower top, the maximum amplitude of the dynamic translational motion (combined surge, sway, and heave displacement), as well as the maximum mean translational motion (even if this is not an optimization criterion) are selected for each DLC simulation case. The five highest values each with the corresponding DLC simulation cases are presented in Table 5.8.

It strikes that for both the total inclination angle and the horizontal nacelle acceleration, which are the two most important optimization criteria for the FOWT system, one and the same DLC simulation case, namely DLC16_w11_s11_y8, appears among the five most critical DLCs. For the total inclination angle this DLC yields directly the maximum value, while for the horizontal nacelle acceleration it results in the second highest value, close to the maximum obtained with DLC 1.6 at cut-out wind speed. For the translational motions, however, DLC 1.6 at a lower wind speed yields the highest dynamic response, while DLC 1.1 yields the highest values for both the mean displacement and the total translational motion (maximum 28.0 m in DLC11_w11_s7_y-8). For DLC16_w11_s11_y8 the maximum dynamic translational motion is 6.0 m (position 36 of all 54 DLC simulation cases) and the maximum mean translational motion is 20.2 m (position 9 of all 54 DLC simulation cases), while the total translational motion is the eighth largest with 25.9 m. As for the translational motion the overall goal is to reduce the dynamic part without having a specific constraint on it and the highest mean translational motion is far below the specified constraint of 64.0 m, but also as the greatest attention lies on the optimization criteria inclination and acceleration, DLC16_w11_s11_y8 is directly selected as the critical DLC simulation setting to be used within the optimization iterations.

Table 5.8: The five most critical DLCs for each optimization criterion and the constrained mean translational motion.

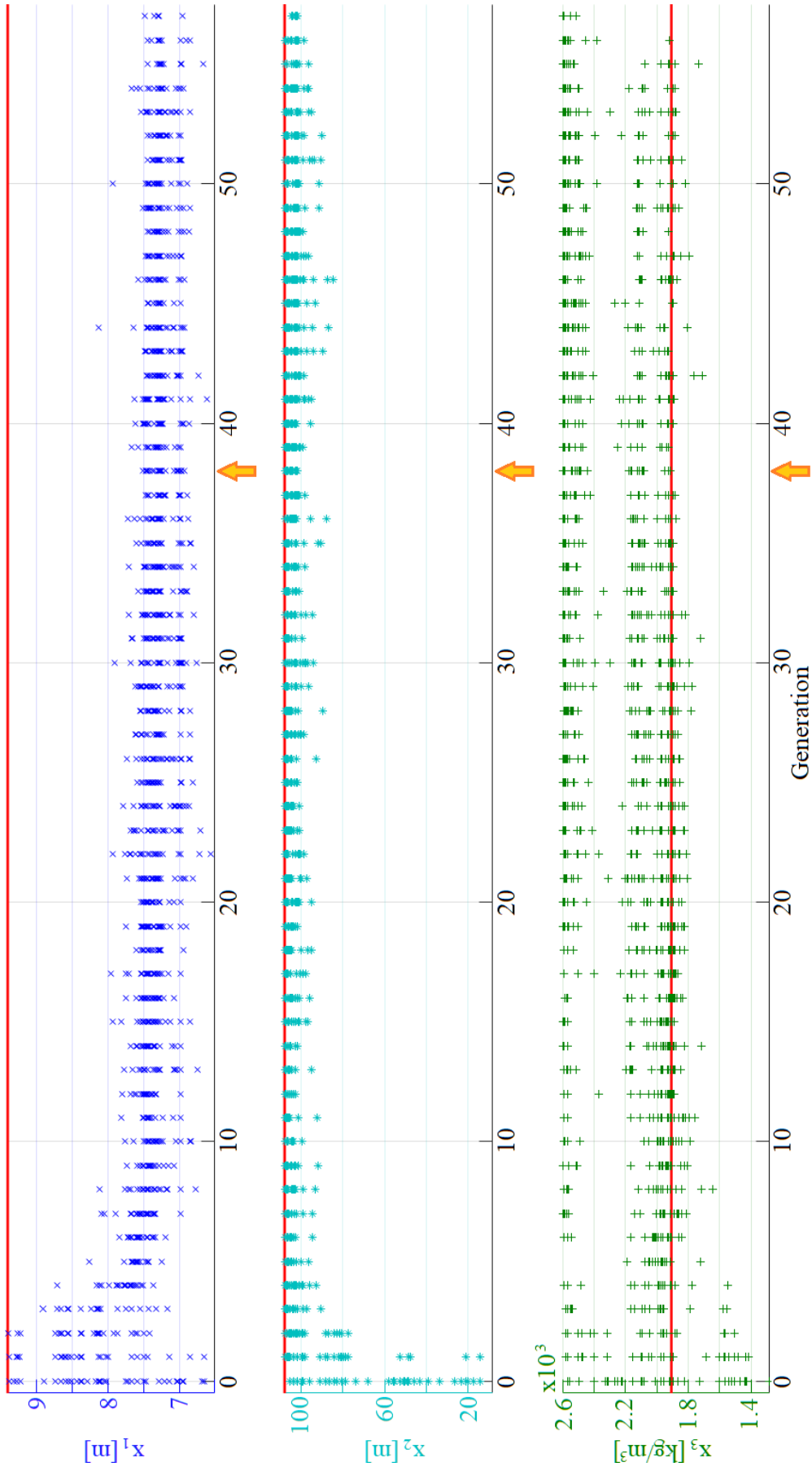
Rank	Total inclination angle		Horizontal nacelle acceleration	
	Simulation case	$\max(t_{\text{tot}})$	Simulation case	$\max(a_{\text{hor,nacelle}})$
1	DLC16_w11_s11_y8	4.9°	DLC16_w25_s16_y0	2.351 m/s ²
2	DLC11_w13_s17_y8	4.7°	DLC16_w11_s11_y8	2.338 m/s ²
3	DLC11_w13_s14_y-8	4.6°	DLC16_w8_s6_y8	2.317 m/s ²
4	DLC16_w11_s12_y8	4.6°	DLC16_w8_s1_y-8	2.306 m/s ²
5	DLC11_w13_s18_y8	4.6°	DLC16_w8_s3_y0	2.301 m/s ²

Rank	Dynamic translational motion		Mean translational motion	
	Simulation case	$\max(s_{\text{dyn,transl}})$	Simulation case	$s_{\text{mean,transl}}$
1	DLC16_w8_s5_y8	11.4 m	DLC11_w11_s10_y0	20.9 m
2	DLC11_w10_s3_y0	10.2 m	DLC13_w11_s10_y0	20.9 m
3	DLC11_w13_s15_y0	10.1 m	DLC11_w11_s9_y0	20.6 m
4	DLC16_w8_s3_y0	10.1 m	DLC13_w11_s9_y0	20.6 m
5	DLC11_w13_s16_y0	9.9 m	DLC16_w11_s10_y0	20.4 m

5.1.4.2 Developments throughout the global design optimization

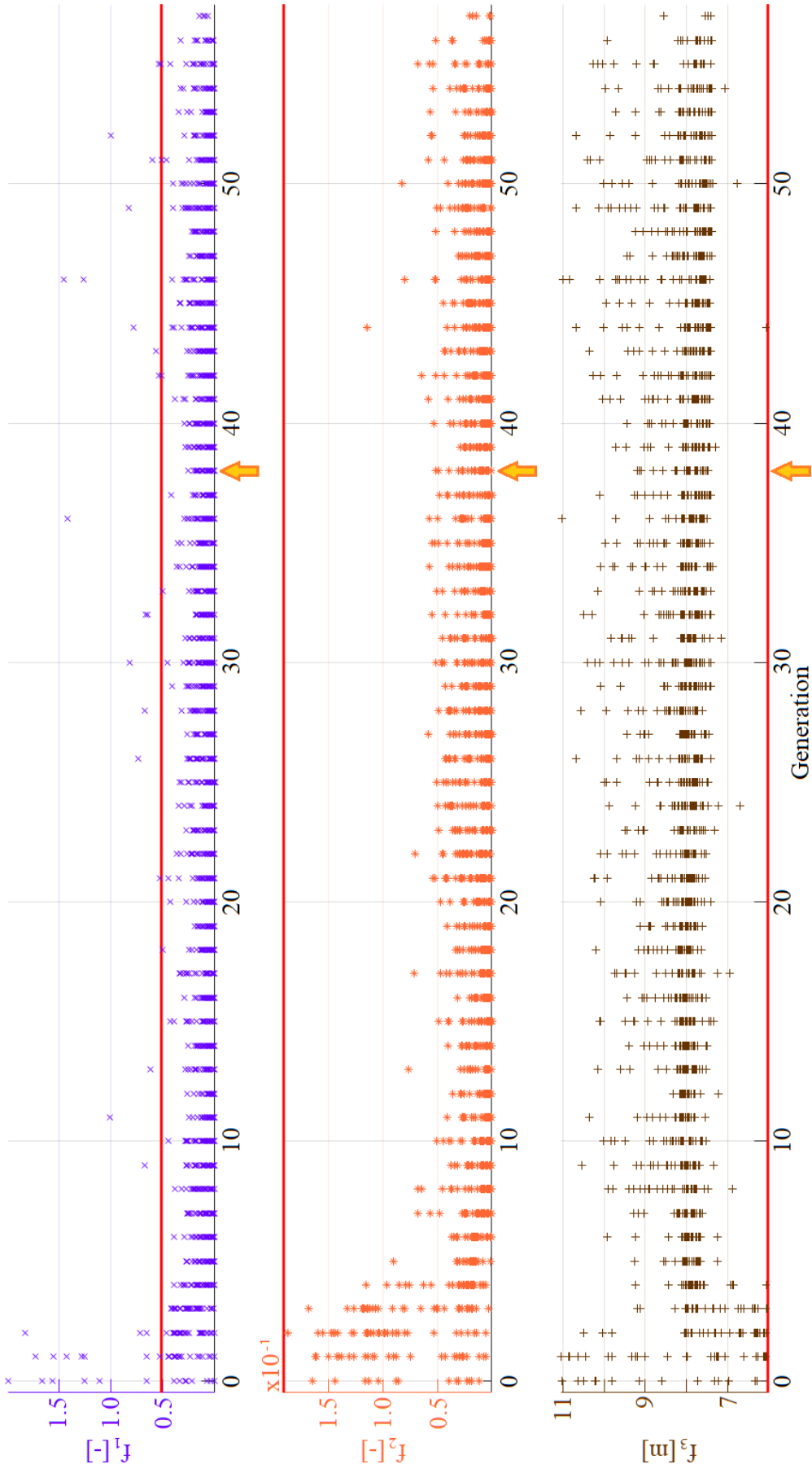
Thus, the optimization is performed with the OC3 phase IV spar-buoy FOWT system model for DLC16_w11_s11_y8, using the optimization settings as described in Section 5.1.3.2 and referring to the definitions in Section 5.1.1. 2,011 simulations are executed, using 36 processors in parallel and taking in total 197 hours. Due to the internal approach of the optimizer (NSGAI) to manage the simulations of individuals within generations in parallel, all 36 individuals are created for a total of 52 generations - corresponding to the start generation 0 up to and including generation number 51. Further individuals are generated up to generation number 57.

Figure 5.2 shows for all simulated individuals the development of their design variables (Figure 5.2(a)) and resulting objective functions (Figure 5.2(b)) throughout the generations. In addition, the values of the original OC3 phase IV spar-buoy FOWT system design are added (red lines) for comparison purposes. It can be seen that the optimizer first selects individuals from the entire allowable value ranges of the design variables. The corresponding spread in the objective functions is obviously large for these first generations. However, throughout the optimization, having evaluated the objective functions and checked the constraints, better and better design variables are selected by the optimizer and the objective functions improve.



(a) Development of the design variables, red lines representing the original values of the OC3 phase IV FOWT system, arrows indicating the selected generation of convergence.

Figure 5.2: Development of the 2,011 individuals throughout generation 0 up to generation 57 within the global design optimization.



(b) Development of the objective functions, red lines representing the original values of the OC3 phase IV FOWT system, arrows indicating the selected generation of convergence.

Figure 5.2: Development of the 2,011 individuals throughout generation 0 up to generation 57 within the global design optimization. (cont.)

Regarding the number of individuals (each represented by a marker) plotted in Figure 5.2, it has to be noted that the incompleteness of generations above generation number 51 is clearly visible. Furthermore, in Figure 5.2(b), the objective functions of not all 36 individuals of generation 0 and generation 1 are plotted, as only the successful designs are evaluated with respect to the optimization objectives. However, due to the high flexibility of the selected optimizer NSGAI, already from the third generation ($G = 2$) on all selected individuals complete the simulations without any failures.

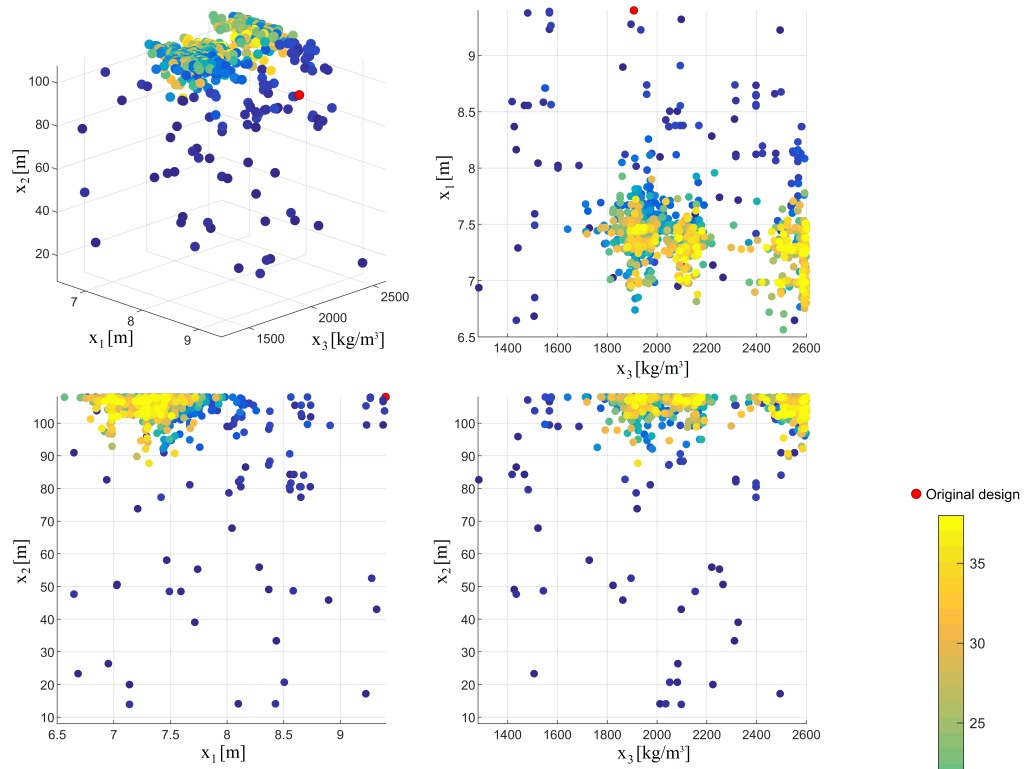
5.1.4.3 The resulting optimum design

Apart from the 29 individuals from the first two generations, which directly demonstrate imperfectness as their simulations fail, the remaining 1,982 individuals perform the simulations with success. From these it is now to select the one optimum individual.

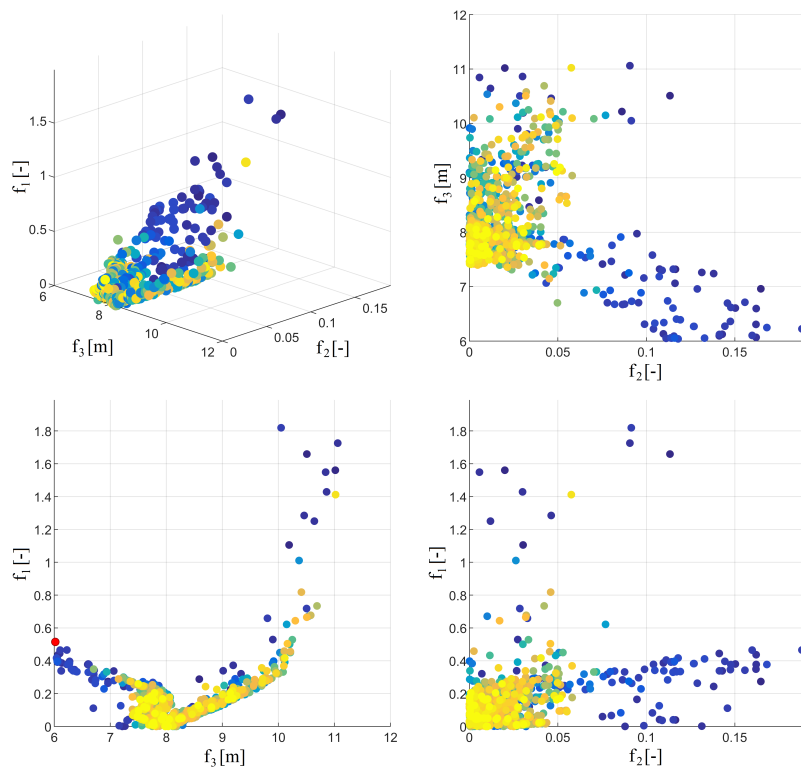
Selection procedure of the optimum solution Before the optimum individual can be selected, first, the convergence of the optimization has to be checked, as already mentioned in Section 5.1.3.2. This is done mathematically by determining the spread of the design parameters - and for comparison reasons also the spread of the objective functions - within each generation. The calculations show that the optimizer converges already within the first ten generations, but then, as the stop criterion (the total number of simulations) is not yet reached, diverges again to try to find an even better solution by increasing the spread within the design parameters again. However, as the optimizer had already found the optimum it converges back to this. This makes up the wavy pattern in the spread of the design variables and the objective functions, which can also directly be seen in Figure 5.2.

Based on these analyses, the overall minimum spread within the design variables is obtained in generation number 38 (with some other local minima in already earlier generations from generation 5 on), as pointed out by arrows in Figure 5.2. This proves again that the selected total number of simulations is sufficiently high for obtaining convergence within the optimization. Furthermore, Figure 5.3 shows 3D and 2D plots for both the development of the design variables, as well as the objective functions from generation 0 up to the selected generation 38. Here (Figure 5.3(a)), it can clearly be seen that the individuals of generation 0 fill out the entire space of the allowable values for the design variables, while the individuals of generation 38 troop together around the optimum. With respect to the objective functions, the 3D plot and even more clearly the 2D plots in Figure 5.3(b) show rather how the developing individuals form a Pareto front, on which most of the individuals of generation 38 are in the corner of optimum performance, indicated by low values for the objective functions.

Thus, from this selected generation of convergence now the final optimum design solution has to be chosen. To do so, first, the prescribed constraints are checked and not complying individuals are rejected. Then, the optimum value for each objective function is determined from the complying individuals within generation 38. These three values together are taken as the utopia point, which hence represents the ideal performance. Then, for each individual within



(a) 3D and 2D plots of the design variables.



(b) 3D and 2D plots of the objective functions.

Figure 5.3: Development of the individuals in the design space within the global design optimization.

generation 38, which fulfills the constraints, its distance to the utopia point is identified by determining from the differences between the inclination, acceleration, and normalized dynamic translational motion objective function values and the corresponding utopia values the overall distance by means of the root of the sum of the differences squared. As the inclination and acceleration objective functions are already normalized with respect to their target values, the absolute difference is computed for these two criteria. However, for the dynamic translational motion, the difference between achieved value and utopia value is normalized with respect to the value of the utopia, to allow for equally weighted consideration of the three optimization objectives. Following this approach, individual number 18 within generation 38 is obtained as the optimum design with the minimum distance to the utopia point. The properties of this optimum individual are presented in the following.

The optimized spar-buoy floater The shape of the optimum spar-buoy floater is drawn schematically in Figure 5.4 and compared to the original spar-buoy floater design, as well as a few exemplary designs of individuals in start generation ($G = 0$), showing the exploited value ranges of the design variables.

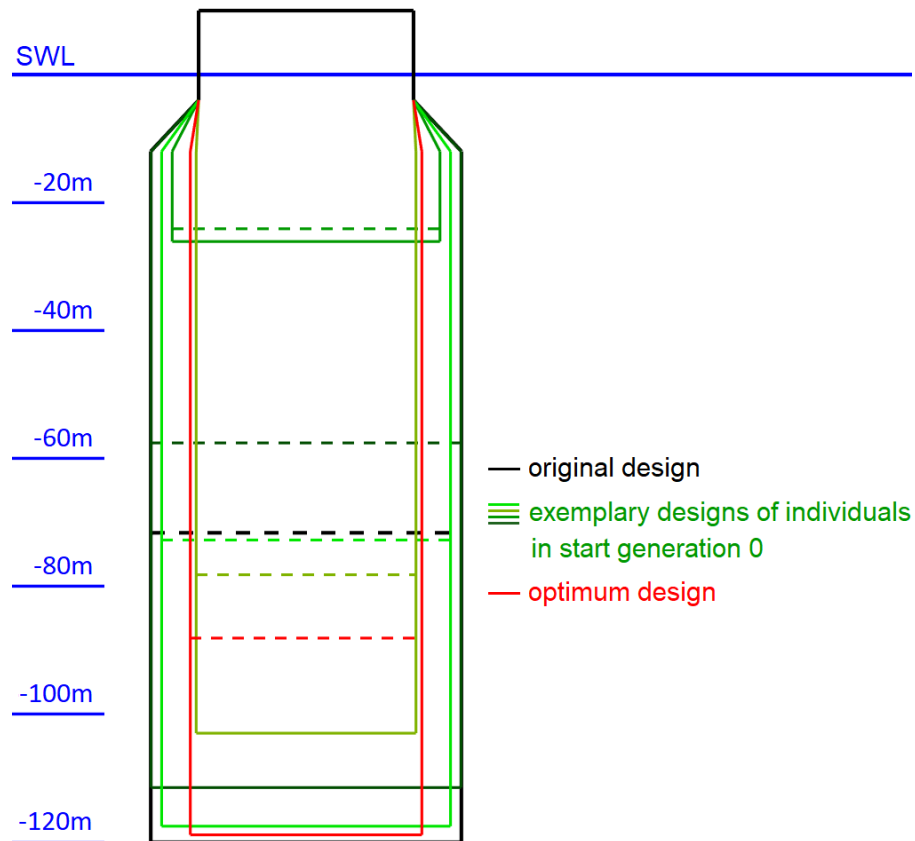


Figure 5.4: Design shapes from the global design optimization in comparison, dashed lines indicating the ballast height.

The specific numbers for the values of the design variables of the determined optimum spar-buoy floating structure are presented in Table 5.9. As it can be seen, when comparing

the values to the original OC3 phase IV spar-buoy floater design, the outer dimensions can be reduced, what is aimed for within the global design optimization task and realized through the specified allowable value ranges for the design variables. In specific, a reduction of the base column diameter by more than 25% is achieved, while the base column height is just 1% smaller than the original design. This reduction of the outer dimensions, however, is only possible as the original OC3 phase IV spar-buoy floater design is - as already indicated at the beginning of Chapter 5 - highly over-dimensioned for safety reasons, which can as well be seen in the very limited system response, as presented in Table 5.10 and discussed in more detail hereinafter. Furthermore, based on the additionally presented values for the structural mass of the spar-buoy, as well as for the ballast mass, a significant reduction in the overall mass of the floating platform is observed. By means of the optimized floater design, the ballast mass is more than halved, while a more than 35% denser ballast material is utilized, and the required structural mass is reduced by almost 24%. On this basis it can be expected to obtain also a drop in the system costs, which is as well an overall objective within this global design optimization task.

Table 5.9: Design variables of the optimum design of the global design optimization task, in comparison with the specified value ranges and original values.

Parameter	Value	Allowable value range	Original value
Base column diameter	7.0 m	[6.5 m, 9.4 m]	9.4 m
Base column height	106.8 m	[8.0 m, 108.0 m]	108.0 m
Ballast density	2,584 kg/m ³	[1,281 kg/m ³ , 2,600 kg/m ³]	1,907 kg/m ³
Ballast height	30.8 m	-	48.4 m
Structural mass	8.77×10^5 kg	-	11.50×10^5 kg
Ballast mass	30.07×10^5 kg	-	63.16×10^5 kg

Table 5.10: Optimization criteria of the optimum design of the global design optimization task, in comparison with the targets, constraints, and original values.

Parameter	Value	Target value	Constraint	Original value
$\max(t_{\text{tot}})$	9.9°	10.0°	$\leq 10.0^\circ$	4.9°
$\max(a_{\text{hor,nacelle}})$	1.910 m/s ²	1.962 m/s ²	≤ 1.962 m/s ²	2.338 m/s ²
$\max(s_{\text{dyn,transl}})$	7.7 m	minimized	≥ 0.0 m	6.0 m
$s_{\text{mean,transl}}$	26.7 m	-	≤ 64.0 m	20.2 m

Performance checks As already indicated within the selection procedure of the optimum solution, the constraints are checked again before selecting the optimum individual. Table 5.9 shows that the chosen values for the design variables fall within the specified allowable value

ranges. In addition to the design variables, also the optimization criteria are approved. Table 5.10 presents the achieved maximum values for the global LSs, as well as the additional constrained mean translational motion parameter. It can be seen that all parameters comply with the defined constraints. Furthermore, the targets for inclination and acceleration are very closely approached. Comparing the results with the maximum values obtained with the original OC3 phase IV spar-buoy FOWT system, it can be observed, at first, that not all constraints are initially fulfilled: the maximum achieved horizontal nacelle acceleration of the original OC3 phase IV spar-buoy floating system exceeds with 2.338 m/s^2 the specified upper limit of 1.962 m/s^2 ; however, the value still lies below $0.3 g$, which can as well be found in some literature as operational limit (Nejad et al. 2017, Huijs et al. 2013). Furthermore, it becomes apparent that both inclination angle and nacelle acceleration are significantly improved with respect to the specified objectives, meaning that the horizontal nacelle acceleration is now within the specified limit, but very close to it, and the maximum total system inclination angle is significantly enlarged - compared to the original maximum angle of 4.9° -, but as well still below the specified operational value of 10.0° . This is closely related to the reduced outer dimensions, as already mentioned and presented in Table 5.9. The translational motions of the optimum design are slightly larger than with the original design; however, the increase in the dynamic motion is minor and the constraint for the mean displacement is still fulfilled with a large clearance to the limit value.

The final check goes to the critical DLC, as already examined and mentioned in Section 5.1.3.1 in step 5. Thus, the 54 DLC simulation cases, as specified in Section 5.1.4.1, are run with the same simulation settings but now with the optimized spar-buoy floater design found beforehand. The evaluation of the time series reveals that the selected critical DLC16_w11_s11_y8 yields the highest horizontal nacelle acceleration. However, for the other optimization objectives DLC16_w11_s11_y8 is not the most critical DLC simulation case. Table 5.11 summarizes the results of the review of the critical DLC. For the dynamic translational motion, DLC16_w11_s11_y8 is already not the most critical DLC simulation case with the original OC3 phase IV spar-buoy FOWT system and just on position 36 in the ranking; whereas with the optimized spar-buoy design it moves up to position 32. A similar change is seen for the constrained mean translational motion parameter. Furthermore, the value obtained with the most critical DLC is only marginally larger than the maximum mean translational motion in DLC16_w11_s11_y8 and still significantly below the set constraint.

Thus, the only relevant difference between the original and optimized design, with respect to the critical DLC simulation case, is the maximum value for the total inclination angle. The selected critical DLC is for the optimized design (with an achieved value of 9.9°) just on position 9 in the ranking and the most critical DLC yields an inclination angle of 11.5° , which exceeds the prescribed operating limit of 10° . The analysis shows that six DLC simulation cases yield maximum inclination angles higher than 10° . Within this global design optimization task, however, this is accepted and no new critical DLC is selected, as spar-buoy FOWT systems should even in a damaged condition persist a maximum inclination angle of 17° (DNV GL 2018c) and in other studies up to 15° are considered as upper limit for a parked FOWT

system in extreme environmental conditions (Hegseth et al. 2020). This means, that with the optimized spar-buoy FOWT it might happen that - in six out of 54 environmental conditions - the wind turbine has to stop operation at certain times, but the system stability would never become critical. In the following (Section 5.1.5.1), some further strategies are proposed and analyses performed.

Table 5.11: Values of the optimization objectives and constrained parameters for the utilized and the most critical DLCs, original and optimized spar-buoy design in comparison.

Parameter	Design	DLC16_w11_s11_y8		Most critical DLC	
		Rank	Value	Value	Simulation case
$\max(t_{\text{tot}})$	Original	1	4.9°	4.9°	DLC16_w11_s11_y8
	Optimized	9	9.9°	11.5°	DLC11_w13_s16_y0
$\max(a_{\text{hor,nacelle}})$	Original	2	2.338 m/s ²	2.351 m/s ²	DLC16_w25_s16_y0
	Optimized	1	1.910 m/s ²	1.910 m/s ²	DLC16_w11_s11_y8
$\max(s_{\text{dyn,transl}})$	Original	36	6.0 m	11.4 m	DLC16_w8_s5_y8
	Optimized	32	7.7 m	13.4 m	DLC16_w8_s5_y8
$s_{\text{mean,transl}}$	Original	9	20.2 m	20.9 m	DLC11_w11_s10_y0
	Optimized	6	26.7 m	27.3 m	DLC16_w11_s10_y0

5.1.5 Discussion of the design optimization approach based on global limit states

Beyond and complementary to the results and analyses presented in Section 5.1.4, some aspects have to be addressed in more detail - as already indicated - and further points need to be discussed. Following up the performance check in Section 5.1.4.3, the issue of addressing various environmental conditions within the global design optimization approach is investigated in Section 5.1.5.1. Afterwards, the plausibility of the found optimum solution is analyzed in Section 5.1.5.2, while in Section 5.1.5.3 the Pareto optimality of the global design optimization is examined as alternative approach for selecting the optimum design solution. Finally, some sensitivities and limitations are elaborated in Section 5.1.5.4.

5.1.5.1 Addressing environmental conditions within the global design optimization approach

With respect to the presented global design optimization approach and demonstrated application example, a sensitive issue is the critical DLC, which is used for the simulations during the optimization. The methodology of utilizing one single critical environmental condition within the iterative optimization process is on the one hand very reasonable, as from a computational (and cost) point of view running the entire DLC set from standards with each individual within the optimization iterations would not be advisable; however, on the other hand, when using only

one DLC simulation case within the optimization procedure, this DLC has to be selected very carefully. Hence, in Section 5.1.3.1 an approach for selecting and approving this one critical DLC is suggested. In the presented application example it turns out that easily the most critical DLC can shift during the optimization, which emphasizes again the relevance of the check at the end and potential adjustments (step 5 of the sequence presented in Section 5.1.3.1).

In the design optimization of the OC3 phase IV spar-buoy, no amendments to the initially selected critical DLC are made, as the target and limit values for the two most important optimization objectives are set with allowance for some tolerance above.

- For the total inclination angle, the maximum operational value of 10° is selected, meaning that the FOWT system remains still stable at higher values but the turbine might have to stop operation. This is accepted for the six out of 54 DLC simulation cases, in which the operational limit is slightly exceeded, but way below extreme limits for a parked or even damaged system (Hegseth et al. 2020, DNV GL 2018c).
- For the horizontal nacelle acceleration, the more conservative value of maximum 0.2 g is selected. This leaves some safety margin for higher values in case that the ranking of criticality of the DLCs changes during the optimization, as even up to 0.3 g is mentioned as common operational limit (Nejad et al. 2017, Huijs et al. 2013).

Apart from the proposed methodology in Section 5.1.3.1, implying re-evaluation and modification of the selected critical DLC, another possible approach is to apply some safety factors to the overall limits for the optimization objectives, as it is indirectly done in the presented application example.

5.1.5.2 Plausibility of the optimum solution obtained from the global design optimization

In addition to the selection and performance of the optimum solution, the obtained optimized floater design itself needs to be discussed. Due to the complexity of FOWT systems and the MO optimization problem, it cannot directly be said how the optimum design will look like, especially as the MO optimization yields actually a set of optimal designs (the Pareto front), as examined in more detail in Section 5.1.5.3. However, based on the prime principle laws of FOWT system responses, a first estimate on the direction, in which the optimization will go, as well as on the expected values compared to the initial system design can be given. Thus, using the static analysis of the global motion response of a floating system, the highest inclination angle is expected at rated wind speed, yielding the highest thrust force and corresponding overturning moment (M), as already indicated in the pre-selection of critical DLCs (Section 5.1.3.1). The static relation between t_{tot} and M is given by means of the system stiffness C , as expressed in Equation 5.9.

$$t_{\text{tot}} = \frac{M}{C} \quad (5.9)$$

Due to the geometry of the spar-buoy floater, the system stiffness in the roll and pitch DOFs are the same and follow Equation 5.10, with the density of water ρ_{water} , the gravitational acceleration g , the diameter D_{WP} of the spar-buoy at the waterplane area, the total mass m_{system} of the entire FOWT system, as well as the vertical positions of the center of buoyancy and center of mass (z_{CoB} and z_{CoG} , respectively), having $z = 0$ at and $z < 0$ below SWL.

$$C = \rho_{\text{water}} g \frac{\pi}{64} D_{\text{WP}}^4 + m_{\text{system}} g (z_{\text{CoB}} - z_{\text{CoG}}) \quad (5.10)$$

Comparing the original maximum total inclination angle (4.9°) with the target value (10.0°), it is obvious that t_{tot} has to be increased within the optimization iterations. Due to the fact that the environmental conditions are unchanged during the optimization, the loading on the turbine can be considered as constant, neglecting an influence on the final overturning moment due to a changed point of rotation because of altered centers of buoyancy and mass. Thus, to enlarge t_{tot} , the system stiffness C has to be reduced. However, as the spar diameter at SWL - corresponding to the diameter of the upper column - is not modifiable, a smaller stiffness can only be obtained by a reduced distance between the centers of buoyancy and mass. This initial estimation of changes between the obtained optimum and the original floater design is examined. The specific numbers for the centers of buoyancy and mass, as well as their vertical distance to each other ($z_{\text{CoB}} - z_{\text{CoG}}$), determined for both the original and the obtained optimum FOWT system as presented in Table 5.12, substantiate the approximate estimations and the reasonability of the optimum floater design solution obtained with the presented global design optimization approach.

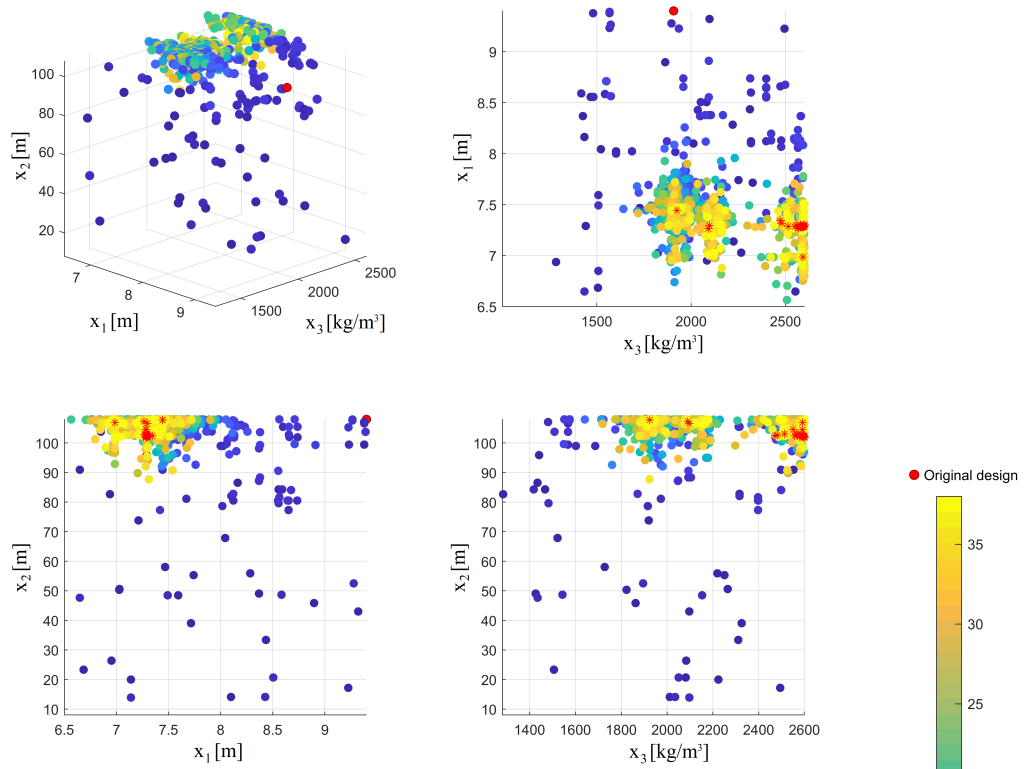
Table 5.12: Comparison of the centers of buoyancy and mass of the original and optimum FOWT systems for interpreting the results obtained with the global optimization approach.

Parameter	Original FOWT system	Optimum FOWT system
z_{CoB}	-62.1 m	-59.9 m
z_{CoG}	-78.0 m	-70.7 m
$z_{\text{CoB}} - z_{\text{CoG}}$	15.9 m	10.8 m

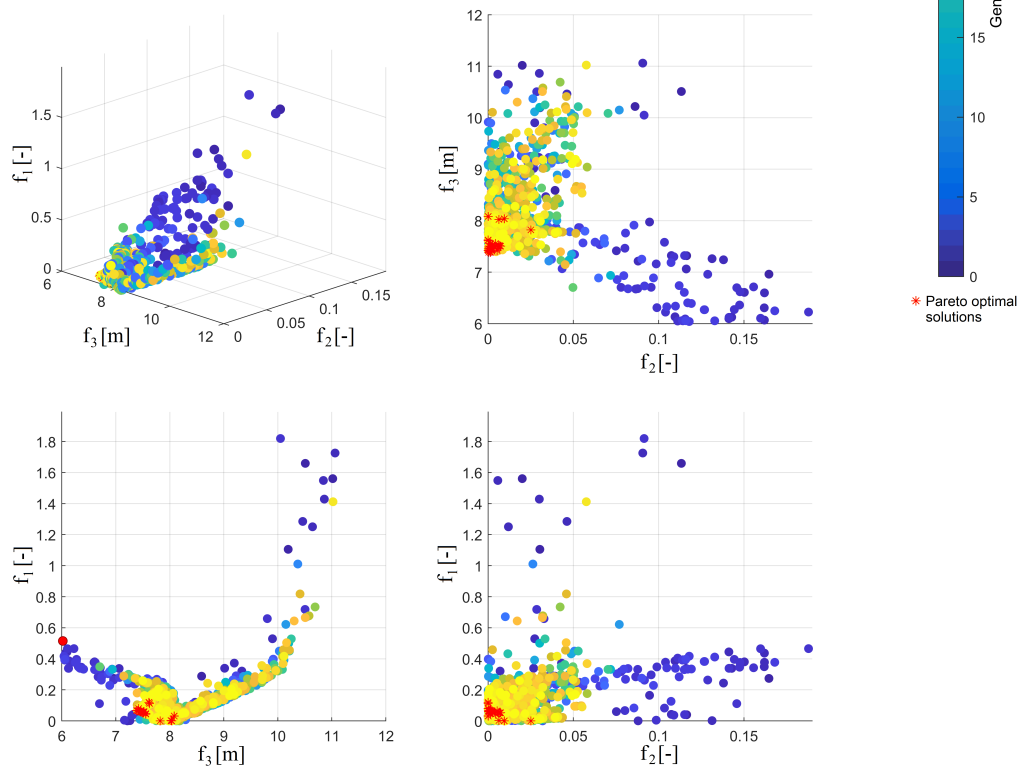
5.1.5.3 Pareto optimality of the global design optimization

As indicated in Section 5.1.5.2, MO optimizations yield a set of feasible solutions. From this, the optimum floater design is selected in Section 5.1.4.3 from the generation with the minimum spread within the design variables and as individual with the shortest distance to the utopia point. The latter is itself defined by the optimum objective function values occurring within the specific generation. However, an alternative approach to analyse MO optimization results follows a non-dominance test to obtain the Pareto optimal solutions.

Thus, the results of the global design optimization are filtered according to Pareto dominance, utilizing the code given in Appendix E. The resulting Pareto optimal solutions are indicated by means of an asterisk in Figure 5.5, which is analogous to Figure 5.3 in Section 5.1.4.3.



(a) 3D and 2D plots of the design variables.



(b) 3D and 2D plots of the objective functions.

Figure 5.5: Development of the individuals and Pareto optimal solutions in the design space within the global design optimization.

Afterwards, having checked the compliance with all constraints, the utopia point is again created out of the optimum value for each objective function, however, now determined from all generations, but considering only the Pareto optimal solutions. The distance of each Pareto optimal solution to the utopia point is determined according to the procedure described in Section 5.1.4.3. Finally, from the 37 Pareto optimal solutions, the one floater design is selected that shows the overall shortest distance to the utopia point, which is similar to the compromise solution mentioned by Gambier (2011), however, utilizes a normalization of the third objective function value (dynamic translational motion) to ensure equally weighted consideration of all three optimization objectives. This final Pareto optimal compromise solution is now individual number 1 from generation 37. Its shape is shown in Figure 5.6 in comparison to the previously selected optimum (individual number 18 from generation 38), while its specific figures for design variables, system parameters, and optimization criteria are presented in Tables 5.13 and 5.14.

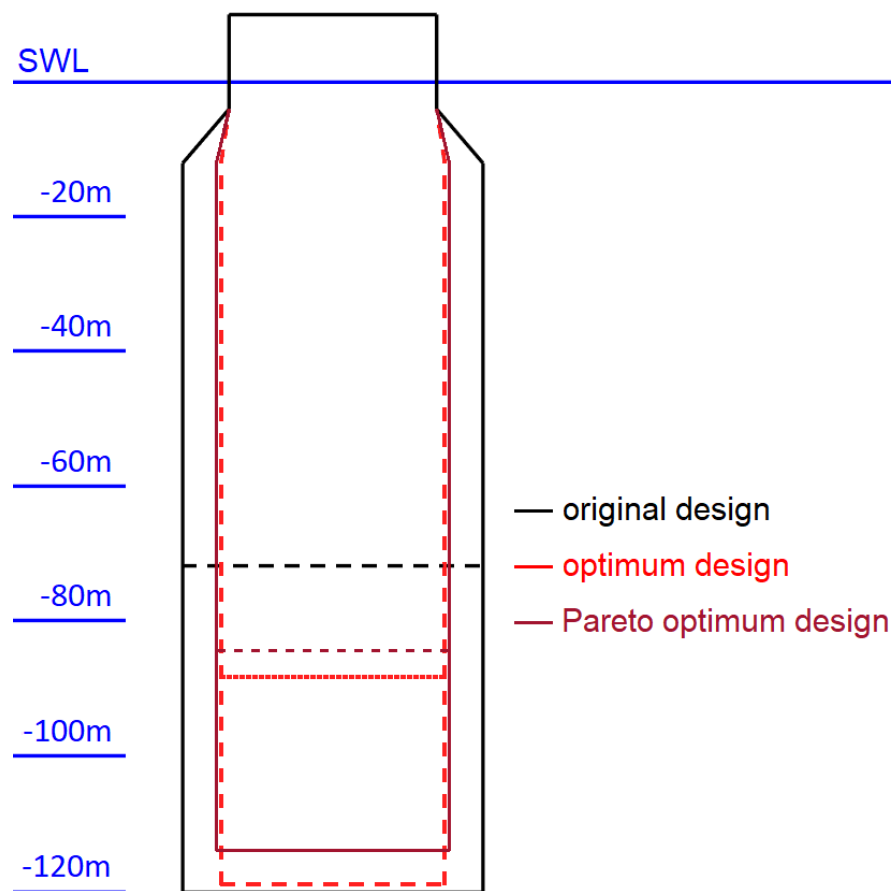


Figure 5.6: Pareto optimum design shape from the global design optimization, in comparison with the optimum from Section 5.1.4.3, dashed lines indicating the ballast height.

This demonstrates that both the optimum selected in Section 5.1.4.3 and the found Pareto optimum are very similar, especially with respect to their base column diameters, ballast densities, and translational motions. The base column height of the Pareto optimum design is, however, a bit smaller and the total system is regarding the structural and ballast mass in both

respects slightly heavier. Regarding the system performance, the Pareto optimum solution shows a less critical total inclination angle, while the horizontal nacelle acceleration is closer to the specified upper limit. Thus, even if both floater design solutions resemble one another, the comparison points out that for MO optimization tasks the selection of the optimum solution is not straight forward and can be done following different techniques, leading to different final design solutions.

Table 5.13: Design variables of the Pareto optimum design of the global design optimization task, in comparison with the optimum from Section 5.1.4.3.

Parameter	Pareto optimum	Optimum (Section 5.1.4.3)
Base column diameter	7.3 m	7.0 m
Base column height	101.8 m	106.8 m
Ballast density	2,600 kg/m ³	2,584 kg/m ³
Ballast height	29.6 m	30.8 m
Structural mass	8.80×10^5 kg	8.77×10^5 kg
Ballast mass	31.56×10^5 kg	30.07×10^5 kg

Table 5.14: Optimization criteria of the Pareto optimum design of the global design optimization task, in comparison with the optimum from Section 5.1.4.3.

Parameter	Pareto optimum	Optimum (Section 5.1.4.3)
$\max(t_{\text{tot}})$	9.6°	9.9°
$\max(a_{\text{hor,nacelle}})$	1.954 m/s ²	1.910 m/s ²
$\max(s_{\text{dyn,transl}})$	7.6 m	7.7 m
$s_{\text{mean,transl}}$	26.2 m	26.7 m

5.1.5.4 Sensitivities and limitations of the global design optimization task

Apart from the final selection procedure of the optimum solution, also already the optimizer and the convergence of the optimization are further aspects of high importance. The convergence of the global design optimization is checked and approved within this study; however, the most appropriate optimizer, as well as its rate of convergence depend on the explicit application example (both the simulated system and the specified optimization problem). Thus, for any other and further study and optimization task, it is highly recommended to perform sensitivity studies on the selection of the suitable optimizer and afterwards as well on approving its convergence within the optimization procedure.

Finally and fundamentally, it has to be emphasized that the presented global design optimization of the OC3 phase IV spar-buoy FOWT system is kept deliberately simple and focuses mainly on the global system performance, as well as on the reduction of the outer dimensions.

However, with the selected design variables (spar-buoy diameter and length, as well as the ballast density), one of the optimization objectives, namely the dynamic translational motion, as well as the constrained mean translational motion, can only be marginally influenced, which is reflected by the increased translational motions of the optimized design compared to the original design, as presented in Tables 5.10 and 5.11. Even though the wave drift forces - contributing to the surge motion - depend on the frontal area of the spar-buoy and, hence, its outer dimensions which are selected as design variables, the decisive influencing factor on the surge motion of a spar-buoy floating wind turbine system is the station-keeping system. Thus, mooring system parameters would have to be added as design variables to directly address the translational motion objective within the optimization. Furthermore, the optimized floating spar-buoy wind turbine system - with reduced floater outer dimensions and more critical, but still safe system inclination - will experience a larger bending moment at the tower base, as well as increased loads in the yaw bearing and at the blade roots, suffer losses in the power output, and impair the performance of the generator speed control. Hence, further local and more detailed criteria - such as (local) structural integrity checks, load and fatigue analyses, or even reliability aspects - as well as additional design variables (for the structure, but also for the mooring system or the turbine control) would have to be incorporated in the presented optimization approach for a high-quality and fully adequate design analysis and optimization.

5.2 Designing a complex geometry offshore wind turbine spar-type floating support structure

From the survey-based study, presented in Section 3.1.2, the conclusion is drawn that the spar-buoy concept is the most mature and has the highest TRL. However, in order to enhance its suitability for multi-MW wind farm deployment, this technology has to be further advanced: the common spar-buoy floater is already very convenient for volume production and certification due to its simple geometry, but to facilitate an accelerated and global market uptake, especially the large floater draft has to be reduced, so that in the end LCoE is reduced and handling simplified.

To overcome the challenges that the highly promising spar-buoy floating platform type still faces, a few researchers have already worked on concepts for advanced spar-type FOWT support structures, which have a reduced draft but still provide sufficient stability (Wright et al. 2019, Yoshimoto & Kamizawa 2019, Zhu et al. 2019, Hirai et al. 2018, Yoshimoto et al. 2018, Yamanaka et al. 2017, Matsuoka & Yoshimoto 2015, Lee 2005). However, different approaches for designing the floating platform are followed and it does not seem that a fully integrated optimization approach is adopted. Other design development studies (Chen et al. 2017, Perry et al. 2007, Bangs et al. 2002) are inspired by the oil and gas industry and deal with so-called truss spar platforms, in which a truss section connects a bottom tank with the floating platform and heave plates can be included. However, only Perry et al. (2007) apply a GA-based optimization for developing a cost-efficient preliminary floating support structure design. Some

other researchers focus on the optimization of the dynamic response of the FOWT system by rather adding and optimizing additional components instead of modifying the spar-type structure itself. Hence, Ding, Li, Ye, Zhou & Wang (2017), Ding, Li, Li, Hao & Ye (2017) use helical strakes - again inspired by the oil and gas industry - and a heave plate, while He et al. (2019) optimize a tuned mass damper by utilizing an artificial fish swarm algorithm. Pham & Shin (2019) add a moonpool, which is optimized together with the commonly shaped spar-type platform, following a three-step and, hence, no integrated optimization approach. The majority of design optimization approaches, however, is based on the common spar-type floater shape and utilizes gradient-based methods (Hegseth et al. 2020, Berthelsen et al. 2012, Fylling & Berthelsen 2011) or GAs (Karimi et al. 2017, Choi et al. 2014). Some applications are purely dealing with the support structure - focusing on basic hydrodynamic analyses, maximum system stability, and minimum material cost (Choi et al. 2014), reduced draft, weight, and cost with at the same time increased power output (Lee et al. 2015), or optimized floater cost and power generation (Gao & Sweetman 2018) - while other design optimization approaches are highly complex and account for optimizing several components of the floating wind turbine system, such as the tower, mooring system, power cable, and/or blade-pitch controller in addition to the floating platform, and focus on extreme loads, structural strength, fatigue life, or power quality in addition to costs and global system responses (Hegseth et al. 2020, Sandner et al. 2014, Fylling & Berthelsen 2011) or distinguish also between different floater types (Karimi et al. 2017, Sclavounos et al. 2008). Even if a reduced draft is often aimed and obtained (Hegseth et al. 2020, Gao & Sweetman 2018, Lee et al. 2015, Sandner et al. 2014) and sometimes the spar-buoy floater is subdivided into several cylindrical sections (Hegseth et al. 2020, Berthelsen et al. 2012, Fylling & Berthelsen 2011) or a broad range of allowable values is considered for the design variables (Karimi et al. 2017, Sclavounos et al. 2008), always common spar-type platform designs are considered, meaning a structure consisting of welded sections, for which reason even Hegseth et al. (2020) limit the maximum allowable taper angle.

Thus, the aim in this section and design optimization application is to demonstrate that, through a more comprehensive fully integrated design optimization approach and by allowing design variables out of a wider range of values, more potential solutions for an advanced spar-type floater design can be captured. Apart from reducing the floater draft, the main objective is cost reduction - expressed in terms of the material used - while global system performance criteria have to be fulfilled. All these requirements regarding design variables and optimization criteria are - together with specific environmental conditions and the fully-coupled aero-hydro-servo-elastic dynamic characteristics of a FOWT system - incorporated into the fully integrated MoWiT-Dymola[®]-Python optimization framework. By means of this, an advanced spar-type FOWT support structure design is aimed to be obtained. The focus of the optimization procedure lies on hydrodynamic and system-level analyses and no further limitations regarding a high detail structural design are added. This way and by considering different structural realization approaches for the resulting optimized geometries, new alternatives of potential and innovative floater design solutions are opened up.

In order to figure out in detail the required characteristics of such a floating platform, first, advanced spar-type floating wind turbine support structures are elaborated in detail in Section 5.2.1 and a reference floating system with corresponding assessment criteria is specified. Based on this, the optimization problem - consisting of design variables, objective function, and constraints - is defined in Section 5.2.2. Subsequently, the automated design optimization of the advanced spar-type floating wind turbine system is performed in Section 5.2.3, including some pre-processing automated DLC simulations, as well as the characterization of the iterative optimization approach. The results of the optimization simulations are presented in Section 5.2.4 and further discussed in Section 5.2.5.

5.2.1 Advanced spar-type floating wind turbine support structures

According to the survey conducted in Section 3.1.2, industry professionals and scientific experts judge the advanced spar-type floating platform - compared to the common spar-buoy floaters, semi-submersibles, TLPs, barges, or any hybrid, multi-turbine, or mixed-energy floating system - to be the most suitable support structure for wind turbines to be deployed in floating offshore wind farms due to their suitability for serial production, possibility of receiving certification, low LCoE, and little demands on the mooring system.

5.2.1.1 Characteristics of advanced spar-type floaters

The common spar-buoy floating platform - as described in detail in Section 3.1.1 - consists of a long relatively slender cylinder which is filled at the bottom end with ballast. The resulting deep center of gravity provides stability against overturning. However, this floating system exhibits some weaknesses, as elaborated in Section 3.1.2.1: due to its deep draft it cannot be deployed in shallow or intermediate waters up to around 100 m (James & Ros 2015), nor can the entire floating wind turbine system be fully assembled in upright position onshore or at harbor sites. The latter fact adds to the already expensive floater, as it makes the overall handling of this long and heavy structure, its assembly, transport, and installation costly. Thus, by

- reducing the draft,
- applying a delta or so called crowfoot connection of the mooring lines to the spar-buoy structure, and/or
- adding stabilizing fins,

the advanced spar-type floating system can benefit from

- a wider range of possible installation sites,
- simplified handling (both construction, assembly, transport, and installation),
- reduced system, as well as construction and transportation costs, as well as
- improved system motion performance.

In particular, these characteristics of advanced spar-type floating platforms are realized in a few - both research and real - concepts. The advanced spar-type floater by the Massachusetts Institute of Technology (Lee 2005) has a relatively shallow draft and gets stability support from a two-layered taut-leg mooring system (Butterfield et al. 2007). Both Hirai et al. (2018) and Yamanaka et al. (2017) use a three-segmented advanced geometry spar, where a larger diameter column makes up the middle part to allow for shortening the overall length of the spar and reducing the system cost, while Zhu et al. (2019) utilize the three elements just in an opposite way, focusing on increased restoring and improved motion performance: the spar element makes up the middle part and interconnects two columns, one with just a slightly larger diameter at the bottom end and another one with a large diameter at the upper end.

Within the Fukushima Floating Offshore Wind Farm Demonstration Project FORWARD an advanced spar-type support structure, developed by Japan Marine United, is utilized for a floating substation (Fukushima Kizuna) and a 5 MW wind turbine (Fukushima Hamakaze) (Yoshimoto & Kamizawa 2019, James & Ros 2015, Main(e) International Consulting LLC 2013). The advanced spar for the floating substation consists of three columns - or so called hulls - placed at the bottom, in the middle, and at the upper end (intersecting the water line) of the spar, so that the floating system is suitable already at around 110 m water depth, the motion performance is improved, and the cost for installation is reduced (Wright et al. 2019, Yoshimoto et al. 2018, Matsuoka & Yoshimoto 2015). The Fukushima Hamakaze was initially using a similarly structured advanced spar, equipped with damping fins for stabilization in sway and heave direction (James & Ros 2015, Main(e) International Consulting LLC 2013); however, after some investigations and studies by Matsuoka & Yoshimoto (2015), finally the advanced spar-type platform for the 5 MW wind turbine consists of just two large columns/hulls at the bottom and top end of the spar and, thus, is optimized with respect to the system restoring and motion performance, as well as the construction cost (Yoshimoto & Kamizawa 2019). Despite these optimizations, the installation of the floating platform - in particular the ballasting operations - turned out to be complex, as the floater has leaned to an angle of 45° when it was brought from the construction draft to a deeper draft, which, however, could be resolved within less than a week (JWPA 2017, Foster 2016).

5.2.1.2 Defining a reference advanced spar-type floating offshore wind turbine system

As starting point of the design optimization towards an advanced spar-type floating platform for an offshore wind turbine, the reference OC3 phase IV spar-buoy floating wind turbine system, presented in Section 3.2, is utilized. The numerical model of the OC3 phase IV spar-buoy FOWT system, as implemented in MoWiT and verified in Section 4.1, is used as basis and modified so that a design of an advanced spar-type floater can be obtained through automated optimization. As this work focuses on the design of the floating platform and not on the mooring system, a shorter, less heavy, and, hence, cheaper advanced spar-type floater design shall be obtained by changing the floater geometry. Different characteristic shapes of advanced spar-type floating platforms are pointed out in Section 5.2.1.1. In this application example, a similar

concept as presented by Zhu et al. (2019) and realized in the Fukushima Hamakaze floating wind turbine system (Yoshimoto & Kamizawa 2019, Matsuoka & Yoshimoto 2015) is applied: the long cylindrical element below the tapered part is divided into three partitions:

1. the base column upper part BC_{up} , which shall serve for gaining buoyancy;
2. the base column middle part BC_{mid} , which mainly provides the separation of parts 1 and 3 to deepen the position of part 3; and
3. the base column lower part BC_{low} , which can be filled with ballast and this way shall shift the center of gravity downwards.

This partitioning is schematically represented in Figure 5.7, showing the unchanged geometric parameters and dimensions for the upper column and tapered part (TP) in a light shade

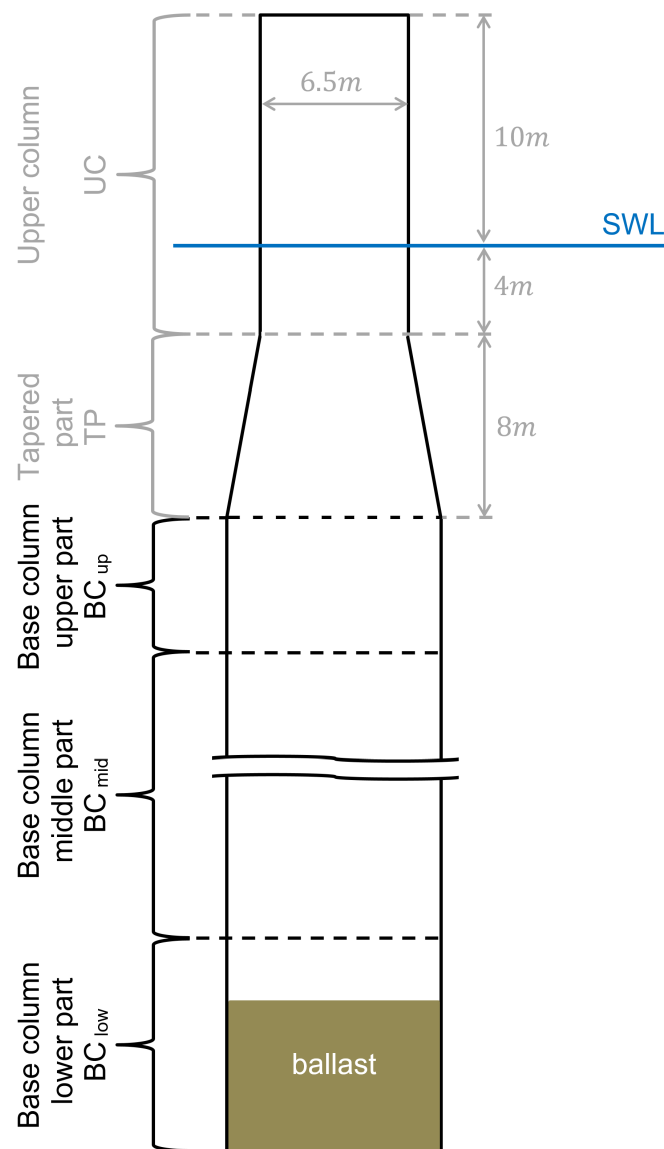


Figure 5.7: Geometrical definitions of the advanced spar-type floating platform.

(gray) and indicating the three sections of the base column together with the ballast filling in the base column lower part.

In order to still represent the original OC3 phase IV floating spar-buoy with the modified MoWiT model, initially the diameters of all three BC parts are set equal to the original base column diameter of 9.4 m and - as a ballast filling is just allowed in BC_{low} - the heights of BC_{up} and BC_{mid} are set equal to machine epsilon, which corresponds to a value of 10^{-15} in Modelica[®], while BC_{low} holds the full original length of 108.0 m. Regarding the hydrodynamic coefficients for the three cylindrical partitions, the same as for the original OC3 phase IV spar-buoy, presented in Section 3.2.2, are applied.

Apart from these modifications, which are directly related to an advanced spar-type floater design, also the material density ρ_{platform} of the support structure and the wall thickness t of the cylindrical spar-buoy elements are changed. As the material density of the OC3 phase IV spar-buoy is not explicitly defined in the definition document by Jonkman (2010), a value of $10,000 \text{ kg/m}^3$ is derived in the model verification (Section 4.1.1.2). However, to better match the common steel properties of offshore structures, a material density of $7,850 \text{ kg/m}^3$ is used for the design of the advanced spar-type floating platform. Furthermore, the wall thickness of the spar structure¹ is changed from the fixed value of 0.0314 m, which is derived in Section 4.1.1.2, to a wall thickness that is adaptable to the specific advanced spar-type floater design. In order to obtain an appropriate wall thickness for a corresponding floater design, a fixed ratio of the support structure structural mass m_{platform} to the displaced mass of water, corresponding to the buoyant mass m_B , is deployed, which is for a spar-type floating platform 0.13 - according to representative values from research designs and academic studies and excluding designs, such as the Hywind demonstrator, which are for safety reasons heavily oversized (Bachynski 2018). Hence, the equivalent structural mass of the advanced spar floater (meaning the mass of the advanced spar-type steel structure excluding the tower and wind turbine, and as well excluding the ballast mass) with certain outer dimensions (diameters D_i and heights H_i) and corresponding displaced volume can be determined following Equation (5.11).

$$\frac{m_{\text{platform}}}{m_B} = 0.13 \quad (5.11)$$

With the resulting structural mass of the advanced spar-type floater of $10.70 \times 10^5 \text{ kg}$, which is a bit lower than the original structural mass of $11.50 \times 10^5 \text{ kg}$, the corresponding appropriate wall thickness, which is kept the same and constant for all parts of the specific advanced spar design, is computed by means of Equation (5.12), which is derived from the expression for the mass of the advanced spar steel structure with a material density of $7,850 \text{ kg/m}^3$ as explained above. In Equation (5.12), H_i and D_i are the heights and diameters of each element, meaning UC, TP, BC_{up}, BC_{mid}, and BC_{low}, while the diameter of the tapered part D_{TP} is determined according to Equation (5.13) as mean of the diameters of UC and BC_{up}.

¹Referring here purely to the circumferential walls of the hollow cylindrical or conical elements, as for base and lid a fixed marginal cap thickness of $1.0 \times 10^{-4} \text{ m}$ is applied, according to the implemented model verified in Section 4.1.1.2.

$$t = \frac{\sum_i (H_i D_i) - \sqrt{[\sum_i (H_i D_i)]^2 - \frac{4}{\pi} \frac{m_{\text{platform}}}{\rho_{\text{platform}}} \sum_i H_i}}{2 \sum_i H_i} \quad (5.12)$$

$$D_{\text{TP}} = \frac{D_{\text{UC}} + D_{\text{BC,up}}}{2} \quad (5.13)$$

This way, a wall thickness of 0.0372 m is obtained for the original OC3 phase IV spar-buoy with reduced material density (7,850 kg/m³) and adopted structural mass to displaced mass ratio of 0.13. This wall thickness value lies within the acceptable range, based on available data for the semi-submersible floating platform from phase II of OC4.

As the advanced spar-type floater design optimization does not focus on the mooring system, as mentioned above and due to the fact that the mooring system itself could be covered in a separate optimization task, any change in the restoring system characteristics due to shifted fairlead positions is prevented by utilizing constant (the original) resulting mooring system properties, as already applied in the global design optimization task in Section 5.1.1.1. This means that - independent of possible attachment points to the reshaped floating platform - the resulting stiffness of each mooring line is taken from the system motion, assuming the original fairlead positions as defined in Table 3.13 in Section 3.2.2. A realistic mooring system design for the finally obtained optimized floating platform, which represents the considered resulting mooring system properties, can then afterwards be obtained through a subsequent optimization, which might even be manual - depending on the degree of complexity - as it is applied in studies for designing equivalent mooring systems (Molins et al. 2015, Udoh 2014). However, having not included the mooring system as design variable within the optimization of the floating spar-type platform, further system performance improvements due to modified mooring system parameters or fairlead positions - in addition to an optimized support structure design - are limited. This, however, leaves open the possibility of subsequent fine tuning of the design solution obtained through optimization based on hydrodynamic and system-level analyses. By addressing the mooring system in a successive but separate optimization algorithm, the dynamic response of the FOWT system, as well as the mooring line tension itself, can be significantly improved by considering an advanced and more complex optimization problem, in which - apart from various line diameters and lengths - different mooring line arrangements and distribution forms can be utilized, the optimum number of lines within the mooring system and best fairlead position elaborated, different mooring types used or even mixed within segmented lines, and also clump weights incorporated (Tafazzoli et al. 2020, Barbanti et al. 2019, Men et al. 2019, Chen et al. 2017).

5.2.1.3 Assessment criteria for designing an optimized advanced spar-type floater

The focus in this application example lies on obtaining an advanced spar-type floating platform, which is characterized through a limited draft and reduced structural cost, but still shows good hydrodynamic performance. Any detailed structural integrity checks are not addressed in this work, but can be added for a more extensive optimization approach. However, by focusing

only on hydrodynamics and global system performance without defining any restrictions regarding structural aspects, floater designs, which would have been discarded when performing structural integrity checks and as they would be unfeasible to be realized with conventional structural approaches, can still be captured as potential solutions when considering different structural realization approaches.

The only structural related focus, considered in this approach, is the minimization of the structural cost. This is represented through the steel volume of the floater, which is finally specified as objective of the optimization problem, as formally declared in Section 5.2.2.2.

In order to achieve the shortened length of the advanced spar-type floater, the allowable draft of the system is limited to the original draft of the OC3 phase IV floating wind turbine system as maximum value, as well as to a recommended minimum value of 15.0 m (Ng & Ran 2016). The resulting allowable total height of the base column has to be distributed to the three partitions. As, however, this distribution is not restricted, keeping also the option of utilizing not all three BC parts, the minimum allowable value for the height of each of the BC parts is machine epsilon (10^{-15} m) - as a zero value is unfeasible from a modeling point of view. For the ballast height, it additionally has to be guaranteed that it does not exceed the actual height of BC_{low} . The resulting allowable value ranges based on the draft limits are summarized in Table 5.15.

Table 5.15: Allowable value ranges addressing the draft limits for the advanced spar-type floater.

Limit	Allowable draft	Resulting H_{BC}	$H_{BC,up}$	$H_{BC,mid}$	$H_{BC,low}$	$H_{ballast}$
Min	15.0 m	3.0 m	10^{-15} m	10^{-15} m	10^{-15} m	10^{-15} m
Max	120.0 m	108.0 m	108.0 m	108.0 m	108.0 m	108.0 m

The applied concept of a three-segmented advanced spar-type floater with elements for buoyancy, distance, and ballast shall not only allow different heights but also different diameters of these elements. Thus, the allowable value range for the diameter of each of the BC parts is set from machine epsilon - due to the same modeling feasibility reason - to 120.0 m. The maximum diameter is chosen deliberately large - corresponding to the total maximum draft of the floating system - to ensure that the border of feasible solutions is well captured. From the manufacturing point of view, cylindrical offshore structures with diameters of more than 10.0 m are realistic: various sources (Sif Group 2020, Windkraft-Journal 2019) state a value of 11.0 m, the reference semi-submersible floating platform from phase II of OC4 has an upper column diameter of 12.0 m (Robertson et al. 2014), and the diameter of the spar-buoy utilized in the Hywind Scotland floating wind farm (Equinor 2020b, 2017) is even up to 14.5 m large. However, looking at other floating platform solutions, such as the Damping Pool[®] floater by Ideol (Ideol 2020) with outer dimensions of 36 m x 36 m and a resulting diagonal length of almost 51 m or again the OC4 phase II semi-submersible platform (Robertson et al. 2014) with an overall outer dimension of almost 82 m in diameter, shows that floating structures with a large overall outer diameter can be obtained without being restricted to the manufacturing feasibil-

ity limits for pure cylinders. Thus, from a hydrodynamic point of view, a cylindrical offshore structure with very large diameter can be realized as well through several smaller diameter cylinders being clustered together in a circle, representing similar hydrodynamic behavior and characteristics. Finally, attention has to be drawn on the minimum possible diameter of the BC parts, which always has to be at least as large as twice the actual wall thickness corresponding to the specific advanced spar-type floater design.

Having modified the diameters and heights of the three BC parts, as well as the ballast filling height, and having adjusted the wall thickness according to the structural mass to displaced mass ratio, as defined in Section 5.2.1.2, the ballast density has to be adjusted to match the original floating equilibrium between buoyancy force, system weight, and downward mooring force, so that the original hub height is maintained. In order to exclude unfeasible system solutions, in which material would have to be removed from the system (realized for example by reducing the material density) to meet this equilibrium condition, it has to be ensured that the actual resulting ballast density of the specific advanced spar-type floater design carries a positive value. However, in order to account for truly realistic ballast densities, also the uppermost allowable value of the ballast density has to be constrained. Within the global design optimization application example (Section 5.1.1.1) densities for common and cheap materials to be used as ballast for a floating spar-buoy are explored. The densest material included is sandstone (or other rocks) with a density of about $2.6 \times 10^3 \text{ kg/m}^3$. Apart from sand, sand mixed with water, concrete, or rocks, MagnaDense (heavyweight concrete) is as well used in industry as high density material² (LKAB Minerals 2020, 2018). With MagnaDense densities of up to $5.0 \times 10^3 \text{ kg/m}^3$ can be obtained (LKAB Minerals 2019). Even if minimization of the structure material volume is defined as objective function - as stated at the beginning of this section - in order to represent the structural cost, the cost of the two potential densest ballast materials is elaborated to avoid significant larger ballast costs when utilizing MagnaDense instead of the common cheap materials pointed out in Section 5.1.1.1. However, when comparing the material prices for sandstone (Alibaba.com 2020b) (for the ballast density limit of $2.6 \times 10^3 \text{ kg/m}^3$) and MagnaDense(Alibaba.com 2020a) (for the ballast density limit of $5.0 \times 10^3 \text{ kg/m}^3$), it turns out that both ballast materials have a similar cost of around 150 \$ per ton, which is less than 20% of the material cost for structural (raw) steel of about 700 \$ per tonne (Butcher 2018, Grogan 2018, Michael 2018). Thus, the ballast density is constrained to a maximum of $5.0 \times 10^3 \text{ kg/m}^3$.

Apart from these more geometry related assessment criteria, there are three performance related criteria that the advanced spar-type FOWT system has to fulfill, which are the same as applied for the global design optimization task (Section 5.1.1.2) and with which risks and consequences for system components or the entire FOWT system are associated, as listed in Table D.1 in Appendix D. For the global system performance of a FOWT maximum allowable values are prescribed for

²Floating offshore wind project manager at a leading company in offshore industry, personal communication, 6 February 2020.

1. the total inclination angle of the system to the vertical:
for system rotational stability reasons a maximum total inclination angle of 10.0° is allowed in operational conditions (Katsouris & Marina 2016, Kolios et al. 2015, Huijs et al. 2013);
2. the total horizontal acceleration at the tower top:
due to sensitive components in the nacelle and to prevent any issues with the lubrication, the nacelle acceleration - corresponding to the acceleration at the tower top - is limited, depending on the specific wind turbine, to a maximum of 0.2 to 0.3 times the gravitational acceleration constant (Nejad et al. 2017, Huijs et al. 2013, Suzuki et al. 2011); herein the lower value of 1.962 m/s^2 is used following the conservative approach applied in the global design optimization task (Section 5.1.1.2); as well as
3. the mean translational motion of the floating system:
based on experience, the static translational displacement of a (non TLP-type) FOWT system, corresponding to the mean of the translational motion, is restricted to 0.2 times the water depth (320.0 m in the case of the OC3 phase IV spar-buoy floating system), and hence to 64.0 m in this application.

5.2.2 Definition of the optimization problem for designing an advanced spar-type floater

For obtaining an optimized advanced spar-type floater design, following the assessment criteria - as outlined in Section 5.2.1.3 - and using the modified floating wind turbine system model - as described in Section 5.2.1.2 - as basis, an iterative optimization approach (explained in more detail in Section 5.2.3.2) is carried out. This optimization approach requires the definition of the optimization problem, which is based on the formal expression given in Section 4.2.3.1 and comprises the modifiable design variables (Section 5.2.2.1), the objective function to be minimized (Section 5.2.2.2), as well as the constraints to be fulfilled (Section 5.2.2.3) - as declared in the following.

5.2.2.1 Design variables of the advanced spar-type floating wind turbine system

Based on the derivation of the modified spar-buoy floater model for enabling the design of an advanced spar-type floating platform (Section 5.2.1.2), the design variables vector $X = \{x_1, x_2, \dots, x_6, x_7\}$ with the following seven ($k = 7$) elements is defined according to the declarations given in Table 5.16.

Table 5.16: Declaration of the seven design variables of the optimization problem for designing an advanced spar-type floater.

Design variable	Formal expression	Description
x_1	$D_{BC,up}$	Diameter of base column upper part
x_2	$D_{BC,mid}$	Diameter of base column middle part
x_3	$D_{BC,low}$	Diameter of base column lower part
x_4	$H_{BC,up}$	Height of base column upper part
x_5	$H_{BC,mid}$	Height of base column middle part
x_6	$H_{BC,low}$	Height of base column lower part
x_7	$H_{ballast}$	Height of ballast within base column lower part

5.2.2.2 Objective function for the advanced spar-type floating wind turbine system

As stated in Section 5.2.1.3, just one objective function ($l = 1$) is specified, which corresponds to the structure material volume of the advanced spar-type floating platform (Table 5.17). This objective function (f_1) is to be minimized, as defined at the beginning of Section 5.2.2.

Table 5.17: Declaration of the objective function of the optimization problem for designing an advanced spar-type floater.

Objective function	Formal expression	Description
$f_1 (system(X))$	$\frac{m_{platform}}{\rho_{platform}}$	Spar structure material volume

5.2.2.3 Constraints for the advanced spar-type floating wind turbine system

Section 5.2.1.3 covers already the assessment criteria for designing an optimized advanced spar-type floating platform. These make up - apart from the objective function - 25 constraints, which are all specified as inequality constraints - hence, $m = 0$ (for the equality constraints h_i) and $n = 25$ (for the inequality constraints g_i). These shall all take on values less or equal to zero, as expressed formally in Section 4.2.3.1. The definitions of the inequality constraints are listed in Table 5.18.

Table 5.18: Definition of the 25 inequality constraints of the optimization problem for designing an advanced spar-type floater.

Inequality constraint	Formal expression	Description
$g_1(x_1)$	$10^{-15} \text{ m} - x_1$	Allowable value range of x_1
$g_2(x_1)$	$x_1 - 120.0 \text{ m}$	Allowable value range of x_1
$g_3(x_2)$	$10^{-15} \text{ m} - x_2$	Allowable value range of x_2
$g_4(x_2)$	$x_2 - 120.0 \text{ m}$	Allowable value range of x_2
$g_5(x_3)$	$10^{-15} \text{ m} - x_3$	Allowable value range of x_3
$g_6(x_3)$	$x_3 - 120.0 \text{ m}$	Allowable value range of x_3
$g_7(x_4)$	$10^{-15} \text{ m} - x_4$	Allowable value range of x_4
$g_8(x_4)$	$x_4 - 108.0 \text{ m}$	Allowable value range of x_4
$g_9(x_5)$	$10^{-15} \text{ m} - x_5$	Allowable value range of x_5
$g_{10}(x_5)$	$x_5 - 108.0 \text{ m}$	Allowable value range of x_5
$g_{11}(x_6)$	$10^{-15} \text{ m} - x_6$	Allowable value range of x_6
$g_{12}(x_6)$	$x_6 - 108.0 \text{ m}$	Allowable value range of x_6
$g_{13}(x_7)$	$10^{-15} \text{ m} - x_7$	Allowable value range of x_7
$g_{14}(x_7)$	$x_7 - 108.0 \text{ m}$	Allowable value range of x_7
$g_{15}(\text{system}(X))$	$\max(\iota_{\text{tot}}) - 10.0^\circ$	Maximum total inclination angle
$g_{16}(\text{system}(X))$	$\max(a_{\text{hor,nacelle}}) - 1.962 \text{ m/s}^2$	Maximum horizontal nacelle acceleration
$g_{17}(\text{system}(X))$	$s_{\text{mean,transl}} - 64.0 \text{ m}$	Mean translational motion
$g_{18}(x_4, x_5, x_6)$	$3.0 \text{ m} - (x_4 + x_5 + x_6)$	Minimum draft
$g_{19}(x_4, x_5, x_6)$	$x_4 + x_5 + x_6 - 108.0 \text{ m}$	Maximum draft
$g_{20}(x_6, x_7)$	$x_7 - x_6$	Ballast filling height within BC_{low}
$g_{21}(\text{system}(X))$	$-\rho_{\text{ballast}}$	Allowable value range of ballast density
$g_{22}(\text{system}(X))$	$\rho_{\text{ballast}} - 5.0 \times 10^3 \text{ kg/m}^3$	Allowable value range of ballast density
$g_{23}(\text{system}(X))$	$0.5 \times 10^{-15} \text{ m} + t - 0.5x_1$	Wall thickness and diameter of BC_{up}
$g_{24}(\text{system}(X))$	$0.5 \times 10^{-15} \text{ m} + t - 0.5x_2$	Wall thickness and diameter of BC_{mid}
$g_{25}(\text{system}(X))$	$0.5 \times 10^{-15} \text{ m} + t - 0.5x_3$	Wall thickness and diameter of BC_{low}

5.2.3 Approach for automated design optimization of an advanced spar-type floater

The final automated design optimization of the reference advanced spar-type floating wind turbine system described in Section 5.2.1.2 consists of

1. pre-processing automated system simulations for identifying the simulation conditions to be considered within the optimization (Section 5.2.3.1), as well as
2. the actual iterative optimization approach for obtaining an optimized advanced spar-type floating platform design (Section 5.2.3.2).

Both utilize the MoWiT-Dymola[®]-Python framework for automated simulation and optimization, presented in detail in Section 4.2.

5.2.3.1 Pre-processing automated system simulations

As it is not practical - for reasons of high computational effort - to simulate for each design considered within the iterative optimization approach the full set of DLCs recommended by standards, such as IEC or DNV GL, and as not all DLCs may be relevant or design driving for the specified optimization problem, the same approach as described in Section 5.1.3.1 and applied within the global design optimization task is adopted. In this, first, a limited number of DLCs, critical for the considered FOWT system and design optimization problem, is selected. For the considered advanced spar-type floating wind turbine system, described in Section 5.2.1, and the corresponding optimization problem stated in Section 5.2.2, three DLCs according to IEC 61400-3-1 (IEC 2019*b*) - the same as considered in the global design optimization task (Section 5.1.3.1) - are selected:

- DLC 1.1 around rated wind speed (explicitly at 10.0 m/s, 11.4 m/s, and 13.0 m/s), as well as
- DLC 1.3 and
- DLC 1.6, both at 8.0 m/s, 11.4 m/s (rated wind speed), and 25.0 m/s (cut-out wind speed).

These are chosen to cover highest thrust loads and corresponding system inclination and mean translational displacement at rated wind speeds, as well as maximum dynamic responses in extreme turbulent wind conditions or at severe irregular sea states, as the maximum total inclination angle, the maximum horizontal nacelle acceleration, and the mean translational motion make up three (g_{15} , g_{16} , and g_{17}) of the optimization constraints defined in Section 5.2.2.3, which need to be checked and adhered to.

From these selected three DLCs, 54 environmental conditions are defined, which correspond to 18 different environmental settings per DLC as summarized in Table 5.7 in Section 5.1.4.1. Thus, in each DLC turbulent wind with three different mean wind speeds and corresponding longitudinal turbulence intensity are considered. Per wind speed six different

wind seed numbers are accounted to capture the randomness of turbulent wind. Three different yaw misalignment angles are used and combined with two seeds each to reduce the overall number of simulation cases. The irregular sea state, prevailing in all three DLCs, is specified through the significant wave height and peak period. Furthermore, each realization of the turbulent wind with a different wind seed uses as well a different wave seed to represent again the randomness of irregular waves. Finally, a current speed is specified for each wind speed.

These 54 system simulations are already performed in Section 5.1.4.1 with the original OC3 phase IV spar-buoy FOWT system and are here again carried out, however, now with the modified reference floating system from Section 5.2.1.2. The simulations are executed automatically, utilizing the MoWiT-Dymola[®]-Python framework for automated simulation and optimization, as specified in detail in Section 4.2.1.4.

From the total simulation time of 800 s, the last 600 s (excluding any transients at the beginning) are evaluated with respect to the system performance criteria. The results, presented in Section 5.1.4.1, show that DLC 1.6 at rated wind speed (11.4 m/s) with wind seed number 11 and yaw misalignment angle of 8° is most critical for the total inclination angle of the system and yields the second highest value (just less than 1% lower than the maximum value obtained from all DLCs) for the horizontal nacelle acceleration. The mean translational motion is in general far off the limit value and is just less than 3.5% of the overall maximum value for the above mentioned critical DLC. For the modified advanced spar-type floating system, the five highest values for the three performance parameters and corresponding DLC simulation cases, as well as the position of the above described most critical DLC for the original OC3 phase IV floating wind turbine system are presented in Table 5.19. This shows that DLC 1.6 at rated wind speed with wind seed number 11 and yaw misalignment angle of 8° (DLC16_w11_s11_y8) is still of high criticality for the modified reference advanced spar-type floating system. It scores not the highest for the performance criteria; however, the total inclination angle of the system is almost 96% of the highest value obtained in the 54 DLC simulations, the horizontal nacelle acceleration is even almost 99% of the highest value occurring, and the mean translational motion is just less than 1% lower than the maximum value obtained.

Thus, DLC16_w11_s11_y8 (DLC 1.6 at 11.4 m/s wind speed with wind seed number 11 and yaw misalignment angle of 8°) is used - as already deployed in the global design optimization application example (Section 5.1.4.1) - for defining the environmental conditions for the system simulations throughout the subsequent iterative optimization approach, which is specified in detail in Section 5.2.3.2. As, however, it is not ensured that the outcome of the DLC results comparison - based on the reference advanced spar-type floating wind turbine system - does not change for the optimized floater design, the 54 environmental conditions will be simulated subsequent to the design optimization process and the criticality of the DLCs will be assessed again, as covered in Section 5.2.4.4.

Table 5.19: The highest values for the three performance parameters and corresponding DLC simulation cases, based on the modified reference advanced spar-type floating system.

Rank	Total inclination angle		Horizontal nacelle acceleration	
	Simulation case	$\max(t_{\text{tot}})$	Simulation case	$\max(a_{\text{hor,nacelle}})$
1	DLC16_w11_s8_y-8	3.9°	DLC16_w25_s16_y0	2.339 m/s ²
2	DLC16_w11_s10_y0	3.9°	DLC16_w25_s14_y-8	2.322 m/s ²
3	DLC16_w11_s7_y-8	3.9°	DLC16_w8_s5_y8	2.313 m/s ²
4	DLC16_w11_s11_y8	3.8°	DLC16_w11_s7_y-8	2.312 m/s ²
5	DLC16_w11_s12_y8	3.6°	DLC16_w11_s11_y8	2.311 m/s ²

Rank	Mean translational motion	
	Simulation case	$s_{\text{mean,transl}}$
1	DLC16_w11_s9_y0	19.5 m
2	DLC11_w11_s9_y0	19.5 m
3	DLC13_w11_s9_y0	19.5 m
4	DLC16_w11_s12_y8	19.4 m
5	DLC16_w11_s8_y-8	19.4 m
6	DLC16_w11_s11_y8	19.3 m

5.2.3.2 Specification and execution of the iterative optimization approach

The pre-processing DLC simulations mentioned in Section 5.2.3.1, as well as the actual iterative optimization approach, are executed in an automated manner by means of the MoWiT-Dymola[®]-Python framework for automated simulation and optimization, which is described in Section 4.2.1.4. As displayed in Figure 4.24 in Section 4.2.3, the iterative optimization algorithm coupled to the programming framework requires in addition to the model and simulation information also the definition of the optimization problem and specification of the optimizer.

Optimization problem The optimization problem comprises the specification of design variables, objective functions, as well as constraints. This is defined and described in detail in Section 5.2.2 and, hence, consists of seven design variables (diameters and heights of each of the three BC parts, as well as height of the ballast), one objective function for the structure material volume of the advanced spar-type floater, and 25 inequality constraints (14 for the allowable value ranges of the design variables, three for the floating system performance, two for the draft requirements, and six for compliance checks regarding the filling capacity and actual ballast height, feasible ballast densities, as well as the cylinder diameters and wall thicknesses). These

are directly implemented in the MoWiT-Dymola[®]-Python framework, based on the definitions given in Section 5.2.2.

Optimizer From the broad range of available algorithms and methods presented in Table 4.9, only gradient-free optimization algorithms can be chosen for the application to complex fully-coupled wind energy systems modeled by means of MoWiT, as already indicated in Sections 4.2.3.2 and 4.2.4.1. From the implemented and tested MO optimizers NSGAI, NSGAIII, and SPEA2 - all from Platypus - NSGAI is found to be the most suitable optimizer for the MO optimization problem in the global design optimization task on a common floating offshore spar-buoy wind turbine system (Section 5.1.3.2). Two further optimization algorithms ALPSO and COBYLA, which are both single-objective optimizers from OpenMDAO, are deployed in other application examples on wind turbine systems, as presented in Sections 4.2.4.1 and 4.2.4.2. Due to the fact that the optimization problem considered in this application for designing an advanced spar-type floater holds only one objective function, as defined in Section 5.2.2.2, a single-objective optimizer could be adopted. However, as the parallelization of the system simulations within the iterative optimization algorithm is not viable due to the consecutive approach adopted by these optimizers, and due to the fact that a huge number of iterations is demanded for such a complex system with such a sophisticated and heavily constrained optimization problem, the single-objective optimizers are discarded due to reasons of inefficiency with respect to the required computational time. Thus, in this application it is stuck to the well-performing - both with respect to the convergence speed and the compliance rate concerning the constraints - MO optimizer NSGAI.

For the genetic algorithm NSGAI, which follows the principle of Darwin's theory of evolution - meaning having individuals which develop further and further each generation towards performing better with respect to the fitness (objective) function -, the number of individuals in each generation (the population size) and the stop criterion for terminating the iterative optimization algorithm have to be defined, as already stated in Section 4.2.3.2.

- Due to the complex optimization problem with seven design variables and 25 constraints, the population size is set equal to the maximum possible number of processors, on which simulations can be run simultaneously. On an AMD Ryzen Threadripper 2990WX 32-Core Processor with 64-bit system and 64 virtual processors 60 processors could be used for parallel simulations. Hence, 60 individuals are considered in each generation.
- The stop criterion for terminating the iterative optimization algorithm is defined through the total number of simulations to be performed, while the convergence is checked separately when post-processing the simulation results. As the convergence speed is not known ahead of the execution of the specific optimization problem, the experience from the global design optimization application example, presented in Section 5.1, is used and the total number of simulations is increased to account for the much more complex optimization problem considered in this application example. Hence, the resulting number of generations being simulated is roughly tripled, so that a total number of simulations

of 10,000 is chosen, corresponding to more than 166 full generations with 60 individuals each.

Optimization algorithm Now, having defined and modeled the FOWT system as described in Section 5.2.1.2, stating the simulation settings as given in Table 5.20, having specified the optimization problem (Section 5.2.2), and having selected the optimizer and corresponding parameter values as outlined beforehand, the iterative optimization algorithm can be executed by means of the MoWiT-Dymola[®]-Python framework for automated simulation and optimization.

Table 5.20: Simulation settings of the optimization algorithm for designing an advanced spar-type floater.

Simulation variable	Value	Note
Simulation interval	from 0 s to 800 s	The first 200 s are accounted for as pre-simulation time to exclude any transients.
Output interval length	0.05 s	
Solver	Rkfix4	
Fixed integrator step-size	0.01 s	

Within the iterative optimization algorithm, the values of the design variables for the 60 individuals of the first generation ($G = 0$) are selected by the optimizer based on the specified allowable value ranges. All individuals are simulated in parallel on the available 60 processors and analyzed afterwards by the optimizer with respect to their fitness - meaning the objective function - and their compliance with the constraints based on the resulting time series, evaluated between 200 s and 800 s. As also simulations may have failed (due to too bad performance or instability of the considered floating wind turbine system), the simulated time is checked against the specified simulation stop time (800 s according to Table 5.20). In case of an unsuccessful simulation and hence incomplete time series, the parameters of interest addressed in the constraints g_{15} to g_{17} for the system performance are not taken by evaluating the time series but are set equal to twice the maximum allowable value, meaning

- $\max(t_{\text{tot}})|_{\text{failing system}} = 2 \cdot 10.0^\circ = 20.0^\circ$
 $\Rightarrow g_{15}(\text{system}(X)|_{\text{failed}}) = 20.0^\circ - 10.0^\circ = 10.0^\circ \not\leq 0$
- $\max(a_{\text{hor,nacelle}})|_{\text{failing system}} = 2 \cdot 1.962 \text{ m/s}^2 = 3.924 \text{ m/s}^2$
 $\Rightarrow g_{16}(\text{system}(X)|_{\text{failed}}) = 3.924 \text{ m/s}^2 - 1.962 \text{ m/s}^2 = 1.962 \text{ m/s}^2 \not\leq 0$
- $s_{\text{mean,transl}}|_{\text{failing system}} = 2 \cdot 64.0 \text{ m} = 128 \text{ m}$
 $\Rightarrow g_{17}(\text{system}(X)|_{\text{failed}}) = 128 \text{ m} - 64.0 \text{ m} = 64.0 \text{ m} \not\leq 0$

This way, it can be ensured that unsuccessful simulations do not comply with all constraints and, hence, are undesirable design solutions, which the optimizer then discards from further selection of well-performing individuals.

Having evaluated the simulated individuals of generation 0, the optimizer selects the design variables for the individuals of the next generation ($G = 1$), again in accordance with the specified allowable value ranges, but also based on the fitness and constraints compliance rate of each of the previous individuals. Then, the loop of simulating the individuals, evaluating each system with respect to the objective function and constraints, and re-selecting values (from the allowable value ranges) for the design variables of the individuals of the next generation based on the performance of the individuals in the previous generation is repeated as long as the number of executed simulations is still below the specified total number of simulations of 10,000. This iterative optimization algorithm ends when the stop criterion is reached - the final results are now available.

5.2.4 Results of the automated design optimization of an advanced spar-type floater

The optimization algorithm with the specified optimization settings is executed; however, the simulation run has to be interrupted due to a required system restart. At that time already 8,133 individuals have been simulated. To complete the specified 10,000 simulations without having any disruptive effects on the final results, the optimization is continued by providing the individuals of the last wholly simulated generation 133 as start population of the subsequent optimization execution, utilizing the operator `InjectedPopulation` available in Platypus. Thus, the optimization run takes effectively about 744 hours and comprises 10,011 individuals simulated in total, ranging from generation 0 up to generation 166, with full populations up to and including generation 165.

5.2.4.1 Developments throughout the iterative optimization process

Figure 5.8 shows in light blue for all simulated individuals of the optimization run the values for the design variables x_1 to x_7 , as defined in Section 5.2.2.1. The values of the design variables of the reference advanced spar-type floating wind turbine system, covered in Section 5.2.1.2, are plotted additionally as red lines for comparative purposes. Post-processing of the simulation results and checking the constraints yield the dark blue recolored individuals which comply with all specified constraints. The finally selected optimum, which is presented in Section 5.2.4.3, is marked with a yellow filled circle framed in orange.

The developments of the design variables throughout the iterative optimization process show that in the first generations, the optimizer selects individuals covering the entire design space; however, none of the first is meeting all requirements. With more generations, the compliance rate is significantly increased, while it slightly decreases again when the focus of minimizing the objective function is coming more to the fore again. Overall, the spread in the design variables is decreased for more generations being simulated and for some design variables the change in their values is even very limited for the individuals which comply with all constraints. This indicates that the optimization algorithm is converging, though it has not

yet fully converged, which is underlined by the fact that the optimum originates from the last generation.

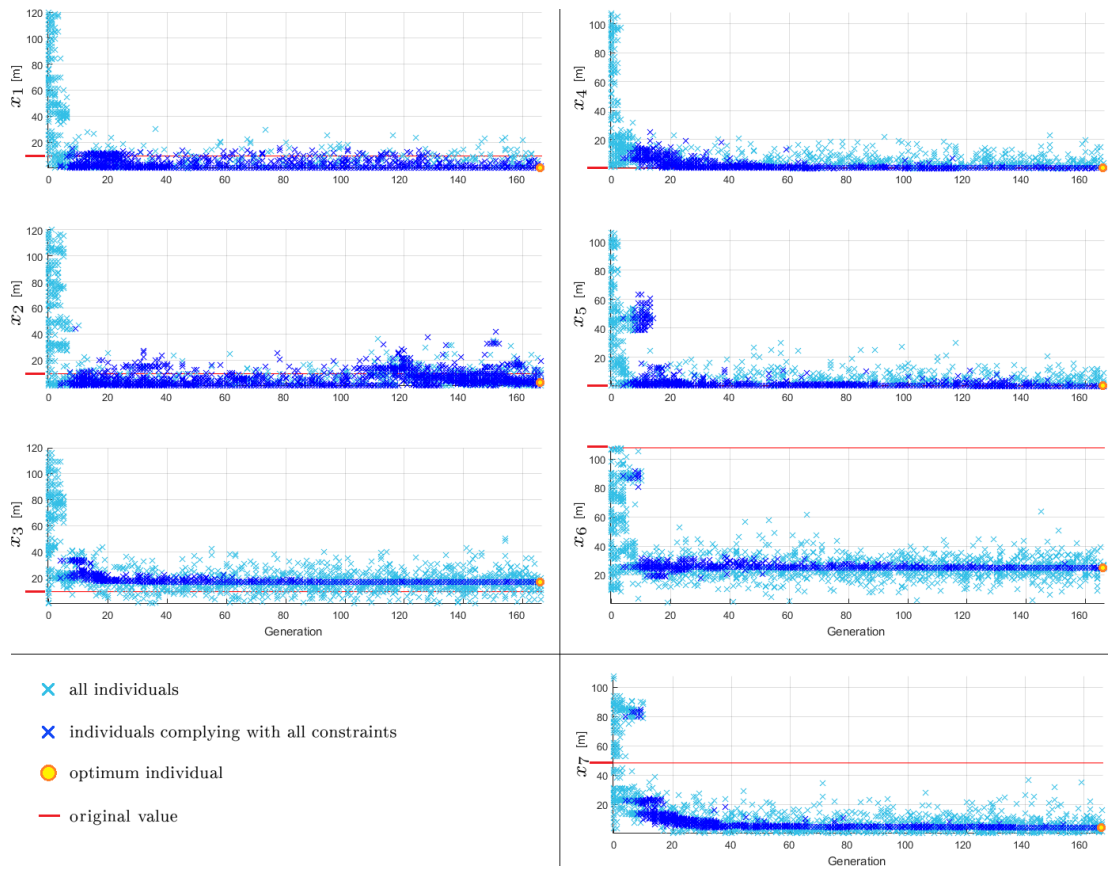


Figure 5.8: Development of the design variables throughout the iterative optimization process for designing an advanced spar-type floater.

Similarly, the developments of the constraints g_{15} to g_{25} throughout the iterative optimization process are analyzed and presented in Figure 5.9. The first 14 constraints for the allowable value ranges of the design variables are excluded, as they are not constraints that are evaluated after the simulation, but are taken into account ahead of the simulations when the optimizer selects the design variables for the new individuals and, hence, are never violated. This can clearly be seen in Figure 5.8, where all individuals lie within the allowable value ranges of the design variables. In Figure 5.9, the light cyan crosses indicate the results for all simulated individuals, while the individuals which simultaneously comply with all constraints are recolored in dark bluish green. The limits of the inequality constraints, which should all be less or equal to zero, are indicated in red and the finally selected optimum is marked again with a yellow filled circle framed in orange. For g_{21} and g_{22} it has to be noted that the ordinate is limited to $[-1 \times 10^4, 1 \times 10^4]$ for reasons of clarity, as a few more individuals yield values in the order of magnitude of six.

For g_{18} to g_{20} and g_{23} to g_{25} , which are directly related to and dependent on the design variables, the developments of the constraints show a similar behavior as the developments of the corresponding design variables throughout the iterative optimization process. For the other

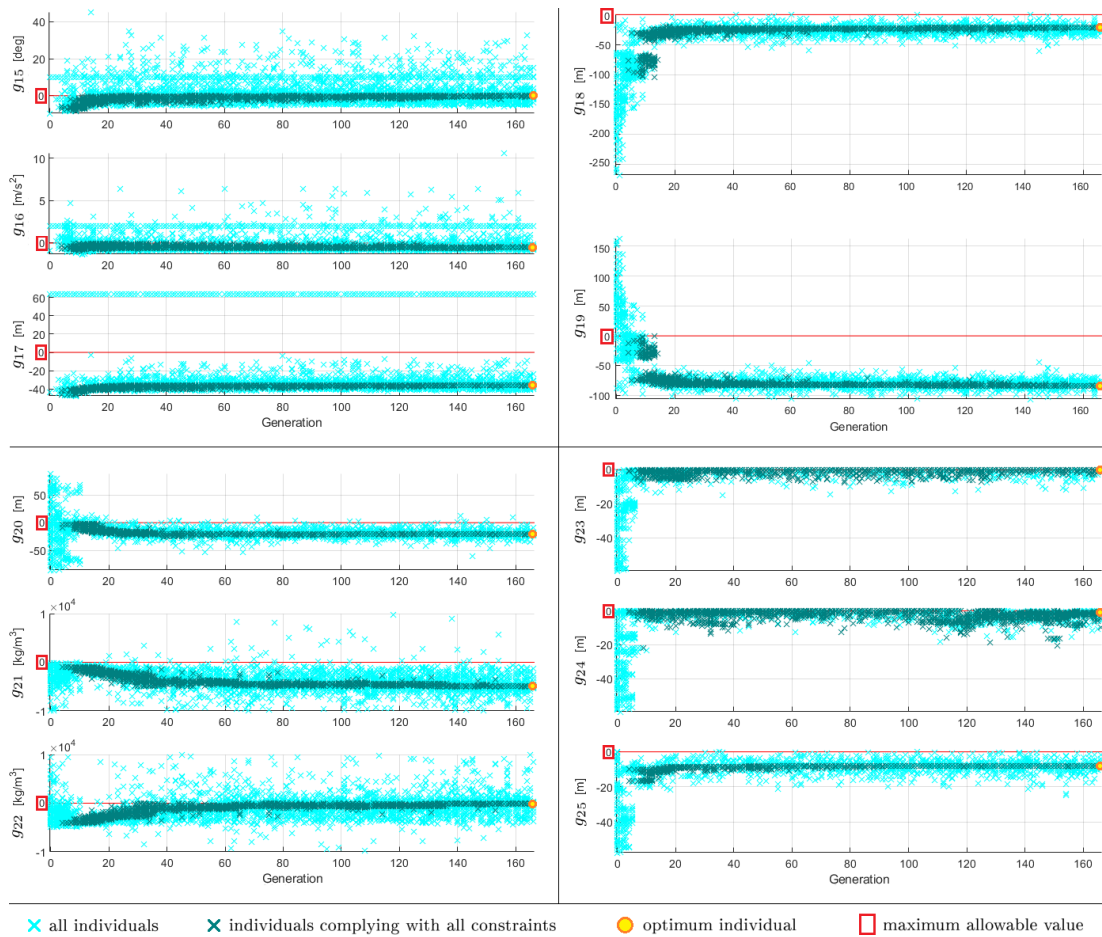


Figure 5.9: Development of the constraints throughout the iterative optimization process for designing an advanced spar-type floater.

constraints, the trend is rather different, having a large spread in the results throughout the simulated generations. The fact that for g_{15} to g_{17} only a few distinguishable individuals are plotted in the first generations is caused by the large number of unsuccessful simulations in the first trials of the optimizer, for which reason the performance variables are set to the undesired values, as explained in Section 5.2.3.2, and, hence, are all the same for all failing systems. This is as well visible throughout the generations, as there is a line at the specified undesired value formed by the individuals that do not complete the simulations successfully.

5.2.4.2 Advanced spar-type floater geometries in the design space

As presented and mentioned in Section 5.2.4.1, the individuals of the first generations cover the entire design space, specified through the allowable value ranges prescribed by means of the constraints g_1 to g_{14} . The individuals that comply with all constraints, however, are in a much more narrow area of the design space. In Figure 5.10, the geometric design variables x_1 to x_6 of these individuals, setting height and diameter of each BC part in correlation, are plotted in light blue unfilled circles. The original and optimum designs are highlighted by red and orange-framed yellow filled circles, respectively. From these individuals, which comply with

all constraints, seven examples are selected to demonstrate the diversity of potential (meaning successful but maybe not yet optimum) advanced spar-type floater geometries. These examples are schematically drawn with green lines in Figure 5.10 together with the original shape in black and having represented the ballast heights in dashed lines. The corresponding figures for design variables, performance parameters, objective function, and further resulting geometrical and structural parameters of the presented examples are outlined in Table 5.21. These numbers also underline that - when evaluating g_1 to g_{25} - none of the inequality constraints is violated.

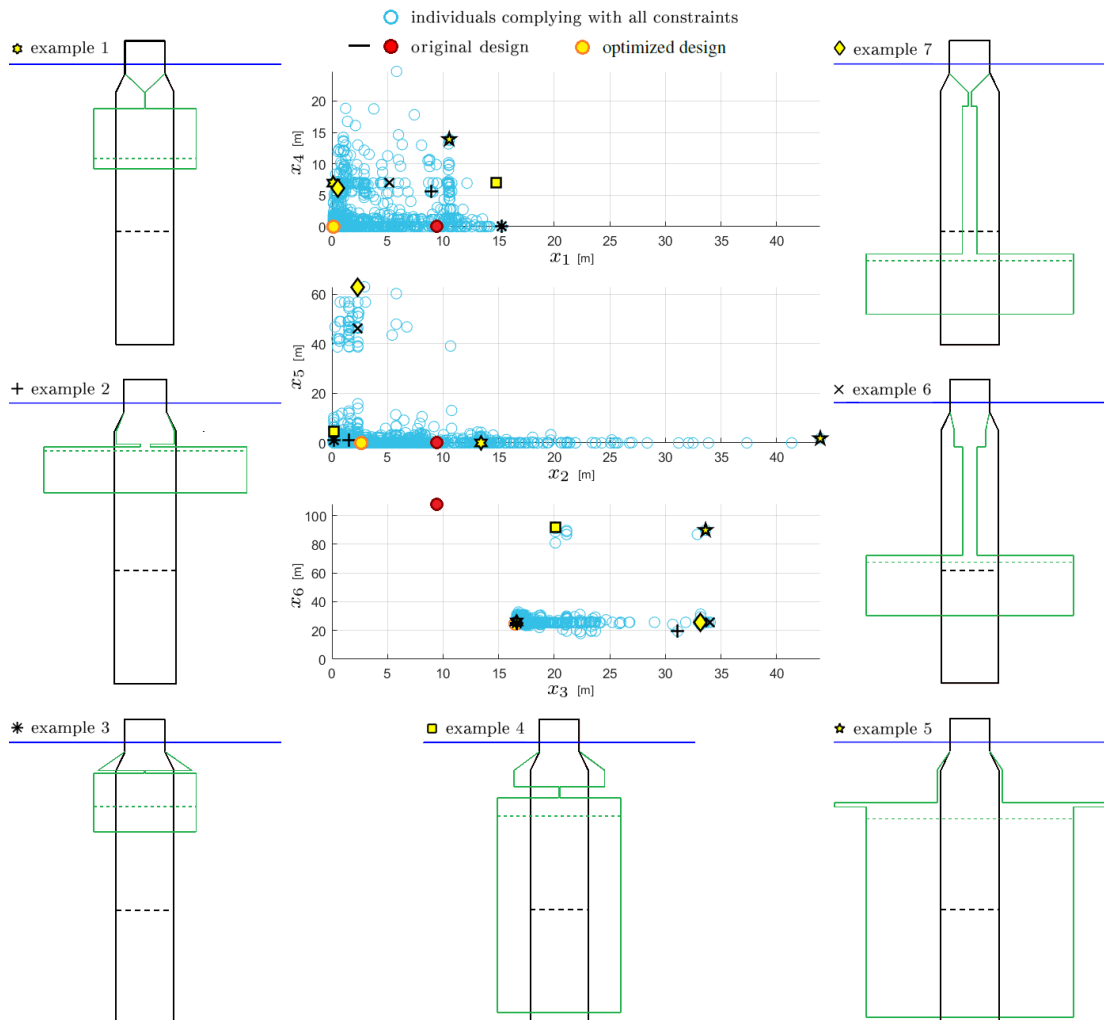


Figure 5.10: Exemplary potential advanced spar-type floater geometries selected from the individuals complying with all constraints.

Looking at the floater geometries presented in Figure 5.10, it becomes clear that not all of these shapes can be realized with conventional structural solutions, where cylindrical sections are welded together. It has to be emphasized that these results are solely based on the hydrodynamic and system-level analyses, as specified within the optimization problem. Other additional types of analyses - addressing structural integrity, manufacturability, and localized design - can, hence, deem some of the presented potential design solutions unfeasible, which is discussed in some more detail in Section 5.2.5.3. However, the advantage of this methodology

Table 5.21: Key figures of the exemplary potential advanced spar-type floater geometries.

Ex.	Gen.	Ind.	x_1 [m]	x_2 [m]	x_3 [m]	x_4 [m]	x_5 [m]	x_6 [m]	x_7 [m]
1	115	45	0.1	13.4	16.6	6.9	2×10^{-3}	25.9	4.6
2	14	15	8.9	1.5	31.1	5.6	1.2	19.5	17.8
3	78	32	15.3	0.2	16.6	2×10^{-2}	1.1	25.0	10.7
4	8	6	14.8	0.2	20.1	7.0	4.7	92.0	84.0
5	9	45	10.6	43.9	33.6	13.9	1.8	89.8	84.7
6	10	8	5.2	2.3	34.0	7.0	46.3	25.7	22.7
7	9	57	0.5	2.3	33.2	6.2	62.9	25.7	22.7

Ex.	$\max(t_{\text{tot}})$ [°]	$\max(a_{\text{hor,nacelle}})$ [m/s ²]	$s_{\text{mean,transl}}$ [m]
1	9.9	1.337	28.2
2	5.0	1.231	22.2
3	9.3	1.724	27.3
4	2.6	1.955	17.5
5	1.6	1.664	21.1
6	3.9	1.447	21.1
7	4.6	1.159	22.1

Ex.	Draft [m]	ρ_{ballast} [kg/m ³]	t [m]	f_1 [m ³]	m_{platform} [kg]	Ballast mass [kg]
1	44.8	4,585	0.0578	99.1	77.78×10^4	45.44×10^5
2	38.3	1,003	0.1052	266.2	20.90×10^5	13.55×10^6
3	38.2	2,156	0.0580	107.7	84.55×10^4	50.04×10^5
4	115.6	1,037	0.0797	530.1	41.62×10^5	27.61×10^6
5	117.5	1,008	0.1344	1428.6	11.21×10^6	75.70×10^6
6	91.0	1,022	0.1135	407.9	32.02×10^5	21.11×10^6
7	106.8	1,013	0.1106	384.8	30.21×10^5	19.87×10^6

- by focusing only on the hydrodynamics - is that a new range of potential floater designs is opened up and shapes like these presented in Figure 5.10 can still be considered as feasible

solutions when different structural realization approaches are applied. These approaches can range from truss structures to tendons to realize large diameter changes, as well as very thin elements, without utilizing tapered sections or having issues with the structural integrity. Idea and impulse provider for such different structural realization approaches can, for example, be the oil and gas industry (Chen et al. 2017, Perry et al. 2007, Bangs et al. 2002) or innovative floating platform concepts, such as the TetraSpar by Stiesdal A/S (Stiesdal 2019) or the pendulum-stabilized Hexafloat floater by Saipem, realized in the AFLOWT project (Richard 2019).

5.2.4.3 The optimized advanced spar-type floater

Due to the single-objective nature of the optimization problem, the selection of the optimum solution happens directly through evaluating the one and only objective function. This means that from all individuals that comply with all constraints, this is chosen as optimum which exhibits the lowest value for the structure material volume of its advanced spar-type floating platform design.

First, looking at the development of the objective function f_1 throughout the iterative optimization process, as presented in Figure 5.11, the trend of all simulated individuals (plotted in light green) shows a significant minimization of the objective function - clearly below the original value of 136.3 m^3 , indicated in Figure 5.11 by a red line - after a large spread in the first generations.

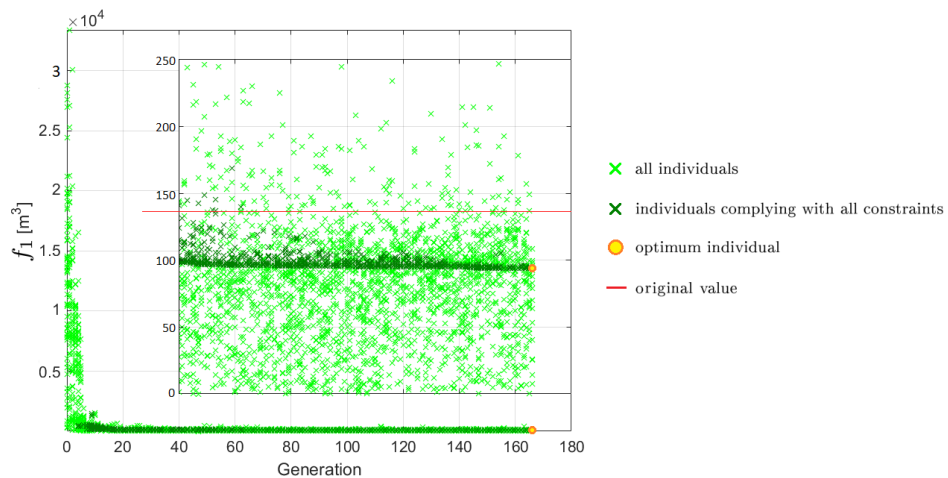


Figure 5.11: Development of the objective function throughout the iterative optimization process for designing an advanced spar-type floater.

Zooming into the objective function results from generation 40 on, as included in Figure 5.11, provides a much clearer indication of the development of the minimum structure material volume for the individuals which comply with all constraints (recolored in dark green): they aggregate to an asymptote. This is already visible in early generations; however, the spread in the objective function results of the individuals complying with all constraints is decreasing with more generations being simulated. This asymptotic clustering of the individuals which

comply with all constraints to a minimum objective function value on the one hand states the convergence of the iterative optimization process and on the other hand portends that there will be several - more or less similar (elaborated in the following) - design solutions, which yield comparable low structure material volumes that are all very close to the minimum value observed.

The individual with the minimum structure material volume is pointed out in Figure 5.11 by means of a yellow filled circle framed in orange. This design solution yields a reduction of the structure material volume of more than 31% compared to the original (modified) advanced spar-type floating platform. The fact that this optimum solution is just found in the last simulated generation states that full convergence is not yet reached, despite the converging trend in most of the design variables and constraints, as well as in the objective function. Nevertheless, due to the asymptotic aggregation of the individuals mentioned above, the first ten minimum objective function results from the individuals which comply with all constraints are evaluated. This results - as some individuals yield the same objective function value - into 16 individuals with a just by $2.8 \times 10^{-4}\%$ increased structure material volume, comparing the tenth lowest with the minimum value, and shapes that are difficult to distinguish from each other. This proves the above mentioned anticipation that - due to the convergence of the iterative optimization process and the aggregation of the individuals' objective function results to an asymptote - several very similar advanced spar-type floater design solutions of comparable low structure material volumes are found.

The geometry of the optimized advanced spar-type floater shape (red line) is shown schematically in Figure 5.12 in comparison to the original floating platform drawn in black. The key figures of the optimized advanced spar-type floater geometry are presented in Table 5.22. The found design solution is - as already mentioned - out of the last generation, indicating that the optimizer is still searching for individuals with lower structure material volume; however, the improvement within the last simulated generations is negligible as outlined above. Both Figure 5.12 and Table 5.22 indicate the following design development trend within the iterative optimization process: to reduce the structure material volume

- the overall length of the floating platform is significantly decreased compared to the original geometry - the draft of the advanced spar-type floater is, however, still significantly away from the minimum allowable draft of 15 m;
- the width of the bottom part of the support structure is enlarged, while
- the upper and middle parts are almost left out, leading to this significant constriction in the tapered part; and
- a very low ballast volume is obtained through a significantly increased ballast density, utilizing MagnaDense or high density concrete as ballast material.

The system performance - maximum total inclination angle, maximum horizontal nacelle acceleration, and mean translational motion - points out that the maximum total inclination

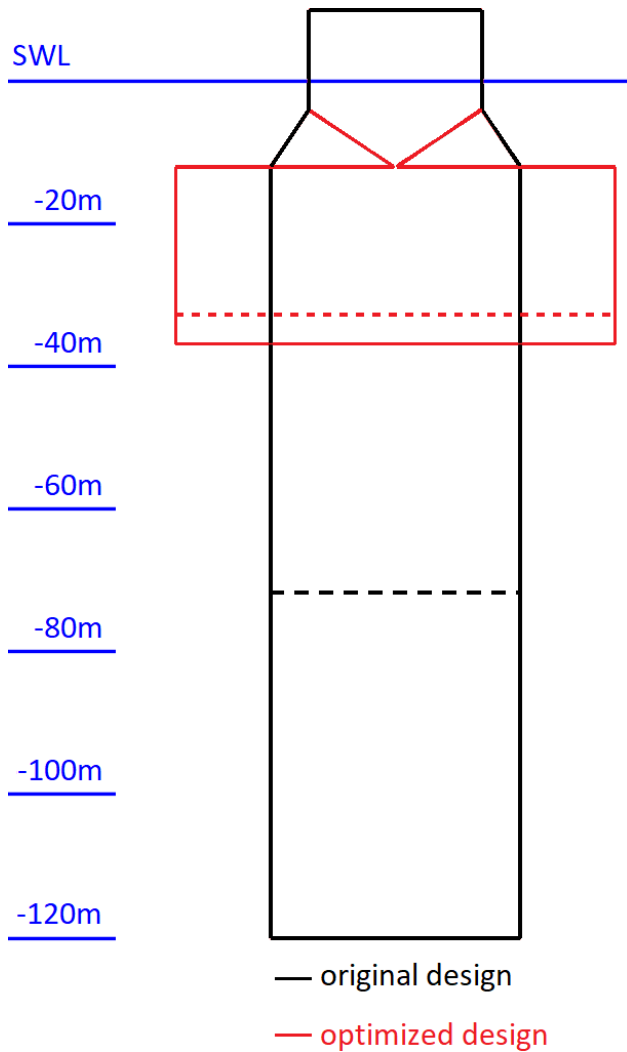


Figure 5.12: The optimized advanced spar-type floater geometry in comparison with the original shape.

Table 5.22: Key figures of the optimized advanced spar-type floater.

Key figure	Value
Generation	166
Individual	51
x_1	0.1 m
x_2	2.7 m
x_3	16.5 m
x_4	1×10^{-3} m
x_5	3×10^{-8} m
x_6	24.8 m
x_7	4.1 m
$\max(I_{\text{tot}})$	10.0°
$\max(a_{\text{hor,nacelle}})$	1.426 m/s^2
$s_{\text{mean,transl}}$	28.4 m
Draft	36.8 m
ρ_{ballast}	$4,855 \text{ kg/m}^3$
t	0.0571 m
f_1	93.9 m^3
m_{platform}	$73.73 \times 10^4 \text{ kg}$
Ballast mass	$42.67 \times 10^5 \text{ kg}$

angle is the most critical performance criterion, as the obtained value from the optimized design is equal to the specified upper limit of 10° .

Overall, the shape of the optimized advanced spar-type floater design resembles rather a submerged thick barge-type floater, hanging below the upper column element. This constriction in the tapered part is significant and would not directly be technically feasible, both from a manufacturing point of view and with respect to structural integrity. The reason for the current shape obtained is the connection of the upper column to the upper BC part, which, however, is, as well as the middle BC part, negligible. Thus, the tapered part could directly connect the end of the upper column with the top of the lower BC part, which is mainly purely the base column of the advanced spar-type floater. The change in required structure material would be not that significant; however, the related change in the displaced water volume has to be taken into account by adjusting the structure mass and by carefully evaluating the system performance due to the shifted center of buoyancy. This realization by means of a tapered section, however, comes with a large diameter change and corresponding large taper angle, which may

be critical for both hydrodynamic load calculations and manufacturing, as discussed in more detail in Sections 5.2.5.2 and 5.2.5.3. However, the structural issues due to the geometrical configuration of the optimized floater as presented in Figure 5.12, or as well as due to the large diameter change when utilizing a tapered section, become void when eliminating the negligible upper and middle BC parts and connecting the upper column and lower BC part by means of a number of rigid slender braces or some tendons instead of using a tapered segment. These manufacturing solutions go beyond the conventional structural realization approach of welding cylindrical sections together, but they make the found optimized floater design solution feasible and are expected to represent similar system performance. The fitness of the floater solution proposed by the optimizer is underlined due to its similarity to the most novel and alternative solutions suggested by the research community, such as the Stiesdal's TetraSpar (Stiesdal 2019) or the Hexafloat by Saipem (Richard 2019).

5.2.4.4 Performance of the optimized advanced spar-type floating system in different environmental conditions

With the design solution for the advanced spar-type FOWT platform obtained from the optimization run, finally, the DLCs that are selected for the pre-processing automated system simulations for choosing the most critical DLC (as presented in Section 5.2.3.1) are rerun to check whether a shift in the most critical DLC happens. The criticality is again assessed by evaluating the fully-coupled system performance criteria (maximum total inclination angle, maximum horizontal nacelle acceleration, and mean translational motion) and analyzing the corresponding constraints g_{15} to g_{17} . The highest values and corresponding DLC simulation cases, as well as the values obtained with the selected DLC 1.6 at rated wind speed with wind seed number 11 and yaw misalignment angle of 8° , are presented in Table 5.23.

For the design solution from the optimization run, there is a shift in the criticality of the DLCs observed. The smallest change in the order of criticality of the 54 environmental conditions happens in the horizontal nacelle acceleration. Still the cases from DLC 1.6 at cut-out wind speed, as well as around rated wind speed, are most critical, but the DLC used within the iterative optimization algorithm is still among the first ten with an acceleration value that is almost 12% lower compared to the maximum obtained from all simulated DLCs. This, however, is itself still more than 17% below the maximum allowable horizontal nacelle acceleration and, hence, uncritical, which - on a side note - is not the case for the original floating spar-buoy wind turbine system. A significant increase in the resulting performance values and considerable change in the order of criticality of the environmental conditions is obtained for the mean translational motion. Here, the selected DLC for the optimization process drops down from the originally sixth position to the 22nd, while it is just 10% below the highest value achieved, which is still less than half of the maximum allowable value and, hence, again uncritical. However, the most severe shift in the criticality of the DLCs happens for the total inclination angle of the system. As indicated in Section 5.2.4.3, the maximum allowable value is already reached in the environmental condition considered for the optimization approach. This DLC, however,

Table 5.23: The highest values for the three performance parameters and corresponding DLC simulation cases, based on the optimized advanced spar-type floating system.

Rank	Total inclination angle		Horizontal nacelle acceleration	
	Simulation case	$\max(t_{\text{tot}})$	Simulation case	$\max(a_{\text{hor,nacelle}})$
1	DLC11_w13_s18_y8	12.1°	DLC16_w25_s17_y8	1.620 m/s ²
2	DLC11_w11_s10_y0	12.0°	DLC16_w25_s18_y8	1.618 m/s ²
3	DLC13_w11_s10_y0	12.0°	DLC16_w25_s13_y-8	1.550 m/s ²
4	DLC11_w11_s7_y-8	11.9°	DLC16_w25_s16_y0	1.521 m/s ²
5	DLC13_w11_s7_y-8	11.9°	DLC16_w25_s15_y0	1.480 m/s ²
10			DLC16_w11_s11_y8	1.426 m/s ²
30	DLC16_w11_s11_y8	10.0°		

Rank	Mean translational motion	
	Simulation case	$s_{\text{mean,transl}}$
1	DLC11_w13_s15_y0	31.6 m
2	DLC11_w11_s9_y0	31.4 m
3	DLC13_w11_s9_y0	31.4 m
4	DLC11_w13_s17_y8	30.6 m
5	DLC11_w11_s12_y8	30.3 m
22	DLC16_w11_s11_y8	28.4 m

is for the obtained optimized design solution no longer prevailing but just on the 30th position, meaning that 29 other environmental conditions (mostly from DLC 1.1 and DLC 1.3, as well as some others from DLC 1.6) exceed the specified upper limit by up to more than 20%. In these environmental conditions, the floater designs obtained from the optimization run would have to stop operation, while the overall system stability is not expected to be critical, as commonly much higher values for a parked floating wind turbine system in extreme environmental conditions are acceptable, such as 15° considered by Hegseth et al. (2020). However, to avoid reduced system availability, the occurring changed criticality of the DLCs has to be addressed already during the optimization - by for example considering safety factors for such critical and design-driving performance criteria - and the performance in all environmental conditions can be further improved by subsequent optimization of the currently unaltered mooring system. These options are discussed in more detail in Section 5.2.5.1.

5.2.5 Discussion of the results of the automated design optimization of an advanced spar-type floater

In addition to the presented, analyzed, and discussed results in Section 5.2.4, these are addressed in more detail and further aspects are discussed in the following.

5.2.5.1 Desirable performance of the optimized advanced spar-type FOWT system in different environmental conditions

Based on the results and findings from the DLC simulations with the optimized advanced spar-type floating wind turbine system design, it is recommended to take some safety factors for the maximum allowable performance values into account. If the horizontal nacelle acceleration would have been exceeded in some of the 54 environmental conditions, it would not have been that critical, as a maximum allowable value of up to 0.3 times the gravitational acceleration constant - and not only 0.2 times as applied - is often accepted, as already mentioned in Section 5.2.1.3. The specific maximum allowable values for an operating FOWT system have to be provided by the turbine manufacturer or operator. Thus, maybe a higher inclination angle is still acceptable; however, if 10° are really the uppermost tolerated angle, a value of 8° or maximum 9° shall be used for the optimization constraint.

A reduced maximum allowable total inclination angle can as well afterwards be applied in the post-processing of the results and this way an in all 54 environmental conditions well-performing floater design can be obtained, with the downside that a larger structure material volume is required and that this design does not represent an optimized solution.

A profitable option, hence, is to adjust the - currently excluded and unchanged - mooring system properties and layout design. By modifying these in a subsequent optimization task, the optimized floater design can be retained and at the same time the performance of the FOWT system in all considered environmental conditions improved - in this case especially the system inclination.

Apart from the considered 54 environmental conditions, however, the optimized FOWT system design has to prove to withstand any potential environmental and operational condition during its design life. Thus, for a subsequent more realistic analysis, the entire set of DLCs recommended by standards,

- considering more realistic environmental conditions by accounting for various natural periods per considered sea state,
- capturing the low frequency dynamics of the floating wind turbine system through utilization of longer simulation times, and
- including also load cases with occurrence of a fault - such as grid loss - or with other transient loads - due to, for example, gusts - which might cause high accelerations and extreme loads,

has to be considered - at least in the pre-selection and final reassessment of the selected critical load case.

5.2.5.2 Enhanced hydrodynamic calculations for advanced spar-type floater geometries

Considering the wide design space - especially the broad allowable value ranges for the structural diameters - and the extreme environmental conditions, included in the DLC simulations, some refinements in the model with respect to the hydrodynamic calculations are suggested.

- For an accurate representation of the hydrodynamic loads on the floating structure, the hydrodynamic coefficients have to be recalculated for each specific diameter. While the horizontal added mass coefficient, as well as the total inertia force, are already determined in dependency of the actual structural diameter and wave number, as the MacCamy-Fuchs approach is applied for each column element separately, the horizontal drag coefficient is currently not altered from the original value of 0.6. This is a valid assumption for large diameters already at low flow velocities; however, for small diameter structures, which can occur within the optimization algorithm, an around twice as large horizontal drag coefficient might be applicable (Clauss et al. 1992). In the vertical (heave) direction, both added mass and drag coefficients are currently unchanged, while a vertical Froude-Krylov excitation force is considered, accounting for the difference between UC diameter and the diameter at the floater base. Especially for geometries with large diameter changes, as well as with large diameters, which can be regarded as heave plates, the hydrodynamic coefficients will differ from the original values for a continuous cylinder as the OC3 phase IV spar-buoy. Furthermore, the vertical Froude-Krylov excitation force would have to be adjusted to the specific geometry, when the lower BC part is connected by means of trusses or tendons to the upper column, to account for the differences between each upper and lower surfaces. This both - changes in the hydrodynamic coefficients in heave direction and adjusted vertical Froude-Krylov excitation force - will mainly affect the heave motion of the floating system, as well as the roll and pitch motions in some respect. With the geometry obtained from the optimization, however, it is expected to experience less strong system responses if the hydrodynamic coefficients are adjusted accordingly - which would benefit for example the system inclination - while the system responses will increase slightly if the vertical Froude-Krylov excitation force is determined accurately for the considered geometry.
- For more extreme environmental conditions with extreme waves and similar structures as obtained with the optimization run, which tend to have a large diameter directly at or close to the top of the BC, the event that the upper surface of such a large diameter cylinder becomes dry (which is not the case with the obtained advanced spar-type geometry) has to be accounted for when calculating the added mass and damping coefficients in order to not overestimate the heave and pitch added mass and, thus, to not underestimate the horizontal nacelle acceleration in case of more energetic sea states. Furthermore, having a horizontal surface close to the water surface - in the presented settings with a minimum distance of 12 m - could be as well critical structurally or maybe due to the impossibility of common service vessels to approach the wind turbine. However, it has to be noted that it is aimed to establish a floating platform optimized with respect to the

hydrodynamics. This, then, needs to be compromised imposing other prevailing constraints, such as structural limits - as discussed in Section 5.2.5.3 in more detail again - or accessibility, for which for example walk-to-work solutions with a gangway can be exploited.

- The applied MacCamy-Fuchs approach is in principle just valid for cylinders with vertical walls and not for cylinders with abrupt changes of diameters, leading to conical sections or even large horizontal surfaces anywhere along the column (the latter one, however, is considered again by means of the vertical Froude-Krylov excitation force, as discussed previously). If the MacCamy-Fuchs approach is applied to conical structures, the wave load from especially waves with low periods will be underestimated. This could be in the order of magnitude of up to 8% or 14% for a cone angle of around 6.7° or 12.2° , respectively, and could affect wave periods of 3 s to 6 s or 3.5 s to 7 s, according to investigations on a tapered bottom-fixed offshore wind turbine support structure (Leimeister, Spill, Dose, Foglia, Siegl, Karch, Heins, Schümann, Dührkop & Hartmann 2019). Thus, this potential underestimation of the hydrodynamic loading is mostly relevant for the environmental conditions of DLC 1.1, as well as for the below and at rated wind speed cases of DLC 1.3. For the design solution proposed in Section 5.2.4.3, in which the bottom end of the upper column is directly connected with the large diameter lower BC part, the taper angle would amount to 32° . Any hydrodynamic calculations based on the MacCamy-Fuchs approach would no longer be meaningful if the design solution is realized by means of a solid tapered part. Thus, the alternative suggestion of having instead a number of rigid slender braces would be favored. In order to ensure valid computation of the hydrodynamics already within the optimization approach, another constraint on the maximum taper angle shall be added, as implemented with a limit of 10° by Hegseth et al. (2020). This aspect is, however, less critical when allowing for different structural solutions, where trusses or tendons prevent any utilization of strongly tapered sections.

5.2.5.3 Structural realization of advanced spar-type floater geometries

As addressed and discussed in Sections 5.2.4.2 and 5.2.4.3, the geometrical configuration of the potential and optimized advanced spar-type floaters as presented in Figures 5.10 and 5.12 may not be technically feasible from a structural integrity and manufacturability point of view, adopting the standard manufacturing solutions. For obtaining a high detail structural design, further localized analyses and assessments regarding the manufacturability have to be performed subsequently. However, structural integrity checks for buckling or stress concentration and for accounting for a realistic and adjustable base and lid thickness, which is currently just set to a fixed marginal value, can as well directly be integrated in the definition of the optimization problem.

Nonetheless, based on the assumptions and focus of this application example, which is on hydrodynamic and system-level analyses, a significantly improved and more cost-efficient floater can be achieved. This is as well feasible when considering different structural realization

approaches, such as braces and truss structures or tendons, as already used in the oil and gas industry (Chen et al. 2017, Perry et al. 2007, Bangs et al. 2002) or utilized in innovative floater concepts (Richard 2019, Stiesdal 2019), instead of following purely the conventional structural approach of welding cylindrical and tapered sections together.

5.2.5.4 The true matter of costs

Finally and admittedly, for really considering an optimization of the wind turbine system cost, the ratio of CapEx to AEP (annual energy production) or even the LCoE, which additionally takes OpEx - and sometimes also costs of decommissioning - into account, would have to be considered to be minimized. This way, a real trade-off between saved material costs, changed expenditure of manufacturing and maintaining the system, and different system performance, and, hence, affected AEP can be found. However, this requires a more holistic and complex approach, considering annual environmental distributions at the location of interest, calculations for the full life-time of the system, as well as knowledge of possible manufacturing processes and related costs. The present work can be further expanded in the future to take into account these steps and aspects.

5.3 Brief digression and outlook: larger MW-class floater designs without upscaling? - a direct optimization approach

Exploitation of deeper waters and installation of larger wind turbines are current and future trends of the offshore wind industry. While different platforms are developed and prototypes of FOWTs are already installed and tested, as presented in Section 3.1.1.2, floating support structures still need to conform with the increasing scale of wind turbines. The design process of (floating) wind turbine systems is very extensive and of iterative character, as already discussed in Chapter 4. However, to avoid designing a floating support structure for a larger wind turbine completely from scratch, advantage is taken of the experience with existing systems and upscaling procedures are used for dimensioning larger structures. Notwithstanding, subsequent optimization and modification are required to obtain an efficient final design, as standard upscaling procedures are only suitable for obtaining a first rough draft of an upscaled design. As discussed by Leimeister (2016), the theoretical scaling laws do not account for technological developments, such as lighter and high-strength materials for rotor blades, site-specific conditions and constraints, or further improvements due to, for example, economic interests. Thus, based on the upscaled support structure design, further modifications and optimization steps have to be performed until the final floater design for a larger wind turbine is obtained.

To save effort, the digression in this section proposes the design of a floating platform for a larger wind turbine, which is directly obtained through optimization, thus, eliminating the intermediate step of upscaling. By means of this approach, only a few initial adaptations are required to consider the changed wind turbine weight - hence, ensuring floatation - and to take account of the new wind turbine tower base diameter. All other modifications of the floating

support structure are covered within an optimization procedure, which is based on user-defined design variables, value ranges, and optimization criteria. The result of this automatic direct optimization is then a support structure design, which is suited for a pre-defined larger wind turbine and specified site and is also optimized with respect to user-defined criteria.

The OC3 phase IV spar-buoy FOWT system (Jonkman 2010), as specified as reference system in Section 3.2, serves as basis for the application of the direct optimization approach. By this means, a support structure for a 7.5 MW wind turbine - Fraunhofer's IWT-7.5-164 (Popko, Thomas, Sevinc, Rosemeier, Bätge, Braun, Meng, Horte, Balzani, Bleich, Daniele, Stoevesandt, Wentingmann, Polman, Leimeister, Schümann & Reuter 2018) - shall be obtained from a floater, which is initially designed for a 5 MW wind turbine - NREL 5 MW (Jonkman et al. 2009). Thus, in addition to the already specified 5 MW-class reference FOWT system (Section 3.2), the target 7.5 MW reference wind turbine is introduced at first in Section 5.3.1. Afterwards (Section 5.3.2), the methodology is explained. On this basis, the specific design conditions, such as the simulation load case, design variables, optimization criteria, and optimization parameters, are set in Section 5.3.3. The results (Section 5.3.4) show the development of the design throughout the optimization process, as well as the final floater design for the 7.5 MW wind turbine and its performance. The outcomes and applied approach are finally discussed in Section 5.3.5.

5.3.1 Target larger MW-class reference wind turbine

In this application, the OC3 phase IV spar-buoy supporting the NREL 5 MW reference wind turbine, as described in Section 3.2, is used as basis FOWT system and hence as input to the direct optimization approach. The final goal of the direct optimization is to obtain a floating spar-buoy, which suits the 7.5 MW IWT-7.5-164 reference wind turbine, which is introduced in more detail hereinafter.

The IWT-7.5-164 (Popko, Thomas, Sevinc, Rosemeier, Bätge, Braun, Meng, Horte, Balzani, Bleich, Daniele, Stoevesandt, Wentingmann, Polman, Leimeister, Schümann & Reuter 2018) is a state-of-the-art upwind 7.5 MW reference wind turbine, which is designed by Fraunhofer IWES according to wind turbine class I and turbulence category A. This turbine has three blades and a direct drive generator. Further properties of the RNA are given in Table 5.24.

For this wind turbine, different support structures exist for an onshore system (with a tower) or two different offshore systems (with monopile, transition piece, and tower). The monopile-based offshore wind turbine system "Offshore TANDEM" (Popko, Thomas, Sevinc, Rosemeier, Bätge, Braun, Meng, Horte, Balzani, Bleich, Daniele, Stoevesandt, Wentingmann, Polman, Leimeister, Schümann & Reuter 2018), which served as basis for the joint research project TANDEM (Leimeister, Spill, Dose, Foglia, Siegl, Karch, Heins, Schümann, Dührkop & Hartmann 2019), is used in this study; however, for this application, the monopile is removed and the transition piece is cut at 10.0 m above SWL, which corresponds to the top of the floating platform. This way, the hub height of the IWT-7.5-164 remains unchanged, when

it is placed on top of the floating platform. The relevant parameters of the support structure, considering the shortened transition piece, are presented in Table 5.25.

Table 5.24: Properties of the IWT-7.5-164 reference wind turbine RNA (Popko, Thomas, Sevinc, Rosemeier, Bätge, Braun, Meng, Horte, Balzani, Bleich, Daniele, Stoevesandt, Wentingmann, Polman, Leimeister, Schümann & Reuter 2018).

Parameter	Value
Rotor diameter	163.4 m
Hub height	111.6 m
RNA mass	536.8×10^3 kg
Cut-in, rated, cut-out wind speed	3.0 m/s, 11.7 m/s, 25.0 m/s

Table 5.25: Properties of the IWT-7.5-164 reference wind turbine support structure (Leimeister, Spill, Dose, Foglia, Siegl, Karch, Heins, Schümann, Dührkop & Hartmann 2019, Popko, Thomas, Sevinc, Rosemeier, Bätge, Braun, Meng, Horte, Balzani, Bleich, Daniele, Stoevesandt, Wentingmann, Polman, Leimeister, Schümann & Reuter 2018).

Parameter	Value
Tower top elevation, diameter, thickness	107.6 m, 3.0 m, 0.025 m
Tower base elevation, diameter, thickness	21.6 m, 7.0 m, 0.035 m
Transition piece diameter, thickness (at 10 m above SWL)	7.0 m, 0.090 m
Tower material density	7,850 kg/m ³
Transition piece material density	7,850 kg/m ³
Support structure mass (from 10 m above SWL)	491.5×10^3 kg

5.3.2 Methodology of the direct optimization approach

To generate a new floater design for a larger MW-class wind turbine on the basis of a smaller existing FOWT system, first, the FOWT system has to be modeled, comprising the basis design, replacing the wind turbine, and adjusting some parameters to ensure system conformity. This model is then further processed within the optimization framework.

The reference OC3 phase IV FOWT system is already implemented in MoWiT and verified, as covered in Section 4.1. Due to the component-based structure of MoWiT, the original NREL 5 MW wind turbine can easily be replaced with the IWT-7.5-164 wind turbine by exchanging the models for rotor, nacelle, and operating control, as well as the tower subcomponent model within the support structure model. However, due to the different wind turbine dimensions (mass and transition piece diameter at 10 m above SWL, referred to in the following as tower base diameter), some initial adaptations are required before the model can be given as input to the optimization framework.

Thus, the spar-buoy geometry is partially modified by increasing the upper column diameter from the initial 6.5 m to 7.0 m to fit the new tower base diameter of the IWT-7.5-164. This changed parameter affects the floater structural mass for the upper column and the tapered part up to 12.0 m below SWL, but also the displaced water volume from 12.0 m below SWL to the water line. The change in the equivalent buoyancy mass and the structural mass can be determined directly from the original and modified spar-buoy geometry. Hence, the buoyancy mass is increased by around 46.7×10^3 kg, while the floating structure becomes 8.9×10^3 kg heavier. Furthermore, the exchanged wind turbine on top of the floater results in an additional mass increase of 428.6×10^3 kg. These changed buoyancy and structural masses are accounted for in the determination of the ballast height, which is internally calculated in the MoWiT model to ensure floatation of the FOWT system with maintained hub height, and yield a ballast filling height of 45.38 m for this initially adapted FOWT system.

Furthermore, the wind turbine controller needs to be adjusted to avoid negative aerodynamic damping, as now the IWT-7.5-164 is on top of a floating platform. For this purpose, the integral and proportional controller gains K_I and K_P are modified, following the general descriptions and recommendations given by Hansen et al. (2005), as well as adopting the approach used by Leimeister (2016). Hence, the damping ratio of the response ζ_c (associated with the equation of motion for the rotor-speed error), required for the determination of K_P , is set equal to 0.7. In addition, the controller natural frequency $\omega_{c,nat}$ needs to be defined. As the controller should be slower than the system response, the pitch natural frequency of the OC3 phase IV FOWT system, obtained by means of the verification simulations (Section 4.1) with the MoWiT model as 0.1985 rad/s (Table 4.6), is taken and reduced by a factor of 1.3, according to the approach suggested by Leimeister (2016). This yields a controller natural frequency of $\omega_{c,nat} = 0.1527$ rad/s. Together with the 7.5 MW wind turbine specific drivetrain and blade-pitch controller parameters, as given in Table 5.26, the controller gains are computed according to Equations 5.14 and 5.15 for a direct drive wind turbine and, hence, set to $K_I=0.00141924$ and $K_P=0.01300953$ s.

Table 5.26: Properties of the IWT-7.5-164 reference wind turbine drivetrain and blade-pitch controller (Leimeister 2016, Sevinc et al. 2016).

Parameter	Symbol	Value
Diameter of generator rotor	$D_{gen,rotor}$	4.5 m
Mass of generator rotor	$m_{gen,rotor}$	39.3×10^3 kg
Inertia of drivetrain*	$I_{drivetrain}$	99,478 kg m ²
Rated rotational speed of drivetrain shaft	Ω_{rated}	10.0 rad/s
Sensitivity of the aerodynamic power to the rotor-collective blade-pitch angle	$\frac{\partial P}{\partial \theta}$	-16.35×10^6 W/rad

* The drivetrain inertia is determined following Equation 5.16.

$$K_I = \frac{I_{\text{drivetrain}} \Omega_{\text{rated}} \omega_{c,\text{nat}}^2}{-\frac{\partial P}{\partial \theta}} \quad (5.14)$$

$$K_P = \frac{2I_{\text{drivetrain}} \Omega_{\text{rated}} \zeta_c \omega_{c,\text{nat}}}{-\frac{\partial P}{\partial \theta}} \quad (5.15)$$

$$I_{\text{drivetrain}} = \frac{1}{8} m_{\text{gen,rotor}} D_{\text{gen,rotor}}^2 \quad (5.16)$$

This model of the FOWT system, consisting of the OC3 phase IV spar-buoy and the IWT-7.5-164 wind turbine with the required initial adaptations, as summarized in Table 5.27, is given as input to the optimization framework. The MoWiT-Dymola[®]-Python framework for automated simulation and optimization, as developed and introduced in Section 4.2, is utilized. The specific design and optimization conditions, comprising as well the definition of the optimization problem and the selection of the optimizer, are specified hereinafter (Section 5.3.3).

Table 5.27: Required initial adaptations of the OC3 phase IV spar-buoy floater model with the IWT-7.5-164 on top.

Parameter	Adapted value	Original value
Diameter of upper column	7.0 m	6.5 m
Height of ballast within base column	45.38 m	48.37 m
Integral controller gain	0.00141924	-
Proportional controller gain	0.01300953 s	-

5.3.3 Design conditions for the direct optimization approach

The design and optimization conditions for the design of a spar-buoy floating support structure supporting the IWT-7.5-164, based on the 5 MW-class OC3 phase IV floater and obtained through a direct optimization approach, is closely related to the global design optimization task presented in Section 5.1. Thus, only the main and final settings are presented in the following once again, while for the detailed information on derivations and argumentations just the references to the corresponding sections are provided.

5.3.3.1 Design-relevant load case

The iterative optimization procedure is carried out based on design-relevant load cases, used to simulate the considered floating system and to derive the performance criteria from the simulation results. For this first utilization of the direct optimization approach, only one design-relevant load case is selected based on the investigations on critical DLCs, as well as the DLC simulation results and analyses performed in Sections 5.1.3.1 and 5.1.4.1, respectively. Assuming similar system behavior of the IWT-7.5-164 FOWT system, the same environmental condition - namely, DLC 1.6 at rated wind speed and with the turbulent wind seed number

11 and a yaw misalignment angle of 8° - is transferred to the initially adjusted floating wind turbine system and used for the simulations within the direct optimization application.

5.3.3.2 Optimization problem

The object of interest in the direct optimization approach is the spar-buoy floating structure; however, the upper column is initially already adjusted to fit the larger tower base diameter of the 7.5 MW wind turbine. Hence, the design variables, which are to be modified during the direct optimization approach, concern the base column geometry (diameter and height), as well as the ballast. The latter is defined through its density and filling height within the base column. As the ballast density is prescribed by available filling materials - as investigated in Section 5.1.1.1 - it is selected as the third design variable, while the ballast height is not a direct design variable as it depends on the system parameters and chosen design variables and is determined internally to ensure floatation of the wind turbine system. With regard to the structural parameters - similar to the global design optimization task (Section 5.1.1.1) - only the diameter and height of the base column are selected as design variables, whereas the original wall thickness remains unchanged, as the objective of the optimization is not the design strength, but rather focuses on the hydrodynamic behavior of the FOWT system. Furthermore, the mooring system properties again remain unchanged, as the yaw stability is not analyzed explicitly in the direct optimization application, but it would have to be considered as design variable as well, if the entire system stability is to be optimized.

For the three design variables, the allowable value ranges, as well as their values in the initially adjusted FOWT design are presented in Table 5.28. For the spar-buoy base column diameter the lower limit is prescribed by the tower base diameter of the IWT-7.5-164, while the upper limit is inspired by the original value and chosen to be not significantly larger for the ease of handling and manufacturing, but still considering a potential increase in size due to the upscaling to a larger MW-class wind turbine. For the same reasons of handleability and manufacturability, the original base column height is set as upper limit for this design variable, with an option to be reduced by up to 40.0 m. Here it has to be noted, that the lower bound is not set as small as in the global design optimization task, as the resulting optimum floater still requires a base column height of more than 100 m (Sections 5.1.4.3 and 5.1.5.3). The potential ballast density values originate from the density ranges of cheap materials, such as sand with varying water content, rocks, or clay (Engineering ToolBox 2010, 2009), as investigated in

Table 5.28: Design variables and allowable value ranges for the direct optimization application, in comparison to the values for the initially adjusted FOWT system.

Variable	Lower bound	Upper bound	Initial value
D_{BC}	7.0 m	10.0 m	9.4 m
H_{BC}	68.0 m	108.0 m	108.0 m
$\rho_{ballast}$	1,281 kg/m ³	2,600 kg/m ³	1,907 kg/m ³

detail in Section 5.1.1.1. Apart from the ballast type, which is conditional on available lower-cost material, the upper bounds for the geometric parameters are shaped by the additional objective of limiting the outer dimensions of the floating system to facilitate the handling and manufacturing processes, but also to prevent a significant loss in the structural strength as this is excluded from the analysis. Different user-specific objectives and set value ranges would definitely affect the results. This is addressed again in Section 5.3.5.

Within the formulation for determining the ballast filling height as a function of the system mass and buoyancy mass (both are directly derived from the geometric parameters), it is checked that the ballast height never becomes negative, nor exceeds the base column height. If the settings of the design variables would violate one of these constraints, either the ballast density or floater material density is modified - according to the definitions given in Section 5.1.1.1 - to overcome this issue. With having this defined within the MoWiT model, it is ensured that the ballast height remains within these boundaries during the entire optimization iterations.

The optimization goal is similar to that of the global design optimization task (Section 5.1.1.2): obtain an appropriate floating support structure - in this case now for a 7.5 MW wind turbine - so that this FOWT system is stable and complies with general global performance criteria. The direct optimization application as well neither focuses on the structural strength nor on the loading on the structure, such as fatigue due to system eigenfrequencies. These aspects, however, can be integrated by adding more optimization objectives, which are based on post-processed parameters and analyses.

Thus, similarly to the definitions in Section 5.1.2.2 and based on the associated potential risks and consequences investigated in Table D.1 in Appendix D, three objective functions are specified, addressing the platform total inclination angle for stability and wind turbine operational reasons, the nacelle acceleration because of sensitive components within the nacelle, and the translational motion (here it refers to the overall combined mean and dynamic translational motion) due to motion restrictions of the power cable. To avoid oversizing of the FOWT system, which would only yield dispensable high safety factors but an overpriced design, common operational limits are set as objectives. The target values and constraints are summarized in Table 5.29.

Table 5.29: Objectives for the direct optimization application, including target values and constraints.

Parameter	Target value	Constraint
Total inclination angle	10.0°	$\leq 10.0^\circ$
Horizontal nacelle acceleration	1.962 m/s ²	$\leq 1.962 \text{ m/s}^2$
Translational motion	minimized	$\geq 0.0 \text{ m}$

5.3.3.3 Optimization settings

Based on the experience gained within the global design optimization task and as the design and optimization conditions for this direct optimization application are similar - with respect to

the complexity of the considered system, as well as the considered MO optimization problem - to the conditions for the global design optimization task, the evolutionary algorithm NSGAI is chosen again. Thus, the direct optimization approach is carried out by means of the MoWiT-Dymola[®]-Python framework and with the NSGAI optimizer from Platypus. Due to limited computational capacities, the population size for this first direct optimization application is set to 36 individuals in each generation and the total number of simulations to be run is defined as 1,080, which would correspond to 30 generations (29 plus the start population with number 0). These are less generations than simulated in the global design optimization (Section 5.1.3.2) and not even covering the generation in which the optimum of the global design optimization is found (Section 5.1.4.3); however, based on the convergence behavior, discussed in Section 5.3.4.1, the chosen settings prove to provide satisfactory results.

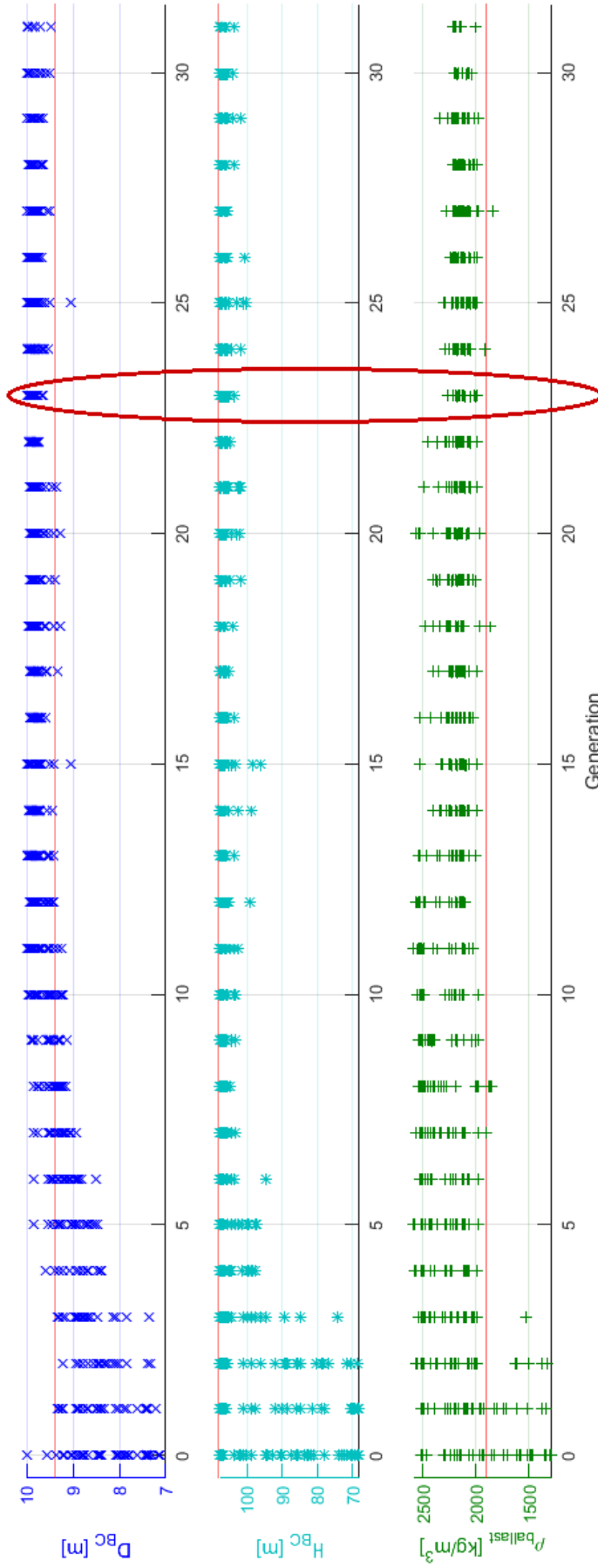
5.3.4 Results of the direct optimization application

The results of the direct optimization approach, applied to the initially adapted OC3 phase IV spar-buoy with the IWT-7.5-164 on top, are presented in the following, first (Section 5.3.4.1), showing the results throughout the optimization process and, then (Section 5.3.4.2), focusing on the final floater design, which is obtained from the direct optimization approach to be appropriate for supporting the IWT-7.5-164.

5.3.4.1 Developments throughout the direct optimization iterations

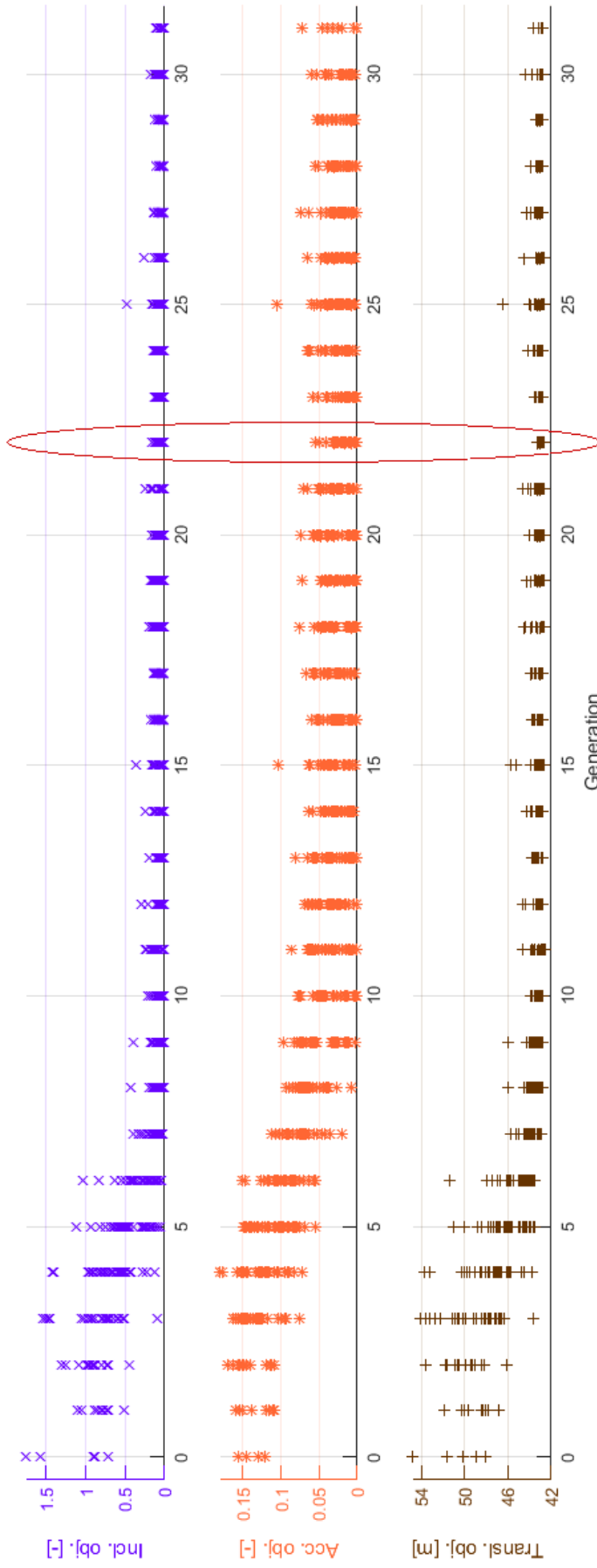
Within the direct optimization procedure, finally, 1,097 individuals are created, simulated, and evaluated. The number differs slightly from the specified number of total simulations of 1,080, as defined in Section 5.3.3.3, due to the internal management (within the MoWiT-Dymola[®]-Python framework and the utilized optimizer NSGAI) of running simulations in parallel. This way, individuals from generation 0 up to generation 31 are created, while the last full generation - meaning containing all 36 individuals - is generation number 26.

Within each generation, the design variables for the individuals are chosen by the optimizer from the specified value ranges and based on the objectives obtained from the previously simulated individuals. Hence, a trend from a broad spread of selected values for the design variables towards better and better values is clearly visible throughout the optimization procedure, as visualized in Figure 5.13(a). The corresponding trend in the obtained optimization objectives (Figure 5.13(b)) shows as well decreasing spreads and, what is most important, an improvement with respect to the objectives set. In Figure 5.13(b), it is noticeable that in the first few generations not for all 36 individuals an objective function value is plotted. The reason for this is that, at the start of the optimization procedure, individuals from the entire allowable value ranges for the design variables are created. These, however, do not all perform that well and some might be instable, which causes an early termination of the simulation. The effectively simulated time is taken as criterion for identifying such unsuccessful simulations, which are then assigned undesirable objectives to ensure exclusion of these designs - analogously to the approach discussed and presented in Section 4.2.3.3 and applied in Section 5.1.3.2.



(a) Development of the design variables in comparison to the initial values (red lines).

Figure 5.13: Development of the individuals throughout the simulated generations in the direct optimization approach, the generation selected based on the first and used approach (thick line) or the second selection option (thin line) is encircled.



(b) Development of the optimization objectives.

Figure 5.13: Selected individuals throughout the simulated generations in the direct optimization approach. (cont.)

5.3.4.2 Spar-buoy design for the IWT-7.5-164

From the 1,097 individuals, obtained within the direct optimization approach, the optimum and final appropriate spar-buoy floater design for the IWT-7.5-164 wind turbine has to be found. The method and criteria for the selection of the optimum geometry are described firstly and, then, the obtained FOWT system is presented and analyzed.

Selection of the floater design resulting from the direct optimization approach As the specified stop criterion, defined through the total number of simulations, which corresponds approximately to a maximum number of generations, is set based on the limited computational capacity, first, the generation has to be determined at which the optimization algorithm has converged before it starts diverging again. To do so, two selection options are considered: based on the minimum spread of the design variables (as applied in the global design optimization task, covered in Section 5.1.4.3) or based on the minimum spread of the objectives. The first option would yield generation 23, the latter generation 22, to be considered for determining the optimum individual, as highlighted in Figures 5.13(a) and 5.13(b) in dark red. As the point of interest in this application example is the convergence of the optimization to one optimum design, the first selection method, based on the minimum spread of the design variables, is used and, hence, generation 23 is taken for finding the best individual in it.

For the selection of the optimum individual, the same procedure as applied in the global design optimization task (Section 5.1.4.3) is utilized. Thus, the following steps are taken.

1. The minimum value for each of the three objectives is identified, comparing all individuals within generation 23. These three values, which originate from different individuals in generation 23, are used as utopia for the objectives.
2. For each individual in generation 23, the distance of its objectives to the utopia point is determined by means of the root of the sum of the three individual distances squared. Here, it has to be noted that the distances for the total inclination angle and horizontal nacelle acceleration objectives are calculated directly, as these objectives are already normalized, as indicated in Table 5.4, while the distance for the translational motion objective, which is by definition just directly the translation value, is now normalized with respect to the utopia value for the translational motion.
3. Doing so, the individual within generation 23, which yields the minimum distance of its objectives to the utopia point, is determined to be the optimum solution.

The final floater geometry resulting from the direct optimization approach Following this selection approach, the final floater geometry of the most appropriate spar-buoy design to support the IWT-7.5-164 is obtained. Its values for the design variables are presented in Table 5.30. This also demonstrates that all values lie within the specified allowable value ranges. A schematic drawing, comparing the original OC3 phase IV spar-buoy for the NREL 5 MW wind turbine with the initially adapted spar-buoy floater for the IWT-7.5-164 wind

turbine, which deals as input to the direct optimization approach, and the final optimized spar-buoy geometry for the IWT-7.5-164 wind turbine, is shown in Figure 5.14.

Table 5.30: Design variables of the final design obtained from the direct optimization approach, in comparison with the specified allowable value ranges and original values.

Design variable	Final value	Allowable value range	Original value
Base column diameter	9.89 m	[7.0 m, 10.0 m]	9.4 m
Base column height	106.42 m	[68.0 m, 108.0 m]	108.0 m
Ballast density	2,127 kg/m ³	[1,281 kg/m ³ , 2,600 kg/m ³]	1,907 kg/m ³

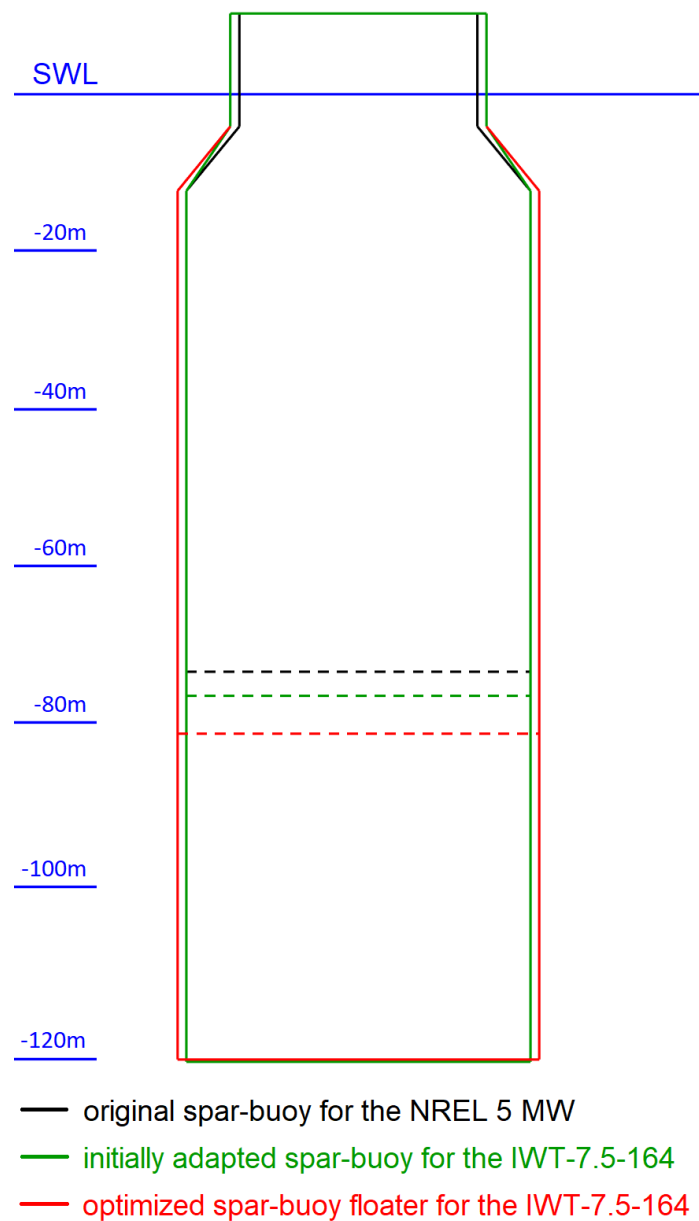


Figure 5.14: Spar-buoy geometry obtained from the direct optimization approach, in comparison with the original and initially adapted geometries, dashed lines indicating the ballast height.

Due to the fact that two potential methods are initially considered for the selection of the generation, at which the optimization has converged, the results obtained when using the second alternative based on the minimum spread of the objectives (yielding generation 22) are determined as well and compared in Table 5.31 to the final results (from the selected generation 23) presented above. This shows that, for both obtained individuals, the spar-buoy design variables, as well as the calculated distances of the objectives to the utopia point, differ only marginally. But still, the final optimum spar-buoy geometry, selected from the individuals within generation 23, and, hence, following the approach as chosen and described earlier, scores higher.

Table 5.31: Comparison of the results for the two generation selection methods for determining the optimum spar-buoy floater geometry resulting from the direct optimization approach.

Parameter	Generation 23	Generation 22
Base column diameter	9.89 m	9.88 m
Base column height	106.42 m	106.42 m
Ballast density	2,127 kg/m ³	2,114 kg/m ³
Distance to utopia point	0.0218	0.0254

Performance of the 7.5 MW FOWT system To prove the suitability of the obtained final spar-buoy geometry, the performance of the FOWT system, consisting of the IWT-7.5-164 wind turbine and the optimum floater design, outlined in Table 5.30 and Figure 5.14, is analyzed. This means that the considered design-relevant load case, according to the definition in Section 5.3.3.1, is simulated with the obtained 7.5 MW FOWT system and the maximum value for each of the defined optimization objectives, specified in Section 5.3.3.2, is taken from the output time series. The results are presented in Table 5.32 and it can clearly be seen that all constraints are met, while still the objective parameters are close to the target values.

Table 5.32: Performance of the spar-buoy FOWT system design obtained with the direct optimization approach.

Parameter	Value	Target value	Constraint
Total inclination angle	9.86°	10°	≤10°
Horizontal nacelle acceleration	1.929 m/s ²	1.962 m/s ²	≤1.962 m/s ²
Translational motion	42.92 m	minimized	≥0 m

5.3.5 Discussion of the direct optimization approach

By means of the presented direct optimization approach, a floating support structure design for a larger wind turbine is obtained based on a smaller existing FOWT system. The finally

achieved design is based on the specified design conditions, as described in Section 5.3.3, and also highly dependent on their settings. Hence, different choices will yield different designs, each optimum for the specific design conditions considered.

In this digression, the focus is placed upon the global system performance and hydrodynamic behavior of the FOWT. Neither the structural design strength, nor the loading on the structure - implying frequency response analyses -, nor the overall system stability are assessed and integrated in the direct optimization approach. However, the current functionality already indirectly checks the requirement of having the system natural frequencies far from the wave spectra peak frequencies by minimizing the system response, but can also easily be extended by adding more detailed checks, as well as further criteria and optimization objectives, such as for the structural strength or loads and fatigue. Furthermore, a more sophisticated design optimization, implying the design strength but also, for instance, the mooring system, would as well require the definition of additional design variables, such as the wall thickness, the fairlead and anchor positions, the mooring line length, and its extensional stiffness.

In general, the settings have to be selected carefully to ensure that the direct optimization approach can be successful. When still intending an upscaling to a larger MW-class wind turbine, this has to be taken into account in the definition of the boundaries for the allowable value ranges of the design variables, to allow for obtaining a stable FOWT system in the end. Furthermore, there is large freedom in the selection of design variables, both with respect to the variable itself and the number of variables. The optimization objectives will definitely also influence the final optimum design. The objectives selected in this application example can be considered as general parameters for the global performance of a FOWT system; however, for more detailed assessment and design of a FOWT system there are almost no limits to the objectives. But still this has to be treated with caution, as this is always subject to a cost-benefit calculation. This aspect is also the reason for just selecting one design-relevant load case, which is then used during the direct optimization approach, instead of running an entire DLC set in each iteration with all individuals. But still it needs to be proved that the obtained optimum FOWT system design performs as required in various environmental conditions. Finally, the achieved optimum design will also depend on the optimization settings; however, due to the preceding study and comparison, it is expected that the selected optimizer NSGAI is suitable for the presented application. The number of simulations to be run is of course again a trade-off between cost or time and benefit and the user has to define up to which accuracy and convergence tolerance the optimization has to be performed. In the end, the final selection of the optimum design out of the huge number of created and simulated individuals depends again on the point of interest and selected approach. However, as shown in Section 5.3.4.2, the resulting optimum designs differ not significantly if the methods are reasonable and the optimization algorithm has run sufficiently long so that a convergence is clearly visible.

In general, however, the presented direct optimization approach has high potential for future applications due to the fast development of the wind turbine technology towards larger and larger MW-classes. This allows that especially floating concepts, which still have to gain competitiveness with bottom-fixed wind turbine system solutions and other renewable energy

devices, can already now get prepared for the trend towards larger wind turbine MW-classes. By means of the presented direct optimization approach, in which the intermediate step of up-scaling is eliminated, the design process of larger MW-class FOWT support structures becomes faster, more efficient, and more economical.

Chapter 6

Reliability-based design optimization of a spar-type floating offshore wind turbine support structure

Even though the costs for offshore wind has already decreased over the last few years (WindEurope 2019a), more cost reduction is required to make offshore wind energy - and especially floating solutions - economic and competitive with other renewable energy systems. In addition, more flexible design provisions would enable more innovation and allow for an accelerated market uptake of floating offshore wind. To this end structures could adhere to a goal-setting design approach, where reliability is the key driving criterion and concepts of structural reliability can be adopted in order to systematically account for uncertainties and different design criteria. Optimization based on structural RA concepts is highly relevant for considering the wide range of prevailing uncertainties - coming from environmental loads, manufacturing processes, or material properties (Hu 2018, Yang et al. 2018, Li et al. 2017, Hu et al. 2016, Yang et al. 2015). These uncertainties may significantly affect the dynamic system response, but are not accounted for in DDO methods which are commonly used for offshore structures (Hu 2018, Yang et al. 2015, Lee et al. 2014).

There is a broad range of structural RA methods, which can be classified in different ways, such as local and sampling methods (Huang et al. 2017a,b) or analytical and stochastic methods, as done and presented in Section 2.1.3. By means of statistical surrogate modeling methods - such as kriging, RSM, or regression analysis (Section 2.3.2.2) - a system representation can be created (Huang et al. 2017a). The final RA can be performed either on the real system or on such a derived system representation. The most common analytical RA methods are - as described in Sections 2.1.3.1 and 2.3.1.2 - FORM and SORM, which are based on Taylor expansion, while stochastic approaches - covered in Sections 2.1.3.2 and 2.3.2 - can follow sampling methods, as for example MCS, LHS, or IS (Huang et al. 2017a,b). Commonly, combinations

Note: This chapter is based on the publication by Leimeister & Kolios (2020).

of these methods, such as RSM or LHS for creation of an approximate metamodel and MCS, FORM, or SORM for finally determining the reliability, are applied - especially when it comes to offshore wind turbine systems which are of high complexity (Shittu et al. 2020). Consequently, alternative approaches and simplifications are required for the even more complex and computationally highly demanding RBDO of offshore wind turbine systems. Thus, in addition to the application examples presented in Section 2.3.4, response surface approximation (Kang et al. 2009), fractional moment reliability analysis method (Yang et al. 2018), environmental contour method (Velarde et al. 2019), surrogate modeling combined with an ensemble learning method (Pillai et al. 2019), or an advanced first-order second moment method (Park & Park 2014) can be found in studies on RBDO of offshore wind turbine system components. Even if MCS and sampling-based RBDO methods are recommended for systems with nonlinear or intricate design sensitivity (Hu 2018), these are highly computationally intensive as they require a large number of iterations. Thus, MCS is often just used for the final reliability calculation, based on predetermined response surface approximation models, surrogate models, or Latin hypercube metamodels (Li et al. 2017, Yang et al. 2015). A stepwise refinement, as applied by Hu et al. (2016), where surrogate models are just created for a more detailed RBDO at predetermined hotspots, may as well be more efficient. Finally, another approach that is adopted in some research studies - as well with the focus on efficiency enhancement - is the decoupling of the reliability assessment and the design optimization (Stieng & Muskulus 2020, Lee et al. 2014).

In some first studies on RBDO in relation to offshore wind turbine systems (Stieng & Muskulus 2020, Pillai et al. 2019, Velarde et al. 2019, Hu et al. 2016, Depina & Eiksund 2015, Yang et al. 2015), the cost reduction objective is augmented by constraints addressing reliability aspects, such as reduced fatigue damage. These RBDO application examples deal with different single components of the system, such as blades (Hu 2018, Hu et al. 2016), drivetrain (Li et al. 2017), tower (Park & Park 2014), transition piece (Lee et al. 2014), or various bottom-fixed support structures (monopiles, gravity-based foundations, or tripods) (Stieng & Muskulus 2020, Velarde et al. 2019, Depina & Eiksund 2015, Yang et al. 2015, Kang et al. 2009); however, the only component of a FOWT system addressed in a RBDO study is the mooring system (Pillai et al. 2019, Clark & Paredes 2018). This emphasizes the significantly increased level of difficulty, when - in addition to including the reliability aspect into design optimization - also the much more complex system of a FOWT is considered.

Thus, in this chapter the RBDO of FOWTs is addressed. A proven concept, by which means the combination of FOWT system design optimization and reliability assessment is feasible, as well as reasonable with respect to computational effort and elapsed time, is developed. Due to the already high complexity and fully-coupled system dynamics of FOWTs, a simple design example is elaborated in this first approach. In the highly flexible framework for RBDO, the reliability criterion can be specified as objective function or also addressed as constraint within the design optimization. The latter option is adopted in the presented application example due to computational limitations. With success of this first application example, having obtained positive results, the presented concept and framework can be used for more complex and ad-

vanced RBDO problems on FOWT systems. This way, the presented methodology can pave the way to reliable structures of FOWTs and reduced uncertainties in the system designs.

In the following, first (Section 6.1), the RBDO problem is presented. The challenges and solutions for the realization and numerical implementation of this RBDO problem are discussed and detailed in Section 6.2. The presented RBDO methodology is applied to an exemplary spar-buoy FOWT system, as described in Section 3.2, and the results are presented in Section 6.3 and further discussed in Section 6.4.

6.1 Definition of the RBDO problem

The RBDO is applied to the reference OC3 phase IV spar-buoy FOWT system, presented in Section 3.2, and for certain design-critical environmental conditions elaborated in Section 6.1.4. In the global DDO example presented in Section 5.1, the same system is optimized with respect to its global performance, while limiting the outer dimensions of the floater. Based on this, LSs, uncertainties in form of stochastic variables, and reliability criteria are incorporated in the optimization problem, following the general formulation given in Section 4.2.3.1. For a RBDO problem, a target reliability has to be specified as objective function. An alternative - the reliability-constrained design optimization, as realized in this application example due to computational limitations - is to address the reliability criteria in the constraints of the optimization problem. Thus, the finally selected design variables and objective functions, LSs, environmental conditions, stochastic variables, and reliability criteria, as well as optimization constraints, are specified in Sections 6.1.1 to 6.1.7.

6.1.1 The design variables of the RBDO problem

The RBDO problem is - as already stated - based on the global design optimization task presented in Section 5.1. Hence, to allow for comparisons between the DDO and the RBDO, the selection of the design variables and corresponding allowable value ranges is done analogously to the elaborations in Section 5.1.1.1. Thus, not altering the transition between tower and floater base - meaning the upper column down to the bottom end of the tapered part - three design variables for modifying the spar-buoy floater are defined: base column diameter, base column height, and ballast density, as declared in Table 6.1. Other floater properties, such as material density, wall thickness, or resulting mooring stiffness, are kept unchanged.

Table 6.1: Declaration of the three design variables and their allowable value ranges of the RBDO problem.

Design variable	Formal expression	Allowable value range	Original value
x_1	D_{BC}	[6.5 m, 9.4 m]	9.4 m
x_2	H_{BC}	[8.0 m, 108.0 m]	108.0 m
x_3	$\rho_{ballast}$	[1,281 kg/m ³ , 2,600 kg/m ³]	1,907 kg/m ³

Allowable value ranges for the three selected design variables are specified to limit on the one hand the outer dimensions of the floater, which would positively affect the required material and resulting structural costs, and on the other hand to consider only feasible design solutions with respect to existing and affordable ballast materials. Thus, the original values for the base column diameter and height are set as upper bound for the allowable value ranges. The lower bound for the base column diameter is prescribed by the tower base diameter to avoid any constriction of the support structure, while for the base column height the minimum draft of the floating system is decisively. As cost-efficient ballast materials, sand with different water contents, concrete, and rocks are considered. This leads to the allowable value ranges for the design variables, as presented in Table 6.1 together with the original values of the OC3 phase IV spar-buoy. These limitations on the allowable values for the design variables are addressed by means of the inequality constraints g_1 to g_6 , outlined in Section 6.1.7.

6.1.2 The objective functions of the RBDO problem

As the reliability criteria are - in this application example - not defined as objective functions but rather as optimization constraints, the same objective functions as specified for the DDO (Section 5.1.2.2) are utilized - again for comparative reasons. Thus, focusing on the global dynamic FOWT system performance and based on the associated potential risks and consequences, as investigated in Table D.1 in Appendix D, the total system inclination angle and horizontal nacelle acceleration shall approach but not exceed a maximum allowable value, which is set in each case according to common values (Nejad et al. 2017, Katsouris & Marina 2016, Kolios et al. 2015, Huijs et al. 2013, Suzuki et al. 2011), while the dynamic translational motion is to be reduced at all. Thus, the objective functions are defined as given in Table 6.2, while the non-exceedance of maximum allowable values are addressed by means of the inequality constraints g_7 to g_9 (Section 6.1.7).

Table 6.2: Declaration of the three objective functions of the RBDO problem.

Objective function	Formal expression	Description
$f_1(system(X))$	$\frac{ \max(t_{tot}) - 10.0^\circ }{10.0^\circ}$	Total inclination angle criterion
$f_2(system(X))$	$\frac{ \max(a_{hor,nacelle}) - 1.962 \text{ m/s}^2 }{1.962 \text{ m/s}^2}$	Horizontal nacelle acceleration criterion
$f_3(system(X))$	$\max(s_{dyn,transl})$	Dynamic translational motion criterion

6.1.3 The limit states of the RBDO problem

In the final reliability assessment, LSs are to be considered. Thus, two parameters that might become critical for the considered optimization objectives (Section 6.1.2) and are also judged

in other studies (Matha et al. 2014, Bachynski et al. 2013, Huijs et al. 2013, Bachynski & Moan 2012) as important parameters for LS analyses are selected and discussed in the following.

6.1.3.1 Bending stress at the tower base

The tower base fore-aft and side-side bending moments depend highly on the thrust force, as well as on the degree of dampening in fore-aft and side-side motion, and are influenced by the floater motion. The overall bending moment experienced at the tower base is derived as the combined fore-aft and side-side tower base bending moment (M_{TB}). Relating this to the cross-sectional area at the tower base with diameter D_{TB} (6.5 m) and wall thickness t_{TB} (0.027 m) according to Equation 6.1, the combined tower base bending stress (σ_{TB}) is obtained.

$$\sigma_{TB} = \frac{32}{\pi} \frac{D_{TB}}{D_{TB}^4 - (D_{TB} - 2t_{TB})^4} M_{TB} \quad (6.1)$$

For this bending stress at the tower base, the LS is defined as follows:

- the common construction steel is S355 with a minimum yield stress of 355.00 MPa (Gentils et al. 2017, DNV 2014);
- a partial safety factor of 1.35 is applied according to standards and guidelines (IEC 2019a,b,c, GL 2010);
- the resulting limit for the allowable stress amounts to 262.96 MPa.

This limit defines both the LS for the reliability assessment and the ultimate tower base bending stress.

6.1.3.2 Breaking strength of each mooring line

The tension in the mooring lines at the fairleads is influenced by the floater motion and highly depends on the thrust force and wave loading. Based on the coordinate system presented in Figure 4.3 and the mooring line configuration with one mooring line (ML1) facing away from the wind (positive x -direction) parallel to the x -axis and two lines (ML2 and ML3) facing towards the wind (negative x -direction) with an aperture angle of 120° (ML2 in positive y -direction and ML3 in negative y -direction), higher tensions are expected in ML2 and ML3. Relating the mooring line tension (F_{MLi}) to the sectional area of the mooring line with diameter D_{MLi} (0.090 m) according to Equation 6.2, the stress in the mooring line (σ_{MLi}) is obtained.

$$\sigma_{MLi} = \frac{4}{\pi} \frac{F_{MLi}}{D_{MLi}^2} \quad (6.2)$$

For the breaking strength related to the tensional stress in each mooring line, the LS is define as follows:

- the common studless mooring chain R4 (Kim et al. 2014, Huijs et al. 2013) is utilized with a break load of 8,167 kN for a chain diameter of 0.090 m (Vicinyay 2012), resulting into a break stress of 1,283.77 MPa;

- a design safety factor of 1.67 is applied according to standards and guidelines (DNV GL 2016*b*, BSI 2013);
- the resulting limit for the allowable stress amounts to 768.73 MPa.

Additionally to this LS, used for the reliability assessment, the ultimate LS tension is set equal to 60% of the maximum break load according to standards and guidelines (DNV GL 2016*b*, BSI 2013), leading to a maximum allowable stress of 770.26 MPa. This is used as constraint for the maximum stress occurring in the mooring lines during the analyses.

6.1.4 The design load case of the RBDO problem

For designing a FOWT system, standards and technical specifications by IEC, DNV, and DNV GL recommend a huge set of DLCs for various environmental conditions and turbine operational states to be considered. However, the highly iterative character of the development of a system design, including design optimization, forces a compromise between computational effort and comprehensiveness of load analyses. Thus, commonly only certain critical load cases are investigated in system and design analyses, as discussed and applied in the global design optimization (Section 5.1.3.1). Following the presented five-step approach, the same objectives (defined and described in Section 6.1.2) as utilized in the global design optimization, but now - additionally - also the LS parameters (selected and specified in Section 6.1.3) have to be considered when choosing the critical DLC to be used within the RBDO.

Due to the focus on the maximum global system performance and the ultimate nature of the LSs, 54 environmental conditions from operational DLCs for ultimate analyses are selected from IEC standard 61400-3-1 (IEC 2019*b*), which are the same as considered in the global design optimization (Section 5.1.3.1), based on the following argumentation:

- 18 conditions for DLC 1.1 around rated wind speed (10.0 m/s, 11.4 m/s, 13.0 m/s) with normal turbulent wind, normal irregular waves, and normal current, as the largest system inclination and mean translational motion, as well as tower base bending stress and stress in the upwind mooring lines (ML2 and ML3), are expected to be driven by the highest thrust force occurring at rated wind speed;
- 18 conditions for DLC 1.3 below, at, and above rated wind speed (8.0 m/s, 11.4 m/s, 25.0 m/s) with extreme turbulent wind, but normal irregular waves and normal current, as for a wind-dominated site the largest nacelle acceleration and dynamic translational motion are expected to be driven by the high fluctuations in the wind loading; and
- 18 conditions for DLC 1.6 below, at, and above rated wind speed (8.0 m/s, 11.4 m/s, 25.0 m/s) with normal turbulent wind and normal current, but severe irregular waves, as for a wave-dominated site the largest nacelle acceleration and dynamic translational motion are expected to be driven by the high fluctuations in the wave loading.

In each DLC three yaw misalignment angles (-8° , 0° , 8°) and two discrete seed numbers (each for wind and waves) per yaw misalignment angle are considered. This leads, combined

with the three different wind speeds addressed in each DLC, to the mentioned 18 conditions per DLC.

Fully-coupled system simulations in time-domain are performed with the specified reference FOWT system (Section 3.2) for these environmental conditions, utilizing the MoWiT-Dymola[®]-Python framework and taking advantage of its suitability for automated simulation of DLCs, as presented in Section 4.2.2. The evaluated system parameters are on the one hand the optimization objectives defined in Section 6.1.2, as well as a fourth constrained performance parameter - the mean translational motion - and on the other hand the LS parameters specified in Section 6.1.3.

From the set of 54 environmental conditions, the three DLC settings that turn out to be most critical to some of the evaluated system parameters are presented in Table 6.3, following the same naming convention DLCx_wW_sS_yY as specified in Section 4.2.2.2. The criticality of each case for each parameter of interest is expressed in terms of the position of the specific case within all 54 simulated conditions.

Table 6.3: Criticality of specific DLC settings for evaluated system parameters of the RBDO problem.

Parameter		DLC11_ w11_s10_y0	DLC16_ w11_s8_y-8	DLC16_ w11_s11_y8
$\max(t_{\text{tot}})$	Rank	21	1	5
	Value	4.4°	5.1°	4.8°
$\max(a_{\text{hor,nacelle}})$	Rank	33	3	1
	Value	0.706 m/s ²	2.324 m/s ²	2.334 m/s ²
$\max(s_{\text{dyn,transl}})$	Rank	16	26	40
	Value	7.6 m	7.1 m	5.7 m
$s_{\text{mean,transl}}$	Rank	5	10	9
	Value	20.7 m	20.5 m	20.5 m
$\max(\sigma_{\text{TB}})$	Rank	35	1	3
	Value	127.61 MPa	204.74 MPa	202.14 MPa
$\max(\sigma_{\text{ML1}})$	Rank	33	47	46
	Value	113.89 MPa	108.39 MPa	108.57 MPa
$\max(\sigma_{\text{ML2}})$	Rank	2	32	13
	Value	207.35 MPa	194.70 MPa	201.74 MPa
$\max(\sigma_{\text{ML3}})$	Rank	1	12	35
	Value	210.36 MPa	202.25 MPa	193.68 MPa

Further assessment, rating total inclination angle and horizontal nacelle acceleration as the two most important performance parameters and noticing that the highest mooring line stress

achieved in all simulated cases is way below the specified LS (less than one third of it) while the tower base bending stress reaches a much closer value to the corresponding LS (almost 80% of it), yields the selection of DLC 1.6

- at 11.4 m/s wind speed,
- with seed number 8 for the normal turbulence model,
- yaw misalignment angle of -8° ,
- severe sea state (SSS) with 50 years recurrence period, and
- irregular waves of 10.4 m significant wave height and 14.7 s peak period

as design driving and most critical load case for the considered optimization objectives and LSs given in Sections 6.1.2 and 6.1.3.

6.1.5 The stochastic variables of the RBDO problem

As the considered FOWT is just a reference system, which is not operating at or designed for an explicit offshore site - only the water depth is prescribed, however, no information on annual distributions of wind and waves is available - the environmental parameters, used within the DLC setup (Section 6.1.4) based on equations and relations provided in standards, are selected as uncertain parameters in this application example, which are then accounted for in the reliability analysis. In specific, the mean value of the turbulent wind speed (11.4 m/s in the selected critical DLC), as well as the significant wave height of the irregular waves in the severe sea state (10.4 m in the selected critical DLC), are taken.

To define a stochastic variable, its type of distribution and statistical coefficients have to be specified. This is done in Sections 6.1.5.1 and 6.1.5.2 for the two selected uncertain parameters.

6.1.5.1 Statistical properties for the wind speed

For the wind speed V (long-term n -minute average speed), a Weibull distribution can be assumed, according to the classification notes 30.6 by DNV (1992). The Weibull distribution parameters are derived from data at an offshore site, which shall represent realistic site conditions for the considered FOWT system, as well as a mean wind speed of 11.4 m/s as stated in the selected critical DLC (Section 6.1.4). Considering the locations of the Hywind demonstrator (west of Karmøy) and the Hywind Scotland pilot park (east of Peterhead), the database by Fugro GEOS (2001) for the northern North Sea and central North Sea areas is investigated. Here it strikes that at grid point 14715 in the northern North Sea the mean wind speed in month December matches exactly the required value of 11.4 m/s. To the available data on percentage exceedance, a two-parameter Weibull distribution¹ is fitted. The obtained parameters and statistical coefficients are summarized in Table 6.4.

¹Mathematical expressions for the two-parameter Weibull distribution can be found in Appendix F in Equations F.1 to F.5.

Table 6.4: Statistical coefficients of the stochastic variable wind speed.

Parameter	Symbol	Value
Weibull scale factor	b	12.8 m/s
Weibull shape factor	c	2.659
Mean wind speed	$\mu(V)$	11.4 m/s
Standard deviation	$\sigma(V)$	4.6 m/s
Least square error of fit	-	$4.8 \times 10^{-4} \text{ m}^2/\text{s}^2$

6.1.5.2 Statistical properties for the significant wave height

For the significant wave height H_s , the classification notes 30.6 by DNV (1992) prescribe a three-parameter Weibull distribution². Such a three-parameter Weibull distribution is derived by DNV (1992) from scatter data in the North Sea - hence, the similar region considered already in Section 6.1.5.1. The provided and determined parameters are the following.

- Weibull scale factor $b = 2.290 \text{ m}$
- Weibull shape factor $c = 1.385$
- Weibull location parameter $a = 0.594 \text{ m}$
- Mean significant wave height $\mu(H_s) = 2.7 \text{ m}$
- Standard deviation $\sigma(H_s) = 1.5 \text{ m}$

As, however, the sea state considered in the selected DLC (Section 6.1.4) is severe, an extrapolation to such an extreme significant wave height is required. In an application example in the classification notes 30.6 (DNV 1992), an extreme three-hour event is considered. Following the same approach, the cumulative density function (CDF) for the significant wave height in SSS ($F_{\text{SSS}}(H_s)$) is derived according to Equation 6.3 from the common CDF ($F(H_s)$) with accounting for the reference period of the extreme event by means of N , as expressed in Equation 6.4 for a three-hour extreme event.

$$F_{\text{SSS}}(H_s) = [F(H_s)]^N \quad (6.3)$$

$$N = \frac{365 \frac{d}{y} 24 \frac{h}{d}}{3 \frac{h}{y}} = 2920 \quad (6.4)$$

Based on this³, the distribution parameters and statistical coefficients for the stochastic variable H_s are derived and presented in Table 6.5.

²Mathematical expressions for the three-parameter Weibull distribution can be found in Appendix G in Equations G.1 to G.4.

³The further mathematical expressions for the three-parameter Weibull distribution parameters for the SSS extreme event can be found in Appendix G in Equations G.5 to G.7.

Table 6.5: Statistical coefficients of the stochastic variable significant wave height.

Parameter	Symbol	Value
Weibull scale factor	b	2.290 m
Weibull shape factor	c	1.385
Weibull location parameter	a	0.594 m
Reference period of extreme event	-	3 h
Mean significant wave height for SSS	$\mu_{\text{SSS}}(H_s)$	11.4 m
Standard deviation	$\sigma_{\text{SSS}}(H_s)$	1.1 m

The mean value is by about 9.6% larger than the significant wave height specified in the selected critical DLC (Section 6.1.4), but still close enough for such an extreme event, so that these site distribution values are utilized for the stochastic variable H_s .

6.1.6 The reliability criteria of the RBDO problem

Various standards, technical specifications, and classification notes by IEC, DNV, DNV GL, and ISO (International Organization for Standardization) are reviewed regarding the target value for the reliability index β to be considered. While IEC (2019*a,b,c*) recommend a nominal annual failure probability of 5×10^{-4} , corresponding to $\beta = 3.291$, and refers to ISO 2394 (ISO 2015), which defines the allowable probability of failure in dependency on the amount of the relative cost of safety measure and the magnitude of the consequences of failure, DNV (2014, 1992) and DNV GL (2018*c*) recommend for the same reference period of one year a nominal failure probability of 1×10^{-4} , corresponding to $\beta = 3.719$, which is even tightened in case of unacceptable consequences of failure to a failure probability of 1×10^{-5} , corresponding to $\beta = 4.265$.

In the considered case of a single FOWT system under normal operating condition in SSS - as specified in Section 6.1.4 - and, hence, being unmanned, the consequences of failure are likely neither related to human injuries, nor to impacts to other structures or the environment, and most probably have mainly financial repercussions, for which reason the target safety level is set to a maximum allowable failure probability of 1×10^{-4} or a minimum required reliability index of $\beta = 3.719$, respectively. This has to be fulfilled for all four LS parameters - bending stress at the tower base, as well as stresses in ML1, ML2, and ML3 - defined in Section 6.1.3, while accounting for the uncertainties in the environmental conditions, specified through the two stochastic variables V and H_s stated in Section 6.1.5.

6.1.7 The constraints of the RBDO problem

The specified optimization problem comes with no ($m = 0$) equality constraint (h_i) and 18 ($n = 18$) inequality constraints (g_i), as presented and declared in Table 6.6 and described in more detail in the following.

Table 6.6: Declaration of the 18 inequality constraints of the RBDO problem.

Inequality constraint	Formal expression	Description
$g_1(x_1)$	$6.5 \text{ m} - x_1$	Allowable value range of x_1
$g_2(x_1)$	$x_1 - 9.4 \text{ m}$	Allowable value range of x_1
$g_3(x_2)$	$8.0 \text{ m} - x_2$	Allowable value range of x_2
$g_4(x_2)$	$x_2 - 108.0 \text{ m}$	Allowable value range of x_2
$g_5(x_3)$	$1,281 \text{ kg/m}^3 - x_3$	Allowable value range of x_3
$g_6(x_3)$	$x_3 - 2,600 \text{ kg/m}^3$	Allowable value range of x_3
$g_7(\text{system}(X))$	$\max(\iota_{\text{tot}}) - 10.0^\circ$	Maximum total inclination angle
$g_8(\text{system}(X))$	$\max(a_{\text{hor,nacelle}}) - 1.962 \text{ m/s}^2$	Maximum horizontal nacelle acceleration
$g_9(\text{system}(X))$	$-\max(s_{\text{dyn,transl}})$	Maximum dynamic translational motion
$g_{10}(\text{system}(X))$	$s_{\text{mean,transl}} - 64.0 \text{ m}$	Mean translational motion
$g_{11}(\text{system}(X))$	$3.719 - \beta(\sigma_{\text{TB}})$	Minimum required reliability of the tower base bending stress LS
$g_{12}(\text{system}(X))$	$3.719 - \beta(\sigma_{\text{ML1}})$	Minimum required reliability of the tensional stress LS for ML1
$g_{13}(\text{system}(X))$	$3.719 - \beta(\sigma_{\text{ML2}})$	Minimum required reliability of the tensional stress LS for ML2
$g_{14}(\text{system}(X))$	$3.719 - \beta(\sigma_{\text{ML3}})$	Minimum required reliability of the tensional stress LS for ML3
$g_{15}(\text{system}(X))$	$\max(\sigma_{\text{TB}}) - 262.96 \text{ MPa}$	Maximum tower base bending stress
$g_{16}(\text{system}(X))$	$\max(\sigma_{\text{ML1}}) - 770.26 \text{ MPa}$	Maximum tensional stress in ML1
$g_{17}(\text{system}(X))$	$\max(\sigma_{\text{ML2}}) - 770.26 \text{ MPa}$	Maximum tensional stress in ML2
$g_{18}(\text{system}(X))$	$\max(\sigma_{\text{ML3}}) - 770.26 \text{ MPa}$	Maximum tensional stress in ML3

The first ten constraints are corresponding to the inequality constraints already prevailing in the DDO application example (Section 5.1.2.3). These are g_1 to g_6 for the allowable value ranges of the design variables specified in Section 6.1.1, g_7 to g_9 for defining the direction from which the objective functions on the global system performance parameters mentioned in Section 6.1.2 shall be approached, as well as g_{10} for another global system performance parameter - the mean translational motion that shall not exceed 20% of the water depth, based on a rule of thumb.

Up to now, the optimization problem defined through the three design variables x_1 to x_3 (Section 6.1.1), the three objective functions f_1 to f_3 (Section 6.1.2), and the above mentioned first ten inequality constraints g_1 to g_{10} is already significantly constrained, but describes just

a DDO problem. Thus, for stating a RBDO problem, the reliability criteria for the four LS parameters given in Section 6.1.3, with considering environmental uncertainties by means of the two stochastic variables specified in Section 6.1.5, have to be added. Defining them through additional objective functions would put much more restrictions on the optimization problem. This would not necessarily inhibit the convergence of the algorithm, but would significantly slow it down. Due to computational limitations, hence, the reliability criteria are integrated as constraints for the lower limit - the minimum required reliability of the system LS parameters. This entails g_{11} to g_{14} for limiting the lowest allowable value for the reliability index obtained for the tower base bending stress, as well as the stress in each mooring line.

Furthermore, as already indicated in Section 6.1.3, the maximum values for the tower base bending stress and the stresses in the three mooring lines are limited to not exceed the corresponding ultimate stress values. This adds four more inequality constraints: g_{15} to g_{18} .

6.2 Numerical implementation of the RBDO problem

The realization of the RBDO problem defined in Section 6.1 utilizes on the one hand the MoWiT-Dymola[®]-Python framework - as presented and described in detail in Section 4.2 - for executing automatically fully-coupled system simulations with the FOWT, as well as performing automatically the optimization task, and requires on the other hand two levels of pre-processing, covered in Sections 6.2.1 and 6.2.2, before addressing finally the iterative RBDO process, described in Section 6.2.3. The subsequent post-processing of the results is covered in Sections 6.3.2 and 6.3.3. A flowchart of these modular steps is presented in Figure 6.1.

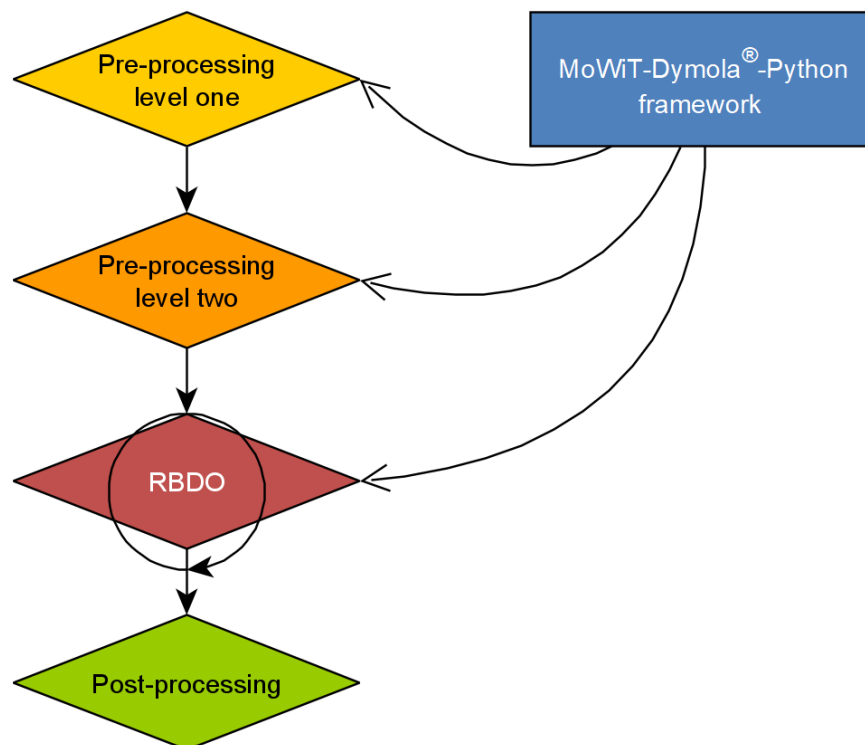


Figure 6.1: Flowchart of modular steps for realizing the RBDO problem.

6.2.1 Pre-processing level one

Ahead of performing any RBDO task on the FOWT, some preparatory investigations, simulations, and studies are required. At first, the approach and boundary conditions for the reliability assessment of one specific system have to be elaborated. This comprises the specification of the environmental conditions in terms of a DLC, under which the system is investigated, as well as the LSs, which are to be considered in the reliability assessment; the choice and definition of uncertain parameters, which are then handled as stochastic variables with specific statistical properties; the selection of a specific reliability analysis method to be followed to determine the reliability index for each LS; and, finally, the investigation of the plausibility of the settings and results, as well as their closeness to reality. The flowchart of these pre-processing level one steps is presented in Figure 6.2. This approach has similarities regarding its structure with other studies on reliability assessments of complex renewable energy systems (Shittu et al. 2020, Kolios et al. 2018, Wang & Kolios 2017); however, the decisions on the DLC and LSs are primarily driven by the optimization objectives of the RBDO problem and the selection of the reliability analysis method already takes account of the final application within the iterative RBDO process.

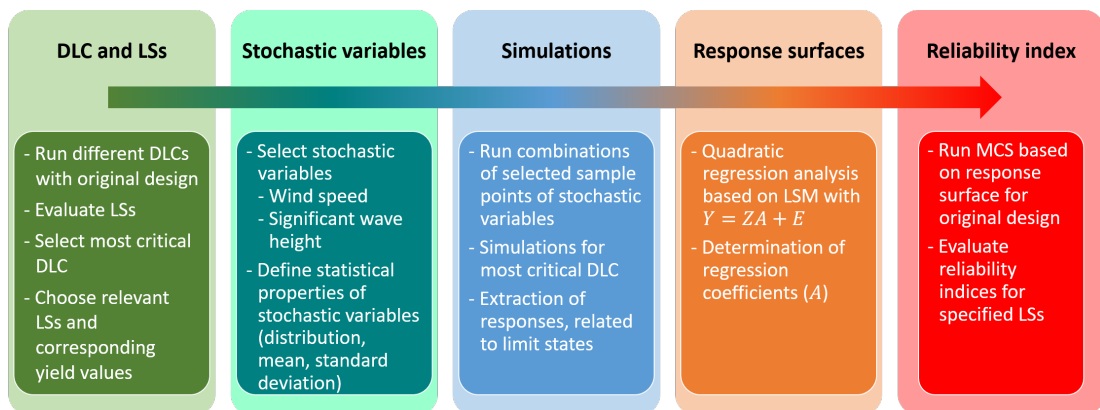


Figure 6.2: Pre-processing level one flowchart for elaborating the approach and boundary conditions for the reliability assessment of one specific system.

6.2.1.1 Determination of DLCs, LSs, and stochastic variables

The reliability assessment of the floating wind turbine system to be optimized is done for a specific DLC, focusing on certain LSs, and considering uncertainties through stochastic variables. The LSs are selected based on the defined objective functions (Section 6.1.2) and specified in Section 6.1.3. The selection procedure for choosing a critical environmental condition is presented in Section 6.1.4. For this, fully-coupled system simulations are required, as already mentioned. These are performed automatically and in parallel utilizing the MoWiT-Dymola[®]-Python framework described in Section 4.2.1.4. As the evaluation of the system response in a DLC is based on ten-minute time series, each DLC simulation is run for 800 s, which allows for sufficient (200 s) pre-simulation time, in which any initial transients have already decayed.

The final post-processing, in which the maximum occurring values for the parameters of interest (system performance and LSs) are extracted from the time series, is, hence, always based on the last 600 s.

Based on the found critical DLC, the stochastic variables V and H_s and their statistical properties are defined in Section 6.1.5. As not all possible combinations of the stochastically distributed wind speed and significant wave height can be elaborated in the subsequent reliability assessment, sample points for which the reliability analysis shall be performed have to be specified. As the wind speed follows a non-normal distribution (Section 6.1.5.1), five sample points of the stochastic variable are taken from the 5th to 95th percentile range⁴ and, additionally, directly the mean value, as the distribution is not symmetric. All selected sample points for the stochastic variable V are presented in Table 6.7.

Table 6.7: Sample points of the stochastic variable wind speed.

Statistical parameter	Wind speed
5th percentile	4.2 m/s
25th percentile	8.0 m/s
50th percentile	11.2 m/s
Mean value	11.4 m/s
75th percentile	14.5 m/s
95th percentile	19.4 m/s

For the significant wave height for SSS, which is as well non-normal distributed (Section 6.1.5.2), the sample points are again composed by five values taken from the 5th to 95th percentile range⁵, as well as the mean value. The corresponding peak period T_p is determined - as done in the DLC specification and explained in detail in Section 5.1.4.1 - according to Equation 5.6. This uses the upper bound of the peak period range specified in the IEC standard 61400-3 (IEC 2009) in order to realize a peak-shape parameter which is as close as possible to one, as discussed in Section 5.1.4.1. This, namely, reflects a Pierson-Moskowitz spectrum, which follows the concept of a fully developed sea - what is the condition at such a far offshore and deep water site as considered for the location of the spar-buoy FOWT system (Section 6.1.5). The selected sample points for the stochastic variable H_s and the corresponding peak periods are summarized in Table 6.8.

⁴The corresponding mathematical derivation is presented in Appendix F in Equation F.6.

⁵The corresponding mathematical derivation is presented in Appendix G in Equation G.8.

Table 6.8: Sample points of the stochastic variable significant wave height.

Statistical parameter	Significant wave height	Peak period
5th percentile	9.8 m	14.3 s
25th percentile	10.5 m	14.8 s
50th percentile	11.2 m	15.3 s
Mean value	11.4 m	15.4 s
75th percentile	12.0 m	15.8 s
95th percentile	13.5 m	16.8 s

6.2.1.2 Evaluation of reliability index

The reference FOWT system (Section 3.2) is simulated according to the determined critical DLC (Section 6.1.4), however, replacing the values for wind speed and significant wave height (as well as peak period) by any combination of the selected sample points of the two stochastic variables (Section 6.2.1.1). Thus, a total of 36 simulations (each of 800 s simulation length) are performed and the system responses related to the specified LSs (Section 6.1.3) are extracted from the last 600 s (excluding any transients within the first 200 s of the simulation) - similarly as done in the DLC simulations and described in Section 6.2.1.1. Through the 36 values for each LS parameter, a response surface is developed by means of a quadratic regression analysis based on the least squares method (LSM) (Shittu et al. 2020, Kolios et al. 2018, Kolios 2010, Choi et al. 2007). The quadratic regression model of the considered case, with

- a 36 x 4 matrix Y , containing the values for each LS parameter at all simulated stochastic variables combinations;
- a 36 x 5 matrix Z of $[1 \ V \ V^2 \ H_s \ H_s^2]$ for each of the 36 simulated combinations;
- a 5 x 4 matrix A , containing the regression coefficients $[a_0 \ a_1 \ a_2 \ a_3 \ a_4]^T$ for each LS parameter; and
- the 36 x 4 error matrix E ,

is expressed in Equation 6.5.

$$Y = ZA + E \quad (6.5)$$

The regression coefficients for each LS parameter, contained in the matrix A , are derived following Equation 6.6.

$$A = \left(Z^T \cdot Z \right)^{-1} \cdot Z^T \cdot Y \quad (6.6)$$

SRSM is commonly used as basis for analytical - using FORM or SORM - or stochastic - using MCS or other sampling methods - reliability analyses for determining the reliability in-

dex, as pointed out in Section 2.1.3.2. FORM and SORM come with a similar affordable computational effort independent on the resulting failure probability, while MCS becomes more and more computationally expensive when aiming to accurately cover larger and larger probabilities of failure. However, the failing convergence of the iterative calculations within the HL-RF (Hasofer Lind - Rackwitz Fiessler) method - an extension of the HL approach for dealing as well with non-normal distributed stochastic variables, which are transformed at first into equivalent normal distributions (Choi et al. 2007, Rackwitz & Flessler 1978) - applied within FORM, is a widely discussed issue that appears for specific conditions, such as nonlinear LS functions or complicated phenomena (Huang et al. 2017a, Makhduomi et al. 2017, Ramesh et al. 2017, Keshtegar & Miri 2013, Yang et al. 2006, Zhang & Kiureghian 1995), as well as the herein considered RBDO problem. Thus, it is decided to directly use MCS in combination with SRSM. Applying the response surfaces, which are already derived, means that no more system simulations are required. Just more computational effort for the MCS - namely, evaluating Equation 6.5 for a certain number r of random samples of V and H_s - is needed, depending on the order of magnitude of r . Based on a rule of thumb, r should be one or two orders of magnitude higher than the probability of failure that shall be covered accurately enough. As the limit for an acceptable reliability index is 3.719, as derived in Section 6.1.6, which corresponds to a probability of failure of 1×10^{-4} , r is set equal to 1×10^6 , which sufficiently captures the limit for an acceptable reliability index (including as well some higher values) and at the same time comes with a reasonable computational effort, as Equation 6.5 can be evaluated for 1×10^6 different Z -matrices in just about half a minute on a conventional computer.

Thus, each 1×10^6 random values for wind speed and significant wave height are generated, based on their distribution type and statistical coefficients given in Tables 6.4 and 6.5, respectively. Performing the MCS by solving Equation 6.5 with a now $10^6 \times 5$ Z -matrix, covering the random set of the stochastic variables, and counting for each LS parameter all events j , in which the specified limit for the LS parameter (Section 6.1.3) is exceeded, the reliability index for each LS parameter is derived according to Equation 6.7, with the inverse of the normal cumulative density function Φ^{-1} .

$$\beta = \Phi^{-1} \left(1 - \frac{j}{r} \right) \quad (6.7)$$

This yields infinite (meaning zero failure events) for all LS parameters, which is because of the very safe distance between the obtained maximum values for the LS parameters in the system simulations and the allowable limits specified in Section 6.1.3. This is already noticeable in the initial DLC simulations presented in Table 6.3 and gets more clear when comparing the limit values with the maximum values obtained from the 36 simulations for the sample points of the stochastic variables, as presented in Table 6.9.

A reduction of the allowable maximum values to for example 225.00 MPa for σ_{TB} and 230.00 MPa for σ_{MLi} proves with reliability index values between 2.74 and 4.47 the approach and sufficient order of magnitude of r . Even if the stress in the mooring lines is expected not to become critical to the specified limit when changing the FOWT design during the sub-

sequent RBDO (Section 6.2.3), the bending stress at the tower base could become critical to the reliability index limit, as larger stresses are expected for higher system inclination angles. The considered DLC and specified statistical properties of the stochastic variables are, hence, judged as realistic and appropriate for the defined application example.

Table 6.9: Comparison of the limit values and the maximum LS parameter values obtained from the 36 stochastic simulations.

Limit state parameter	Maximum value	Limit value	β
σ_{TB}	218.79 MPa	262.96 MPa	∞
σ_{ML1}	148.69 MPa	768.73 MPa	∞
σ_{ML2}	196.80 MPa	768.73 MPa	∞
σ_{ML3}	215.58 MPa	768.73 MPa	∞

6.2.2 Pre-processing level two

Integrating reliability assessment into design optimization, which is of iterative nature, requires some additional investigations on how the reliability index for each single system design appearing within an optimization algorithm can be determined in an efficient manner. Performing 36 simulations for the sample points of the stochastic variables - as done in Section 6.2.1.2 with the original FOWT system - but now with each individual design obtained in an iterative RBDO process, would make the total number of simulations and the required computational effort skyrocket and, hence, is definitely not the most efficient way to assess the reliability of each of these FOWT system designs. Thus, in this concept, response surfaces - on which basis the reliability index can be determined, as already presented in Figure 6.2 and described in Section 6.2.1.2 - are generated for a limited number of floating system designs lying within the optimization design space. The obtained regression coefficient sets, which each define a system-specific response surface, build the basis for an interpolation approach, used later on during the iterative optimization algorithm in order to determine the regression coefficients - and based on these perform the reliability assessment - of each single system design appearing within the optimization algorithm. The steps for generating various response surfaces in the optimization design space are presented in Figure 6.3 and described in more detail in Sections 6.2.2.1 and 6.2.2.2. Furthermore, the derivation and quality assessment of the interpolation approach, which serves as time- and computationally efficient method for the reliability assessment within the iterative RBDO, are detailed in Section 6.2.2.3.

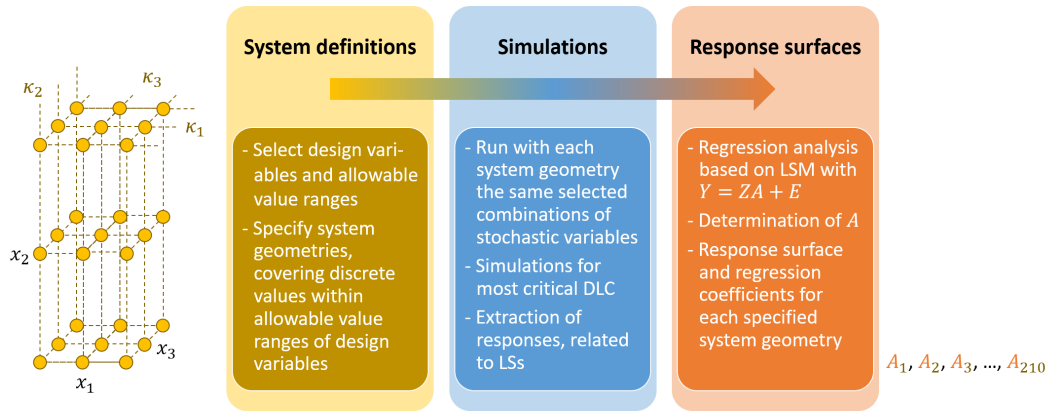


Figure 6.3: Pre-processing level two flowchart for generating response surfaces in the optimization design space.

6.2.2.1 Definition of discrete floater geometries in the design space

During the RBDO, the FOWT system designs can vary within the allowable value ranges of the design variables, as specified in Section 6.1.1. Within this optimization design space, for each optimization variable five discrete values, evenly spaced in the corresponding allowable value range, are selected, as well as the original system parameter value if not yet included. This leads to five values for the base column diameter, five values for the base column height, and six values for the ballast density, as presented in black in Table 6.10. Thus, combining all discrete values for the optimization variables with each other, 150 system geometries are selected.

Table 6.10: Discrete values of the design variables for the selected floater geometries in the optimization design space, initial selection in black, further added values in red.

Base column diameter x_1 [m]					
6.5	7.225	7.95	8.675	9.4	
Base column height x_2 [m]					
8.0	33.0	45.5	58.0	70.5	83.0 108.0
Ballast density x_3 [kg/m ³]					
1281	1610.75	1907	1940.5	2270.25	2600

6.2.2.2 Generation of response surfaces

For each of the 150 system geometries, specified in Section 6.2.2.1, simulations for all 36 combinations of the sample points of the stochastic variables (Section 6.2.1.1) for the selected critical DLC condition (Section 6.1.4) are performed and the maximum values for the specified

LS parameters (Section 6.1.3) extracted from the time series (again between 200 s and 800 s). Following the approach described in Section 6.2.1.2, response surfaces and the corresponding regression coefficients are derived for each system geometry. As, however, not all combinations of the discrete optimization variables yield stable FOWT designs, it is not striking that some simulations fail due to bad system performance and do not complete the total 800 s simulation time. These failing designs are excluded and the regression coefficients are just set to NaN (not a number).

Analyzing the results, it is noted that none of the FOWT systems with a base column height of either 8.0 m or 33.0 m is stable and still for base column heights of 58.0 m and 83.0 m several system simulations fail when combined with low base column diameters and low ballast densities. Thus, two more discrete values for the base column height are added, presented in red in Table 6.10, recombined with the other two design variables, simulated, and evaluated. This way, the separation area between stable and failing FOWT system designs is narrowed down and a total of 72 successfully simulated designs are obtained, while 138 show unstable behavior.

Overall, 210 system geometries are considered and a total of 7,560 simulations are performed. Utilizing the MoWiT-Dymola[®]-Python framework, this takes about 185 hours on an AMD Ryzen Threadripper 2990WX 32-Core Processor with 64-bit system and using all of its 64 virtual processors for parallel execution of the simulations.

In order to prove that the quadratic regression analysis with $Z = [1 \ V \ V^2 \ H_s \ H_s^2]$ is sufficient, the responses (Y) are re-computed based on the determined regression coefficients (Equation 6.5) and compared - by means of the coefficient of determination R^2 - with the maximum values obtained directly from the system simulations. This comparison can only be done for the 72 successfully simulated system geometries. For all those corresponding 288 LS parameter results, except for three, R^2 values of at least 0.96 (mostly even above 0.99) are obtained. This proves that the selected quadratic regression analysis approach is sufficient for the considered system and problem.

6.2.2.3 Interpolation of response surfaces for arbitrary floater geometries in the design space

During the optimization, the design variables can take on any value within the allowable value ranges in any combination with each other. The system geometries for which response surfaces are generated, however, are just 210 discrete combinations of five (κ_1), six (κ_3), and seven (κ_2) values for the design variables. In order to interpolate the regression coefficients of the pre-simulated system geometries for any geometry appearing during the optimization, first, the closest neighbors of a design χ in the optimization design space have to be found. In the three-dimensional space - defined through the three design variables - these are eight (2^3) neighbors, as indicated in Figure 6.4.

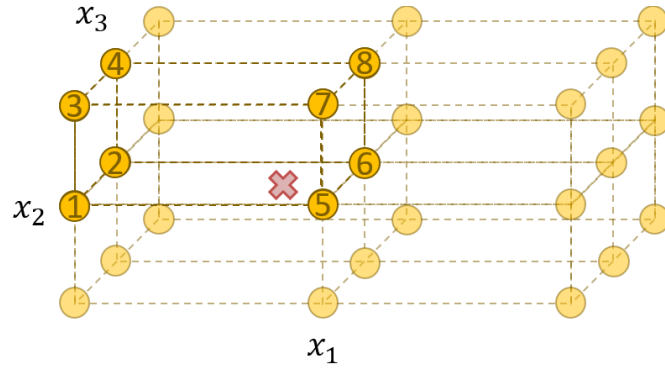


Figure 6.4: Eight closest neighbors of design χ in the optimization design space.

For each design variable, the values of the left ($x_{i,\text{left}}$) and right ($x_{i,\text{right}}$) neighbors (smaller and larger compared to the value of design χ) are determined according to Equation 6.8⁶ for the base column diameter, as well as Equations 6.9⁶ and 6.10⁶ for the base column height and ballast density, respectively, including case distinctions due to the different spacing (Δ) between the discrete values. To find the closest discrete value out of the values listed in Table 6.10 and collated in vectors \vec{x}_1 , \vec{x}_2 , and \vec{x}_3 , the function `nearest`, described in Appendix H, is utilized.

$$\begin{aligned} \Delta_1 &= 0.725 \text{ m} \\ x_{1,\text{left}} &= \text{nearest} \left(\vec{x}_1, 6.5 \text{ m} + \Delta_1 \text{floor} \left(\frac{x_{1,\chi} - 6.5 \text{ m}}{\Delta_1} \right) \right) \\ x_{1,\text{right}} &= \text{nearest} (\vec{x}_1, x_{1,\text{left}} + \Delta_1) \end{aligned} \quad (6.8)$$

if ($(x_{2,\chi} \geq 33 \text{ m})$ and $(x_{2,\chi} < 83 \text{ m})$) :

$$\Delta_2 = 12.5 \text{ m}$$

else :

$$\Delta_2 = 25 \text{ m} \quad (6.9)$$

$$x_{2,\text{left}} = \text{nearest} \left(\vec{x}_2, 8.0 \text{ m} + \Delta_2 \text{floor} \left(\frac{x_{2,\chi} - 8.0 \text{ m}}{\Delta_2} \right) \right)$$

$$x_{2,\text{right}} = \text{nearest} (\vec{x}_2, x_{2,\text{left}} + \Delta_2)$$

⁶As the interpolation approach is utilized within the iterative optimization algorithm (Section 6.2.3.2) performed by means of the MoWiT-Dymola[®]-Python framework, the equations are presented in Python coding style and the Python function `floor` from the `math` module is utilized for rounding a value to the closest integer, which is less than or equal to the input value.

$$\begin{aligned}
& \text{if} \left(\left(x_{3,\chi} \geq 1,610.75 \frac{\text{kg}}{\text{m}^3} \right) \text{ and } \left(x_{3,\chi} < 1,907 \frac{\text{kg}}{\text{m}^3} \right) \right) : \\
& \quad \Delta_3 = 296.25 \frac{\text{kg}}{\text{m}^3} \\
& \quad x_{3,\text{left}} = 1,610.75 \frac{\text{kg}}{\text{m}^3} \\
& \text{elif} \left(\left(x_{3,\chi} \geq 1,907 \frac{\text{kg}}{\text{m}^3} \right) \text{ and } \left(x_{3,\chi} < 1,940.5 \frac{\text{kg}}{\text{m}^3} \right) \right) : \\
& \quad \Delta_3 = 33.5 \frac{\text{kg}}{\text{m}^3} \\
& \quad x_{3,\text{left}} = 1,907 \frac{\text{kg}}{\text{m}^3} \\
& \text{else} : \\
& \quad \Delta_3 = 329.75 \frac{\text{kg}}{\text{m}^3} \\
& \quad x_{3,\text{left}} = \text{nearest} \left(\vec{x}_3, 1,281 \frac{\text{kg}}{\text{m}^3} + \Delta_3 \text{floor} \left(\frac{x_{3,\chi} - 1,281 \frac{\text{kg}}{\text{m}^3}}{\Delta_3} \right) \right) \\
& \quad x_{3,\text{right}} = \text{nearest} (\vec{x}_3, x_{3,\text{left}} + \Delta_3)
\end{aligned} \tag{6.10}$$

In the next step, the position of design χ with respect to its eight neighbors is determined in terms of factors λ_1 , λ_2 , and λ_3 as fraction of the distances between the surrounding neighbors, as given in Equation 6.11 generalized for design variable i .

$$\lambda_i = \frac{x_{i,\chi} - x_{i,\text{left}}}{\Delta_i} \tag{6.11}$$

Based on these factors, weights w_{P_i} are calculated for the neighboring points P_1 to P_8 based on the closeness of the neighbors to design χ . The weights are determined according to Equation 6.12 for the numbering of the neighbors indicated in Figure 6.4.

$$\begin{aligned}
w_{P_1} &= (1 - \lambda_1)(1 - \lambda_2)(1 - \lambda_3) \\
w_{P_2} &= (1 - \lambda_1)(1 - \lambda_2)\lambda_3 \\
w_{P_3} &= (1 - \lambda_1)\lambda_2(1 - \lambda_3) \\
w_{P_4} &= (1 - \lambda_1)\lambda_2\lambda_3 \\
w_{P_5} &= \lambda_1(1 - \lambda_2)(1 - \lambda_3) \\
w_{P_6} &= \lambda_1(1 - \lambda_2)\lambda_3 \\
w_{P_7} &= \lambda_1\lambda_2(1 - \lambda_3) \\
w_{P_8} &= \lambda_1\lambda_2\lambda_3
\end{aligned} \tag{6.12}$$

The weights are used to interpolate the regression coefficients of each neighboring point A_{P_i} , following Equation 6.13, to obtain the regression coefficients A_χ for defining the response surface of design χ . Within this calculation it is checked whether the regression coefficients of any neighbor is NaN to ensure that only numeric values are added up. In case that all eight neighbors fail in the system simulations, a zero vector is assigned to the regression coefficients

of design χ , which is later on (Section 6.2.3.2) utilized for excluding such designs from the set of potential satisfying solutions.

$$A_{\chi} = \sum_{i=1}^8 w_{P_i} A_{P_i} \quad (6.13)$$

To verify the accuracy of the applied interpolation approach, 32 control points - as given in Table 6.11 - are defined, for which in each case the 36 system simulations for the sample points of the stochastic variables are performed. A couple of these control points are selected to lie in between the discrete values of one design variable, while matching a specified discrete value of the other two design variables, and some further are completely between the grid points defined by the discrete values of the design variables.

Table 6.11: Control design geometries for verifying the accuracy of the interpolation approach.

$x_2 = 108.0 \text{ m}$ and $x_3 = 1,907 \text{ kg/m}^3$						
x_1 [m]	6.8625	7.0	7.7	8.3125	9.3	
$x_2 = 83.0 \text{ m}$ and $x_3 = 2,600 \text{ kg/m}^3$						
x_1 [m]	7.5875	8.2		9.0375		
$x_1 = 9.4 \text{ m}$ and $x_3 = 1,907 \text{ kg/m}^3$						
x_2 [m]	51.75	62.0	76.75	106.0		
$x_1 = 8.675 \text{ m}$ and $x_3 = 2,600 \text{ kg/m}^3$						
x_2 [m]	57.0	64.25	80.0	95.5		
$x_1 = 9.4 \text{ m}$ and $x_2 = 108.0 \text{ m}$						
x_3 [kg/m ³]	1,445.875	1,850	1,923.75	2,200	2,435.125	
$x_1 = 8.675 \text{ m}$ and $x_2 = 83.0 \text{ m}$						
x_3 [kg/m ³]	1,300	1,758.875	1,935	2,105.375	2,500	
Further combinations						
x_1 [m]	9.0375	9.3	7.0	8.3125	8.2	7.7
x_2 [m]	62.0	95.5	106.0	76.75	80.0	95.5
x_3 [kg/m ³]	2,500	1,300	1,850	1,923.75	1,758.875	2,200

For these 32 control points, from which just one system design fails during the simulations, the regression coefficients are calculated based on the above presented interpolation approach. First, again the coefficient of determination is computed for the simulation results and the quadratic regression analysis results (Equation 6.5). The 124 LS parameter results corresponding to the 31 successful control design geometries score higher than 0.99, except for two with a minimum R^2 of 0.97. Due to these very high values for the coefficient of determination, the comparison of the interpolated results with the values obtained directly from the simulations yields similar values to the comparison of the interpolated results with the quadratic regression analysis results. This yields for just six out of 124 LS parameter results a R^2 value below 0.9, however, of minimum 0.84. The affected designs lie on the margins of the design space or the separation area between stable and failing FOWT system designs, for which the interpolation is less accurate - but still very good - due to some NaN values, which are excluded from the regression coefficients calculation. Overall, the presented interpolation approach proves to be of very high precision and, thus, can be applied for determining the regression coefficients of the individual system designs appearing within the highly iterative optimization approach.

6.2.3 RBDO process

Based on the pre-processing done in Sections 6.2.1 and 6.2.2, now the actual task can be addressed. The RBDO is performed with the reference FOWT system described in Section 3.2 for the optimization problem (design variables, objective functions, and optimization constraints) specified in Section 6.1 and implying the selected LSs, stochastic variables, and reliability criteria. In addition to the optimization problem, also an optimizer needs to be chosen (Section 6.2.3.1) and the iterative RBDO algorithm has to be defined (Section 6.2.3.2), incorporating the reliability assessment based on the beforehand derived response surfaces in the optimization design space and the interpolation approach described in Section 6.2.2. The overall interaction between the components of the RBDO approach is shown in Figure 6.5.

6.2.3.1 Selection of the optimizer

Based on previous comparisons of different optimizers and the experience from and application in other design optimization tasks, presented in Chapter 5, the same optimizer as utilized for the DDO example (Section 5.1), on which this RBDO application is based, is selected: NSGAII from Platypus.

In the DDO approach 36 individuals and a total of 2,011 simulations are considered for the MO optimizer and show good convergence, as defined in Section 5.1.3.2 and presented in Section 5.1.4. As, however, the present RBDO task is much more complex and heavily constrained, the total number of simulations is significantly increased and set equal to 10,000, as already applied in the design optimization of an advanced spar-type floater (Section 5.2.3.2). The number of individuals in each generation is as well enlarged and set equal to 60, based on the available processors on the utilized computational machine (an AMD Ryzen Threadripper

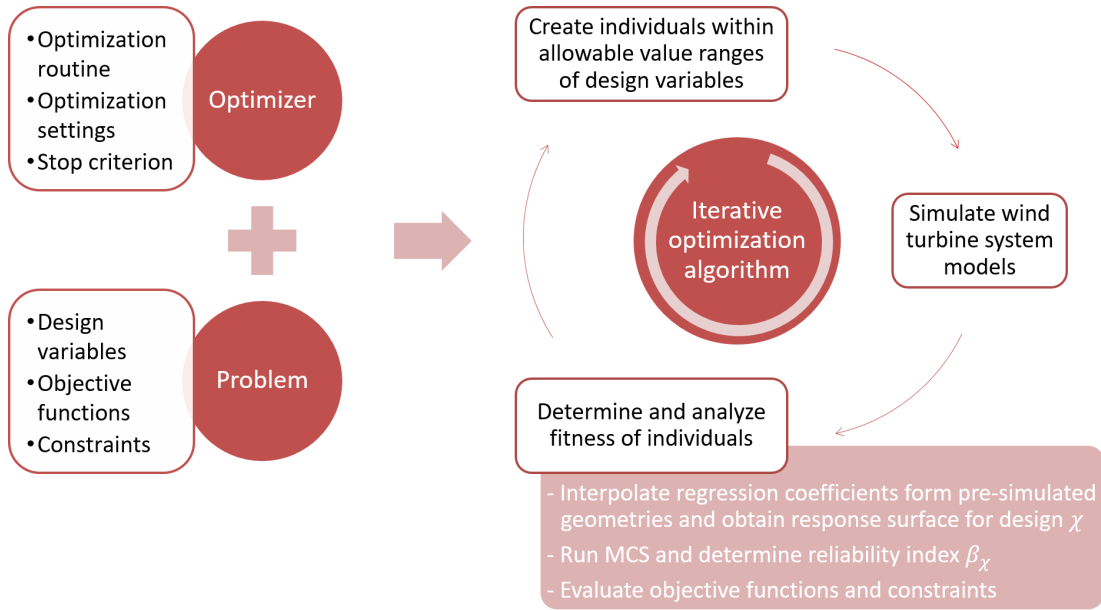


Figure 6.5: Flowchart of the RBDO approach, including its components and their interaction.

2990WX 32-Core Processor with 64-bit system and 64 virtual processors), so that parallel simulation of the individuals in one generation is feasible.

6.2.3.2 Specification of the iterative RBDO algorithm

The iterative optimization algorithm for the considered RBDO problem, performed with NS-GAII and integrated into the MoWiT-Dymola[®]-Python framework, works as follows (Figure 6.5).

0. The start population (individuals of generation 0) are selected purely based on the specified allowable value ranges for the design variables, given in the inequality constraints g_1 to g_6 (Table 6.6).
1. Each individual wind turbine system model is simulated for the specified critical DLC (Section 6.1.4) for a period of 800 s, using Rkfix4 as solver with fixed integrator step-size of 0.01 s, and the system parameters are written in an .csv-file with an output interval length of 0.05 s.
2. From the last 600 s (discarding any transients in the first 200 s) of the time series, the maximum values for the system performance parameters (l_{tot} , $a_{hor,nacelle}$, $s_{dyn,transl}$, $s_{mean,transl}$) and the LS parameters (σ_{TB} , σ_{ML1} , σ_{ML2} , σ_{ML3}) are extracted and used for evaluating the objective functions f_1 to f_3 (Table 6.2), as well as the inequality constraints g_7 to g_{10} and g_{15} to g_{18} (Table 6.6). For g_{11} to g_{14} , first, the regression coefficients for the specific individual design and the four LS parameters are determined according to the interpolation approach (Section 6.2.2.3), based on which afterwards the reliability indices are calculated by means of MCS (Section 6.2.1.2) and then substituted in the corresponding inequality constraints.

3. A new set of individuals for the next generation is created by the optimizer, based on the fitness (performance with respect to objective functions and inequality constraints) of the individuals in the current generation and again in accordance with the allowable value ranges for the design variables.
4. Steps 1. to 4. are iterated until the specified maximum number of simulations (10,000) is reached.

As already addressed in Section 6.2.2, some FOWT system geometries might fail and not complete the total simulation time. For these unstable system designs, the evaluation of the objective functions and inequality constraints (step 2.) is addressed in a different way. As such poorly performing individuals shall not be considered by the optimizer for any further recombination, the values for the system performance parameters and LS parameters for evaluating f_1 to f_3 (Table 6.2), g_7 to g_{10} , and g_{15} to g_{18} (Table 6.6) are set to the following undesirable values:

- $\max(t_{\text{tot}}) |_{\text{failing system}} = 2 \cdot 10.0^\circ = 20.0^\circ$
- $\max(a_{\text{hor,nacelle}}) |_{\text{failing system}} = 2 \cdot 1.962 \text{ m/s}^2 = 3.924 \text{ m/s}^2$
- $\max(s_{\text{dyn,transl}}) |_{\text{failing system}} = -1 \text{ m}$
- $s_{\text{mean,transl}} |_{\text{failing system}} = 2 \cdot 64.0 \text{ m} = 128.0 \text{ m}$
- $\max(\sigma_{\text{TB}}) |_{\text{failing system}} = 2 \cdot 262.96 \text{ MPa} = 525.93 \text{ MPa}$
- $\max(\sigma_{\text{ML1}}) |_{\text{failing system}} = 2 \cdot 770.26 \text{ MPa} = 1540.53 \text{ MPa}$
- $\max(\sigma_{\text{ML2}}) |_{\text{failing system}} = 2 \cdot 770.26 \text{ MPa} = 1540.53 \text{ MPa}$
- $\max(\sigma_{\text{ML3}}) |_{\text{failing system}} = 2 \cdot 770.26 \text{ MPa} = 1540.53 \text{ MPa}$

For the calculation of the reliability index, MCS based on the interpolated regression coefficients is as well not performed in case of an incomplete time series. In this case, $\beta = 0$ is set for all LS parameters for the failing system design. This is an undesirable value for the reliability index and ensures that the corresponding inequality constraints g_{11} to g_{14} (Table 6.6) are violated. Setting all regression coefficients to zero if all eight neighboring designs fail in the system simulations, as mentioned in Section 6.2.2.3, leads to the same result.

Another particularity - when evaluating the reliability criteria - has to be addressed, namely the case that MCS yields infinite for the reliability index, what already happens in the evaluation of the reliability index of the original design of the reference FOWT system (Section 6.2.1.2). This is an indicator that the maximum value occurring in the time series of the LS parameter is much below the specified limit value and, hence, the corresponding reliability index value cannot be captured by the chosen amount of random samples ($r = 1 \times 10^6$). As the formal expressions for g_{11} to g_{14} , as given in Table 6.6, can only be evaluated with a real number, in these cases, where MCS yields infinite for the reliability index, $\beta = 2 \cdot 3.719 = 7.438$ is set instead, ensuring full compliance with the inequality constraints g_{11} to g_{14} .

6.3 Results of the RBDO of the spar-type floating support structure

During the RBDO execution, two interruptions - due to system shutdown and grid disconnection - occur. To continue the highly time-consuming iterative RBDO, the last fully simulated generation is used as start population of the next run, utilizing from Platypus the operator `InjectedPopulation`. The effective time for all 10,000 simulations, excluding the duplicate generations at the point of continuation, amounts about 695 hours. Individuals of generations 0 up to including 171 are created, while in the last generations not all 60 individuals yet exist.

6.3.1 Progression within the iterative RBDO process

The design variables of all individuals created and simulated within the RBDO are presented in Figure 6.6. This shows that at the beginning, the optimizer utilizes the entire design space, defined through the allowable value ranges of the design variables as specified in the inequality constraints g_1 to g_6 declared in Table 6.6, to select individuals. This large spread, however, diminishes in the further generations - very fast for the base column height, a bit slower for the base column diameter, and after around 20 to 30 generations also for the ballast density. It is interesting to see that, for the base column height and ballast density, the individuals in the end tend to cluster around the original value of the reference FOWT system, while the base column diameter approaches a much lower value compared to the original one.

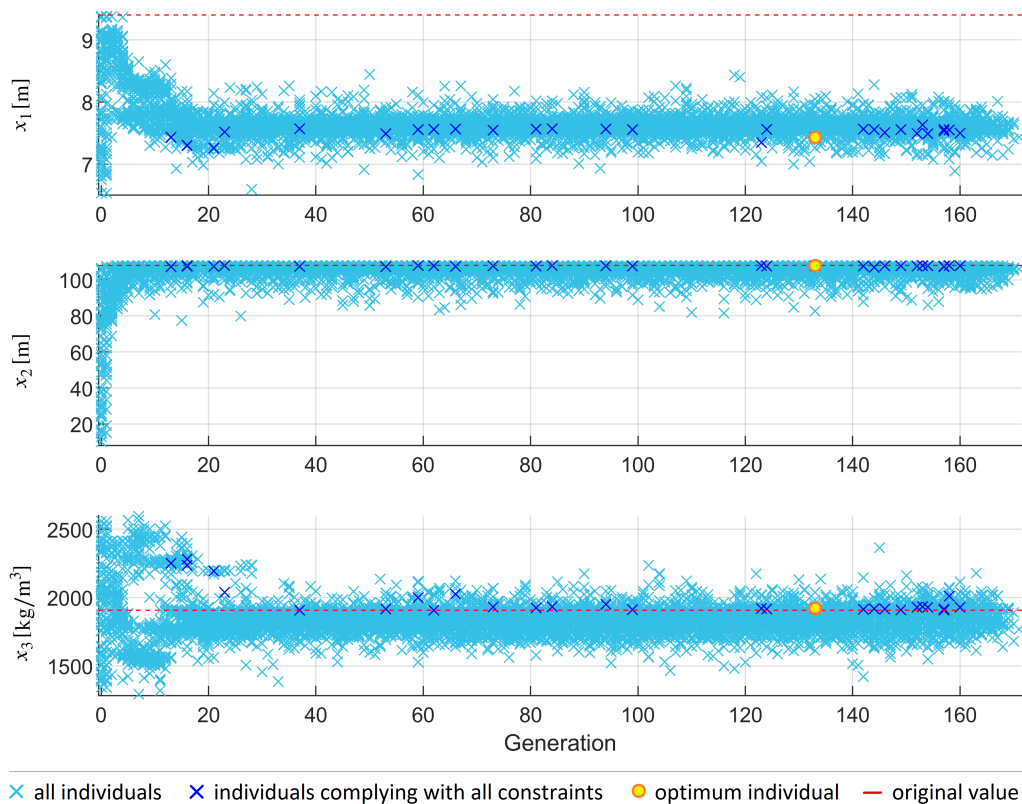


Figure 6.6: Development of the design variables throughout the iterative RBDO approach.

Similarly, Figures 6.7 to 6.9 present the resulting values of all individuals for the inequality constraints g_7 to g_{18} . The critical performance parameters are clearly the total inclination angle and horizontal nacelle acceleration, while both dynamic and mean translational motion values always - apart from some failing individuals in generations 0 and 1 - comply with the constraints, as visible in Figure 6.7. Looking at the reliability criteria (Figure 6.8) and the maximum allowable stresses (Figure 6.9), it becomes clear that both constraints are connected, as they all depend on the maximum stress values obtained. Thus, in both cases, the stress in the mooring lines is highly safe, what is already perceived in Section 6.2.1.2, while the tower base bending stress exceeds for some individuals the maximum allowable target.

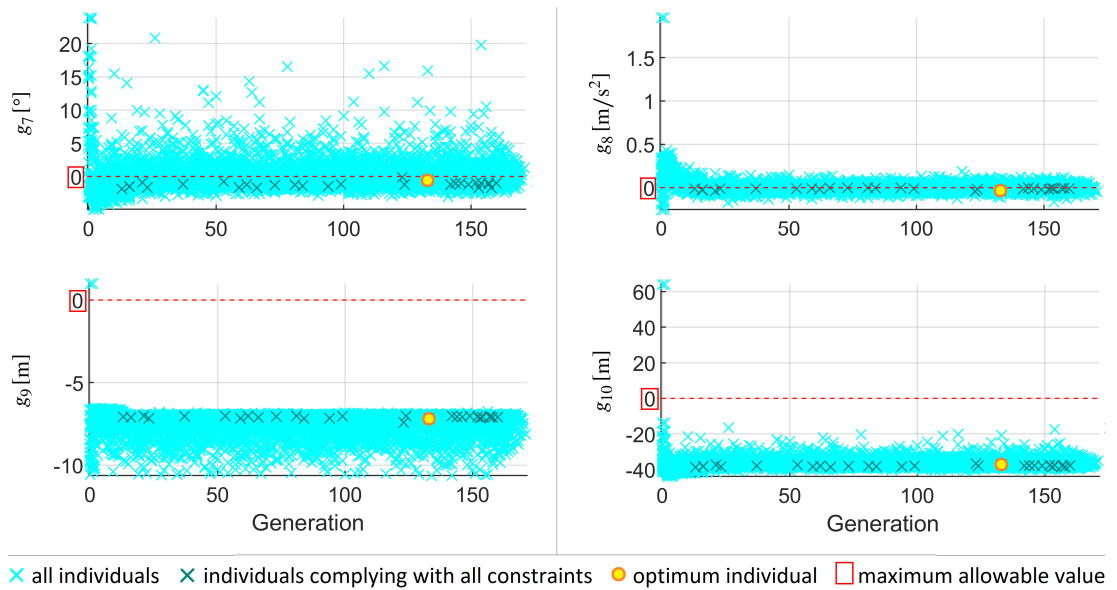


Figure 6.7: Development of the performance constraints throughout the iterative RBDO approach.

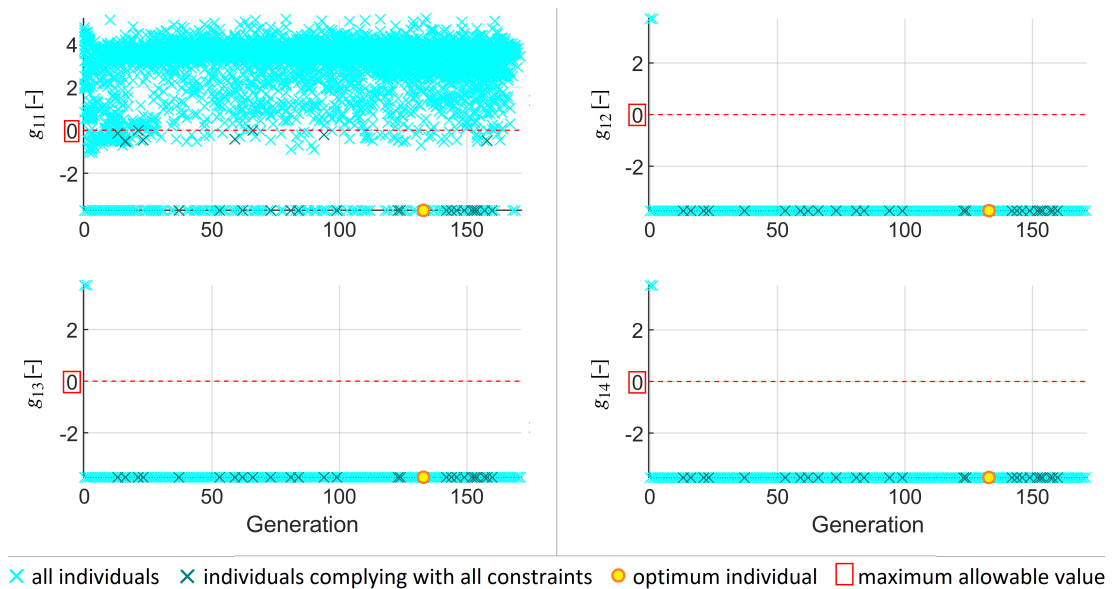


Figure 6.8: Development of the reliability constraints throughout the iterative RBDO approach.

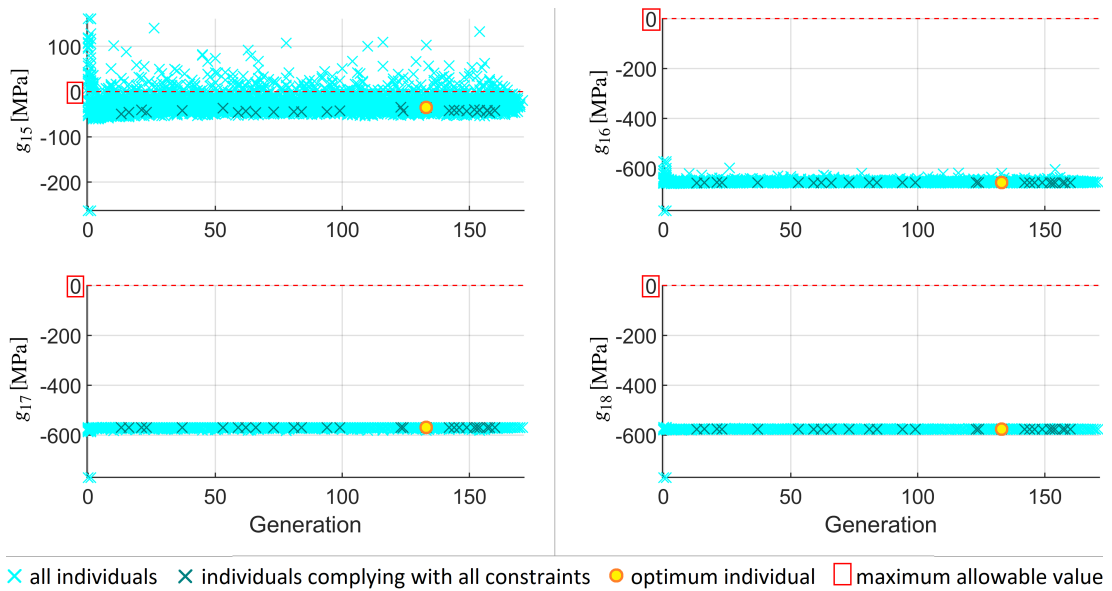


Figure 6.9: Development of the constraints on the maximum stresses throughout the iterative RBDO approach.

Finally, the development of the objective functions throughout the iterative RBDO process is presented in Figure 6.10. The largest spread in the results is as well perceived in the first generations. Most of the individuals score better in the total inclination angle objective (f_1)

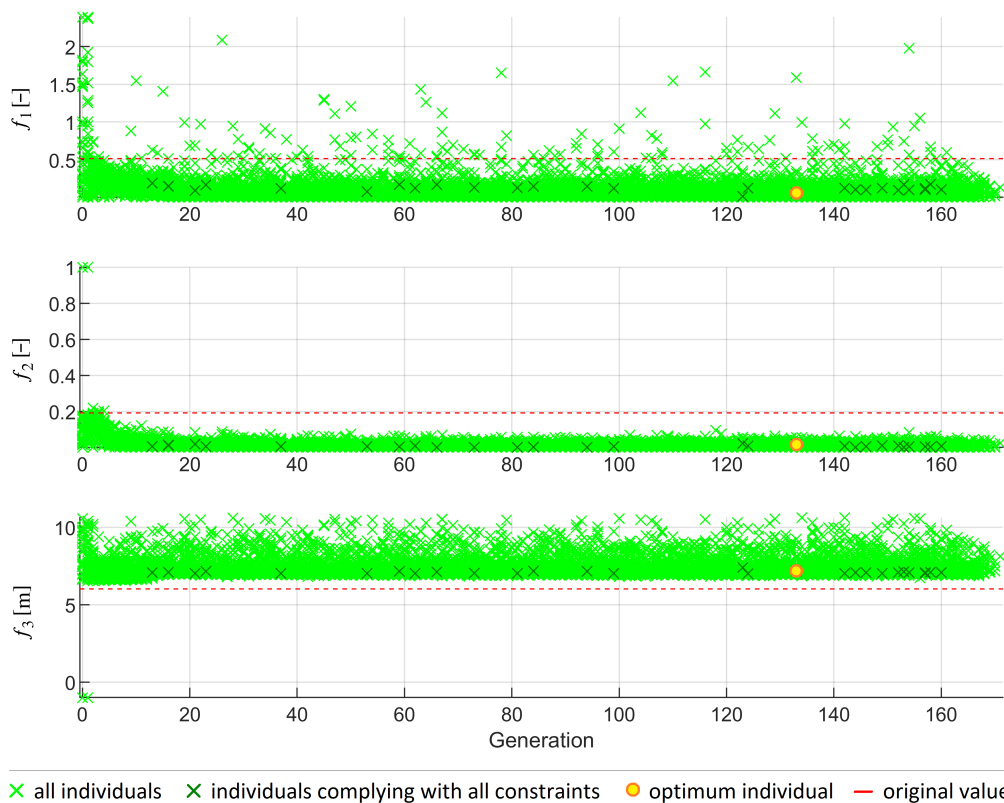


Figure 6.10: Development of the objective functions throughout the iterative RBDO approach.

than the original design. For the horizontal nacelle acceleration objective (f_2), the value is significantly reduced compared to the objective function result of the original reference FOWT system. Only the resulting value for the dynamic translational motion objective (f_3) is slightly increased compared to the original floating system.

6.3.2 Selection of the optimized FOWT system design solution

To select the optimized FOWT system design solution from the 10,000 simulated individuals, first, the individuals that violate one or more constraints have to be excluded from the further analyses. These individuals that comply with all constraints at the same time are indicated in the development plots (Figures 6.6 to 6.10) by darker-colored crosses. In the first generations no individual meets all requirements, but from generation 13 on some individuals can fulfill them. These are just a few at the beginning, but become more and more, especially from generation 140 on.

From these individuals that comply with all constraints, the optimum solution is selected, following a similar approach as applied in the DDO example (Section 5.1.4.3).

1. The utopia - theoretically best possible performing system design - is defined through the minimum value for each objective function, occurring within the individuals that meet all the requirements.
2. The distance of each individual that complies with all constraints to utopia is determined, taking the square root of the sum of squares of the differences between the individual's objective function value and the utopia's one. Here it has to be noted that the difference between the dynamic translation objective function values is normalized by the utopia objective function value to allow comparable weightings of all three objective functions, as the total inclination angle and horizontal nacelle acceleration objective functions are already normalized, as declared for f_1 and f_2 , respectively, in Table 6.2.
3. The individual with the smallest resulting distance to utopia is selected as the optimized FOWT system design solution and is indicated in all presented development plots (Figures 6.6 to 6.10) by means of a yellow filled circle framed in orange.

This design solution is individual 58 of generation 133. A schematic drawing of this RBDO-based optimized design shape is presented in Figure 6.11 in red, together with the original OC3 phase IV reference FOWT indicated in black. The key figures of the optimized design solution in comparison to the original reference FOWT system are set out in Table 6.12.

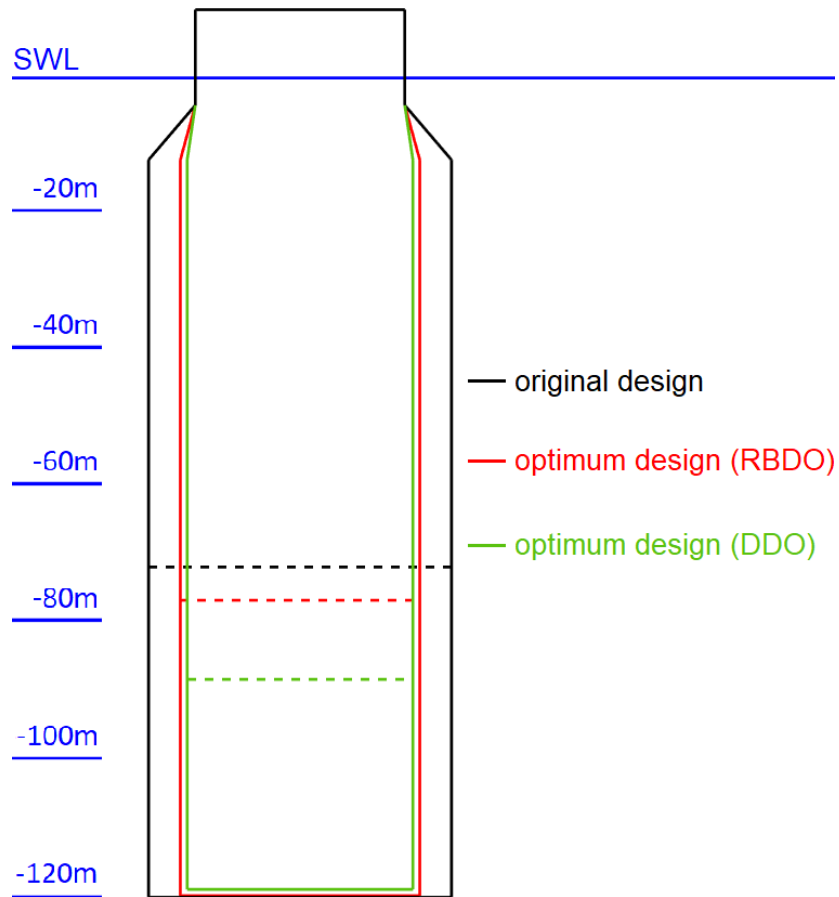


Figure 6.11: Original, RBDO-, and DDO-based optimized design shapes in comparison, ballast heights indicated by dashed lines.

While base column height and ballast density are similar to the original system design, the base column diameter is significantly reduced, what is already reflected by Figure 6.6. The horizontal nacelle acceleration of the original floating system exceeds the specified limit and is now in the optimized design solution below but close to it, while the total inclination angle, which is for the original design just less than half of the defined maximum allowable value, is for the optimized FOWT system as well close but below the limit. The reliability index for all LSs is in both the original and the optimized designs beyond twice the specified minimum required value. While increasing just slightly the considered stresses, the overall structural mass of the floating spar-buoy can be reduced by almost 20% and the ballast mass by around 44%.

Table 6.12: Key figures of the selected RBDO-based optimized design solution in comparison to the original reference FOWT system values.

	Target/allowable value	Optimized design	Original system
D_{BC}	[6.5 m, 9.4 m]	7.4 m	9.4 m
H_{BC}	[8.0 m, 108.0 m]	107.8 m	108.0 m
$\rho_{ballast}$	[1,281 kg/m ³ , 2,600 kg/m ³]	1,921.5 kg/m ³	1,907 kg/m ³
$H_{ballast}$	-	43.3 m	48.4 m
$\max(t_{tot})$	$\leq 10^\circ$	9.4°	4.9°
$\max(a_{hor,nacelle})$	$\leq 1.962 \text{ m/s}^2$	1.930 m/s ²	2.338 m/s ²
$\max(s_{dyn,transl})$	$\geq 0.0 \text{ m}$	7.2 m	6.0 m
$s_{mean,transl}$	$\leq 64.0 \text{ m}$	26.9 m	20.2 m
$\beta(\sigma_{TB})$	≥ 3.719	7.438 (∞)	7.438 (∞)
$\beta(\sigma_{ML1})$	≥ 3.719	7.438 (∞)	7.438 (∞)
$\beta(\sigma_{ML2})$	≥ 3.719	7.438 (∞)	7.438 (∞)
$\beta(\sigma_{ML3})$	≥ 3.719	7.438 (∞)	7.438 (∞)
$\max(\sigma_{TB})$	$\leq 262.96 \text{ MPa}$	228.02 MPa	204.74 MPa
$\max(\sigma_{ML1})$	$\leq 770.26 \text{ MPa}$	113.15 MPa	108.39 MPa
$\max(\sigma_{ML2})$	$\leq 770.26 \text{ MPa}$	200.65 MPa	194.70 MPa
$\max(\sigma_{ML3})$	$\leq 770.26 \text{ MPa}$	194.05 MPa	202.25 MPa
Structural mass	-	$9.30 \times 10^5 \text{ kg}$	$11.50 \times 10^5 \text{ kg}$
Ballast mass	-	$35.43 \times 10^5 \text{ kg}$	$63.16 \times 10^5 \text{ kg}$

6.3.3 Final checks with the optimized FOWT system design solution

Finally, the full DLC set investigated in Section 6.1.4 is simulated and analyzed analogically with the selected RBDO-based optimized FOWT system design solution. Comparing the results from the 54 DLC simulations with the original reference FOWT system (Section 6.1.4), yields the following conclusions.

- t_{tot}

There is a significant shift in the order of criticality of the DLCs. The considered DLC, which is most critical for the original FOWT system, is for the RBDO-based optimized design solution just on position 25. There are in total 13 other environmental conditions - mostly from DLC 1.1 and DLC 1.3 at either 11.4 m/s or 13.0 m/s wind speed - that yield maximum total inclination angle values above the specified limit (10°), with a highest value of 10.8°. Thus, the consequence would be that the optimized FOWT system has to stop operation for these environmental conditions if the limit is strict. This might

affect the overall power output; however, the highest total inclination angle occurring does not lead to an overall instability of the floating system, as already discussed in Sections 5.1.4.3 and 5.1.5.1.

- $a_{hor,nacelle}$

For the original FOWT system there are already two more critical environmental conditions; for the RBDO-based optimized design solution now there are three other DLCs yielding a bit higher maximum horizontal nacelle acceleration. Two of them are exceeding with 1.990 m/s^2 and 1.965 m/s^2 marginally the specified upper limit. As, however, even up to 0.3 times the gravitational acceleration (corresponding to 2.943 m/s^2) are in some applications considered as allowable maximum horizontal nacelle acceleration (Nejad et al. 2017, Huijs et al. 2013), these values are judged as uncritical.

- $s_{dyn,transl}$

The considered critical DLC, which is already just on position 26 for the original system design, is now for the RBDO-based optimized solution just on position 41, but yields a similar value. The highest value obtained for the maximum dynamic translational motion is with 14.2 m for just one case a bit larger compared to the original FOWT system, while the remaining numbers are of a similar order of magnitude as before.

- $s_{mean,transl}$

There is no significant change in the order of criticality of the considered critical DLC compared to the other 53 environmental conditions. For all cases, the mean translational motion is increased compared to the original FOWT system, however, is with a highest value of 28.1 m still way below the maximum allowable value of 64.0 m.

- σ_{TB}

There is a shift in the order of criticality of the DLCs, as now the considered critical DLC is no longer yielding the highest tower base bending stress, but is just on the sixth position. The highest value for σ_{TB} is with 236.24 MPa about 8.22 MPa higher than for the applied critical DLC but still 26.72 MPa below the maximum allowable value. Thus, this shift is neither critical for the maximum allowable stress value nor for the minimum required reliability index.

- σ_{MLi}

There is no significant change in the order of criticality of the considered critical DLC compared to the other 53 environmental conditions. The highest stresses in the mooring lines obtained are as well of the same order of magnitude compared to the original system simulations and, thus, are still way below the maximum allowable value, resulting in reliability indices way beyond the minimum required value.

To approve again the applied interpolation approach for determining the regression coefficients and on their basis the reliability index, also all stochastic environmental conditions

specified in Section 6.2.1.1 are simulated with the RBDO-based optimized FOWT system design solution. The simulation and analysis results show a high accuracy of the interpolation approach. The coefficient of determination is with $R^2 = 0.98$ for the tower base bending stress the lowest (but still very high), while R^2 is above 0.99 for the stresses in the mooring lines.

6.4 Discussion of the RBDO approach applied to floating offshore wind turbine support structures

RBDO of FOWT systems are a highly complex process; however, the results presented in Section 6.3 prove the proper functioning of the developed and applied RBDO approach. Nevertheless, some further discussions, analyses, and recommendations for future work are provided in the following. These address the convergence of the iterative RBDO (Section 6.4.1), investigate a comparison of the DDO and RBDO approaches and results (Section 6.4.2), take up again the issue regarding the criticality of DLCs (Section 6.4.3), and deal with the incorporation of the reliability aspect within a RBDO (Section 6.4.4).

6.4.1 Full convergence of the RBDO

The results of the RBDO approach, presented in Section 6.3, already show a clear tendency even if full convergence is not yet reached with the simulated 10,000 individuals. This, however, is mainly a matter of computational capacity. As towards the end more and more individuals, which are additionally of similar shape, comply with all constraints, the achieved solution can be judged as already significantly improved compared to the original design and expected to be close to the final real optimum obtained when performing more simulations.

6.4.2 DDO and RBDO in comparison

Comparison of the RBDO-based optimized FOWT system design solution with the optimum design obtained by means of the DDO approach ($D_{BC} = 7.0 \text{ m}$, $H_{BC} = 106.8 \text{ m}$, $\rho_{\text{ballast}} = 2,583 \text{ kg/m}^3$; $\max(\iota_{\text{tot}}) = 9.9^\circ$, $\max(a_{\text{hor,nacelle}}) = 1.910 \text{ m/s}^2$, $\max(s_{\text{dyn,transl}}) = 7.7 \text{ m}$), as presented in Tables 5.9 and 5.10 in Section 5.1.4.3 and indicated additionally in green in Figure 6.11, makes clear that inclusion of reliability criteria prevents from a slightly higher reduction in the outer dimensions of the spar-buoy, while the system performance parameters are less critical. This is reasonable as, for example, a larger total inclination angle of the floating system would result into higher bending stresses in the tower base, which itself would reduce the corresponding reliability index.

6.4.3 Environmental conditions considered within the RBDO

The shifts in the order of criticality of the DLCs, experienced and presented in Section 6.3.3, emphasizes the relevance of careful selection of one or some environmental conditions to be considered within the design optimization, as well as well thought out specification of the

targets and limits in the objective functions and constraints. The single critical DLC chosen in this application example is sufficient for the purpose of this study to illustrate the realization of RBDO with a FOWT system and the applicability of the MoWiT-Dymola[®]-Python framework to such a complex optimization problem. Since this proves to be successful, it can be proceeded in future work to inclusion of more DLCs. However, a trade-off between compliance with all environmental conditions and computational efficiency of the highly time-consuming RBDO process is required. A potential approach could be to use just a few (or only one) critical DLC(s) but to apply safety factors to the targets in the objective functions and constraints. The practicality of this strategy is already underlined by the obtained results: the case that a higher limit for the horizontal nacelle acceleration - than specified in this application - is as well common practice, provides already a good example for specifying a reasonable target value, while a small exceedance of this - in maybe other environmental conditions - not directly leads to a really critical value. This could then be correspondingly applied to the total inclination angle limit.

6.4.4 Reliability criteria and analysis method within the RBDO approach

The inclusion of reliability criteria by means of quadratic regression and MCS proves to work; however, there are still alternatives and potential improvements to be discussed and recommended for future work.

6.4.4.1 Performing the reliability analysis

Utilization of the MCS method limits the covered range of reliability index values or requires unreasonable high computational resources. For the specified limit of $\beta = 3.719$ the MCS with $r = 1 \times 10^6$ random samples is both sufficient and acceptable with respect to the computational effort. For higher flexibility, an alternative or modified HL-RF method could be more suitable. This, however, implies that the existing HL-RF method is customized for the applied regression model and considered complex FOWT system, so that convergence of the iterative calculations within the HL-RF method is ensured and FORM can be applied for the reliability index calculation.

6.4.4.2 Addressing the reliability criteria

The method to implement reliability criteria can be diverse. The applied open end solution, with just having a lower limit for the reliability index, can be substantiated by the fact that the specified objectives - approaching the maximum allowable system performance values - will lead to an already limited reliability index value. The results of the RBDO emphasize this tendency, as for the tower base bending stress a large number of individuals fail to comply with the corresponding reliability constraint. Some individuals exhibit slightly higher values for the reliability index than required, while others' reliability index can no longer be captured by the chosen amount of random samples in the MCS.

Thus, having additionally an upper limit could be more realistic. This could be, for example a probability of failure of 1×10^{-6} , corresponding to $\beta = 4.753$, which is not extremely over-conservative as a failure probability of 1×10^{-6} is also a common value. However, in this case r in the MCS would have to be adjusted accordingly to capture as well this higher reliability index, which on the other hand would require more computational capacity - as already discussed before. Constraining the reliability index from both sides might as well have the drawback that - if the reliability criteria are not the dominant constraints - β might not lie within the allowable value ranges.

For actually realizing RBDO, the reliability criteria should directly be implemented as objective functions. The constraints for the lower limit would then still be required, while the additional specification of an upper limit is not mandatory and maybe a bit redundant. Changing from the realized reliability-constrained design optimization to RBDO, would put much more restrictions on the optimization problem and, hence, its realization is - after the success of this study - just a matter of computational resources.

6.4.4.3 Final statement on the realized approach

For this application - to show the functionality of coupling optimization with reliability assessment of FOWT systems - the presented approach is fully sufficient. More constraints would only require more computational capacity, as more individuals per generation have to be considered and overall more simulations need to be performed.

Chapter 7

Discussion

Some main opportunities, but also challenges of the reliability assessment of (floating) offshore wind turbine systems are already pointed out in Section 2.4. Thus, the high complexity and novelty of FOWT concepts already makes any reliability-based design process or assessment difficult. This is even amplified due to the variety of uncertainties, which are not only prevailing in the wind turbine system itself - because of uncertainties in manufacturing processes or material properties - but also come from the environment, which the system is exposed to. These uncertainties are even more complex in case of a FOWT system, as this has to deal with both wind and waves, currents and buoyancy, more complex dynamic couplings, as well as the additional mooring system, which behaves non-linear and is afflicted with further uncertainties. This brings RBDO methods to the fore, whose main strength is to consider uncertainties directly within the design process of the system, which is at the same time optimized with respect to its reliability, mass, performance, or cost, as some examples. However, this capability in particular requires significant computational effort. Thus, finally, combined theories - including as well approaches allowing for computational simplifications - are most promising for the reliability assessment and effort-efficient RBDO of FOWT systems.

These aspects are also experienced within this research work. At first, the high complexity of FOWT systems with their fully-coupled dynamics make modeling and simulation for any system analysis or design development indispensable. There are various numerical tools developed and used by the research community. While these tools mostly have the main physical relations in common, the approaches on how and in which detail these are implemented, which components are included, what assumptions and simplifications are made, what input is required and what results can be provided, how and what analyses are performed, and to which extend the tools are flexible or can even be adjusted to specific user interests and applications, vary widely. Thus, because of its holistic representation of a FOWT system, its great versatility and broad application range, as well as its expandability and modifiability due to being directly the developer, MoWiT is utilized for the development of an aero-hydro-servo-elastic coupled model of dynamics for FOWTs. Despite the fact that FOWT system simulation results from other numerical tools exist for the OC3 phase IV spar-buoy, the code-to-code verification holds already some challenges as only insufficient data and information is available. Thus,

assumptions on system parameters and simulation settings are required; however, taking these into account in the analysis and comparison of the results, the MoWiT model can be verified to some extent. But any application of a numerical model is only as good and meaningful as the model is realistically representing the reality. This entails the step of validation, which requires real measurement data. And this, however, is a major and quite common problem: measurement data is not only relevant for realistic modeling of complex systems, but also for detailed and meaningful reliability assessments, as already pointed out in Sections 2.3.6.1 and 2.4. Thus, even if the developed and applied FOWT system model in MoWiT is verified, any validation is still pending due to the lack of real data and it has to be assumed that the numerical model represents reasonably realistically the real system behavior.

The high complexity of design optimization tasks, especially when they are reliability-based, not only requires numerical models of the FOWT system, but also necessitates automation of the execution of simulations - either for system analyses or within an iterative optimization algorithm. Thus, benefiting from the highly flexible MoWiT models for fully-coupled aero-hydro-servo-elastic simulations of FOWTs, a holistic framework for automated simulation and optimization is developed around. The framework itself is coded in Python, as this programming language fits perfectly to and complements very well the modeling and simulation environments MoWiT and Dymola[®]. Thus, all in all, the developed MoWiT-Dymola[®]-Python framework enables automated execution of a variety of fully-coupled aero-hydro-servo-elastic simulations of FOWTs in a time-efficient manner and by utilizing parallelization, including automated setup and consecutive simulation and analysis of sets of DLCs, as well as highly flexible, comprehensive, and user-specific definition and realization of optimization problems with having a wide choice of sophisticated optimization tools for the selection for the specific application. However, the more capabilities and options are available, the better thought out the use and application has to be. Thus, for instance, the considered highly complex spar-buoy FOWT system modeled by means of MoWiT can only be handled by gradient-free optimizers, while gradient-based ones might be a better and more efficient choice if the considered system can be represented through a single differentiable system equation. Furthermore, an optimization problem with several objectives can either be written in one single objective function, using as well weight factors, or dealt with individually by utilizing a MO optimizer. The final outcome and success of an optimization algorithm also depends on the chosen settings: the specified stop criterion has to ensure that the optimization has already fully converged, while the specific optimizer could either find a local - which varies with the starting point - or the global optimum solution, whereas the one and only optimum is hardly existing in case of MO optimization problems and the final solution has to be selected from a set of Pareto optimal solutions, which allows again for different approaches. Thus, for each optimization task and application a sensitivity study is highly recommended in order to choose the optimization settings which are most appropriate for the specific problem and system - in the case of a single- or multi-objective design optimization of the OC3 phase IV spar-buoy floating support structure, modeled by means of MoWiT, the genetic algorithm NSGAI is found to be suitable.

For the final RBDO application, on the one hand, the previously mentioned benefit of RBDO to consider prevailing uncertainties in the design process can be turned to account. Hence, the missing real measurement data, which is required for the still pending validation of the MoWiT model of the FOWT system, can still be addressed to some extent by defining stochastic variables for environmental parameters. Of course, if any real measurement data is not available, mostly the corresponding statistical properties are missing as well; however, standards, recommended practices, or classification notes provide information on what statistical distribution which environmental parameter commonly follows. To finally derive the further required statistical coefficients, the known distribution can be fitted to other existing data, such as probability of occurrence or percentage of exceedance, without the need for measurement time series. This way, the uncertain environmental parameters wind speed and significant wave height can be considered within the RBDO performed in this research work; however, if even no data for deriving the statistical coefficients is available, assumptions would have to be taken, their reasonability subsequently proven, and - if applicable - the statistical parameters tuned.

On the other hand, however, RBDO has the drawback of large computational effort, which might even increase with the complexity of the system of interest. This exactly might be the reason why RBDO has not yet been applied to FOWT systems. Design optimization of single components of a FOWT are already feasible, as well as some simple RBDO tasks on less complex wind turbine components, but the increased level of difficulty of design optimization including reliability criteria combined with the highly complex system of a FOWT is challenging and requires a specific approach. Therefore, a concept for computationally and time-efficient RBDO of FOWT systems is developed in this research. The main idea is to outsource the computationally intensive part of the reliability assessment from the iterative optimization process. Thus, some time- and resource consuming pre-processing simulations and analyses for generating response surfaces for different FOWT systems within the optimization design space and under all combinations of the considered stochastic variables are accepted, while the final calculation of the reliability indices for each design considered within the iterative optimization process is simplified and, hence, significantly sped up by interpolating the response surfaces (obtained in the pre-processing) to the specific design. Thus, just some minor additional computational resources are required for the pre-processing simulations, while the computational effort within the RBDO process is comparable to a (deterministic) design optimization task without any reliability criteria. However, the main challenge is the complexity of the optimization problem, which is increased when adding reliability criteria, but even an optimization problem without any reliability criteria but with several objectives and/or constraints can already be very complex and, hence, very computationally intensive. This is observed in the different optimization applications addressed in this research work: while the global design optimization (Section 5.1) with three design variables, three objective functions, and ten constraints requires just about 1,400 simulations until the optimum design is found, the optimization problem for designing an advanced spar-type floater (Section 5.2) with seven design variables, just one objective function, but 25 constraints, as well as the RBDO (Chapter 6) with again just three design variables, three objective functions, but 18 constraints, are not yet fully

converged even after 10,000 simulations, though a clear trend is already discernible. Thus, for any design optimization task, independent of if it is reliability-based or not, a deliberated trade-off between the complexity of the optimization problem and the corresponding computational effort has to be found.

Apart from the complexity, also the difficulty of implementing the optimization problem into the framework and adapting the numerical model correspondingly will increase when considering a higher level of detail, as well as technological innovations. This becomes clear in the presented design optimization applications.

- One aspect are the environmental conditions. Throughout the application examples elaborated within this research work, one critical DLC is determined based on pre-processing analyses. The FOWT system is then simulated and optimized under this specific environmental condition. Subsequent analyses of the found optimized design in various environmental conditions are indispensable and performed. These, however, in some cases turn out to have changed - during the optimization - their criticality with respect to the defined objectives and/or set constraints. In the presented applications, no further iterations with an adjusted DLC are performed and some reduced operational time of the FOWT system due to an exceedance of operational limits in certain environmental conditions is accepted, as the overall system stability is not endangered. However, for a finally optimized FOWT system, its operability in various environmental conditions has to be envisaged as well. This is, however, again a trade-off between computational effort and - now - level of detail with respect to the considered environmental conditions. Avoiding a significant increase of the required computational resources, safety factors might be applied to the most critical performance parameters, so that the FOWT system is still optimized for one critical DLC, but leaving a safety margin of higher system responses in other environmental conditions. An alternative or supplement to this would be to perform with the found optimum floating support structure a subsequent design optimization, which focuses then on previously excluded components, such as the mooring system. Following this approach, the obtained optimized floater can be kept, while its performance throughout different environmental conditions can be further improved by modifying the mooring system properties. Compared to the approach of accounting for safety factors for critical performance parameters, the subsequent optimization of, for example, the mooring system comes with a second optimization process; however, this would be still much more computationally efficient than performing with each design considered within the iterative optimization process simulations for a full set of DLCs.
- The optimization application for designing an advanced spar-type floating support structure additionally points out the tougher demands on the numerical model. First of all, as elaborated in Section 5.2.1.2, the original FOWT system model needs to be modified to allow for geometrical changes according to the specified design variables and envisaged advanced spar-type structure. To the newly defined parameters initial values have to be assigned, so that still the originally considered floating system is represented. But - what

is more demanding - the broader range of geometries allowed within the iterative design optimization requires some more refinements and additional cases to be considered in the hydrodynamic calculations, as discussed in detail in Section 5.2.5.2. Consequently, all hydrodynamic coefficients have to be recalculated for each diameter of all structural partitions and specific designs considered within the iterative optimization process. Furthermore, the implemented computation of the vertical Froude-Krylov force would have to be adjusted to account for the differences between upper and lower surfaces of each partition. Moreover, further possible cases - depending on the geometry and environmental condition - have to be considered, so that the added mass and damping coefficients - and, hence, the resulting system response - are correctly calculated even if some parts of the structure temporarily might become dry. Finally, limitations of implemented calculation approaches, such as the validity of the MacCamy-Fuchs approach for cylinders with vertical walls, have to be accounted for and either more generally valid theories or different approaches depending on the specific case have to be implemented in the numerical model, or the optimization problem has to be constrained such that the validity or acceptable range of validity of the utilized calculation approaches is never violated.

- The specific case of using a direct optimization approach for obtaining a larger MW-class floater design without upscaling, as investigated in Section 5.3, points out the relevance of carefully selecting the optimization settings. The allowable value ranges for the design variables, as well as the chosen design variables itself, have to be appropriate for the formulated optimization problem. In the application example it is possible to limit the outer dimensions of the spar-buoy directly or very close to the original system parameters, while still aiming for a larger wind turbine to be supported - only because the reference OC3 phase IV FOWT system is heavily oversized. However, in case of using an already optimized floating support structure as basis for the direct optimization approach, it would have to be allowed for larger values for the geometrical parameters. Furthermore, the design variables and optimization objectives have to be selected compatibly - as already addressed in Section 5.1.5.4. This means that a modification of the values of the design variables should directly or at least indirectly cause a change in the objective functions.
- With respect to the reliability criteria, it has to be noted again - as already discussed in Section 6.4.4 - that the current approach represents a reliability-constrained design optimization approach. This is not a matter of implementation in the optimization framework, as the reliability criteria can easily be defined either as constraints or as objective functions, but rather a compromise between computational effort and exact reliability target definition. The optimization problem without any reliability criteria is already significantly constrained. Adding four more objective functions for the reliability criteria to the already specified three performance-related objective functions would certainly place very high demands on the computational effort. However, having the design variables and optimization objectives, as well as the reliability criteria, compatibly selected - as al-

ready pointed out and recommended in the previous item - the reliability criteria can still be incorporated in a time- and computationally efficient, as well as meaningful, manner, without directly formulating objective functions for the reliability criteria. Thus, as the objectives for the system performance - approaching the maximum allowable values for total inclination angle and horizontal nacelle acceleration - entail a reduction in the reliability index values for the tower base bending stress and tensional stress in at least the two upwind mooring lines, the constraints on the minimum required reliability index are sufficient for the presented application example. However, for other applications, the direct formulation of objective functions for the reliability criteria might be most appropriate for representing a RBDO.

- Finally, as discussed in all application examples elaborated within this research work, the currently more global performance-based or cost-oriented design optimizations must not ignore any structural aspects. Due to the high flexibility of the developed and applied MoWiT-Dymola[®]-Python framework, additional output parameters for forces and moments at specific positions and parts of the structure can easily be implemented and defined in the MoWiT model, and their subsequent processing for performing structural integrity checks or local buckling calculations coded in Python and included as constraints in the optimization problem. This, however, requires information on the structure itself, such as its specific characteristics and strengths or resistances, increases the complexity of the optimization problem, and assumes certain manufacturing methods and geometries for the structural realization (mainly cylindrical sections welded together). The structural information, which is very likely to be afflicted with uncertainties, can directly be incorporated through stochastic variables in the RBDO process. The second aspect of increased complexity is already discussed and a careful compromise between computational effort and level of detail and complexity of the optimization problem has to be found. However, allowing alternative manufacturing and structural realization solutions could positively affect the complexity of the optimization problem, as presented and discussed in the optimization approach for designing an advanced spar-type floating support structure (Section 5.2). Thus, by not including any detailed structural integrity checks and focusing only on hydrodynamic and system-level analyses, but allowing for different concept solutions and alternative structural realization approaches - such as truss elements or tendons as connecting elements - less constraints for the optimization problem have to be defined and a cost-efficient highly innovative optimized floater design can be achieved.

Thus, the final optimum design solution obtained by means of any optimization process is just a reflection of the user-specific definitions and considerations. However, a higher level of detail considered within the design optimization not always directly implies higher computational effort if the optimization settings are carefully selected and when keeping an open mind for technological innovations.

Chapter 8

Conclusions

In this research thesis, a concept for enabling RBDO of FOWTs is developed - starting from the assessment of reliability analysis methods and their suitability for offshore wind turbine systems, continuing with the numerical modeling of highly complex FOWT systems, as well as their automated simulation and processing within optimization tasks, and finally ending with specific approaches for performing DDO and RBDO tasks on a spar-buoy FOWT support structure. The work conducted within this research thesis is briefly summarized in Section 8.1 and the outcome and contributions to knowledge, research, as well as industry, are elaborated in Section 8.2. Finally, the thesis closes with an outlook (Section 8.3) and some final concluding remarks (Section 8.4).

8.1 Summary of the chapters

The thesis commences in Chapter 1 with a short introduction to the research work. Based on the potential of the floating offshore wind technology, as well as the challenges towards the next generation FOWTs, the main aim and single objectives of this thesis are defined. Thus, within the research work, finally, guidelines for RBDO of FOWT support structures are to be derived, based on existing standards but as well being applicable to novel concepts. The single steps for achieving these objectives - building the structure of the thesis - are outlined and the publications in connection with this research thesis listed.

Chapter 2 presents a review of reliability-based methods for risk assessment, which have been most used so far for the assessment of offshore wind and marine renewable energy systems. Based on the current practices in offshore applications, a comprehensive subcategorization of qualitative and quantitative techniques is carried out. The presented qualitative methods are mainly structured as failure mode analyses, tree and graphical analyses, as well as the more rarely used hazard analyses. Within the quantitative methods, it is differentiated between ana-

Note: This chapter is partially based on the publications by Leimeister, Collu & Kolios (2020), Leimeister & Kolios (2020), Leimeister, Kolios & Collu (2020*a,b*), Leimeister, Kolios, Collu & Thomas (2020), Leimeister (2019), Leimeister, Kolios, Collu & Thomas (2019), Leimeister & Kolios (2018), and Leimeister, Kolios & Collu (2018) in excerpts.

lytical and statistical, as well as Bayesian approaches, RBDO tools, multivariate analyses, and strategies for data pooling. Regarding the reliability assessment of offshore wind turbine systems in particular, it has to be noted that offshore wind turbine systems are very complex with dependent, repairable, or redundant components, dynamic characteristics, and non-linearities; furthermore, they require special consideration regarding the severe offshore site conditions, implying several uncertainties in the motion and stress response of the system due to unknown and complex environmental effects, as well as non-linearities; though, there is little experience with novel structures and lack of reliability data; and last but not least, ethical and economic aspects, such as data confidentiality, as well as time and computational efficiency, have to be preserved. These factors challenge the reliability assessment of offshore wind turbines. The trend towards more complex, efficient, and flexible tools, as well as the approach of combining different techniques is developing and should advance further, also including more advanced sensitivity analysis tools to systematically consider uncertainties which will govern the design and operation of offshore wind turbine systems.

The specifics of FOWT systems are addressed in Chapter 3. Existing concepts of FOWT support structures are in general classified and assessed in more detail with respect to their benefits and drawbacks. In order to elaborate most promising design solutions, ten FOWT support structure types are assessed with respect to ten criteria, focusing in particular on wind farm deployment. A MCDA, based on survey results and utilizing TOPSIS method, is performed. With respect to the decision criteria, LCoE proves to be still most important, while maintenance aspects are placed second - both can be improved by increased system reliability. Regarding the floating concepts, the survey reveals that the advanced spar, directly followed by the most developed standard spar, has the highest potential for multi-MW wind farm deployment. In general a correlation trend between TRL and TOPSIS score emerges. Based on the survey results, the OC3 phase IV spar-buoy FOWT is defined as reference system, which serves as basis for the modeling, simulation, and optimization applications in this thesis.

An aero-hydro-servo-elastic coupled model of dynamics for this reference spar-buoy FOWT system is developed by means of MoWiT in Chapter 4. During implementation, it appears that not all required data is available. Hence, some parameter values - such as wall thickness(es), material densities, or ballast height - need to be derived based on the given information, but also implying some assumptions to be made. Not for all resulting variables - mainly the platform yaw inertia - a perfect match can be obtained, which leads to some anticipated deviations of the MoWiT results to the results from the OC3 phase IV participants. The model is simulated for different load conditions and a comprehensive analysis of the simulation results in comparison to the results from other codes is performed. The initial deviation in the yaw inertia is reflected in a significantly higher natural frequency in yaw, which is encountered in all corresponding time series. Taking account of start-up transients in the time series, the results for the hydro-elastic and aero-hydro-servo-elastic simulations with regular waves, as well as steady wind in the latter case, are highly comparable with the results from the other modeling tools. However, for irregular waves and turbulent wind, discrepancies are observed due to deviations in the input spectra. In post-processing, the differences in the input are reduced,

yielding a better match of the results. Hence, the MoWiT model can still be verified to some extent and found suitable for fully-coupled aero-hydro-servo-elastic simulations of FOWT systems, as well as for optimization applications. Hence, afterwards, a holistic and highly flexible framework for automated simulation and optimization of wind turbine systems, including all system components and their fully-coupled aero-hydro-servo-elastic behavior, is developed. This framework can be used for automated execution and analysis of DLC simulations, as well as for running optimization algorithms, in which the automated simulation execution can still be employed. The framework requires a modeling environment, a simulation engine, as well as the programming framework itself. In case of optimization tasks, the optimization problem, optimizer, and optimization algorithm have to be defined as well. The broad range of applications of such an optimization framework for wind turbine design is shown on the example of the MoWiT-Dymola[®]-Python framework, with the highly flexible modeling environment MoWiT, coupled to the simulation engine Dymola[®], and the extremely advantageous programming language Python. The technical feasibility and proper functioning of this framework is verified by means of a plausibility check and further suitable application cases are discussed.

Utilizing this framework, three design optimization tasks, each applied to the specified reference FOWT system, are presented and elaborated in Chapter 5. These are in particular:

- a global design optimization approach. The optimization example focuses on global limit states and aims for cost reduction by means of reducing the outer dimensions of the floater, as well as using cheap and common ballast materials. This optimization application covers the entire methodology for a design optimization task: 1) starting with the substantiated selection and specification of the design variables and global limit states for the reference FOWT; 2) processing these for the formal description of the optimization problem; 3) continuing with the definition of one critical simulation case, which is used within the optimization iterations; 4) followed by the profound choice of the optimizer and corresponding settings, as well as its approval of convergence; 5) and finishing off with the final selection approach of the optimum and its evaluation. Keeping the scope of this application example in mind, the presented optimization approach and demonstrated results show a successful design optimization of a spar-buoy floating wind turbine system by means of global limit states definitions and utilization of the MoWiT-Dymola[®]-Python framework. The outer dimensions (spar-buoy base column diameter and height) can be reduced by more than 25% and 1%, respectively, which results in almost 24% reduction in structural mass and related material cost. By using a more than 35% denser ballast, but still only requiring less than half of the original ballast mass, a sufficient deep center of mass can be obtained to meet the stability and dynamic performance requirements. These results and the presented methodologies serve as basis for further in-depth and more sophisticated applications of the design optimization approach.
- an automated optimization approach for designing an advanced spar-type floating platform, which is optimized with respect to the change in hydrodynamics and their impact on the main system performance, while structural, manufacturability, or other constraints

are not considered. This approach, following a freer optimization formulation, is taken in order to be able to explore novel design spaces, which can be better from an hydrodynamic point of view, but that may require novel structural realization approaches, as actively investigated by the community (e.g. Stiesdal's TetraSpar and Saipem's Hexafloat). The reference FOWT system is modified by dividing the spar-buoy base column into three distinct partitions, so that sufficient buoyancy, as well as a deep center of gravity, can be obtained. Furthermore, the wall thickness is adjusted based on a common ratio of the support structure's structural mass to the displaced mass of water. The optimization focuses on the minimization of the steel volume of the floater, which represents an approximation of the CapEx of the floating platform. In addition, constraints regarding the outer dimensions (meaning the allowable value ranges of the design variables), the global fully-coupled system performance, the system draft, the ballast, and the geometric integrity are defined. Having selected, based on pre-processing automated system simulations, one DLC which is most critical for the constrained system performance criteria, the iterative optimization algorithm run is performed, utilizing the MoWiT-Dymola[®]-Python framework and using the genetic algorithm NSGAI as optimizer. The analysis of the optimization simulation results shows that the individuals which comply with all prescribed constraints aggregate as for their objective function values to an asymptote. The results from the optimization run emphasize the complexity of the optimization problem and indicate that - despite the large number of simulations and the asymptotic clustering to a minimum objective function - full convergence is not yet obtained. Nevertheless, the applied iterative optimization algorithm yields an advanced spar-type floating support structure design, which has a by more than 31% reduced structure material volume compared to the original floating platform, meets all global performance criteria for the considered critical DLC, has an overall draft of just 36.8 m, utilizes MagnaDense or high density concrete as ballast material, and resembles a submerged thick barge-type floater. The operability is - taking the maximum allowable system performance values as strict obligation for operating ability - limited to 46.3% of the considered 54 environmental conditions. This, however, can be much more extended when modifying subsequently the currently unchanged mooring system properties and layout. Based on the applied hydrodynamic and system-level analyses, an optimized initial advanced spar-type floater design is obtained, which has to be further refined by incorporating structural checks into the optimization process, but can be realized by means of innovative structural approaches, which utilize trusses or tendons instead of solely welding cylindrical sections together.

- a direct optimization approach, by which means a floating support structure for a larger MW-class wind turbine is obtained, based on an existing smaller FOWT system design, without using the intermediate step of upscaling. The input to this direct optimization algorithm only requires minor initial adaptations of the original FOWT system model, as well as the specification of the design conditions - such as the design variables which

are to be modified during the optimization, the optimization objectives which should be focused on, the environmental conditions which are used for the system simulations, as well as the optimization settings. Even if the final result highly depends on the choice for these design conditions, an appropriate FOWT system design, which fulfills the specified requirements and performs well with respect to the defined objectives, can be obtained automatically by means of this direct optimization approach.

The final proven concept for RBDO of FOWT systems is developed, presented, and applied to the reference FOWT system in Chapter 6. This application example enhances the DDO - the global design optimization presented in Chapter 5, which targets a less over-dimensioned floating structure by aiming for more critical but still save operational global performance - by incorporating reliability criteria and accounting for environmental uncertainties. The presented methodology for integrating the reliability aspect into the design optimization comprises: 1) the specification of LSs, environmental conditions, stochastic variables, and reliability criteria relevant to the reference FOWT system; 2) the subsequent definition of the RBDO problem, comprising design variables, objective functions, and optimization constraints; 3) a level one pre-processing to elaborate an appropriate reliability assessment approach, which utilizes MCS based on quadratic regression analysis; 4) a subsequent level two pre-processing to develop and approve an interpolation approach for deriving the regression coefficients for any floater geometry based on pre-generated response surfaces for a set of discrete floater geometries within the optimization design space; 5) the definition of the RBDO process including the selection of an optimizer; 6) and the final application of the RBDO with subsequent post-processing of the results. Both the selected reliability assessment approach and the developed interpolation approach are of high accuracy, represented by high values for the coefficient of determination. The iterative RBDO itself is not more computationally intensive than the DDO; however, much more iterations are required due to the significantly stronger constrained optimization problem. This is as well underlined by the much slower convergence rate of the RBDO results. Nevertheless, a clear tendency is already visible in the simulation results and an improved floater geometry is obtained that meets all specified constraints - including the reliability criteria - and performs well for the selected and most of the other considered environmental conditions, while it needs just around 80% of the original floater's steel mass, as well as around 44% less ballast mass. Thus, this final application example demonstrates that reliability assessment and design optimization of FOWT systems can be combined, but it as well emphasizes the high complexity of such tasks.

Finally, the main aspects of the presented studies, elaborated methodologies, applied approaches, and analyzed results are discussed in Chapter 7. These address the benefit of RBDO methods to account for uncertainties, as well as the drawback to require high computational effort, both substantiated by reviewed literature and made experiences within this research work. Furthermore, the problem of missing or incomplete data is not only prevalent for reliability assessments, but also for validation of numerical models. When it comes to the automation of simulations and execution of optimization tasks, the relevance of sensitivity studies and careful

selection of optimization settings for any specific problem and considered system is elaborated. But also for the definition of the (reliability-based) design optimization problem, the considered environmental condition(s), design variables and optimization objectives, allowable value ranges and constraints, validity of implemented theories, and detail of analyses have to be chosen compatibly and thoughtfully. Cost-efficient realization of complex RBDO tasks on FOWT systems can happen through an elaborated and structured approach, as developed and proposed in this research thesis, as well as through careful selection of the optimization settings - as already mentioned - and by being open for technological innovations - as addressed as well in this research work when designing an advanced spar-type floating support structure.

8.2 Thesis contributions to knowledge, research, and industry

The contribution of this research thesis to knowledge, as well as its relevance for research and industry, are elaborated in the following. Each of the defined (Section 1.3) and successfully realized objectives is assessed with respect to novelty, scientific soundness, and value, as presented in Table 8.1. This knowledge, as well as the experience gained and approaches developed and applied, are disseminated in the course of the research thesis through several paper publications in scientific journals, as well as oral and poster presentations at scientific conferences, as listed in Section 1.5 and Appendix A.

Overall, the main contribution of this thesis to knowledge, research, as well as industry, is the developed concept for combining FOWT design optimization and reliability assessment, which is based on the immensely versatile aero-hydro-servo-elastic coupled numerical MoWiT model of dynamics for FOWTs and the highly flexible and multifunctional holistic MoWiT-Dymola[®]-Python framework for automated simulation and optimization of FOWT systems, both as well developed and verified within this research work. This fulfills the overall aim of this research thesis to derive guidelines for reliability-based design optimization of floating wind turbine support structures, taking into account target safety levels and failure mechanisms from existing standards and applying them in such novel concepts.

The novelty of this research thesis is, at first, the coupling of design optimization with reliability assessment of FOWT systems, as this has not yet been addressed and realized before. The developed approach is based on a profound review, classification, and assessment of reliability-based methods for risk analysis specific to the offshore and marine renewable energy industry and their applicability to offshore wind turbine systems. Furthermore, the RBDO approach is based on and utilizes an aero-hydro-servo-elastic coupled model of dynamics for FOWT systems and a framework for automated simulation and optimization, which are both novel due to their holistic approach, high flexibility, multifunctionality, and broad applicability. Apart from the novelty of including reliability assessment in the design optimization of FOWT systems, the approaches are in general highly future-oriented. This begins with the MCDA of FOWT concepts, which includes advanced approaches - such as hybrid, multi-turbine, or mixed-energy designs - and focuses already on the suitability of floating support structures for offshore wind farm deployment (by the way, there is currently just one floating wind farm of

five units in operation); continues with the application of a comprehensive fully integrated optimization approach for designing an innovative advanced spar-type floating support structure by exploring as well alternative structural realization solutions and innovative materials; and, finally, even reaches to a brief digression on direct optimization without the intermediate step of upscaling to address the current trend in the wind turbine technology towards larger and larger MW-class wind turbines.

The systematic conduct of the literature reviews, implying as well opinions and experiences of knowledgeable academic and industrial experts, the comprehensive analyses for verifying the developed fully-coupled model of dynamics for FOWTs and the approval of the proper functioning of the established framework for automated simulation and optimization, which additionally draws from a wide choice of sophisticated optimization tools, the adherence to common and well-known approaches, recommendations from standards and classifications, and real environmental statistical data for selecting optimization and simulation settings, as well as the detailed assessment of all simulation results - focusing on convergence criteria, elaborating different selection procedures, and utilizing the coefficient of determination - all this proves the scientific soundness of the applied methods and approaches.

The work performed in the course of this thesis is of high significance for both research and industry. The relevance of the thesis topic is underlined by the number of published papers in scientific journals, their stats on how they are received by the academic and industrial audience, as well as the high acceptance rate for presentations at scientific conferences. The elaborated and applied approaches are future-oriented, address the current issues and challenges related to FOWT support structures and their accelerated market uptake, focus on computationally and time-efficient realization of design processes and detailed assessment of FOWT systems, account for cost factors, reliability criteria, as well as innovations, and allow for user-specific applications. These all add value to the floating offshore wind industry, which is as well experienced - being employed as research associate at Fraunhofer IWES - based on recently incoming requests from the industry on potential applications of the optimization framework, as well as discussed and elaborated research projects and industrial orders on related topics. Some of them are further outlined in Section 8.3.2.

Table 8.1: Contribution of the successfully realized objectives to knowledge, assessed with respect to novelty, scientific soundness, and value.

Objective 1: *Review and classify reliability methods applied in the offshore and marine renewable energy industry and derive from these methods suitable procedures and potential future approaches for reliability assessment applications to offshore wind turbine systems.*

Novelty	Scientific soundness	Value
<i>What is new?</i>	<i>What methods are applied and how are they validated?</i>	<i>To whom is the work significant?</i>
<p>The performed literature review and classification of various reliability-based methods for risk analysis specific to the offshore and marine renewable energy industry, with the focus on literature that has been published since 2010 and a specific interest on potential reliability assessment applications to offshore wind turbine systems, has not yet been existing before.</p>	<p>A systematic literature review forms the basis for the classification of reliability methods applied in the offshore and marine renewable energy industry, as well as the derivation of suitable future procedures for reliability assessment applications to offshore wind turbine systems. This systematic literature review is performed word-based (using "reliability" and "offshore") and time-based (from 2010 onwards), with a specific focus on offshore wind turbines, ensuring that all relevant papers (more than 100 in total and additionally several conference publications) are captured.</p>	<p>The review is not only of interest for researchers and academics, but also valuable for the offshore wind and marine renewable energy industry, which is currently employing and further investigating such methods. The relevance of these elaborations is underlined by the stats of the corresponding journal paper publication (Leimeister & Kolios 2018): within the two years of publication, the paper has already been cited 23 times and read about 170 times with in total more than 7,265 views - based on the stats from Elsevier (2020), Mendeley (2020), and ResearchGate (2020).</p>

Table 8.1: Contribution of the successfully realized objectives to knowledge, assessed with respect to novelty, scientific soundness, and value. (cont.)

Objective 2: *Assess the large diversity of existing FOWT support structures with respect to their suitability for offshore wind farm deployment and future development trends.*

Novelty <i>What is new?</i>	Scientific soundness <i>What methods are applied and how are they validated?</i>	Value <i>To whom is the work significant?</i>
<p>The review and subsequent MCDA is not only based on the currently existing concepts for FOWT support structures, but is already future-oriented - as it focuses on the suitability of floating support structures for offshore wind farm deployment - and includes expert opinions.</p>	<p>The review of existing FOWT concepts goes beyond the main categories based on the stabilizing mechanisms and also includes advanced approaches, as well as even hybrid, multi-turbine, or mixed-energy solutions. In addition to sound SWOT analyses of the main floater types, the broad categories are assessed through MCDA, based on a survey answered completely by seven knowledgeable academic and industrial experts, with an average of more than five and a half years (and maximum ten years) of experience in the field of floating offshore wind.</p>	<p>The review and results of the MCDA are of high value for university-, as well as industry-based researchers, as it supports in showing the potential and also the required development trends, so that the floating offshore wind technology can gain a strong market position for offshore wind farms.</p>

Table 8.1: Contribution of the successfully realized objectives to knowledge, assessed with respect to novelty, scientific soundness, and value. (cont.)

<p>Objective 3: <i>Develop a verified aero-hydro-servo-elastic coupled numerical model of dynamics for FOWTs, as well as a holistic framework for automated simulation and optimization of FOWT systems.</i></p>	<p>Novelty <i>What is new?</i></p>	<p>Scientific soundness <i>What methods are applied and how are they validated?</i></p>	<p>Value <i>To whom is the work significant?</i></p>
<p>The novelty of the developed fully-coupled MoWiT model of dynamics for FOWTs - compared to the variety of other numerical tools for modeling wind turbine systems - is the combined holistic approach and highly flexible application potential, ranging from modeling different (onshore/offshore, bottom-fixed/floating) state-of-the-art wind turbine systems and environmental conditions, to the application for real-time simulations, combination with MATLAB® and Simulink, as well as automated DLC simulations or system and component optimization by means of the developed MoWiT-Dymola®-Python framework. This framework is - compared to other existing tools and approaches - as well holistic, highly flexible, and multifunctional, as it contains the numerical wind turbine system model, the corresponding simulation tool, as well as a programming framework, which can be used for various tasks and applications and extended through user-specific definitions.</p>	<p>The MoWiT model is developed according to the definitions for the OC3 phase IV spar-buoy FOWT system and verified to some extent analogously to the code-to-code comparisons performed in phase IV of the OC3 project, while further in-depth analyses of the results are supplemented. The devised framework uses the already developed MoWiT model for aero-hydro-servo-elastic simulations of FOWT systems and draws from a wide choice of sophisticated optimization tools. Furthermore, the proper functioning of the established framework and correct implementation of the optimization routine are approved by means of a plausibility check.</p>	<p>The presented development and verification approach of the numerical FOWT model of dynamics, as well as the developed highly flexible and multifunctional framework for automated simulation and optimization, are in general relevant to research and industry, as modeling and simulation are indispensable for FOWT systems and as the development process of such engineering systems is very complex, requires a huge number of simulations, and implies iterative steps for design optimization. The developed MoWiT model adds one more result to cross-code comparisons and, hence, is of value for researchers and academics working on numerical FOWT models. In addition, as the MoWiT model is already partly verified against other numerical tools, it gains in importance for industrial applications and work performed at Fraunhofer IWES for both research and industry. Furthermore, the framework can be applied to different optimization and simulation tasks within research and industrial projects.</p>	

Table 8.1: Contribution of the successfully realized objectives to knowledge, assessed with respect to novelty, scientific soundness, and value. (cont.)

Objective 4: *Apply the developed model and framework to different design optimization tasks on a FOWT system.*

Novelty	Scientific soundness	Value
<i>What is new?</i>	<i>What methods are applied and how are they validated?</i>	<i>To whom is the work significant?</i>
<p>The global design optimization of the spar-buoy FOWT system is the first application of the developed framework for automated simulation and optimization to a design optimization task. Furthermore, to address the challenges of the highly promising spar-buoy floater concept and to design an advanced spar-type support structure, a fully integrated optimization approach is adopted. More potential and innovative floater design solutions can be captured with the freer optimization formulation, which allows design variables out of a wider range of values, focuses on hydrodynamic and system-level analyses, does not require that stringent limitations on the structure, and considers different structural realization approaches. The finally presented and developed direct optimization approach is highly future-oriented, as it significantly reduces the number of steps when designing a floating support structure for a larger MW-class wind turbine by directly optimizing the floater design without performing the intermediate step of upscaling.</p>	<p>The global, advanced, and direct design optimization approaches utilize the developed MoWiT model, checked MoWiT-Dymola[®]-Python framework, and a sophisticated genetic optimization algorithm. Furthermore, the state-of-the-art reference wind turbine IWT-7.5-164 is used for the larger MW-class floating system. For the selection of DLCs and specification of optimization objectives and constraints, common approaches and standard recommendations are followed. Moreover, the current trends in the floating offshore wind industry and experience from industrial experts directly involved in the development process of innovative floating support structure solutions are taken into account, when defining allowable value ranges of system parameters (both geometry- and material-related), as well as when assessing the optimization results. The results are additionally analyzed in detail, focusing both on convergence and different selection procedures, including consideration of Pareto optimality.</p>	<p>As design optimization of FOWT systems is of high relevance for an accelerated market uptake, the established and applied optimization approaches - forming a sound basis for more advanced optimization tasks - are of high value for both further research applications, as well as for supporting industries in the design process and decision making. Furthermore, the specific focus on innovative FOWT support structures, including alternative materials and structural realization methods, as well as the investigated and proposed direct optimization approach for speeding up the design process of larger MW-class floating platforms, are valuable studies for the research community, but mostly relevant for the industry and the future trend of the floating offshore wind technology, as cost-efficiency is focused and at the same time innovative solutions are investigated. This also allows the floating support structure industry to be on a par with the fast development trend in the wind turbine technology towards larger MW-classes.</p>

Table 8.1: Contribution of the successfully realized objectives to knowledge, assessed with respect to novelty, scientific soundness, and value. (cont.)

Objective 5: *Develop a proven concept for coupling design optimization with reliability assessment of FOWT systems in a computationally and time-efficient manner.*

Novelty	Scientific soundness	Value
<i>What is new?</i>	<i>What methods are applied and how are they validated?</i>	<i>To whom is the work significant?</i>
<p>The developed and applied concept, combining floating wind turbine design optimization and reliability assessment, is the first of its kind. The novelty is to address uncertainties in the design process of FOWT systems through incorporation of reliability criteria in the optimization process - all in all in a time-efficient manner by means of a developed interpolation approach based on response surfaces.</p>	<p>The approach for RBDO of FOWT systems utilizes the developed MoWiT model, checked MoWiT-Dymola[®]-Python framework, and a sophisticated genetic optimization algorithm. Furthermore, common approaches, recommendations from standards and classifications, as well as real environmental statistical data, are followed and used when selecting DLCs, specifying the optimization objectives and constraints, declaring the limit states, defining the stochastic variables, and formulating the reliability criteria. Common and sophisticated methods for assessing the reliability are investigated and applied. Finally, the accuracy of both the selected reliability assessment approach and the developed interpolation approach is checked and verified through very high values for the coefficient of determination.</p>	<p>The application of RBDO to FOWT systems is highly relevant with respect to economic efficiency, as well as for considering prevailing uncertainties. The developed RBDO method for FOWT support structures – the first of its kind – is of high relevance for the offshore wind industry and wind farm operators, as it will pave the way to reliable structures for FOWTs and reduced uncertainties in the system designs.</p>

8.3 Future work and outlook

The outlook is two-tired: focusing on future work required to overcome the perceived and currently still prevailing limitations (Section 8.3.1), as well as addressing future applications of the research outcomes (Section 8.3.2).

8.3.1 Efforts to overcome limitations

Despite the successful verification of the system-only analyses, as well as the system responses in regular and steady environmental conditions - taking the required assumptions and missing information into account - the numerical MoWiT model for representing the aero-hydro-servo-elastic coupled dynamics of FOWT systems has to be further improved, to better capture various environmental inputs, to more accurately represent advanced physical relations, and to increase the flexibility for its application to highly innovative floating support structure geometries and designs. Thus, in particular, the improvement and separate verification of the environmental spectra for both turbulent wind and irregular waves generated by means of MoWiT is envisaged. The basic MoWiT model of the reference OC3 phase IV spar-buoy FOWT system is already modified in Section 5.2.1.2 to allow for the realization of an advanced spar-type floater design; however, the hydrodynamic calculations as well have to be enhanced accordingly, as discussed in detail in Section 5.2.5.2. Thus, the further development of MoWiT has to incorporate geometry-dependent hydrodynamic coefficients, utilize a more sophisticated and design-independent calculation approach for - especially the vertical - hydrodynamic loads, consider extreme events and special load impacts, and account for the validity range of already enhanced calculation approaches when dealing with various structural geometries. Finally, to ensure the realistic representation of the real behavior of a FOWT system, the MoWiT model has to be validated with real measurement data, as soon as this is available.

In general, to facilitate the computational efficiency of the entire (reliability-based) design optimization approach, both the numerical model and the code implemented in the optimization framework have to be further enhanced. Currently real-time simulations with MoWiT models of onshore wind turbine systems are already feasible; however, the increased complexity of offshore and floating systems comes with increased computational effort. Optimizing the code and improving the computational efficiency are ongoing development works on MoWiT, as well as the MoWiT-Dymola[®]-Python framework.

With respect to RBDO - as discussed in detail in Section 6.4.4 - the reliability criteria can already now be implemented as objective functions, which, however, currently entails significantly increased computational effort. Thus, the improvements regarding the optimized code - mentioned beforehand - will definitely benefit a realization of design optimization tasks with reliability-based objectives. Furthermore, it is aimed for the future to precisely capture a definite value for the reliability index in a time- and computationally efficient manner. The currently realization by means of MCS is only suitable due to the low limit of the reliability index specified in the application example. However - as initially also envisaged and tried - in the end, the reliability index calculation should be based on an alternative or modified HL-RF

method. Due to the well-known convergence issues for certain applications, this has to be studied in more detail in future work, so that a customized HL-RF method suitable for the applied optimization problem and considered complex FOWT system is found or developed.

8.3.2 Future applications of the research outcomes

The broad range of applications of the MoWiT-Dymola[®]-Python framework for automated simulation and optimization is already pointed out and discussed in Section 4.2.4. In the following, more specific future potential application examples of the developed framework are presented, based on recently incoming requests from the industry, as well as discussed and prepared research projects and industrial orders.

The capability of the MoWiT-Dymola[®]-Python framework of performing tasks in an automated manner can be at first utilized for the automated execution of especially a huge number of simulations. This is required for simulating DLCs - as already applied in this research work - and performing load analyses, but can further be extended to a comparative analysis of different wind turbine systems in the same environmental conditions - meaning running the entire set of DLCs not only with one but several different wind turbine models. Additionally, the automated execution of simulations is highly beneficial when aiming for generating for a wind turbine system, for instance, response amplitude operators for different environmental loading conditions.

The extended capability of the MoWiT-Dymola[®]-Python framework of performing optimization tasks can be utilized for realizing various conceivable design, system, or component optimization tasks, requiring different levels of detail. Thus, as already indicated in Section 4.2.4.3, the wind turbine controller can be tuned and optimized in order to realize an adaption to different wind turbine systems and environmental conditions, to optimize the operational management of a single wind turbine or an entire wind farm for reducing the loads on the system and increasing the overall farm power output, as well as to control the wind turbine operation with the focus on its remaining lifetime and best utilization. With respect to design optimization tasks, as already addressed in Section 4.2.4.4 and covered in detail by means of the exemplary approaches presented in Chapters 5 and 6, there is a whole spectrum of imaginable and possible applications, such as:

- the development of a rough design for obtaining an initial cost estimate already at an early stage of the project planning - as financial institutes and insurance companies have to be convinced of the planned wind farm project already way before the detailed engineering phase;
- the detailed design optimization of a wind turbine support structure for a specific site and certain prevailing constraints and requirements, including as well structural integrity checks;
- the reliability-based design optimization of a wind turbine support structure to focus on lifetime-related aspects and reduce the required maintenance and repair work;

- the design of wind turbine support structures for different sites, based on an already optimized design solution;
- the elaboration of the best option for a planned wind farm - meaning investigating which wind turbine MW-class would be most efficient and economic for the considered site and planned project;
- the preparation of (especially floating) support structure designs for the current rapid wind turbine trend towards larger MW-class turbines, including an estimate on costs, dimensions, and loads on the structure; and
- the optimization of a first draft innovative wind turbine support structure design.

8.4 Concluding remarks

In the course of the research thesis, a highly flexible and fully-coupled numerical model of dynamics of a FOWT system is developed, verified to some extent, and utilized together with a developed holistic framework for automated simulation and optimization throughout a number of application examples for design optimization of floating support structures for offshore wind turbines. The degree of complexity is further and further increased, starting with global limit states, continuing with innovative geometrical shapes and realization methods, briefly touching upon the future development towards larger MW-class wind turbines and the commonly associated upscaling process, and, finally, ending with the realization of both design optimization and reliability assessment of a FOWT system at the same time.

The elaborations demonstrate the high complexity of FOWT systems, RBDO tasks, and of course the combination of both; however, they also show and prove that the coupling of FOWT design optimization with reliability assessment is possible and can be realized in a time- and computationally efficient manner, when applying a thoughtful approach.

RBDO is already highly relevant for considering prevailing uncertainties directly within the design process and at the same time achieving a cost-efficient design solution. The knowledge and outcomes of this research thesis add to the significance of RBDO of FOWTs and, hence, are of high value for both research and industry, offering a broad range of future applications with invaluable benefits for the floating offshore wind industry and support for an accelerated market uptake of the floating offshore wind technology.

Appendices

Appendix A

Additional dissemination activities

Additionally to the paper publications in scientific journals, listed in Section 1.5, parts of the research work are presented at the following scientific conferences.

- Leimeister, M. & Ward, D. (2017), ‘REMS CDT research on floating wind’, oral presentation at the *3rd REMS Annual Conference, Cranfield, United Kingdom, September 18-19, 2017*.
- Leimeister, M. (2017), ‘Global limit states for the design of floating wind turbine support structures’, oral presentation at the *13th eawe PhD Seminar, Cranfield, United Kingdom, September 20-22, 2017*.
- Leimeister, M., Kolios, A. & Collu, M. (2018), ‘Critical review of floating support structures for offshore wind farm deployment’, poster presentation at the *15th Deep Sea Offshore Wind R&D Conference, EERA DeepWind’2018, Trondheim, Norway, January 17-19, 2018*.
- Leimeister, M. (2019), ‘Python-Modelica framework for automated simulation and optimization’, oral presentation at the *13th International Modelica Conference, Regensburg, Germany, March 4-6, 2019*.
- Leimeister, M. (2019), ‘Optimization of floating support structures’, oral presentation at the *4th REMS Annual Conference, Glasgow, United Kingdom, May 23-24, 2019*.
- Leimeister, M. (2019), ‘Larger MW-class floater designs without upscaling? – a direct optimization approach’, oral presentation at the *ASME 38th International Conference on Ocean, Offshore and Arctic Engineering, Glasgow, Scotland, UK, June 9-14, 2019*.
- Leimeister, M. (2019), ‘MDAO of wind turbine systems for various applications, using Python and Modelica’, oral presentation at the *Wind Energy Science Conference 2019, Cork, Ireland, June 17-20, 2019*.
- Leimeister, M. (2020), ‘Optimization of floating wind support structures for cost-reduction and preparation for innovations in wind turbine technology’, oral presentation at the *Floating Offshore Wind 2020, Online (Aberdeen, UK), October 7-8, 2020*.

Appendix B

Statistics of DLC 4.2

The numerical comparison of the statistics - in form of minimum, mean, maximum, and standard deviation values - from the DLC 4.2 simulation with irregular waves is given in Tables B.1 to B.7 for the considered parameters.

Table B.1: Wave elevation statistics (in m) from DLC 4.2 from OC3 phase IV codes and MoWiT in comparison, **deviations** are highlighted in **red**.

Statistics	OC3 mean	OC3 min	OC3 max	MoWiT	MoWiT deviation
Minimum	-5.5807	-6.4400	-4.7322	-3.2456	+31.4% to +49.6%
Mean	-0.0017	-0.0352	0.0092	0.1207	+443.3% to $+1.2 \times 10^3\%$
Maximum	5.0790	4.2337	6.6900	3.2456	-51.5% to -23.3%
Stand. dev.	1.5832	1.4920	1.9773	2.2959	+16.1% to +53.9%

Table B.2: Platform surge motion statistics (in m) from DLC 4.2 from OC3 phase IV codes and MoWiT in comparison, **deviations** are highlighted in **red**.

Statistics	OC3 mean	OC3 min	OC3 max	MoWiT	MoWiT deviation
Minimum	-3.3505	-4.6930	-1.8170	-1.0557	+41.9% to +77.5%
Mean	-0.1598	-1.3636	0.2958	0.0088	-97.0% to +100.6%
Maximum	2.9966	1.4121	4.9000	1.0491	-78.6% to -25.7%
Stand. dev.	1.0280	0.7442	1.2832	0.6947	-45.9% to -6.7%

Table B.3: Platform heave motion statistics (in m) from DLC 4.2 from OC3 phase IV codes and MoWiT in comparison, **deviations** are highlighted in **red**.

Statistics	OC3 mean	OC3 min	OC3 max	MoWiT	MoWiT deviation
Minimum	-0.6242	-0.8686	-0.3630	-0.2217	+38.9% to +74.5%
Mean	0.0145	-0.0048	0.0630	-0.2169	$-4.4 \times 10^3\%$ to -444.3%
Maximum	0.6732	0.3943	0.9931	-0.2112	-153.6% to -121.3%
Stand. dev.	0.2142	0.1343	0.3549	0.0026	-99.3% to -98.1%

Table B.4: Platform pitch motion statistics (in deg) from DLC 4.2 from OC3 phase IV codes and MoWiT in comparison, **deviations** are highlighted in **red**.

Statistics	OC3 mean	OC3 min	OC3 max	MoWiT	MoWiT deviation
Minimum	-1.3885	-1.6900	-1.1030	-0.6033	+45.3% to +64.3%
Mean	-0.0021	-0.0759	0.1643	-0.0515	-131.4% to +32.1%
Maximum	1.5053	1.0902	2.2200	0.5017	-77.4% to -54.0%
Stand. dev.	0.4781	0.3788	0.6270	0.3861	-38.4% to +1.9%

Table B.5: Tower-top fore-aft shear force statistics (in kN) from DLC 4.2 from OC3 phase IV codes and MoWiT in comparison, **deviations** are highlighted in **red**.

Statistics	OC3 mean	OC3 min	OC3 max	MoWiT	MoWiT deviation
Minimum	-818.6	-968.7	-675.3	-454.7	+32.7% to +53.1%
Mean	-1.5	-7.5	8.3	-1.1	-112.9% to +85.6%
Maximum	845.2	715.6	943.7	453.4	-52.0% to -36.6%
Stand. dev.	238.1	221.1	245.3	317.2	+29.3% to +43.5%

Table B.6: Tower-top fore-aft bending moment statistics (in kNm) from DLC 4.2 from OC3 phase IV codes and MoWiT in comparison, **deviations** are highlighted in **red**.

Statistics	OC3 mean	OC3 min	OC3 max	MoWiT	MoWiT deviation
Minimum	-5.4×10^3	-1.1×10^4	-3.3×10^3	-2.5×10^3	+24.4% to +77.3%
Mean	-906.4	-1.4×10^3	601.4	-1.4×10^3	-328.2% to +4.2%
Maximum	3.0×10^3	355.2	9.9×10^3	-260.8	-173.4% to -102.6%
Stand. dev.	1.0×10^3	530.4	2.4×10^3	776.7	-67.4% to +46.4%

Table B.7: Downstream fairlead tension statistics (in kN) from DLC 4.2 from OC3 phase IV codes and MoWiT in comparison, **deviations** are highlighted in **red**.

Statistics	OC3 mean	OC3 min	OC3 max	MoWiT	MoWiT deviation
Minimum	791.1	536.0	882.8	854.8	−3.2% to +59.5%
Mean	953.3	904.4	1.1×10^3	907.6	−20.0% to +0.4%
Maximum	1.1×10^3	929.2	1.7×10^3	957.7	−44.3% to +3.1%
Stand. dev.	53.6	7.9	181.0	32.6	−82.0% to +311.3%

Appendix C

Statistics of DLC 5.3

The numerical comparison of the statistics - in form of minimum, mean, maximum, and standard deviation values - from the DLC 5.3 simulation with irregular waves and turbulent wind is given in Tables C.1 to C.13 for the considered parameters.

Table C.1: Wave elevation statistics (in m) from DLC 5.3 from OC3 phase IV codes and MoWiT in comparison, **deviations** are highlighted in **red**.

Statistics	OC3 mean	OC3 min	OC3 max	MoWiT	MoWiT deviation
Minimum	-5.2739	-5.8400	-4.5990	-3.2456	+29.4% to +44.4%
Mean	-0.0026	-0.0352	0.0092	0.0956	+371.8% to +935.7%
Maximum	4.7815	4.2337	5.0840	3.2456	-36.2% to -23.3%
Stand. dev.	1.6065	1.4920	1.9773	2.2946	+16.0% to +53.8%

Table C.2: Wind speed statistics (in m/s) from DLC 5.3 from OC3 phase IV codes and MoWiT in comparison, **deviations** are highlighted in **red**.

Statistics	OC3 mean	OC3 min	OC3 max	MoWiT	MoWiT deviation
Minimum	9.6860	6.2960	11.6000	11.4535	-1.3% to +81.9%
Mean	16.9765	11.6818	18.3935	17.4750	-5.0% to +49.6%
Maximum	23.1860	15.1200	25.1300	22.4952	-10.5% to +48.8%
Stand. dev.	2.4818	1.9452	2.6690	1.8384	-31.1% to -5.5%

Table C.3: Platform surge motion statistics (in m) from DLC 5.3 from OC3 phase IV codes and MoWiT in comparison, **deviations** are highlighted in **red**.

Statistics	OC3 mean	OC3 min	OC3 max	MoWiT	MoWiT deviation
Minimum	6.5274	2.0168	15.2762	8.0755	-47.1% to +300.4%
Mean	14.2786	5.8164	24.7603	11.3390	-54.2% to +95.0%
Maximum	22.9980	10.4593	38.0489	14.2555	-62.5% to +36.3%
Stand. dev.	3.2317	1.4129	6.6082	1.1624	-82.4% to -17.7%

Table C.4: Platform heave motion statistics (in m) from DLC 5.3 from OC3 phase IV codes and MoWiT in comparison, **deviations** are highlighted in **red**.

Statistics	OC3 mean	OC3 min	OC3 max	MoWiT	MoWiT deviation
Minimum	-1.2479	-1.7048	-0.8807	-0.7968	+9.5% to +53.3%
Mean	-0.2240	-0.4101	-0.0173	-0.3893	-2.2 × 10 ³ % to +5.1%
Maximum	0.7375	0.3448	1.0191	-0.0205	-105.9% to -102.0%
Stand. dev.	0.4259	0.2626	0.5779	0.1597	-72.4% to -39.2%

Table C.5: Platform pitch motion statistics (in deg) from DLC 5.3 from OC3 phase IV codes and MoWiT in comparison, **deviations** are highlighted in **red**.

Statistics	OC3 mean	OC3 min	OC3 max	MoWiT	MoWiT deviation
Minimum	0.1508	-0.7656	1.0512	0.3473	-67.0% to +145.4%
Mean	2.8102	1.1912	4.6988	2.3567	-49.8% to +97.8%
Maximum	5.5084	3.6456	8.6379	4.1972	-51.4% to +15.1%
Stand. dev.	1.1025	0.6258	2.2428	0.7097	-68.4% to +13.4%

Table C.6: Platform yaw motion statistics (in deg) from DLC 5.3 from OC3 phase IV codes and MoWiT in comparison, **deviations** are highlighted in **red**.

Statistics	OC3 mean	OC3 min	OC3 max	MoWiT	MoWiT deviation
Minimum	-2.8602	-4.5918	-0.1371	-1.8569	-1.3 × 10 ³ % to +59.6%
Mean	-0.1384	-0.3682	-0.0002	0.1489	+140.4% to +8.6 × 10⁴%
Maximum	2.8284	0.1463	4.1148	2.1273	-48.3% to +1.4 × 10 ³ %
Stand. dev.	0.9825	0.0581	1.4656	0.7398	-49.5% to +1.2 × 10 ³ %

Table C.7: Tower-top fore-aft shear force statistics (in kN) from DLC 5.3 from OC3 phase IV codes and MoWiT in comparison, **deviations** are highlighted in **red**.

Statistics	OC3 mean	OC3 min	OC3 max	MoWiT	MoWiT deviation
Minimum	-525.8	-580.5	-446.3	-353.7	+20.7% to +39.1%
Mean	523.6	417.2	625.6	314.5	-49.7% to -24.6%
Maximum	1.7×10^3	1.5×10^3	1.9×10^3	925.4	-50.4% to -39.9%
Stand. dev.	327.4	300.6	374.8	350.0	-6.6% to +16.4%

Table C.8: Tower-top fore-aft bending moment statistics (in kNm) from DLC 5.3 from OC3 phase IV codes and MoWiT in comparison, **deviations** are highlighted in **red**.

Statistics	OC3 mean	OC3 min	OC3 max	MoWiT	MoWiT deviation
Minimum	-5.7×10^3	-7.9×10^3	-3.7×10^3	-2.3×10^3	+38.4% to +71.0%
Mean	991.5	-425.8	1.6×10^3	3.0×10^3	+79.6% to +795.5%
Maximum	7.5×10^3	6.9×10^3	8.2×10^3	9.5×10^3	+15.9% to +37.6%
Stand. dev.	1.9×10^3	1.3×10^3	2.3×10^3	1.9×10^3	-19.0% to +43.0%

Table C.9: Downstream fairlead tension statistics (in kN) from DLC 5.3 from OC3 phase IV codes and MoWiT in comparison, **deviations** are highlighted in **red**.

Statistics	OC3 mean	OC3 min	OC3 max	MoWiT	MoWiT deviation
Minimum	564.8	456.7	621.6	674.1	+8.4% to +47.6%
Mean	668.7	575.3	726.4	721.7	-0.7% to +25.4%
Maximum	777.7	685.7	840.0	787.1	-6.3% to +14.8%
Stand. dev.	45.8	34.4	69.5	23.6	-66.1% to -31.4%

Table C.10: Upstream fairlead tension statistics (in kN) from DLC 5.3 from OC3 phase IV codes and MoWiT in comparison, **deviations** are highlighted in **red**.

Statistics	OC3 mean	OC3 min	OC3 max	MoWiT	MoWiT deviation
Minimum	993.0	966.7	1040.1	987.1	-5.1% to +2.1%
Mean	1.1×10^3	1.0×10^3	1.3×10^3	1.1×10^3	-16.8% to +0.8%
Maximum	1.3×10^3	1.1×10^3	1.7×10^3	1.1×10^3	-33.9% to -1.3%
Stand. dev.	66.9	35.7	162.1	26.9	-83.4% to -24.6%

Table C.11: Generator power statistics (in kW) from DLC 5.3 from OC3 phase IV codes and MoWiT in comparison, **deviations** are highlighted in **red**.

Statistics	OC3 mean	OC3 min	OC3 max	MoWiT	MoWiT deviation
Minimum	4.1×10^3	3.8×10^3	4.3×10^3	1.6×10^3	−63.2% to −59.0%
Mean	5.1×10^3	5.0×10^3	5.2×10^3	4.7×10^3	−9.7% to −6.7%
Maximum	5.8×10^3	5.2×10^3	6.0×10^3	5.3×10^3	−11.5% to +1.2%
Stand. dev.	309.4	174.4	381.8	508.2	+33.1% to +191.4%

Table C.12: Rotor speed statistics (in rpm) from DLC 5.3 from OC3 phase IV codes and MoWiT in comparison, **deviations** are highlighted in **red**.

Statistics	OC3 mean	OC3 min	OC3 max	MoWiT	MoWiT deviation
Minimum	9.8675	9.2700	10.3200	6.4171	−37.8% to −30.8%
Mean	12.1864	12.1662	12.2095	10.8476	−11.2% to −10.8%
Maximum	14.2706	14.0500	14.4024	13.6663	−5.1% to −2.7%
Stand. dev.	0.8298	0.7435	0.9231	1.5016	+62.7% to +102.0%

Table C.13: Out-of-plane blade-tip deflection statistics (in m) from DLC 5.3 from OC3 phase IV codes and MoWiT in comparison, **deviations** are highlighted in **red**.

Statistics	OC3 mean	OC3 min	OC3 max	MoWiT	MoWiT deviation
Minimum	−1.7581	−2.4453	−1.3810	−4.3522	−215.1% to −78.0%
Mean	1.8017	1.5810	2.1870	2.0758	−5.1% to +31.3%
Maximum	5.3812	5.0540	5.8790	7.0813	+20.5% to +40.1%
Stand. dev.	1.0941	1.0550	1.1710	1.8944	+61.8% to +79.6%

Appendix D

Potential risks and consequences associated with global system performance criteria

Table D.1: Potential risks and consequences associated with global system performance criteria, adapted from Bhattacharya (2019) and extended.

Criterion	Potential risks and consequences in case of too large values
Total inclination angle	<ul style="list-style-type: none">• Risk of wind turbine shutdown due to exceeded total inclination angle critical to the operation of the system;• Reduced efficiency of the wind turbine due to inclined rotor plane area;• Reduced clearance between blade and tower and risk of collision due to weight-induced blade bending when the FOWT system is strongly tilted out of the wind;• Increased demands on and potential failure of the yaw system (motor and brake) to control the position when the FOWT system is strongly tilted out of the wind;• Increased fatigue and wear of bearings (for both yaw and pitch systems, as well as main shaft) because of changing load direction and amount due to tilting motion of the FOWT system;• Increased demands on and potential failure of the lubrication system to maintain required fluid flow when the FOWT system is strongly inclined;• Risk of exceeding ultimate bending stress at, for example, the tower base due to strongly inclined FOWT system;• Increased bending and potential failure of the power cable at the exit point from the floating platform when the FOWT system is strongly inclined;• Potential buckling and failure of a mooring line at the fairlead due to tilting motion of the FOWT system.

Table D.1: Potential risks and consequences associated with global system performance criteria.
(cont.)

Criterion	Potential risks and consequences in case of too large values
Horizontal nacelle acceleration	<ul style="list-style-type: none"> • Risk of wind turbine shutdown due to exceeded horizontal nacelle acceleration critical to the operation of the system; • Increased demands on and potential failure of the yaw system (motor and brake) to control the position against the direction of the horizontal nacelle acceleration; • Increased fatigue and wear of bearings (for both yaw and pitch systems, as well as main shaft) because of changing frequency and magnitude of load cycles due to increased horizontal nacelle acceleration; • Increased demands on and potential failure of the lubrication system to maintain required fluid flow when the nacelle experiences high horizontal accelerations; • Increased fatigue and potential failure of the power cable due to large dynamic motion in case of high horizontal nacelle accelerations.
Dynamic translational motion	<ul style="list-style-type: none"> • Risk of wind turbine shutdown due to exceeded horizontal nacelle acceleration critical to the operation of the system because of large dynamic translational motion of the FOWT system; • Increased fatigue and wear of bearings (for both yaw and pitch systems, as well as main shaft) because of changing frequency, magnitude, and direction of load cycles due to dynamic translational motion of the FOWT system; • Increased structural fatigue and risk of excitation of a system or component natural frequency due to critical dynamic translational motion of the FOWT system; • Increased fatigue and potential failure of the power cable due to large dynamic translational motion of the FOWT system.
Mean translational motion	<ul style="list-style-type: none"> • Risk of wind turbine capsizes because of mooring or anchoring system failure due to exceeded mean translational motion critical to the operation of the system; • Increased bending and potential failure of the power cable when the floating system experiences a large mean translational motion away from the power cable laying route; • Increased loads on and potential failure of a fairlead due to exceeded mean translational motion critical to the operation of the system; • Increased loads on and potential failure of a mooring line due to exceeded mean translational motion critical to the operation of the system; • Increased loads on and potential failure of an anchor due to exceeded mean translational motion critical to the operation of the system.

Appendix E

Pareto filtering

The results of the global design optimization are filtered according to Pareto dominance. This is performed in MATLAB[®] by means of the following listing, which is based on the code by Simone (2020) but adjusted (line number 15), as the Pareto dominance needs to be for the smaller values.

```
1 function [p,idxs] = paretoFront(p)
2 % Filters a set of points P according to Pareto dominance, i.e.,
   % points that are dominated (both weakly and strongly) are filtered.
3 %
4 % Inputs:
5 % - p : N-by-D matrix, where N is the number of points and D is the
   % number of elements (objectives) of each point.
6 %
7 % Outputs:
8 % - p : Pareto-filtered p.
9 % - idxs : Indices of the non-dominated solutions.
10
11 [i, dim] = size(p);
12 idxs = [1 : i]';
13 while i >= 1
14     old_size = size(p,1);
15     indices = sum( bsxfun( @le, p(i,:), p ), 2 ) == dim;
16     indices(i) = false;
17     p(indices,:) = [];
18     idxs(indices) = [];
19     i = i - 1 - (old_size - size(p,1)) + sum(indices(i:end));
20 end
21 end
```

Appendix F

Characteristics of a two-parameter Weibull distribution

A common two-parameter Weibull distribution (of a parameter $*$) with scale factor b (of unit m/s in case of the considered Weibull distribution of the wind speed applied in Section 6.1.5.1) and unitless shape factor c can be formulated as cumulative density function (CDF) $F(*)$, given in Equation F.1, or its derivative the probability density function (PDF) $f(*)$, given in Equation F.2.

$$F(*) = 1 - e^{-\left(\frac{*}{b}\right)^c} \quad (\text{F.1})$$

$$f(*) = \frac{c}{b} \left(\frac{*}{b}\right)^{c-1} e^{-\left(\frac{*}{b}\right)^c} \quad (\text{F.2})$$

The corresponding mean $\mu(*)$ and standard deviation $\sigma(*)$ can be obtained following Equations F.3 and F.4 and using the gamma function presented in Equation F.5.

$$\mu(*) = b\Gamma\left(1 + \frac{1}{c}\right) \quad (\text{F.3})$$

$$\sigma(*) = b\sqrt{\Gamma\left(1 + \frac{2}{c}\right) - \left[\Gamma\left(1 + \frac{1}{c}\right)\right]^2} \quad (\text{F.4})$$

$$\Gamma(n) = (n-1)! \quad (\text{F.5})$$

The value of the considered parameter (the wind speed in the applied example, as selected in Section 6.1.5.1) that corresponds to a specific percentile p is determined by setting Equation F.1 for the CDF equal to p , leading to Equation F.6.

$$* = b[-\ln(1-p)]^{\frac{1}{c}} \quad (\text{F.6})$$

Appendix G

Characteristics of a three-parameter Weibull distribution

A three-parameter Weibull distribution uses - compared to a two-parameter Weibull distribution - as well a scale factor b (of unit m in case of the considered Weibull distribution of the significant wave height applied in Section 6.1.5.2) and shape factor c (unitless), but has additionally a location parameter a (of unit m in case of the considered Weibull distribution of the significant wave height applied in Section 6.1.5.2). All two-parameter Weibull functions and characteristics can be derived from the corresponding three-parameter Weibull expressions by setting a equal to zero. The three-parameter Weibull cumulative density function (CDF) $F(*)$ and probability density function (PDF) $f(*)$ are given in Equations G.1 and G.2, respectively.

$$F(*) = 1 - e^{-\left(\frac{* - a}{b}\right)^c} \quad (\text{G.1})$$

$$f(*) = \frac{c}{b} \left(\frac{* - a}{b}\right)^{c-1} e^{-\left(\frac{* - a}{b}\right)^c} \quad (\text{G.2})$$

The corresponding mean $\mu(*)$ and standard deviation $\sigma(*)$ are obtained following Equations G.3 and G.4, respectively, using again the gamma function, as already presented in Equation F.5 in Appendix F.

$$\mu(*) = a + b\Gamma\left(1 + \frac{1}{c}\right) \quad (\text{G.3})$$

$$\sigma(*) = b\sqrt{\Gamma\left(1 + \frac{2}{c}\right) - \left[\Gamma\left(1 + \frac{1}{c}\right)\right]^2} \quad (\text{G.4})$$

Considering an extreme event, such as SSS with the number N of extreme events fitting theoretically in one year, the corresponding CDF $F_{\text{SSS}}(*)$ and PDF $f_{\text{SSS}}(*)$ are extrapolated according to Equations 6.3 (given in Section 6.1.5.2) and G.5.

$$f_{\text{SSS}}(*) = [F_{\text{SSS}}(*)]' = N[F(*)]^{N-1} f(*) \quad (\text{G.5})$$

The corresponding mean value $\mu_{SSS}(*)$ and standard deviation $\sigma_{SSS}(*)$ pertained to the extreme event are then obtained following Equations G.6 and G.7, respectively.

$$\mu_{SSS}(*) = \int_0^{\infty} * f(*) d* \quad (G.6)$$

$$\sigma_{SSS}(*) = \sqrt{\int_0^{\infty} (* - \mu_{SSS}(*))^2 f(*) d*} \quad (G.7)$$

The value of the considered parameter in an extreme event (the significant wave height in SSS in the applied example, as selected in Section 6.1.5.2) that corresponds to a specific percentile p is determined by setting Equation 6.3 for the CDF for a SSS event equal to p , leading to Equation G.8.

$$* = a + b \left[-\ln \left(1 - p^{\frac{1}{N}} \right) \right]^{\frac{1}{c}} \quad (G.8)$$

Appendix H

Python function for closest value

In order to find for a given value the closest number out of a vector of numbers, the function `nearest` is introduced. The applied approach is as follows:

1. from the entries in the vector the specific given value is subtracted and the absolute value of this difference is calculated (line number 11);
2. from the resulting vector the position (index) of the minimum entry is determined (line number 12);
3. the number in the vector, which is the closest to the provided value, is found as the entry in the vector with the index determined in step 2 (line number 13).

As this function is required within the interpolation approach (Section 6.2.2.3), which is utilized within the iterative optimization algorithm (Section 6.2.3.2) performed by means of the MoWiT-Dymola[®]-Python framework, the function is coded in Python as written in the following listing.

```
1 def nearest(array, value):
2     # Returns the number in an array, which is the closest to the provided
3     # value.
4     #
5     # Inputs:
6     # - array: Array of numbers.
7     # - value : Number.
8     #
9     # Return:
10    # - array[idx] : Number in array with index idx.
11
12    n = [abs(i-value) for i in array]
13    idx = n.index(min(n))
14    return array[idx]
```

References

- Abimbola, M., Khan, F. & Khakzad, N. (2014), 'Dynamic safety risk analysis of offshore drilling', *Journal of Loss Prevention in the Process Industries* **30**, 74–85. doi: <http://dx.doi.org/10.1016/j.jlp.2014.05.002>.
- Airy, G. B. (1845), 'Tides and waves', *Encyclopedia Metropolitana* (192), 241–396.
- Alibaba.com (2020a), 'Magnadense (schwerer Beton)'.
URL: <https://german.alibaba.com/product-detail/magnadense-heavy-concrete-172429386.html> [Accessed on: 2020-02-05]
- Alibaba.com (2020b), 'Sandstone price per ton'.
URL: <https://www.alibaba.com/showroom/sandstone-price-per-ton.html> [Accessed on: 2020-02-05]
- Arabian-Hoseynabadi, H., Oraee, H. & Tavner, P. J. (2010), 'Failure modes and effects analysis (FMEA) for wind turbines', *International Journal of Electrical Power & Energy Systems* **32**(7), 817–824. doi: <http://dx.doi.org/10.1016/j.ijepes.2010.01.019>.
- Arapogianni, A., Genachte, A.-B., Ochagavia, R. M., Vergara, J. P., Castell, D., Tsouroukdissian, A. R., Korbijn, J., Bolleman, N. C., Huera-Huarte, F. J., Schuon, F., Ugarte, A., Sandberg, J., de Laleu, V., Maciel, J., Tunbjer, A., Roth, R., de la Gueriviere, P., Coulombeau, P., Jedrec, S., Philippe, C., Voutsinas, S., Weinstein, A., Vita, L., Byklum, E., Hurley, W. L. & Grubel, H. (2013), *Deep Water: The next step for offshore wind energy*, European Wind Energy Association, Brussels, Belgium.
URL: www.ewea.org/report/deep-water [Accessed on: 2020-05-26]
- Ashuri, T., Zaaijer, M. B., Martins, J., van Bussel, G. & van Kuik, G. (2014), 'Multidisciplinary design optimization of offshore wind turbines for minimum levelized cost of energy', *Renewable Energy* **68**, 893–905. doi: <http://dx.doi.org/10.1016/j.renene.2014.02.045>.
- Ayyub, B. M. (2014), *Risk Analysis in Engineering and Economics*, 2nd edn, Taylor and Francis, Hoboken, NJ, USA.
- Bachynski, E. E. (2018), Fixed and floating offshore wind turbine support structures, in O. Anaya-Lara, J. O. Tande, K. Uhlen & K. Merz, eds, 'Offshore Wind Energy Technology', Wiley, Hoboken, NJ, pp. 103–142. doi: <http://dx.doi.org/10.1002/9781119097808.ch4>.

- Bachynski, E. E., Etemaddar, M., Kvittem, M. I., Luan, C. & Moan, T. (2013), 'Dynamic analysis of floating wind turbines during pitch actuator fault, grid loss, and shutdown', *Energy Procedia* **35**, 210–222. doi: <http://dx.doi.org/10.1016/j.egypro.2013.07.174>.
- Bachynski, E. E. & Moan, T. (2012), 'Design considerations for tension leg platform wind turbines', *Marine Structures* **29**(1), 89–114. doi: <http://dx.doi.org/10.1016/j.marstruc.2012.09.001>.
- Bai, X., Sun, H. & Sun, L. (2012), Process risk assessment for transportation and installation of jacket considering correlation, in J. S. Chung, ed., 'ISOPE-2012 Rhodes', International Society of Offshore and Polar Engineers, Cupertino, CA, USA, pp. 669–675.
- Baker, J. H. (2014), 'Applying the threat matrix to investigate reliability and maintainability requirements of offshore renewable energy devices', *Underwater Technology: International Journal of the Society for Underwater* **32**(3), 199–206. doi: <http://dx.doi.org/10.3723/ut.32.199>.
- Bangs, A. S., Miettinen, J. A., Silvola, I., Mikkola, T. & Beattie, S. M. (2002), Design of the truss spars for the Nansen/Boomvang field development, in 'Proceedings of the Offshore Technology Conference, Houston, TX, USA, May 6-9, 2002', Offshore Technology Conference. doi: <http://dx.doi.org/10.4043/14090-MS>.
- Baños, R., Manzano-Agugliaro, F., Montoya, F. G., Gil, C., Alcayde, A. & Gómez, J. (2011), 'Optimization methods applied to renewable and sustainable energy: A review', *Renewable and Sustainable Energy Reviews* **15**(4), 1753–1766. doi: <http://dx.doi.org/10.1016/j.rser.2010.12.008>.
- Barbanti, G., Marino, E. & Borri, C. (2019), Mooring system optimization for a spar-buoy wind turbine in rough wind and sea conditions, in F. Ricciardelli & A. M. Avossa, eds, 'Proceedings of the XV Conference of the Italian Association for Wind Engineering, Naples, Italy, September 9-12, 2018', Vol. 27 of *Lecture Notes in Civil Engineering*, Springer International Publishing, Cham, Switzerland, pp. 87–98. doi: http://dx.doi.org/10.1007/978-3-030-12815-9_7.
- Berthelsen, P. A., Fylling, I., Vita, L. & Paulsen, U. S. (2012), Conceptual design of a floating support structure and mooring system for a vertical axis wind turbine, in 'Proceedings of the ASME 31st International Conference on Ocean, Offshore and Arctic Engineering, Rio de Janeiro, Brazil, July 1-6, 2012', American Society of Mechanical Engineers, New York, NY, USA, pp. 259–268. doi: <http://dx.doi.org/10.1115/OMAE2012-83335>.
- Besnard, F. & Bertling, L. (2010), 'An approach for condition-based maintenance optimization applied to wind turbine blades', *IEEE Transactions on Sustainable Energy* **1**(2), 77–83. doi: <http://dx.doi.org/10.1109/TSTE.2010.2049452>.
- Betz, A. (1920), 'Das Maximum der theoretisch möglichen Ausnutzung des Windes durch Windmotoren', *Zeitschrift für das gesamte Turbinenwesen* (26), 307–309.

- BG BAU (2000), *Gewichtstabellen für Turmdrehkranführer*, Arbeitsgemeinschaft der Bau-Berufsgenossenschaften, online.
URL: <http://www.bgbau-medien.de/bau/bau507/1.htm> [Accessed on: 2017-08-01]
- Bharatbhai, M. G. (2015), 'Failure mode and effect analysis of Repower 5M wind turbine', *International Journal of Advance Research in Engineering, Science & Technology* 2(5).
- Bhattacharya, S. (2019), *Design of foundations for offshore wind turbines*, Wiley, Hoboken, NJ, USA.
- Blue H Engineering (2017), *Technology*.
URL: <http://www.blueengineering.com/technology.html> [Accessed on: 2017-12-16]
- Borg, M. & Collu, M. (2015), 'A comparison between the dynamics of horizontal and vertical axis offshore floating wind turbines', *Philosophical transactions A* 373(2035). doi: <http://dx.doi.org/10.1098/rsta.2014.0076>.
- Bossler, A. (2014), Japan's floating offshore wind projects: An overview, in 'energy ocean, Atlantic City, NJ, USA, June 3-5, 2014'.
URL: <https://www.ormanagerconference.com/wp-content/uploads/2014/06/Bossler.pdf> [Accessed on: 2020-07-09]
- Bredmose, H., Larsen, S. E., Matha, D., Rettenmeier, A., Marino, E. & Sætran, L. (2012), *D2.4: Collation of offshore wind-wave dynamics*, Marine Renewables Infrastructure Network.
- BSI (1991), *Quality vocabulary (BS 4778)*, British Standards Institution, London, UK.
- BSI (2001), *Hazard and operability studies (HAZOP studies) - Application guide (BS IEC 61882:2001)*, British Standards Institution, London, UK. doi: <http://dx.doi.org/10.3403/02337615>.
- BSI (2006), *Analysis techniques for system reliability - Procedure for failure mode and effects analysis (FMEA) (BS EN 60812:2006)*, British Standards Institution, London, UK. doi: <http://dx.doi.org/10.3403/30101028>.
- BSI (2010a), *Risk management - Principles and guidelines (BS ISO 31000:2009)*, British Standards Institution, London, UK.
- BSI (2010b), *Risk management - Risk assessment techniques (BS EN 31010:2010)*, British Standards Institution, London, UK.
- BSI (2013), *Petroleum and natural gas industries - Specific requirements for offshore structures: Part 7: Stationkeeping systems for floating offshore structures and mobile offshore units (BS EN ISO 19901-7:2013)*, British Standards Institution, London, UK.

- Bulder, B., van Hees, M. T., Henderson, A. R., Huijsmans, R. H. M., Pierik, J. T. G., Snijders, E. J. B., Wijnants, G. H. & Wolf, M. J. (2002), *Studie naar haalbaarheid van en randvoorwaarden voor drijvende offshore windturbines*, TNO-Bouw, Delft, The Netherlands.
URL: <http://www.offshorewindenergy.org/> [Accessed on: 2017-12-15]
- Butcher, N. (2018), 'The steel tariff and construction cost: Putting it into context', *Archinect News*(April 6).
URL: <https://archinect.com/news/article/150058852/the-steel-tariff-and-construction-cost-putting-it-into-context> [Accessed on: 2020-02-11]
- Butterfield, S., Musial, W., Jonkman, J. & Sclavounos, P. (2007), *Engineering Challenges for Floating Offshore Wind Turbines: Conference Paper NREL/CP-500-38776*, National Renewable Energy Laboratory, Golden, CO, USA.
- Carroll, J., McDonald, A. & McMillan, D. (2016), 'Failure rate, repair time and unscheduled O&M cost analysis of offshore wind turbines', *Wind Energy* **19**(6), 1107–1119. doi: <http://dx.doi.org/10.1002/we.1887>.
- Carswell, W., Arwade, S., Myers, A. & Hajjar, J. (2013), Reliability analysis of monopile offshore wind turbine support structures, in G. Deodatis, B. Ellingwood & D. Frangopol, eds, 'Safety, Reliability, Risk and Life-Cycle Performance of Structures and Infrastructures', Taylor and Francis, London, UK, pp. 223–229.
- Castro Sayas, F. & Allan, R. N. (1996), 'Generation availability assessment of wind farms', *IEE Proceedings - Generation, Transmission and Distribution* **143**(5), 507. doi: <http://dx.doi.org/10.1049/ip-gtd:19960488>.
- Chen, D., Gao, P., Huang, S., Fan, K., Zhuang, N. & Liao, Y. (2017), 'Dynamic response and mooring optimization of spar-type substructure under combined action of wind, wave, and current', *Journal of Renewable and Sustainable Energy* **9**(6), 063307. doi: <http://dx.doi.org/10.1063/1.5017228>.
- Chew, K.-H., Tai, K., Ng, E. & Muskulus, M. (2016), 'Analytical gradient-based optimization of offshore wind turbine substructures under fatigue and extreme loads', *Marine Structures* **47**, 23–41. doi: <http://dx.doi.org/10.1016/j.marstruc.2016.03.002>.
- Choi, E., Han, C., Kim, H. & Park, S. (2014), 'Optimal design of floating substructures for spar-type wind turbine systems', *Wind and Structures* **18**(3), 253–265. doi: <http://dx.doi.org/10.12989/was.2014.18.3.253>.
- Choi, S.-K., Canfield, R. A. & Grandhi, R. V. (2007), *Reliability-based Structural Design*, Springer-Verlag London Limited, London, UK. doi: <http://dx.doi.org/10.1007/978-1-84628-445-8>.
- Chopra, M., Rastogi, R., Kumar, A. V., Sunny, F. & Nair, R. N. (2013), 'Response surface method coupled with first-order reliability method based methodology for groundwater flow

- and contaminant transport model for the uranium tailings pond site', *Environmental Modelling & Assessment* **18**(4), 439–450. doi: <http://dx.doi.org/10.1007/s10666-012-9352-0>.
- Clark, C. E. & Paredes, G. M. (2018), Effects of co-located floating wind-wave systems on fatigue damage of floating offshore wind turbine mooring cables, in 'Proceedings of the ASME 1st International Offshore Wind Technical Conference, San Francisco, CA, USA, November 4-7, 2018', American Society of Mechanical Engineers. doi: <http://dx.doi.org/10.1115/IOWTC2018-1077>.
- Clauss, G. F. & Birk, L. (1996), 'Hydrodynamic shape optimization of large offshore structures', *Applied Ocean Research* **18**(4), 157–171. doi: [http://dx.doi.org/10.1016/S0141-1187\(96\)00028-4](http://dx.doi.org/10.1016/S0141-1187(96)00028-4).
- Clauss, G., Lehmann, E. & Østergaard, C. (1992), *Offshore structures: Volume I: Conceptual Design and Hydromechanics*, Springer-Verlag, London, UK; Berlin/Heidelberg, Germany; New York, NY, USA.
- Cordle, A. & Jonkman, J. (2011), *State of the Art in Floating Wind Turbine Design Tools: Conference Paper NREL/CP-5000-50543*, National Renewable Energy Laboratory, Golden, CO, USA.
- Cruz, J. & Atcheson, M., eds (2016), *Floating Offshore Wind Energy: The Next Generation of Wind Energy*, Springer International Publishing Switzerland, Switzerland. doi: <http://dx.doi.org/10.1007/978-3-319-29398-1>.
- Dai, L., Ehlers, S., Rausand, M. & Utne, I. B. (2013), 'Risk of collision between service vessels and offshore wind turbines', *Reliability Engineering & System Safety* **109**, 18–31. doi: <http://dx.doi.org/10.1016/j.res.2012.07.008>.
- Delorm, T. M., Lu, Y., Christou, A. & McCluskey, P. (2016), 'Comparisons of offshore wind turbine reliability', *Proceedings of the Institution of Mechanical Engineers, Part O: Journal of Risk and Reliability* **230**(3), 251–264. doi: <http://dx.doi.org/10.1177/1748006X15624592>.
- Depina, I. & Eiksund, G. (2015), Reliability-based design optimization of laterally loaded monopile foundations for offshore wind turbines, in V. Meyer, ed., 'Frontiers in offshore geotechnics III', CRC Press/Balkema, Leiden, The Netherlands, pp. 1355–1360.
- Dessault Systèmes (2015a), *Dymola: Dynamic Modeling Laboratory: User Manual Volume 1*, Dessault Systèmes AB, Lund, Sweden.
URL: <http://www.Dymola.com> [Accessed on: 2018-11-12]
- Dessault Systèmes (2015b), *Dymola: Dynamic Modeling Laboratory: User Manual Volume 2*, Dessault Systèmes AB, Lund, Sweden.
URL: <http://www.Dymola.com> [Accessed on: 2018-11-12]

- Ding, Q., Li, C., Li, B., Hao, W. & Ye, Z. (2017), 'Research on the influence of helical strakes and its parameters on dynamic response of platform of floating wind turbine based on optimization method of orthogonal design', *Journal of Solar Energy Engineering* **139**(5), 800. doi: <http://dx.doi.org/10.1115/1.4037091>.
- Ding, Q., Li, C., Ye, Z., Zhou, G. & Wang, D. (2017), 'Research on optimization for dynamic response of platform of floating wind turbine', *Taiyangneng Xuebao/Acta Energetica Solaris Sinica* **38**(5), 1405–1414.
- DNV (1992), *Structural Reliability Analysis of Marine Structures (Classification Notes No. 30.6)*, July 1992 edn, Det Norske Veritas, Norway.
- DNV (2014), *Design of Offshore Wind Turbine Structures (Offshore Standard DNV-OS-J101)*, May edn, Det Norske Veritas AS.
URL: <http://www.dnvgl.com> [Accessed on: 2017-12-19]
- DNV, ed. (2002), *Marine risk assessment*, Vol. 2001/063 of *Offshore technology report*, HSE Books, Sudbury, Canada.
- DNV GL (2015a), *Buckling (Class Guideline DNVGL-CG-0128)*, DNV GL AS, Bristol, UK.
URL: <http://www.dnvgl.com> [Accessed on: 2020-07-09]
- DNV GL (2015b), *Design of offshore steel structures, general - LRFD method (Offshore Standard DNVGL-OS-C101)*, July 2015 edn, DNV GL AS.
URL: <https://www.dnvgl.com/> [Accessed on: 2019-12-16]
- DNV GL (2016a), *Loads and site conditions for wind turbines (Standard DNVGL-ST-0437)*, November edn, DNV GL AS.
URL: <https://www.dnvgl.com/> [Accessed on: 2018-10-09]
- DNV GL (2016b), *Marine operations and marine warranty (Standard DNVGL-ST-N001)*, June 2016 edn, DNV GL AS.
URL: <https://www.dnvgl.com/> [Accessed on: 2020-01-14]
- DNV GL (2017), 'Electrifying the future'.
URL: <https://www.dnvgl.com/> [Accessed on: 2017-12-14]
- DNV GL (2018a), *Bladed Theory Manual: Version 4.9*, Garrad Hassan & Partners Ltd., Bristol, UK.
- DNV GL (2018b), *Bladed User Manual: Version 4.9*, Garrad Hassan & Partners Ltd., Bristol, UK.
- DNV GL (2018c), *Floating wind turbine structures (Standard DNVGL-ST-0119)*, July edn, DNV GL AS.
URL: <http://www.dnvgl.com> [Accessed on: 2018-10-04]

- DNV GL (2020), 'Wind turbine design software - Bladed'.
URL: <https://www.dnvgl.com/energy/generation/software/bladed/index.html> [Accessed on: 2020-06-09]
- Dong, W., Moan, T. & Gao, Z. (2012), 'Fatigue reliability analysis of the jacket support structure for offshore wind turbine considering the effect of corrosion and inspection', *Reliability Engineering & System Safety* **106**, 11–27. doi: <http://dx.doi.org/10.1016/j.res.2012.06.011>.
- Dorf, R. C. (1996), *The engineering handbook*, CRC Press, Boca Raton, FL, USA.
- Elsevier (2020), 'ScienceDirect article: a review of reliability-based methods for risk analysis and their application in the offshore wind industry'.
URL: <https://www.sciencedirect.com/science/article/pii/S1364032118302120> [Accessed on: 2020-08-03]
- Engineering ToolBox (2009), 'Densities of selected solids'.
URL: https://www.engineeringtoolbox.com/density-solids-d_1265.html [Accessed on: 2018-12-12]
- Engineering ToolBox (2010), 'Densities of common materials'.
URL: https://www.engineeringtoolbox.com/density-materials-d_1652.html [Accessed on: 2018-12-12]
- Equinor (2017), 'World's first floating wind farm has started production'.
URL: <https://www.equinor.com/en/news/worlds-first-floating-wind-farm-started-production.html> [Accessed on: 2017-10-18]
- Equinor (2020a), 'How Hywind works'.
URL: <https://www.equinor.com/en/what-we-do/floating-wind/how-hywind-works.html> [Accessed on: 2020-06-11]
- Equinor (2020b), *Hywind Scotland: The world's first commercial floating wind farm*.
URL: <https://www.equinor.com/content/dam/statoil/documents/newsroom-additional-documents/news-attachments/brochure-hywind-a4.pdf> [Accessed on: 2020-06-21]
- European Commission (2013), 'Horizon 2020 - Work Programme 2014-2015: Part 19. General Annexes Revised'.
URL: https://ec.europa.eu/commission/index_en [Accessed on: 2017-12-17]
- European Parliament & Council of the European Union (2009), *Directive 2009/28/EC of the European Parliament and of the Council of 23 April 2009 on the promotion of the use of energy from renewable sources and amending and subsequently repealing Directives 2001/77/EC and 2003/30/EC*, Official Journal of the European Union.
URL: <http://data.europa.eu/eli/dir/2009/28/oj> [Accessed on: 2020-05-14]

- European Parliament & Council of the European Union (2018), *Directive (EU) 2018/2001 of the European Parliament and of the Council of 11 December 2018 on the promotion of the use of energy from renewable sources*, Official Journal of the European Union.
URL: <http://data.europa.eu/eli/dir/2018/2001/oj> [Accessed on: 2020-05-14]
- Faulstich, S., Hahn, B., Lyding, P. & Tavner, P. (2009), Reliability of offshore turbines - identifying risks by onshore experience, in 'Proceedings of the EWEA Offshore 2009, Stockholm, Sweden, September 14-16, 2009', Curran, Red Hook, NY, USA.
- Fenton, J. D. (1985), 'A fifth-order Stokes theory for steady waves', *Journal of Waterway, Port, Coastal, and Ocean Engineering* **111**(2), 216–234. doi: [http://dx.doi.org/10.1061/\(ASCE\)0733-950X\(1985\)111:2\(216\)](http://dx.doi.org/10.1061/(ASCE)0733-950X(1985)111:2(216)).
- Ferdous, R., Khan, F., Sadiq, R., Amyotte, P. & Veitch, B. (2012), 'Handling and updating uncertain information in bow-tie analysis', *Journal of Loss Prevention in the Process Industries* **25**(1), 8–19. doi: <http://dx.doi.org/10.1016/j.jlp.2011.06.018>.
- Figueira, J., Greco, S. & Ehrogott, M., eds (2005), *Multiple Criteria Decision Analysis: State of the Art Surveys*, Vol. 78 of *International Series in Operations Research & Management Science*, Springer Science + Business Media Inc, New York, NY, USA. doi: <http://dx.doi.org/10.1007/b100605>.
- Foster, M. (2016), 'Floating platform keels over in Japan - updated', *Windpower Monthly*.
URL: <https://www.windpowermonthly.com/article/1394760/floating-platform-keels-japan-updated> [Accessed on: 2020-08-01]
- Fraunhofer IWES (2015), *WIND-POOL - Wind Energy Information Data Pool*, Fraunhofer Institute for Wind Energy and Energy System Technology, IWES, Kassel, Germany.
URL: <http://windmonitor.iese.fraunhofer.de/opencms/export/sites/windmonitor/img/Description-of-WInD-Pool.pdf> [Accessed on: 2020-07-09]
- Froude, R. E. (1889), 'On the part played in propulsion by difference in pressure', *Transaction of the Institute of Naval Architects* (30), 390–405.
- Fugro GEOS (2001), *Wind and wave frequency distributions for sites around the British Isles (Offshore Technology Report 2001/030)*, Health and Safety Executive, Norwich, UK.
- Fukushima Offshore Wind Consortium (2017), *Fukushima Floating Offshore Wind Farm Demonstration Project*.
URL: <http://www.fukushima-forward.jp/english/> [Accessed on: 2017-12-16]
- Fylling, I. & Berthelsen, P. A. (2011), WINDOPT: an optimization tool for floating support structures for deep water wind turbines, in 'Proceedings of the ASME 30th International Conference on Ocean, Offshore and Arctic Engineering, Rotterdam, The Netherlands, June 19-24, 2011', American Society of Mechanical Engineers, pp. 767–776. doi: <http://dx.doi.org/10.1115/OMAE2011-49985>.

- Gambier, A. (2011), Performance evaluation of several multi-objective optimization methods for control purposes, in 'Proceedings of 2011 8th Asian Control Conference, Kaohsiung, Taiwan, May 15-18, 2011', IEEE, pp. 1067–1071.
- Gao, J. & Sweetman, B. (2018), 'Design optimization of hull size for spar-based floating offshore wind turbines', *Journal of Ocean Engineering and Marine Energy* **4**(3), 217–229. doi: <http://dx.doi.org/10.1007/s40722-018-0117-y>.
- Garbatov, Y. & Soares, C. G. (2002), 'Bayesian updating in the reliability assessment of maintained floating structures', *Journal of Offshore Mechanics and Arctic Engineering* **124**(3), 139. doi: <http://dx.doi.org/10.1115/1.1493200>.
- Gentils, T., Wang, L. & Kolios, A. (2017), 'Integrated structural optimisation of offshore wind turbine support structures based on finite element analysis and genetic algorithm', *Applied Energy* **199**, 187–204. doi: <http://dx.doi.org/10.1016/j.apenergy.2017.05.009>.
- Gholizad, A., Golafshani, A. A. & Akrami, V. (2012), 'Structural reliability of offshore platforms considering fatigue damage and different failure scenarios', *Ocean Engineering* **46**, 1–8. doi: <http://dx.doi.org/10.1016/j.oceaneng.2012.01.033>.
- GICON (2016), *The GICON®-SOF*.
URL: <http://www.gicon-sof.de/en/sof1.html> [Accessed on: 2017-12-16]
- GL (2010), *IV Rules and Guidelines Industrial Services - Part 1 Guideline for the Certification of Wind Turbines*, Germanischer Lloyd, Hamburg, Germany.
- Glauert, H. (1935), Airplane propellers, in W. F. Durand, ed., 'Aerodynamic Theory', Vol. 11, Springer Berlin Heidelberg, Berlin/Heidelberg, Germany, pp. 169–360. doi: http://dx.doi.org/10.1007/978-3-642-91487-4_3.
- Gosavi, A. (2015), *Simulation-Based Optimization: Parametric Optimization Techniques and Reinforcement Learning*, 2nd edn, Springer, New York, NY, USA.
- Govindji, A.-K., James, R. & Carvallo, A. (2014), *Appraisal of the Offshore Wind Industry in Japan*, Carbon Trust, London, UK.
URL: <https://prod-drupal-files.storage.googleapis.com/documents/resource/public/Offshore%20wind%20in%20Japan%20-%20REPORT.pdf> [Accessed on: 2020-06-09]
- Grogan, T. (2018), 'Steel, aluminum tariffs will hit prices hard through year end', *Engineering News-Record* (March 21).
URL: <https://www.enr.com/articles/44200-steel-aluminum-tariffs-will-hit-prices-hard-through-year-end?v=preview> [Accessed on: 2020-02-11]
- Gumus, S., Kucukvar, M. & Tatari, O. (2016), 'Intuitionistic fuzzy multi-criteria decision making framework based on life cycle environmental, economic and social impacts: the case of U.S. wind energy', *Sustainable Production and Consumption* **8**, 78–92. doi: <http://dx.doi.org/10.1016/j.spc.2016.06.006>.

- Hadka, D. (2015), *Platypus Documentation: Release*.
URL: <https://platypus.readthedocs.io/en/latest/> [Accessed on: 2018-12-13]
- Hagen, B., Simonsen, I., Hofmann, M. & Muskulus, M. (2013), ‘A multivariate Markov weather model for O&M simulation of offshore wind parks’, *Energy Procedia* **35**, 137–147. doi: <http://dx.doi.org/10.1016/j.egypro.2013.07.167>.
- Hall, M., Buckham, B. & Crawford, C. (2014), ‘Hydrodynamics-based floating wind turbine support platform optimization: a basis function approach’, *Renewable Energy* **66**, 559–569. doi: <http://dx.doi.org/10.1016/j.renene.2013.12.035>.
- Hall, M. T. J. (2013), Mooring line modelling and design optimization of floating offshore wind turbines, Master thesis, University of Victoria, Victoria, Canada.
- Hameed, Z., Vatn, J. & Heggset, J. (2011), ‘Challenges in the reliability and maintainability data collection for offshore wind turbines’, *Renewable Energy* **36**(8), 2154–2165. doi: <http://dx.doi.org/10.1016/j.renene.2011.01.008>.
- Hanke, K. (2004), *REpower 5M Prospekt*.
URL: http://www.besco.de/5m_de.pdf [Accessed on: 2017-04-25]
- Hansen, M. H., Hansen, A., Larsen, T. J., Øye, S., Sørensen, P. & Fuglsang, P. (2005), *Control design for a pitch-regulated, variable speed wind turbine (Risø R, Report 1500*, Risø National Laboratory, Roskilde, Denmark.
URL: http://iis-03.risoe.dk/netahtml/risoe/publ_uk.htm
- Härer, A. (2013), Optimierung von Windenergieanlagen-Komponenten in Mehrkörpersimulationen zur Kosten- und Lastreduktion, Diploma, Stiftungslehrstuhl Windenergie Universität Stuttgart, Stuttgart, Germany.
- Hayman, G. (2012), *MLife Theory Manual for Version 1.00: Revised October 19, 2012 for MLife v1.00.00 (Technical Report)*, National Renewable Energy Laboratory, Golden, CO, USA.
- Hayman, G. (2018), ‘NWTC information portal (MLife)’.
URL: <https://nwtc.nrel.gov/MLife> [Accessed on: 2018-10-18]
- Hayman, G. & Buhl, M. (2012), *MLife User’s Guide for Version 1.00: Revised October 19, 2012 for MLife v1.00.00 (Technical Report)*, National Renewable Energy Laboratory, Golden, CO, USA.
- He, C. (1989), Development and application of a generalized dynamic wake theory for lifting rotors, Doctoral thesis, Georgia Institute of Technology, Atlanta, GA, USA.
- He, J., Jin, X., Xie, S. Y., Le Cao, Lin, Y. & Wang, N. (2019), ‘Multi-body dynamics modeling and TMD optimization based on the improved AFSA for floating wind turbines’, *Renewable Energy* **141**, 305–321. doi: <http://dx.doi.org/10.1016/j.renene.2019.04.005>.

- Hegseth, J. M., Bachynski, E. E. & Martins, J. R. (2020), 'Integrated design optimization of spar floating wind turbines', *Marine Structures* **72**, 102771. doi: <http://dx.doi.org/10.1016/j.marstruc.2020.102771>.
- Henderson, A. R. & Witcher, D. (2010), 'Floating offshore wind energy - a review of the current status and an assessment of the prospects', *Wind Engineering* **34**(1), 1–16. doi: <http://dx.doi.org/10.1260/0309-524X.34.1.1>.
- Herbert-Acero, J., Probst, O., Réthoré, P.-E., Larsen, G. & Castillo-Villar, K. (2014), 'A review of methodological approaches for the design and optimization of wind farms', *Energies* **7**(11), 6930–7016. doi: <http://dx.doi.org/10.3390/en7116930>.
- Hirai, T., Sou, A. & Nihei, Y. (2018), Wave load acting on advanced spar in regular waves, in 'Proceedings of the ASME 37th International Conference on Ocean, Offshore and Arctic Engineering, Madrid, Spain, June 17-22, 2018', American Society of Mechanical Engineers, New York, N.Y. doi: <http://dx.doi.org/10.1115/OMAE2018-77821>.
- Hou, P., Zhu, J., MA, K., YANG, G., HU, W. & CHEN, Z. (2019), 'A review of offshore wind farm layout optimization and electrical system design methods', *Journal of Modern Power Systems and Clean Energy* **7**(5), 975–986. doi: <http://dx.doi.org/10.1007/s40565-019-0550-5>.
- Hu, W. (2018), Reliability-based design optimization of wind turbine systems, in W. Hu, ed., 'Advanced Wind Turbine Technology', Vol. 43, Springer International Publishing, Cham, Switzerland, pp. 1–45. doi: http://dx.doi.org/10.1007/978-3-319-78166-2_1.
- Hu, W., Choi, K. K. & Cho, H. (2016), 'Reliability-based design optimization of wind turbine blades for fatigue life under dynamic wind load uncertainty', *Structural and Multidisciplinary Optimization* **54**(4), 953–970. doi: <http://dx.doi.org/10.1007/s00158-016-1462-x>.
- Huang, C., El Hami, A. & Radi, B. (2017a), 'Overview of structural reliability analysis methods - part I: local reliability methods', *Uncertainties and Reliability of Multiphysical Systems* **17**(1). doi: <http://dx.doi.org/10.21494/ISTE.OP.2017.0115>.
- Huang, C., El Hami, A. & Radi, B. (2017b), 'Overview of structural reliability analysis methods - part II: sampling methods', *Uncertainties and Reliability of Multiphysical Systems* **17**(1). doi: <http://dx.doi.org/10.21494/ISTE.OP.2017.0116>.
- Huijs, F., Mikx, J., Savenije, F. & de Ridder, E.-J. (2013), Integrated design of floater, mooring and control system for a semi-submersible floating wind turbine, in 'Proceedings of the EWEA Offshore 2013, Frankfurt, Germany, November 19-21, 2013', European Wind Energy Association, Brussels, Belgium.
- Ideol (2017), 'Ideol winning solutions for offshore wind'.
URL: <http://ideol-offshore.com/en> [Accessed on: 2017-12-16]

- Ideol (2020), ‘Floatgen: Wind power going further offshore’.
URL: <https://floatgen.eu/> [Accessed on: 2020-06-21]
- IEA (2019), *Offshore Wind Outlook 2019*, International Energy Agency, Paris, France.
URL: <https://www.iea.org/reports/offshore-wind-outlook-2019> [Accessed on: 2020-05-14]
- IEC (2009), *Wind turbines - Part 3: Design requirements for offshore wind turbines (International Standard IEC 61400-3:2009-02)*, 1.0 edn, International Electrotechnical Commission, Geneva, Switzerland.
- IEC (2019a), *Wind energy generation systems - Part 1: Design requirements (International Standard IEC 61400-1:2019-02)*, International Standard, 4.0 edn, International Electrotechnical Commission, Geneva, Switzerland.
- IEC (2019b), *Wind energy generation systems - Part 3-1: Design requirements for fixed offshore wind turbines (International Standard IEC 61400-3-1:2019-04)*, 1.0 edn, International Electrotechnical Commission, Geneva, Switzerland.
- IEC (2019c), *Wind energy generation systems - Part 3-2: Design requirements for floating offshore wind turbines (Technical Specification IEC TS 61400-3-2:2019-04)*, 1.0 edn, International Electrotechnical Commission, Geneva, Switzerland.
- ISO (2015), *General principles on reliability for structures (International Standard ISO 2394:2015)*, International Organization for Standardization, Switzerland.
URL: <http://www.worldcat.org/oclc/1121278946> [Accessed on: 2020-04-03]
- Izzo, D. & Biscani, F. (2015), ‘Welcome to PyGMO’.
URL: <https://esa.github.io/pygmo/index.html> [Accessed on: 2018-10-12]
- James, R. & Ros, M. C. (2015), *Floating Offshore Wind: Market and Technology Review*, Carbon Trust, UK.
URL: <https://prod-drupal-files.storage.googleapis.com/documents/resource/public/Floating%20Offshore%20Wind%20Market%20Technology%20Review%20-%20REPORT.pdf> [Accessed on: 2020-06-09]
- Jonkman, B. J. (2009), *TurbSim User’s Guide: Version 1.50 (Technical Report NREL/TP-500-46198)*, National Renewable Energy Laboratory, Golden, CO, USA.
- Jonkman, J. (2010), *Definition of the Floating System for Phase IV of OC3 (Technical Report NREL/TP-500-47535)*, National Renewable Energy Laboratory, Golden, CO, USA. doi: <http://dx.doi.org/10.2172/979456>.
- Jonkman, J. (2018), ‘NWTC information portal (FAST)’.
URL: <https://nwtc.nrel.gov/FAST> [Accessed on: 2018-11-12]
- Jonkman, J. & Buhl, M. (2005), *FAST User’s Guide (Technical Report NREL/EL-500-38230)*, National Renewable Energy Laboratory, Golden, CO, USA.

- Jonkman, J., Butterfield, S., Musial, W. & Scott, G. (2009), *Definition of a 5-MW Reference Wind Turbine for Offshore System Development (Technical Report NREL/TP-500-38060)*, National Renewable Energy Laboratory, Golden, CO, USA. doi: <http://dx.doi.org/10.2172/947422>.
- Jonkman, J. & Musial, W. (2010), *Offshore Code Comparison Collaboration (OC3) for IEA Task 23 Offshore Wind Technology and Deployment (Technical Report NREL/TP-5000-48191)*, National Renewable Energy Laboratory, Golden, CO, USA.
- Journée, J. & Massie, W. W. (2001), *Offshore Hydromechanics*, 1st edn, Delft University of Technology, Delft, The Netherlands.
- JWPA (2017), *Offshore Wind Power Development in Japan*, Japan Wind Power Association.
URL: http://jwpa.jp/pdf/20170228_OffshoreWindPower_inJapan_r1.pdf [Accessed on: 2020-08-01]
- Kahrobaee, S. & Asgarpoor, S. (2011), Risk-based failure mode and effect analysis for wind turbines (RB-FMEA), in 'NAPS 2011', IEEE, Piscataway, NJ, USA, pp. 1–7. doi: <http://dx.doi.org/10.1109/NAPS.2011.6025116>.
- Kang, B.-J., Kim, J.-H. & Kim, Y. (2016), 'Engineering criticality analysis on an offshore structure using the first- and second-order reliability method', *International Journal of Naval Architecture and Ocean Engineering* **8**(6), 577–588. doi: <http://dx.doi.org/10.1016/j.ijnaoe.2016.05.014>.
- Kang, H., Li, Y. & Huan, C. (2009), 'RBDO method research of offshore wind turbine foundation structure', *Taiyangneng Xuebao/Acta Energetica Sinica* **30**(12), 1602–1607.
- Kang, J., Sun, L., Sun, H. & Wu, C. (2017), 'Risk assessment of floating offshore wind turbine based on correlation-FMEA', *Ocean Engineering* **129**, 382–388. doi: <http://dx.doi.org/10.1016/j.oceaneng.2016.11.048>.
- Karadeniz, H., Toğan, V. & Vrouwenvelder, T. (2009), 'An integrated reliability-based design optimization of offshore towers', *Reliability Engineering & System Safety* **94**(10), 1510–1516. doi: <http://dx.doi.org/10.1016/j.ress.2009.02.008>.
- Karimi, M., Hall, M., Buckham, B. & Crawford, C. (2017), 'A multi-objective design optimization approach for floating offshore wind turbine support structures', *Journal of Ocean Engineering and Marine Energy* **3**(1), 69–87. doi: <http://dx.doi.org/10.1007/s40722-016-0072-4>.
- Katsouris, G. & Marina, A. (2016), *Cost Modelling of Floating Wind Farms (ECN Report ECN-E-15-078)*, ECN, Petten, The Netherlands.
- Keshtegar, B. & Miri, M. (2013), 'An enhanced HL-RF method for the computation of structural failure probability based on relaxed approach', *Civil Engineering Infrastructures Journal* **1**, 69–80. doi: <http://dx.doi.org/10.7508/cej.2013.01.005>.

- Khakzad, N., Khan, F. & Amyotte, P. (2013), 'Quantitative risk analysis of offshore drilling operations: a Bayesian approach', *Safety Science* **57**, 108–117. doi: <http://dx.doi.org/10.1016/j.ssci.2013.01.022>.
- Kim, D. H. & Lee, S. G. (2015), 'Reliability analysis of offshore wind turbine support structures under extreme ocean environmental loads', *Renewable Energy* **79**, 161–166. doi: <http://dx.doi.org/10.1016/j.renene.2014.11.052>.
- Kim, H., Choung, J. & Jeon, G.-Y. (2014), Design of mooring lines of floating offshore wind turbine in Jeju offshore area, in 'Proceedings of the ASME 33rd International Conference on Ocean, Offshore and Arctic Engineering, San Francisco, CA, USA, June 8-13, 2014', American Society of Mechanical Engineers, New York, NY, USA. doi: <http://dx.doi.org/10.1115/OMAE2014-23772>.
- Kolios, A. (2010), A multi-configuration approach to reliability based structural integrity assessment for ultimate strength, Doctoral Thesis, Cranfield University, Cranfield, UK.
URL: <http://dspace.lib.cranfield.ac.uk/handle/1826/5717> [Accessed on: 2020-07-09]
- Kolios, A., Borg, M. & Hanak, D. (2015), 'Reliability analysis of complex limit states of floating wind turbines', *Journal of Energy Challenges and Mechanics* **2**(1), 6–9.
- Kolios, A. & Brennan, F. (2009), Reliability based design for novel offshore structures, in 'Proceedings of IRF'2009 - 3rd International Conference on Integrity, Reliability and Failure, Porto, Portugal, July 20-24, 2009'.
- Kolios, A., Collu, M., Chahardehi, A., Brennan, F. P. & Patel, M. H. (2010), A multi-criteria decision making method to compare available support structures for offshore wind turbines, in 'Proceedings of the European Wind Energy Conference and Exhibition 2010, Warsaw, Poland, April 20-23, 2010'.
- Kolios, A., Di Maio, L. F., Wang, L., Cui, L. & Sheng, Q. (2018), 'Reliability assessment of point-absorber wave energy converters', *Ocean Engineering* **163**, 40–50. doi: <http://dx.doi.org/10.1016/j.oceaneng.2018.05.048>.
- Kolios, A. J., Collu, M. & Brennan, F. P. (2010), Reliability of floating foundation concepts for vertical axis wind turbines, in S. F. Estefen, I. P. Pasqualino & S. H. Sphaler, eds, '11th International Symposium on Practical Design of Ships and Other Floating Structures', Vol. 2, COPPE-URRJ, Rio de Janeiro, Brazil, pp. 1483–1491.
- Kolios, A. J., Rodriguez-Tsouroukdissian, A. & Salonitis, K. (2016), 'Multi-criteria decision analysis of offshore wind turbines support structures under stochastic inputs', *Ships and Offshore Structures* **11**(1), 38–49. doi: <http://dx.doi.org/10.1080/17445302.2014.961295>.
- Kolios, A. J., Umofia, A. & Shafiee, M. (2017), 'Failure mode and effects analysis using a fuzzy-TOPSIS method: a case study of subsea control module', *International Journal of*

- Multicriteria Decision Making* **7**(1), 29–53. doi: <http://dx.doi.org/10.1504/IJMCDM.2017.085154>.
- Kolios, A., Mytilinou, V., Lozano-Minguez, E. & Salonitis, K. (2016), ‘A comparative study of multiple-criteria decision-making methods under stochastic inputs’, *Energies* **9**(7), 566. doi: <http://dx.doi.org/10.3390/en9070566>.
- Kosowatz, J. (2015), *Options Bring Challenges to Floating Platforms*, American Society of Mechanical Engineers.
URL: <https://www.asme.org/> [Accessed on: 2017-12-14]
- Koundouri, P., Giannouli, A. & Souliotis, I. (2017), An integrated approach for sustainable environmental and socio-economic development using offshore infrastructure, in ‘Renewable and Alternative Energy’, pp. 1581–1601. doi: <http://dx.doi.org/10.4018/978-1-5225-1671-2.ch056>.
- Krieger, A., Ramachandran, G. K. V., Vita, L., Alonso, P. G., Almería, G. G., Berque, J. & Aguirre, G. (2015), *LIFES50+ Deliverable D7.2 Design Basis: Qualification of innovative floating substructures for 10MW wind turbines and water depths greater than 50m*, DNV GL.
URL: https://lifes50plus.eu/wp-content/uploads/2015/11/D72_Design_Basis_Retyped-v1.1.pdf [Accessed on: 2018-03-28]
- Kristiansen, M. B. (2020), ‘Welcome to HAWC2’.
URL: <https://www.hawc2.dk/hawc2-info> [Accessed on: 2020-07-09]
- Landbø, T. (2017a), *Floating wind will be cheaper than bottom-fixed: wait and see*, Recharge.
URL: <https://www.rechargenews.com/wind/floating-wind-will-be-cheaper-than-bottom-fixed-wait-and-see/2-1-200866> [Accessed on: 2017-11-02]
- Landbø, T. (2017b), OO-Star Wind Floater: An innovative and robust semi-submersible for offshore floating wind, in ‘EU Research & Innovation Day, Seoul, South Korea, November 23-24, 2017’.
- Larsen, T. J. & Hansen, A. M. (2015), *How 2 HAWC2, the user’s manual (Risø-R-Report Risø-R-1597)*, Risø National Laboratory, Roskilde, Denmark.
URL: <http://www.hawc2.dk/> [Accessed on: 2018-10-09]
- Larsen, T. J. & Hanson, T. D. (2007), ‘A method to avoid negative damped low frequent tower vibrations for a floating, pitch controlled wind turbine’, *Journal of Physics: Conference Series* **75**, 012073. doi: <http://dx.doi.org/10.1088/1742-6596/75/1/012073>.
- Lavasani, S. M. M., Wang, J., Yang, Z. & Finlay, J. (2012), ‘Application of MADM in a fuzzy environment for selecting the best barrier for offshore wells’, *Expert Systems with Applications* **39**(3), 2466–2478. doi: <http://dx.doi.org/10.1016/j.eswa.2011.08.099>.

- Lazakis, I. & Ölcner, A. (2016), 'Selection of the best maintenance approach in the maritime industry under fuzzy multiple attributive group decision-making environment', *Proceedings of the Institution of Mechanical Engineers, Part M: Journal of Engineering for the Maritime Environment* **230**(2), 297–309. doi: <http://dx.doi.org/10.1177/1475090215569819>.
- Le, B. & Andrews, J. (2016), 'Modelling wind turbine degradation and maintenance', *Wind Energy* **19**(4), 571–591. doi: <http://dx.doi.org/10.1002/we.1851>.
- Lee, K. H. (2005), Responses of floating wind turbines to wind and wave excitation, Master thesis, Massachusetts Institute of Technology, Cambridge, MA, USA.
URL: <http://hdl.handle.net/1721.1/33564> [Accessed on: 2020-07-09]
- Lee, Y.-J., Ho, C.-Y., Huang, Z. & Wang, Y.-C. (2015), 'Improvements on the output of a spar-type floating wind turbine influenced by wave-induced oscillation', *Journal of Taiwan Society of Naval Architects and Marine Engineers* **34**(2), 55–62.
- Lee, Y.-S., Choi, B.-L., Lee, J. H., Kim, S. Y. & Han, S. (2014), 'Reliability-based design optimization of monopile transition piece for offshore wind turbine system', *Renewable Energy* **71**, 729–741. doi: <http://dx.doi.org/10.1016/j.renene.2014.06.017>.
- Leimeister, M. (2016), Rational upscaling and modelling of a semi-submersible floating offshore wind turbine, Master thesis, Delft University of Technology and Norwegian University of Science and Technology and Fraunhofer Institute for Wind Energy Systems, Trondheim, Norway.
URL: <http://resolver.tudelft.nl/uuid:7f6b5eda-15d8-4228-ad9a-8c27f8c5c258> [Accessed on: 2020-07-09]
- Leimeister, M. (2019), Python-Modelica framework for automated simulation and optimization, in 'Proceedings of the 13th International Modelica Conference, Regensburg, Germany, March 4-6, 2019', Linköping Electronic Conference Proceedings, Linköping University Electronic Press, Linköping, Sweden, pp. 51–58. doi: <http://dx.doi.org/10.3384/ecp1915751>.
- Leimeister, M., Collu, M. & Kolios, A. (2020), 'A fully integrated optimization framework for designing a complex geometry offshore wind turbine spar-type floating support structure', *Wind Energy Science Discussions* (in review). doi: <http://dx.doi.org/10.5194/wes-2020-93>.
- Leimeister, M. & Dose, B. (2018), Validation and development of improved methods for the calculation of wave loads on XXL monopiles, in 'Proceedings of the ASME 37th International Conference on Ocean, Offshore and Arctic Engineering, Madrid, Spain, June 17-22, 2018', American Society of Mechanical Engineers, New York, NY, USA, pp. OMAE2018-77232.

- Leimeister, M. & Kolios, A. (2018), ‘A review of reliability-based methods for risk analysis and their application in the offshore wind industry’, *Renewable and Sustainable Energy Reviews* **91**, 1065–1076. doi: <http://dx.doi.org/10.1016/j.rser.2018.04.004>.
- Leimeister, M. & Kolios, A. (2020), ‘Reliability-based design optimization of a spar-type floating offshore wind turbine support structure’, *Reliability Engineering and System Safety* (in review).
- Leimeister, M., Kolios, A. & Collu, M. (2018), ‘Critical review of floating support structures for offshore wind farm deployment’, *Journal of Physics: Conference Series* **1104**, 012007. doi: <http://dx.doi.org/10.1088/1742-6596/1104/1/012007>.
- Leimeister, M., Kolios, A. & Collu, M. (2020a), ‘Development and verification of an aero-hydro-servo-elastic coupled model of dynamics for FOWT, based on the MoWiT library’, *Energies* **13**(8), 1974. doi: <http://dx.doi.org/10.3390/en13081974>.
- Leimeister, M., Kolios, A. & Collu, M. (2020b), ‘Development of a framework for wind turbine design and optimization’, *Energy Reports* (in review).
- Leimeister, M., Kolios, A., Collu, M. & Thomas, P. (2019), Larger MW-class floater designs without upscaling?: a direct optimization approach, in ‘Proceedings of the ASME 38th International Conference on Ocean, Offshore and Arctic Engineering, Glasgow, Scotland, UK, June 9-14, 2019’, American Society of Mechanical Engineers, New York, NY, USA, pp. OMAE2019–95210. doi: <http://dx.doi.org/10.1115/OMAE2019-95210>.
- Leimeister, M., Kolios, A., Collu, M. & Thomas, P. (2020), ‘Design optimization of the OC3 phase IV floating spar-buoy, based on global limit states’, *Ocean Engineering* **202**, 107186. doi: <http://dx.doi.org/10.1016/j.oceaneng.2020.107186>.
- Leimeister, M., Spill, S., Dose, B., Foglia, A., Siegl, K., Karch, M., Heins, E., Schümann, B., Dührkop, J. & Hartmann, H. (2019), *TANDEM - Towards an Advanced Design of Large Monopiles: Schlussbericht*, Technische Informationsbibliothek (TIB), Hanover, Germany. doi: <http://dx.doi.org/10.2314/KXP:1678117404>.
- Leimeister, M. & Thomas, P. (2017a), The OneWind[®] Modelica library for floating offshore wind turbine simulations with flexible structures, in ‘Proceedings of the 12th International Modelica Conference, Prague, Czech Republic, May 15-17, 2017’, Linköping Electronic Conference Proceedings, Linköping University Electronic Press, Linköping, Sweden, pp. 633–642. doi: <http://dx.doi.org/10.3384/ecp17132633>.
- Leimeister, M. & Thomas, P. (2017b), Verification of MacCamy-Fuchs theory and its influence on wind turbine loading, in ‘Proceedings of DEWEK 2017 - German Wind Energy Conference, Bremen, Germany, October 17-18, 2017’.
- Lemmer, F., Müller, K., Yu, W., Guzman, R. F. & Kretschmer, M. (2016), *Qualification of innovative floating substructures for 10MW wind turbines and water depths greater than*

50m: Deliverable D4.3 Optimization framework and methodology for optimized floater design, LIFES50+ Consortium.

URL: https://lifes50plus.eu/wp-content/uploads/2015/11/D72_Design_Basis_Retyped-v1.1.pdf [Accessed on: 2020-06-09]

Lemmer, F., Müller, K., Yu, W., Schlipf, D. & Cheng, P. W. (2017), Optimization of floating offshore wind turbine platforms with a self-tuning controller, in 'Proceedings of the ASME 36th International Conference on Ocean, Offshore and Arctic Engineering, Trondheim, Norway, June 25-30, 2017', American Society of Mechanical Engineers, New York, NY, USA. doi: <http://dx.doi.org/10.1115/0MAE2017-62038>.

Li, H., Cho, H., Sugiyama, H., Choi, K. K. & Gaul, N. J. (2017), 'Reliability-based design optimization of wind turbine drivetrain with integrated multibody gear dynamics simulation considering wind load uncertainty', *Structural and Multidisciplinary Optimization* **56**(1), 183–201. doi: <http://dx.doi.org/10.1007/s00158-017-1693-5>.

Liu, Y., Li, S., Yi, Q. & Chen, D. (2016), 'Developments in semi-submersible floating foundations supporting wind turbines: a comprehensive review', *Renewable and Sustainable Energy Reviews* **60**, 433–449. doi: <http://dx.doi.org/10.1016/j.rser.2016.01.109>.

LKAB Minerals (2018), 'Floating Offshore Wind 2018'.

URL: <https://www.lkabminerals.com/de/floating-offshore-wind-2018/> [Accessed on: 2018-10-30]

LKAB Minerals (2019), *Non-hazardous material safety data sheet for MagnaDense*, Luleå, Sweden.

URL: <https://www.lkabminerals.com/wp-content/uploads/2019/02/MagnaDense-SDS-12-06INT-19-03.pdf> [Accessed on: 2020-02-05]

LKAB Minerals (2020), 'Ballast for offshore wind turbines'.

URL: <https://www.lkabminerals.com/en/industry-uses/offshore-energy/offshore-wind-structures/> [Accessed on: 2020-06-21]

Llado, M. G. (2015), Structural reliability analysis and robust design of offshore wind turbine support structures, Master thesis, Norwegian University of Science and Technology, Trondheim, Norway.

Löfken, J. O. (2019), 'Das nächste große Ding auf See', *Neue Energie* (August 2019), 34–37.

Lozano-Minguez, E., Kolios, A. J. & Brennan, F. P. (2011), 'Multi-criteria assessment of offshore wind turbine support structures', *Renewable Energy* **36**(11), 2831–2837. doi: <http://dx.doi.org/10.1016/j.renene.2011.04.020>.

Lu, Z., Song, J., Song, S., Yue, Z. & Wang, J. (2010), 'Reliability sensitivity by method of moments', *Applied Mathematical Modelling* **34**(10), 2860–2871. doi: <http://dx.doi.org/10.1016/j.apm.2009.12.020>.

- Luengo, M. & Kolios, A. (2015), 'Failure mode identification and end of life scenarios of offshore wind turbines: a review', *Energies* **8**(8), 8339–8354. doi: <http://dx.doi.org/10.3390/en8088339>.
- MacCamy, R. C. & Fuchs, R. A. (1954), *Wave forces on piles: A diffraction theory*, Technical Memorandum No. 69, Corps of Engineers, Beach Erosion Board, Washington, D.C., USA.
- Mahadevan, S. (2013), Uncertainty quantification for decision-making in engineered systems, in S. Chakraborty & G. Bhattacharya, eds, 'Proceedings of the International Symposium on Engineering under Uncertainty: Safety Assessment and Management (ISEUSAM - 2012)', Springer India, New Delhi, India; Heidelberg, Germany; New York, NY, USA; Dordrecht, The Netherlands; London, UK, pp. 97–117.
- Main(e) International Consulting LLC (2013), *Floating Offshore Wind Foundations: Industry Consortia and Projects in the United States, Europe and Japan: An Overview*.
URL: <https://cdn.website-editor.net/073319e35fa34e6189750e64c2e99060/files/uploaded/Floating%252BOffshore%252BWind%252BPlatforms%252BConsortia%252Bfor%252Bweb.pdf> [Accessed on: 2020-06-09]
- Makhduomi, H., Keshtegar, B. & Shahraki, M. (2017), 'A comparative study of first-order reliability method-based steepest descent search directions for reliability analysis of steel structures', *Advances in Civil Engineering* **2017**(2), 1–10. doi: <http://dx.doi.org/10.1155/2017/8643801>.
- Mardfekri, M. & Gardoni, P. (2015), 'Multi-hazard reliability assessment of offshore wind turbines', *Wind Energy* **18**(8), 1433–1450. doi: <http://dx.doi.org/10.1002/we.1768>.
- Martin, H., Spano, G., Küster, J. F., Collu, M. & Kolios, A. J. (2013), 'Application and extension of the TOPSIS method for the assessment of floating offshore wind turbine support structures', *Ships and Offshore Structures* **8**(5), 477–487. doi: <http://dx.doi.org/10.1080/17445302.2012.718957>.
- Mast, E., Rawlinson, R. & Sixtensson, C. (2015), *TKI Wind op Zee: Market study floating wind in the Netherlands: Potential of floating offshore wind*, RVO (Netherlands Enterprise Agency).
URL: https://www.topsectorenergie.nl/sites/default/files/uploads/Wind%20op%20Zee/Documenten/20160111_Rap_DNVGL_Market_study_floating_wind.pdf [Accessed on: 2020-06-09]
- Matha, D. (2009), *Model Development and Loads Analysis of an Offshore Wind Turbine on a Tension Leg Platform, with a Comparison to Other Floating Turbine Concepts (Subcontract Report NREL/SR-500-45891)*, National Renewable Energy Laboratory, Golden, CO, USA.
- Matha, D., Sandner, F. & Schlipf, D. (2014), 'Efficient critical design load case identification for floating offshore wind turbines with a reduced nonlinear model', *Journal of Physics:*

- Conference Series* **555**, 012069. doi: <http://dx.doi.org/10.1088/1742-6596/555/1/012069>.
- Matsuoka, R. & Yoshimoto, H. (2015), 'Verification of precision concerning the design of advanced spar type structure', *Conference Proceedings The Japan Society of Naval Architects and Ocean Engineers* **20**, 2015S–OS1–1.
- McKinney, W. (2013), *Python for Data Analysis*, O'Reilly, Sebastopol, CA, USA.
- McLeod, R. W. (2015), *Designing for human reliability in the oil, gas, and process industries: Improving return on investment through human factor engineering*, Gulf Professional Publishing, Amsterdam, The Netherlands.
- Men, J., Yan, F. & Ma, Q. (2019), An optimization for the mooring system of a 10-MW spar type floating wind turbine in time domain, in 'Proceedings of the 29th International Ocean and Polar Engineering Conference, Honolulu, HI, USA, June 16-21, 2019', International Society of Offshore and Polar Engineers, pp. 384–389.
- Mendeley (2020), 'Mendeley web catalog: a review of reliability-based methods for risk analysis and their application in the offshore wind industry'.
URL: <https://www.mendeley.com/catalogue/d80bd577-4761-3b01-b765-19d170c1ad1e/>
 [Accessed on: 2020-08-03]
- Michael (2018), 'How much does structural steel fabrication cost?'.
URL: <https://spendonhome.com/structural-steel-fabrication-cost/> [Accessed on: 2018-12-13]
- Modelica Association (2020a), 'Modelica language'.
URL: <https://www.modelica.org/modelicalanguage> [Accessed on: 2020-06-11]
- Modelica association (2020b), 'Modelica Tools'.
URL: <https://www.modelica.org/tools> [Accessed on: 2020-06-09]
- Mokhtari, K., Ren, J., Roberts, C. & Wang, J. (2011), 'Application of a generic bow-tie based risk analysis framework on risk management of sea ports and offshore terminals', *Journal of hazardous materials* **192**(2), 465–475. doi: <http://dx.doi.org/10.1016/j.jhazmat.2011.05.035>.
- Molins, C., Trubat, P., Gironella, X. & Campos, A. (2015), 'Design optimization for a truncated catenary mooring system for scale model test', *Journal of Marine Science and Engineering* **3**(4), 1362–1381. doi: <http://dx.doi.org/10.3390/jmse3041362>.
- Momoh, J. A. & Surender Reddy, S. (2014), Review of optimization techniques for renewable energy resources, in 'Proceedings of PEMWA 2014 IEEE Symposium on Power Electronics and Machines for Wind and Water Applications, Milwaukee, WI, USA, July 24-26, 2014', pp. 1–8. doi: <http://dx.doi.org/10.1109/PEMWA.2014.6912225>.

- Mone, C., Hand, M., Bolinger, M., Rand, J., Heimiller, D. & Ho, J. (2017), *2015 Cost of Wind Energy Review (Technical Report NREL/TP-6A20-66861)*, National Renewable Energy Laboratory, Golden, CO, USA.
- Morison, J. R., Johnson, J. W. & Schaaf, S. A. (1950), 'The force exerted by surface waves on piles', *Journal of Petroleum Technology* **2**(05), 149–154. doi: <http://dx.doi.org/10.2118/950149-G>.
- Musial, W., Butterfield, S. & Boone, A. (2004), Feasibility of floating platform systems for wind turbines, in 'Proceedings of the 42nd AIAA Aerospace Sciences Meeting and Exhibit, Reno, Nevada, January 5-8, 2004', p. 1098. doi: <http://dx.doi.org/10.2514/6.2004-1007>.
- Muskulus, M. & Schafhirt, S. (2014), 'Design optimization of wind turbine support structures - a review', *Journal of Ocean and Wind Energy* **1**(1), 12–22.
- Myhr, A., Bjerkseter, C., Ågotnes, A. & Nygaard, T. A. (2014), 'Levelised cost of energy for offshore floating wind turbines in a life cycle perspective', *Renewable Energy* **66**, 714–728. doi: <http://dx.doi.org/10.1016/j.renene.2014.01.017>.
- Mytilinou, V. & Kolios, A. J. (2017), 'A multi-objective optimisation approach applied to offshore wind farm location selection', *Journal of Ocean Engineering and Marine Energy* **3**(3), 265–284. doi: <http://dx.doi.org/10.1007/s40722-017-0092-8>.
- Mytilinou, V. & Kolios, A. J. (2019), 'Techno-economic optimisation of offshore wind farms based on life cycle cost analysis on the UK', *Renewable Energy* **132**, 439–454. doi: <http://dx.doi.org/10.1016/j.renene.2018.07.146>.
- Mytilinou, V., Lozano-Minguez, E. & Kolios, A. (2018), 'A framework for the selection of optimum offshore wind farm locations for deployment', *Energies* **11**(7), 1855. doi: <http://dx.doi.org/10.3390/en11071855>.
- NAUTILUS (2020), *Product*.
URL: <http://www.nautilusfs.com/en/nuestra-oferta/producto/> [Accessed on: 2020-07-09]
- Nejad, A. R., Bachynski, E. E. & Moan, T. (2017), On tower top axial acceleration and drivetrain responses in a spar-type floating wind turbine, in 'Proceedings of the ASME 36th International Conference on Ocean, Offshore and Arctic Engineering, Trondheim, Norway, June 25-30, 2017', American Society of Mechanical Engineers, New York, NY, USA, pp. OMAE2017–62314. doi: <http://dx.doi.org/10.1115/OMAE2017-62314>.
URL: <http://proceedings.asmedigitalcollection.asme.org/proceeding.aspx?doi=10.1115/OMAE2017-62314>
- Ng, C. & Ran, L., eds (2016), *Offshore Wind Farms: Technologies, Design and Operation*, Vol. number 92 of *Woodhead Publishing series in energy*, Elsevier WP Woodhead Publishing,

- Amsterdam, The Netherlands; Boston/Cambridge, MA, USA; San Diego/San Francisco, CA, USA; Heidelberg, Germany; London/Oxford, UK; New York, NY, USA; Paris, France.
- Nielsen, J. J. & Sørensen, J. D. (2011), ‘On risk-based operation and maintenance of offshore wind turbine components’, *Reliability Engineering & System Safety* **96**(1), 218–229. doi: <http://dx.doi.org/10.1016/j.ress.2010.07.007>.
- Nilsson, D. & Westin, A. (2014), Floating wind power in Norway: analysis of future opportunities and challenges, Master thesis, Lund University, Lund, Sweden.
- NOPSEMA (2017), *Hazard identification and risk assessment (Guidance note N-04600-GN1613)*, National Offshore Petroleum Safety and Environmental Management Authority, Perth, Australia.
- Nwofor, I. F. (2010), Reliability of offshore structures, Master thesis, Cranfield University, Cranfield, UK.
- Nygaard, T. A., de Vaal, J., Pierella, F., Oggiano, L. & Stenbro, R. (2016), ‘Development, verification and validation of 3DFloat; aero-servo-hydro-elastic computations of offshore structures’, *Energy Procedia* **94**, 425–433. doi: <http://dx.doi.org/10.1016/j.egypro.2016.09.210>.
- O’Connor, P. D. T., Newton, D. & Bromley, R. (2002), *Practical reliability engineering*, 4th edn, Wiley, Chichester, UK.
- Offshore Renewable Energy (2014), ‘SPARTA: The performance data exchange platform for offshore wind’.
URL: <https://ore.catapult.org.uk/documents/10619/106434/SPARTA/66bd6331-a17e-430f-b7ad-1c908eeef6da> [Accessed on: 2016-10-09]
- Okoro, U., Kolios, A. & Cui, L. (2017), ‘Multi-criteria risk assessment approach for components risk ranking - the case study of an offshore wave energy converter’, *International Journal of Marine Energy* **17**, 21–39. doi: <http://dx.doi.org/10.1016/j.ijome.2016.12.001>.
- Olle, N. (2016), ‘IRPWind - Research: Work package 7’.
URL: <http://www.irpwind.eu/core-research-projects/workpackage-7> [Accessed on: 2017-06-01]
- Onoufriou, T. & Forbes, V. (2001), ‘Developments in structural system reliability assessments of fixed steel offshore platforms’, *Reliability Engineering & System Safety* **71**(2), 189–199.
- openmdao.org (2016), ‘OpenMDAO 2.4.0 beta documentation: optimizer’.
URL: <http://openmdao.org/twodocs/versions/latest/tags/Optimizer.html#optimizer> [Accessed on: 2018-10-12]

- ORE Catapult (2015), *Floating wind: technology assessment*, Offshore Renewable Energy Catapult.
URL: <https://ore.catapult.org.uk/> [Accessed on: 2017-12-17]
- ORE Catapult (2016), *Introducing TLPWIND UK*, Offshore Renewable Energy Catapult.
URL: <https://ore.catapult.org.uk/> [Accessed on: 2017-12-16]
- Park, Y.-H. & Park, H.-C. (2014), ‘Optimal design of wind turbine tower model using reliability-based design optimization’, *Transactions of the Korean Society of Mechanical Engineers A* **38**(5), 575–584. doi: <http://dx.doi.org/10.3795/ksme-a.2014.38.5.575>.
- Perry, M. J., Halkyard, J. E. & Koh, C. G. (2007), Rapid preliminary design of floating offshore structures using a modified genetic algorithm, in ‘Proceedings of the ASME 26th International Conference on Ocean, Offshore and Arctic Engineering, San Diego, CA, USA, June 10-15, 2007’, American Society of Mechanical Engineers, New York, NY, USA, pp. 777–784. doi: <http://dx.doi.org/10.1115/OMAE2007-29700>.
- Pham, T. D. & Shin, H. (2019), ‘A new conceptual design and dynamic analysis of a spar-type offshore wind turbine combined with a moonpool’, *Energies* **12**(19), 3737. doi: <http://dx.doi.org/10.3390/en12193737>.
- Pillai, A. C., Thies, P. R. & Johannig, L. (2019), ‘Mooring system design optimization using a surrogate assisted multi-objective genetic algorithm’, *Engineering Optimization* **51**(8), 1370–1392. doi: <http://dx.doi.org/10.1080/0305215X.2018.1519559>.
- Popko, W., Huhn, M. L., Robertson, A., Jonkman, J., Wendt, F., Müller, K., Kretschmer, M., Vorpahl, F., Hagen, T. R., Galinos, C., Le Dreff, J.-B., Gilbert, P., Auriac, B., Villora, F. N., Schünemann, P., Bayati, I., Belloli, M., Oh, S., Totsuka, Y., Qvist, J., Bachynski, E., Sørum, S. H., Thomassen, P. E., Shin, H., Vittori, F., Galván, J., Molins, C., Bonnet, P., van der Zee, T., Bergua, R., Wang, K., Fu, P. & Cai, J. (2018), Verification of a numerical model of the offshore wind turbine from the Alpha Ventus wind farm within OC5 phase III, in ‘Proceedings of the ASME 37th International Conference on Ocean, Offshore and Arctic Engineering, Madrid, Spain, June 17-22, 2018’, American Society of Mechanical Engineers, New York, NY, USA, pp. OMAE2018–77589.
- Popko, W., Robertson, A., Jonkman, J., Wendt, F., Thomas, P., Müller, K., Kretschmer, M., Hagen, T. R., Galinos, C., Le Dreff, J.-B., Gilbert, P., Auriac, B., Oh, S., Qvist, J., Sørum, S. H., Suja-Thauvin, L., Shin, H., Molins, C., Trubat, P., Bonnet, P., Bergua, R., Wang, K., Fu, P., Cai, J., Cai, Z., Alexandre, A. & Harries, R. (2019), Validation of numerical models of the offshore wind turbine from the Alpha Ventus wind farm against full-scale measurements within OC5 Phase III, in ‘Proceedings of the ASME 38th International Conference on Ocean, Offshore and Arctic Engineering, Glasgow, Scotland, UK, June 9-14, 2019’, American Society of Mechanical Engineers, New York, NY, USA, pp. OMAE2019–95429.

- Popko, W., Thomas, P., Sevinc, A., Rosemeier, M., Bätge, M., Braun, R., Meng, F., Horte, D., Balzani, C., Bleich, O., Daniele, E., Stoevesandt, B., Wentingmann, M., Polman, J. D., Leimeister, M., Schümann, B. & Reuter, A. (2018), *IWES Wind Turbine IWT-7.5-164 Rev 4*, Fraunhofer Institute for Wind Energy Systems IWES, Bremerhaven, Germany.
- Power Technology (2019), *Floating foundations are the future of deeper offshore wind*.
URL: <https://www.power-technology.com/comment/floating-offshore-wind-2019/> [Accessed on: 2019-06-13]
- Principle Power (2015), 'WindFloat'.
URL: <http://www.principlepowerinc.com/> [Accessed on: 2017-12-16]
- Pritchard, C. L. (2015), *Risk management: Concepts and guidance*, An Auerbach book, 5th edn, CRC Press, Boca Raton, FL, USA.
- PTC (2011), *Windchill® Prediction: Perform Reliability Analyses using Globally Accepted Standards (Data Sheet)*, Parametric Technology Corporation.
URL: <http://www.ptc.com/> [Accessed on: 2017-04-25]
- Python Software Foundation (2020), 'Python'.
URL: <https://www.python.org/> [Accessed on: 2020-06-11]
- Q FWE (2020), *Floating Project Profiles*, Quest Floating Wind Energy.
URL: <https://questfwe.com/projects/> [Accessed on: 2020-06-05]
- Rackwitz, R. & Flessler, B. (1978), 'Structural reliability under combined random load sequences', *Computers & Structures* **9**(5), 489–494. doi: [http://dx.doi.org/10.1016/0045-7949\(78\)90046-9](http://dx.doi.org/10.1016/0045-7949(78)90046-9).
- Ramesh, R. B., Mirza, O. & Kang, W.-H. (2017), 'HLRF-BFGS-based algorithm for inverse reliability analysis', *Mathematical Problems in Engineering* **2017**, 1–15. doi: <http://dx.doi.org/10.1155/2017/4317670>.
- Ramirez, J. R. & Sørensen, J. D. (2011), Non-parametric Bayesian updating within the assessment of reliability for offshore wind turbine support structures, in M. H. Faber, ed., 'Applications of statistics and probability in civil engineering', A Balkema book, CRC, Boca Raton, FL, USA, pp. 1256–1264.
- Rankine, W. (1865), 'On the mechanical principles of the action of propellers', *Transaction of the Institute of Naval Architects* (6), 13–39.
- Rausand, M. & Høyland, A. (2004), *System Reliability Theory: Models, Statistical Methods, and Applications*, Wiley Series in Probability and Statistics - Applied Probability and, 2nd edn, Wiley-Blackwell, Hoboken, NJ, USA.

- Rendón-Conde, C. & Heredia-Zavoni, E. (2015), 'Reliability assessment of mooring lines for floating structures considering statistical parameter uncertainties', *Applied Ocean Research* **52**, 295–308. doi: <http://dx.doi.org/10.1016/j.apor.2015.06.011>.
- ResearchGate (2020), 'ResearchGate publication: a review of reliability-based methods for risk analysis and their application in the offshore wind industry'.
URL: https://www.researchgate.net/publication/325533454_A_review_of_reliability-based_methods_for_risk_analysis_and_their_application_in_the_offshore_wind_industry
 [Accessed on: 2020-08-03]
- Richard, C. (2019), 'Funds for Ireland's first floating demonstrator', *Windpower Monthly*.
URL: <https://www.windpowermonthly.com/article/1579762/funds-irelands-first-floating-demonstrator> [Accessed on: 2019-03-21]
- Robertson, A., Jonkman, J., Masciola, M., Song, H., Goupee, A., Coulling, A. & Luan, C. (2014), *Definition of the Semisubmersible Floating System for Phase II of OC4 (Technical Report NREL/TP-5000-60601)*, National Renewable Energy Laboratory, Golden, CO, USA.
- Robertson, A. N., Gueydon, S., Bachynski, E., Wang, L., Jonkman, J., Alarcón, D., Amet, E., Beardsell, A., Bonnet, P., Boudet, B., Brun, C., Chen, Z., Féron, M., Forbush, D., Galinos, C., Galvan, J., Gilbert, P., Gómez, J., Harnois, V., Haudin, F., Hu, Z., Le Dreff, J.-B., Leimeister, M., Lemmer, F., Li, H., McKinnon, G., Mendikoa, I., Moghtadaei, A., S., N., Oh, S., Pegalajar-Jurado, A., Nguyen, M. Q., Ruehl, K., Schünemann, P., Shi, W., Shin, H., Si, Y., Surmont, F., Trubat, P., Qwist, J. & Wohlfahrt-Laymann, S. (2020), 'OC6 Phase I: investigating the underprediction of low-frequency hydrodynamic loads and responses of a floating wind turbine', *Journal of Physics: Conference Series* **1618**, 032033. doi: <http://dx.doi.org/10.1088/1742-6596/1618/3/032033>.
- Rummelhoff, I. & Bull, S. (2015), *Building the world's first floating offshore wind farm*, Statoil.
URL: <https://www.statoil.com/> [Accessed on: 2017-12-16]
- Sandner, F., Schlipf, D., Matha, D. & Cheng, P. W. (2014), Integrated optimization of floating wind turbine systems, in 'Proceedings of the ASME 33rd International Conference on Ocean, Offshore and Arctic Engineering, San Francisco, CA, USA, June 8-13, 2014', American Society of Mechanical Engineers, New York, NY, USA. doi: <http://dx.doi.org/10.1115/OMAE2014-24244>.
- Scheu, M., Matha, D., Hofmann, M. & Muskulus, M. (2012), 'Maintenance strategies for large offshore wind farms', *Energy Procedia* **24**, 281–288. doi: <http://dx.doi.org/10.1016/j.egypro.2012.06.110>.
- Scheu, M. N., Kolios, A., Fischer, T. & Brennan, F. (2017), 'Influence of statistical uncertainty of component reliability estimations on offshore wind farm availability', *Reliability Engineering & System Safety*. doi: <http://dx.doi.org/10.1016/j.res.2017.05.021>.

- Sclavounos, P., Tracy, C. & Lee, S. (2008), Floating offshore wind turbines: responses in a seastate Pareto optimal designs and economic assessment, *in* 'Proceedings of the ASME 27th International Conference on Ocean, Offshore and Arctic Engineering, Estoril, Portugal, June 15-20, 2008', American Society of Mechanical Engineers, New York, NY, USA, pp. 31–41. doi: <http://dx.doi.org/10.1115/OMAE2008-57056>.
- Sevinc, A., Rosemeier, M., Bätge, M., Braun, R., Meng, F., Steer, L., Shan, M., Horte, D., Balzani, C. & Reuter, A. (2016), *Reference Wind Turbine IWT-7.5-164 Specification, rev.03*, Fraunhofer Institute for Wind Energy and Energy System Technology, Bremerhaven, Germany.
- Seymour, R. J., ed. (1992), *Ocean energy recovery: The state of the art*, American Society of Civil Engineers, New York, NY, USA.
- Shafiee, M. & Dinmohammadi, F. (2014), 'An FMEA-based risk assessment approach for wind turbine systems: a comparative study of onshore and offshore', *Energies* **7**(2), 619–642. doi: <http://dx.doi.org/10.3390/en7020619>.
- Shafiee, M., Finkelstein, M. & Bérenguer, C. (2015), 'An opportunistic condition-based maintenance policy for offshore wind turbine blades subjected to degradation and environmental shocks', *Reliability Engineering & System Safety* **142**, 463–471. doi: <http://dx.doi.org/10.1016/j.res.s.2015.05.001>.
- Shafiee, M. & Kolios, A. (2015), A multi-criteria decision model to mitigate the operational risks of offshore wind infrastructures, *in* T. Nowakowski, ed., 'Safety and reliability', CRC Press, London, UK, pp. 539–547. doi: <http://dx.doi.org/10.1201/b17399-77>.
- Shittu, A. A., Mehmanparast, A., Wang, L., Salonitis, K. & Kolios, A. (2020), 'Comparative study of structural reliability assessment methods for offshore wind turbine jacket support structures', *Applied Sciences* **10**(3), 860. doi: <http://dx.doi.org/10.3390/app10030860>.
- Siegfriedsen, A. & Klumpp, S. (2020), *Research project: Nezy² floating offshore wind turbine*, aerodyn engineering, EnBW.
URL: https://www.enbw.com/media/presse/docs/gemeinsame-pressemittelungen/2020/20200602_fact_sheet_enbw_aerodyn_nezy2_final_eng.pdf [Accessed on: 2020-06-02]
- Sif Group (2020), 'Wind foundations'.
URL: <https://sif-group.com/en/wind/foundations> [Accessed on: 2020-06-21]
- Simone (2020), *Pareto filtering*, MATLAB Central File Exchange.
URL: <https://www.mathworks.com/matlabcentral/fileexchange/50477-pareto-filtering> [Accessed on: 2020-01-13]

- SINTEF Ocean (2017), *SIMO 4.10.3 User Guide*, Trondheim, Norway.
URL: <https://home.hvl.no/ansatte/tct/FTP/V2020%20Hydrodynamikk/Sesam/SESAM%20UM%20Brukermanualer/SIMO%20User%20Manual.pdf> [Accessed on: 2020-07-09]
- Sirnivas, S., Musial, W., Bailey, B. & Filippelli, M. (2014), *Assessment of Offshore Wind System Design, Safety, and Operation Standards (Technical Report NREL/TP-5000-60573)*, National Renewable Energy Laboratory, Golden, CO, USA.
- Song, G., Khan, F., Wang, H., Leighton, S., Yuan, Z. & Liu, H. (2016), 'Dynamic occupational risk model for offshore operations in harsh environments', *Reliability Engineering & System Safety* **150**, 58–64. doi: <http://dx.doi.org/10.1016/j.res.2016.01.021>.
- Stapelberg, R. F. (2009), *Handbook of Reliability, Availability, Maintainability and Safety in Engineering Design*, Springer London, London, UK. doi: <http://dx.doi.org/10.1007/978-1-84800-175-6>.
- Stieng, L. E. S. & Muskulus, M. (2019), 'Load case reduction for offshore wind turbine support structure fatigue assessment by importance sampling with two-stage filtering', *Wind Energy* **22**(11), 1472–1486. doi: <http://dx.doi.org/10.1002/we.2382>.
- Stieng, L. E. S. & Muskulus, M. (2020), 'Reliability-based design optimization of offshore wind turbine support structures using analytical sensitivities and factorized uncertainty modeling', *Wind Energy Science* **5**(1), 171–198. doi: <http://dx.doi.org/10.5194/wes-5-171-2020>.
- Stiesdal, H. (2019), *TetraSpar and TetraBase: Industrialized Offshore Wind Turbine Foundations*, Stiesdal Offshore Technology.
URL: <https://www.stiesdal.com/material/2019/02/Stiesdal-Tetra-01.02.19.pdf> [Accessed on: 2019-02-01]
- Strauss, A. (2016), 'Numerical and monitoring based Markov chain approaches for the fatigue life prediction of concrete structures', *Engineering Structures* **112**, 265–273. doi: <http://dx.doi.org/10.1016/j.engstruct.2016.01.020>.
- Strobel, M., Vorpahl, F., Hillmann, C., Gu, X., Zuga, A. & Wihlfahrt, U. (2011), The OnWind Modelica library for offshore wind turbines - implementation and first results, in 'Proceedings of the 8th International Modelica Conference, Dresden, Germany, March 20-22, 2011', Linköping Electronic Conference Proceedings, Linköping University Electronic Press, Linköping, Sweden, pp. 603–609. doi: <http://dx.doi.org/10.3384/ecp11063603>.
- Sumer, B. M. & Fredsøe, J. (2006), *Hydrodynamics around cylindrical structures*, Vol. 26 of *Advanced series on ocean engineering*, Rev. edn, World Scientific Pub, Singapore; Hackensack, NJ, USA.
URL: <http://search.ebscohost.com/login.aspx?direct=true&scope=site&db=nlebk&db=nlabk&AN=210818>

- Sundrarajan, C., ed. (1995), *Probabilistic Structural Mechanics Handbook: Theory and Industrial Applications*, Springer Science, Dordrecht, The Netherlands. doi: <http://dx.doi.org/10.1007/978-1-4615-1771-9>.
URL: <http://site.ebrary.com/lib/alltitles/docDetail.action?docID=10649723>
- Suzuki, A. (2000), Application of dynamic inflow theory to wind turbine rotors, Doctoral thesis, University of Utah, Salt Lake City, UT, USA.
- Suzuki, K., Yamaguchi, H., Akase, M., Imakita, A., Ishihara, T., Fukumoto, Y. & Oyama, T. (2011), 'Initial design of tension leg platform for offshore wind farm', *Journal of Fluid Science and Technology* **6**(3), 372–381. doi: <http://dx.doi.org/10.1299/jfst.6.372>.
- Taboada, J. V. (2015), 'Comparative analysis review on floating offshore wind foundations (FOWF)', *Ingenieria Naval: Proceedings of the 54th Naval Engineering and maritime Industry Congress, Ferrol, Spain, October 14-16, 2016 Julio/agosto 2016*, 763–775.
- Tafazzoli, S., Shafaghat, R. & Alamian, R. (2020), 'Optimization study of a catenary mooring system for a spar floating wind turbine based on its hydrodynamic responses', *Proceedings of the Institution of Mechanical Engineers, Part M: Journal of Engineering for the Maritime Environment* **12**, 147509022091781. doi: <http://dx.doi.org/10.1177/1475090220917812>.
- Taflanidis, A. A., Loukogeorgaki, E. & Angelides, D. C. (2013), 'Offshore wind turbine risk quantification/evaluation under extreme environmental conditions', *Reliability Engineering & System Safety* **115**, 19–32. doi: <http://dx.doi.org/10.1016/j.res.2013.02.003>.
- Tavner, P. J. (2012), *Offshore wind turbines: Reliability, availability and maintenance*, Vol. 13 of *IET power and energy series*, Institution of Engineering and Technology, London, UK.
- Tavner, P. J., Xiang, J. & Spinato, F. (2007), 'Reliability analysis for wind turbines', *Wind Energy* **10**(1), 1–18. doi: <http://dx.doi.org/10.1002/we.204>.
- The Regents of the University of California (2020), 'Modelica Buildings Library: buildingspy'.
URL: <https://simulationresearch.lbl.gov/modelica/buildingspy/> [Accessed on: 2020-06-11]
- Thomas, P., Gu, X., Samlaus, R., Hillmann, C. & Wihlfahrt, U. (2014), The OneWind® Modelica library for wind turbine simulation with flexible structure - modal reduction method in Modelica, in 'Proceedings of the 10th International Modelica Conference, Lund, Sweden, March 10-12, 2014', Linköping Electronic Conference Proceedings, Linköping University Electronic Press, Linköping, Sweden, pp. 939–948. doi: <http://dx.doi.org/10.3384/ECP14096939>.
- Thöns, S., Faber, M. H. & Rücker, W. (2010), Support structure reliability of offshore wind turbines utilizing an adaptive response surface method, in 'Proceedings of the ASME 29th International Conference on Ocean, Offshore and Arctic Engineering, Shanghai, China, June

- 6-11, 2010', American Society of Mechanical Engineers, New York, NY, USA, pp. 407–416. doi: <http://dx.doi.org/10.1115/OMAE2010-20546>.
- Tichý, M. (1993), *Applied methods of structural reliability*, Vol. 2 of *Topics in safety, reliability, and quality*, Kluwer Acad. Publ, Dordrecht, The Netherlands.
- Troffaes, M. C., Walter, G. & Kelly, D. (2014), 'A robust Bayesian approach to modeling epistemic uncertainty in common-cause failure models', *Reliability Engineering & System Safety* **125**, 13–21. doi: <http://dx.doi.org/10.1016/j.ress.2013.05.022>.
- Udoh, I. E. (2014), A concise methodology for the design of statically-equivalent deep-offshore mooring systems, in 'Proceedings of the ASME 33rd International Conference on Ocean, Offshore and Arctic Engineering, San Francisco, CA, USA, June 8-13, 2014', American Society of Mechanical Engineers, New York, NY, USA. doi: <http://dx.doi.org/10.1115/OMAE2014-23054>.
- Valverde, P. S., Sarmiento, António J. N. A. & Alves, M. (2014), 'Offshore wind farm layout optimization - state of the art', *Journal of Ocean and Wind Energy* **1**(1), 23–29.
- Velarde, J., Kramhøft, C. & Sørensen, J. D. (2019), Reliability-based design optimization of offshore wind turbine concrete structures, in 'Proceedings of the 13th International Conference on Applications of Statistics and Probability in Civil Engineering, ICASP 2019, Seoul, South Korea, May 26-30, 2019'.
- Vicinay (2012), *The future of mooring*, VICINAY CADENAS[®], S.A.
 URL: <http://www.vicinaycadenas.net/brochure/>
- Walter, G., Aslett, L. J. & Coolen, F. P. (2017), 'Bayesian nonparametric system reliability using sets of priors', *International Journal of Approximate Reasoning* **80**, 67–88. doi: <http://dx.doi.org/10.1016/j.ijar.2016.08.005>.
- Walter, G. & Augustin, T. (2009), 'Imprecision and prior-data conflict in generalized Bayesian inference', *Journal of Statistical Theory and Practice* **3**(1), 255–271. doi: <http://dx.doi.org/10.1080/15598608.2009.10411924>.
- Walter, G. & Coolen, F. P. (2016), Sets of priors reflecting prior-data conflict and agreement, in J. P. Carvalho, M.-J. Lesot, U. Kaymak, S. Vieira, B. Bouchon-Meunier & R. R. Yager, eds, 'Information Processing and Management of Uncertainty in Knowledge-Based Systems', Communications in computer and information science, Springer International Publishing, Cham, Switzerland, pp. 153–164.
- Wang, L. & Kolios, A. (2017), A generic framework for reliability assessment of offshore wind turbine monopiles, in C. Guedes Soares & Y. Garbatov, eds, 'Progress in the Analysis and Design of Marine Structures', CRC Press, Milton, Canada, pp. 931–938.

- Wang, L., Kolios, A., Luengo, M. M. & Liu, X. (2016), 'Structural optimisation of wind turbine towers based on finite element analysis and genetic algorithm', *Wind Energy Science Discussions* pp. 1–26. doi: <http://dx.doi.org/10.5194/wes-2016-41>.
- Wayman, E. N. (2006), Coupled dynamics and economic analysis of floating wind turbine systems, Master thesis, Department of Mechanical Engineering, Cambridge, MA, USA.
URL: <http://hdl.handle.net/1721.1/35650> [Accessed on: 2017-09-19]
- WindEurope (2017), *Floating Offshore Wind Vision Statement*, Vol. June 2017, WindEurope, Brussels, Belgium.
- WindEurope (2019a), *Financing and investment trends: The European wind industry in 2018*, WindEurope, Brussels, Belgium.
- WindEurope (2019b), *Offshore Wind in Europe: Key trends and statistics 2018*, WindEurope, Brussels, Belgium.
- Windkraft-Journal (2019), 'Monopiles for wpd's 640 MW Yunlin offshore wind farm in Taiwan', *Windkraft-Journal* (June 14, 2019).
URL: <https://www.windkraft-journal.de/2019/06/14/steelwind-nordenham-ist-von-wpd-die-gruendungsstrukturen-fuer-den-offshore-wind-park-yunlin-in-taiwan-zu-fertigen/136551> [Accessed on: 2020-06-21]
- Withee, J. E. (2004), Fully coupled dynamic analysis of a floating wind turbine system, Doctoral thesis, Massachusetts Institute of Technology, Cambridge, MA, USA.
- Wright, C., Yoshimoto, H., Wada, R. & Takagi, K. (2019), Numerical modelling of a relatively small floating body's wave and low frequency motion response, compared with observational data, in 'Proceedings of the ASME 38th International Conference on Ocean, Offshore and Arctic Engineering, Glasgow, Scotland, UK, June 9-14, 2019', American Society of Mechanical Engineers, New York, NY, USA. doi: <http://dx.doi.org/10.1115/OMAE2019-96443>.
- Yamanaka, S., Hirai, T., Nihei, Y. & Sou, A. (2017), Interaction between advanced spar and regular waves, in 'Proceedings of the ASME 36th International Conference on Ocean, Offshore and Arctic Engineering, Trondheim, Norway, June 25-30, 2017', American Society of Mechanical Engineers, New York, NY, USA. doi: <http://dx.doi.org/10.1115/OMAE2017-61788>.
- Yang, D., Li, G. & Cheng, G. (2006), 'Convergence analysis of first order reliability method using chaos theory', *Computers & Structures* **84**(8-9), 563–571. doi: <http://dx.doi.org/10.1016/j.compstruc.2005.11.009>.
- Yang, H., Zhang, X. & Xiao, F. (2018), Dynamic reliability based design optimization of offshore wind turbines considering uncertainties, in 'Proceedings of the 13th ISOPE Pacific/A-

- sia Offshore Mechanics Symposium, PACOMS 2018, Jeju Island, Korea, October 14-17, 2018', pp. 325–331.
- Yang, H., Zhu, Y., Lu, Q. & Zhang, J. (2015), 'Dynamic reliability based design optimization of the tripod sub-structure of offshore wind turbines', *Renewable Energy* **78**, 16–25. doi: <http://dx.doi.org/10.1016/j.renene.2014.12.061>.
- Yeter, B., Garbatov, Y. & Guedes Soares, C. (2016), Reliability of offshore wind turbine support structures subjected to extreme wave-induced loads and defects, in 'Proceedings of the ASME 35th International Conference on Ocean, Offshore and Arctic Engineering, Busan, Korea, June 18-24, 2016', American Society of Mechanical Engineers, New York, NY, USA, p. V003T02A060. doi: <http://dx.doi.org/10.1115/OMAE2016-54240>.
- Yoshimoto, H. & Kamizawa, K. (2019), Validation of the motion analysis method of floating offshore wind turbines using observation data acquired by full scale demonstration project, in 'Proceedings of the ASME 38th International Conference on Ocean, Offshore and Arctic Engineering, Glasgow, Scotland, UK, June 9-14, 2019', American Society of Mechanical Engineers, New York, NY, USA. doi: <http://dx.doi.org/10.1115/OMAE2019-95828>.
- Yoshimoto, H., Yoshida, H. & Kamizawa, K. (2018), Validation of applicability of low frequency motion analysis theory using observation data of floating offshore substation, in 'Proceedings of the ASME 37th International Conference on Ocean, Offshore and Arctic Engineering, Madrid, Spain, June 17-22, 2018', American Society of Mechanical Engineers, New York, NY, USA. doi: <http://dx.doi.org/10.1115/OMAE2018-77201>.
- Zhang, H., Innal, F., Dufour, F. & Dutuit, Y. (2014), 'Piecewise deterministic Markov processes based approach applied to an offshore oil production system'.
- Zhang, H. & Kiureghian, A. D. (1995), Two Improved algorithms for reliability analysis, in R. Rackwitz, G. Augusti & A. Borri, eds, 'Reliability and Optimization of Structural Systems', Springer US, Boston, MA, USA, pp. 297–304.
- Zhang, R., Tang, Y., Hu, J., Ruan, S. & Chen, C. (2013), 'Dynamic response in frequency and time domains of a floating foundation for offshore wind turbines', *Ocean Engineering* **60**, 115–123. doi: <http://dx.doi.org/10.1016/j.oceaneng.2012.12.015>.
- Zhang, X., Sun, L., Sun, H., Guo, Q. & Bai, X. (2016), 'Floating offshore wind turbine reliability analysis based on system grading and dynamic FTA', *Journal of Wind Engineering and Industrial Aerodynamics* **154**, 21–33. doi: <http://dx.doi.org/10.1016/j.jweia.2016.04.005>.
- Zhang, Y. & Lam, J. S. L. (2015), 'Reliability analysis of offshore structures within a time varying environment', *Stochastic Environmental Research and Risk Assessment* **29**(6), 1615–1636. doi: <http://dx.doi.org/10.1007/s00477-015-1084-7>.

- Zhu, H., Sueyoshi, M., Hu, C. & Yoshida, S. (2019), 'A study on a floating type shrouded wind turbine: design, modeling and analysis', *Renewable Energy* **134**, 1099–1113. doi: <http://dx.doi.org/10.1016/j.renene.2018.09.028>.
- Ziegler, L., Schafhirt, S., Scheu, M. & Muskulus, M. (2016), 'Effect of load sequence and weather seasonality on fatigue crack growth for monopile-based offshore wind turbines', *Energy Procedia* **94**, 115–123. doi: <http://dx.doi.org/10.1016/j.egypro.2016.09.204>.
- Zitrou, A., Bedford, T. & Walls, L. (2016), 'A model for availability growth with application to new generation offshore wind farms', *Reliability Engineering & System Safety* **152**, 83–94. doi: <http://dx.doi.org/10.1016/j.res.s.2015.12.004>.